SUBCELLULAR GLUTATHIONE HOMEOSTASIS AND CHARACTERISATION OF GLUTATHIONE TRANSPORT ACROSS THE PLASMA MEMBRANE IN *ARABIDOPSIS THALIANA*

Inaugural – Dissertation zur Erlangung des Grades
Doktor der Agrarwissenschaften (Dr. agr.)
der Landwirtschaftlichen Fakultät der
Rheinischen Friedrich-Wilhelms-Universität Bonn

vorgelegt von

Sajid Ali Khan Bangash

aus Nowshera, Pakistan

Bonn, 2017

Erstgutachter: Prof. Dr. Andreas Meyer

Zweitgutachter: Prof. Dr. Michael Frei

Tag der Mündlichen Prüfung: 14.12.2017

TABLE OF CONTENTS

SUMMARY

Challenging environmental conditions are known to alter glutathione homeostasis, notably by inducing the accumulation of oxidized glutathione, an effect that may be influential in the perception or transduction of stress signals. The tripeptide glutathione (reduced form: GSH; oxidized form: GSSG) is a key player in maintaining cellular thiol-redox homeostasis. In Arabidopsis, two proteins are responsible for GSH biosynthesis, GSH1 and GSH2. GSH1 is exclusively localized in plastids, while GSH2 is localized in both plastids and cytosol. Thus, GSH synthesis is restricted to plastids and cytosol but there is a requirement for glutathione also in other subcellular compartments with the need for intracellular GSH transport. In addition, there is good indication pointing at long-distance transport of glutathione between different organs. The latter implies the need for transport of glutathione across the plasma membrane which is poorly understood. Null mutants of GSH1 are embryo lethal, while disruption of GSH2 is seedling lethal. In several genetic screens, different *gsh1* mutants with defects in GSH biosynthesis have been identified. However, the effect of these mutations at the subcellular level was still elusive. In this study, the effect of GSH1 mutations on subcellular glutathione distribution was analysed in an allelic series of *gsh1* mutants and wild-type plants. Fluorescent labelling of GSH with monochlorobimane (MCB) and HPLC measurements showed that the total amount of glutathione was affected by the respective mutations. Furthermore, the relative glutathione redox potential (E_{GSH}) in different subcellular compartments measured with redox-sensitive fluorescent protein2 (roGFP2), showed that these mutations differentially affect the subcellular glutathione pool. The data indicate that mutations in GSH1 have a stronger effect on cytosolic and plastidial glutathione homeostasis than on mitochondrial glutathione homeostasis. Furthermore, crossing of *bir6* (a mutant with diminished glutathione turnover) with the severely GSH deficient mutants, *zir1* (a mutant <20 % GSH, and restricted growth phenotype) and *rml1* (a mutant with <5 % GSH and seedling lethal) partially rescued the growth and lethal phenotype respectively, which strongly suggests that the absolute amount of glutathione is responsible for the growth phenotype GSH deficient mutants.

The glutathione concentration is limited by the γ-glutamyl cycle, which is based on glutathione synthesis, degradation and transport. While the γ-glutamyl cycle was suggested as a classical pathway involved in glutathione transport across the plasma membrane there is also evidence for cytosolic glutathione degradation. Under sulfur deficiency, intense MCB fluorescence in γ-glutamyl-cyclotransferase (GGCT) null mutants and diminished MCB fluorescence in wild-type suggests that GGCTs specifically degrade GSH in the cytosol.

While glutathione transport studies in yeast (*Saccharomyces cerevisiae*) have led to identification of Hgt1p as a high affinity glutathione transporter, genes encoding glutathione-specific transporters in the plasma membrane of plants remain largely unknown. To investigate the transport of glutathione across the plasma membrane, the severely glutathione-deficient Arabidopsis mutant *rml1* was analysed using the roGFP2, which are able to monitor the local E_{GSH}. Changes in the fluorescence ratio of roGFP2 expressed in the cytosol of *rml1* with external supply of GSH, in combination with inhibitor studies revealed a highly efficient secondary active uptake of GSH across the plasma membrane. Furthermore, reduction of roGFP2 was only seen with GSH, but not with individual amino acids or GSSG. Additionally, a generated *opt4rml1* double mutant further proved that the oligopeptide transporter 4 (OPT4) reported earlier is not the only GSH transporter in Arabidopsis but is rather complemented by a yet unknown high affinity transporter. These results have major implications for our understanding of the glutathione homeostasis in plants, with a particular focus on subcellular compartmentation, degradation, functionality and transport.

v

ZUSAMMENFASSUNG

Es ist bekannt, das widrige Umweltbedingungen die Glutathion-Homöostase verändern, insbesondere da sie die Anhäufung von oxidiertem Glutathion verursachen. Dieser Effekt könnte bei der Wahrnehmung oder Transduktion von Stresssignalen eine Rolle spielen. Das Tripeptid Glutathion (reduzierte Form: GSH, oxidierte Form: GSSG) ist ein wichtiger Akteur bei der Aufrechterhaltung der zellulären Thiol-Redox-Homöostase. In Arabidopsis sind zwei Proteine, GSH1 und GSH2, für die GSH-Biosynthese verantwortlich. GSH1 ist ausschließlich in Plastiden lokalisiert, während GSH2 sowohl in Plastiden als auch im Zytosol lokalisiert ist. Somit ist die GSH-Synthese auf Plastiden und Zytosol beschränkt, aber da auch ein Bedarf an Glutathion in anderen subzellulären Kompartimenten besteht, ist ein intrazellulärer GSH-Transports notwendig. Darüber hinaus gibt es einige Evidenzen, die auf längere Transportdistanzen von Glutathion zwischen verschiedenen Organen hinweisen. Letzteres impliziert die Notwendigkeit für einen Transport von Glutathion über die Plasmamembran, der noch schlecht verstanden ist. Nullmutanten von GSH1 sind embryo-letal, während ein Defekt von GSH2 erst im Keimlingsstadium letal ist. In mehreren genetischen Screens wurden verschiedene *gsh1*-Mutanten mit Defekten in der GSH-Biosynthese identifiziert. Allerdings war die Wirkung dieser Mutationen auf der subzellulären Ebene noch schwer fassbar. In dieser Studie wurde die Wirkung von GSH1-Mutationen auf die subzelluläre Glutathionverteilung in einer allelischen Serie von *gsh1*-Mutanten und Wildtyp-Pflanzen analysiert. Eine Fluoreszenzmarkierung von GSH mit Monochlorobiman (MCB) und HPLC-Messungen zeigten, dass die Gesamtmenge an Glutathion durch die jeweiligen Mutationen beeinflusst wurde. Darüber hinaus zeigte das relative Glutathion-Redoxpotential (E_{GSH}) in verschiedenen subzellulären Kompartimenten, gemessen mit roGFP2, dass diese Mutationen die subzellulären Glutathion-Pools unterschiedlich beeinflussen. Die Daten zeigen, dass Mutationen in GSH1 eine stärkere Wirkung auf die zytosolische und plastidiäre Glutathionhomöostase haben als auf die mitochondriale Glutathionhomöostase. Darüber hinaus wurde durch die Kreuzung von *bir6* (eine Mutante mit vermindertem Glutathionumsatz) mit den stark GSH-defizienten Mutanten *zir1* (eine Mutante <20% GSH und eingeschränktem Wachstum) und *rml1* (eine Mutante mit <5% GSH und Keimling letal) das Wachstum bzw. der tödliche Phänotyp teilweise gerettet, was stark darauf hindeutet, dass die absolute Menge an Glutathion für denWachstums-Phänotyp der GSH-defizienten Mutanten verantwortlich ist.

Die Glutathion-Konzentration wird durch den γ-Glutamyl-Zyklus definiert, der auf Glutathion-Synthese, Abbau und Transport basiert. Während der γ-Glutamyl-Zyklus als ein klassischer Weg vorgeschlagen wurde, der am Glutathion-Transport über die Plasmamembran beteiligt ist, gibt es auch Hinweise auf einen zytosolischen Glutathionabbau. Unter Schwefelmangel legt eine intensive MCB-Fluoreszenz in γ-Glutamylcyclotransferase (GGCT) Nullmutanten und eine verminderte MCB-Fluoreszenz im Wildtyp nahe, dass GGCTs spezifisch GSH im Zytosol abbauen.

Während Glutathion-Transportstudien in Hefe (*Saccharomyces cerevisiae*) zur Identifizierung von Hgt1p als hochaffinen Glutathion-Transporter geführt haben, sind Gene, die für Glutathion-spezifische Transporter in der Plasmamembran von Pflanzen kodieren, weitgehend unbekannt. Um den Transport von Glutathion über die Plasmamembran zu untersuchen, wurde die stark Glutathion-defiziente Arabidopsis-Mutante *rml1* unter Verwendung von roGFP2 analysiert, das in der Lage ist, das lokale E_{GSH} auszulesen. Änderungen des Fluoreszenzverhältnisses von roGFP2, exprimiert im Zytosol von *rml1* unter externer Zugabe von GSH zeigten in Kombination mit Inhibitorstudien eine hochwirksame sekundäre aktive Aufnahme von GSH über die Plasmamembran. Weiterhin wurde die Reduktion von roGFP2 nur bei Zugabe von GSH, aber nicht bei einzelnen Aminosäuren oder GSSG beobachtet. Darüber hinaus hat eine generierte *opt4rml1*-Doppelmutante nachgewiesen, dass der zuvor berichtete Oligopeptid-Transporter 4 (OPT4) nicht der einzige GSH-Transporter in Arabidopsis ist, sondern eher durch einen noch unbekannten hochaffinen Transporter ergänzt wird. Diese Ergebnisse haben große Auswirkungen auf unser Verständnis der Glutathion-Homöostase in Pflanzen, mit besonderem Augenmerk auf subzelluläre Kompartimentierung, Abbau, Funktionalität und Transport.

1. INTRODUCTION

Life on Earth has to constantly acclimate to an ever changing environment (Sthijns et al., 2016). The first forms of ancient life emerged a long time before oxygenic photosynthesis evolved (roughly 2.5 billion years ago). During that time, the most fundamental metabolic processes was needed to adapt to the reigning reducing conditions, which subsequentially slowly became oxidised due to the uprising of oxygenic photosynthesis (Lyons et al., 2014; Meyer, 2008). Since this environmental change, cells have to adapt to the progressively changed external environment by developing systems that maintained the reduced internal environment. The characteristic features of a reductive system in cells comprises, a redox buffer for reducing oxidants, and/or sensitive switches for modulating protein structure and function to accomplish specific biological roles (Brandes et al., 2009; Groitl and Jakob, 2014; Sen and Packer, 2000). One of the most relevant components of the reducing machinery are thiols (Meyer, 2008).

1.1 Thiols in living organisms

Thiols are a class of organic sulfur by-product defined by the presence of sulfhydryl residues (-SH) at their active site (Figure 1.1 A). They exist in all aerobic life forms and present a wide range of functions. Among these, they coordinate the cellular antioxidant defence network. Chemically, thiols are referred as mercaptans (C-SH), and biological mercaptans are called biothiols. Biothiols can be classified in two types: large molecular weight protein thiols and low molecular weight free thiols (Sen and Packer, 2000). Most aerobic organisms contain high concentration of low molecular weight (LMW) thiols that serve as redox buffers for cell protections against a variety of reactive chemical species (Roos and Messens, 2011; Van Laer et al., 2013). The most common LMW thiols are, glutathione, cysteine, coenzyme A, homocysteine and lipoic acid. They can be organism–specific, for example mycothiol in *Actinomycetes*, bacillithiol in *Firmicutes*, γ-glutamylcysteine (γ-EC) in *Halobacteria* and lactic acid bacteria, trypanothione in some parasitic protozoa (*Trypanosomes*), coenzyme M and coenzyme B in methanogenic archaea and ergothioneine in fungi and *Mycobacteria* (Poole, 2015).

The thiol-group of cysteine is highly sensitive to loss of electrons or oxidation and serves as an active site for most biologically important thiols. The redox properties of cysteine allow the formation of intra, and intermolecular disulfide bridges (-S-S-) between two thiols (2-SH) residues upon oxidation (Figure 1.1 B). Disulfide bridges enable proper protein folding and the formation of stable multi protein complexes. High affectability of thiols to oxidation likewise renders protein thiols incredibly vulnerable against oxidative damage. Since thiols are highly sensitive to oxidative conditions, their presence in

proteins makes them vulnerable to oxidative damage (Meyer, 2008; Sen and Packer, 2000).
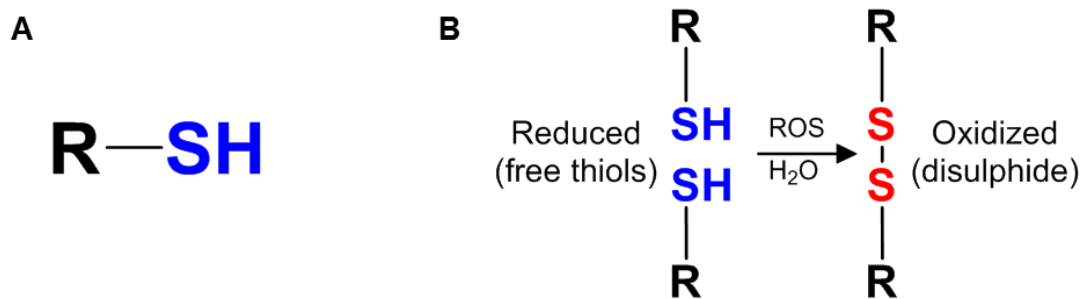
Figure 1.1: Structure and oxidation of thiols. (A) R represents an alkyl or other organic substituent and SH functional group called sulfhydryl group or thiol. **(B)** Oxidation of reduced thiols via reactive oxygen/nitrogen species (RO/NS) results in oxidised disulfide and water.

Thiol oxidation affects structural and catalytic properties of proteins, which may trigger downstream processes. Cells have developed sophisticated mechanisms that allow recovery of such proteins through reduction of thiol residues, preventing loss of proteins. A wide range of redox active enzymes facilitates the reversible oxidation and reduction of thiols. These enzymes include thioredoxins (TRXs) (Buchanan and Balmer, 2005), glutaredoxins (GRXs) (Li, 2014; Xing et al., 2006), sulfiredoxin (SRX) (Park et al., 2009), peroxiredoxins (PRX) (Dietz, 2003; Dietz et al., 2006) and protein disulfide isomerases (PDIs) (Frand et al., 2000; Parakh and Atkin, 2015). Efficient redox control can be ensured only if a redox buffer stabilizes the system and the most important one is a tripeptide called glutathione (Meyer, 2008).

1.2 Glutathione

In 1888, Rey-Pailhades found that yeast and other cells contain a compound that reacts spontaneously with elemental sulfur to give hydrogen sulfide, which by the time was named "philothione" (from the Greek for "love" and "sulfur"). After diverse proposed ideas, glutathione structure was finally established to be a tripeptide (Hopkins, 1929; Meister, 1988b; Simoni et al., 2002). Glutathione is the most abundant non-enzymatic LMW thiol, being found in nearly all organisms, with some exceptions in plants, fungi, prokaryotes and archaea, where they depend on other sulfur compounds besides or as an alternative to glutathione. These fascinating differences can be found in different macro and micro-organisms, such as halobacteria and lactic acid bacteria which use γ-glutamylcysteine (γ-EC)and thiosulfate as alternative to glutathione (Newton and Javor, 1985). Likewise, trypanosomes substitute glutathione by trypanothione (Fairlamb et al., 1985). Furthermore, some plants species (e.g. cereals and legumes) have glutathione homologues, in which C-terminal glycine residue of glutathione is replaced with an

amino acid other than glycine (Klapheck, 1988; Klapheck et al., 1992; Meuwly et al., 1993). The homoglutathione (γ-Glu-Cys-β-Ala) is also found in many legumes besides glutathione (Klapheck, 1988). Moreover, cereals contain another homologue of glutathione, hyroxymethylGSH (γ-Glu-Cys-Ser) (Okumura et al., 2003), and a glutathione reductase that can reduce the disulfide of these homologues (Noctor et al., 2012; Oven et al., 2001).

1.2.1 Glutathione biosynthesis and structure

Glutathione synthesis takes place in two ATP-dependent consecutive steps, catalysed by two different enzymes. First, cysteine and glutamate are combined by the action of the enzyme glutamate-cysteine ligase (GSH1, EC 6.3.2.2), generating the intermediate γ-EC. Secondly, glutathione synthase (GSH2, EC 6.3.2.3) catalyses the conjugation of glycine to γ-EC and the creation of the tripeptide glutathione (GSH) (Meister, 1988a) (Figure 1.2 A). GSH is composed of three amino acids: L-glutamate, L-cysteine and glycine with a γ-peptide bond between the amine group of cysteine and the γ-carboxyl group of the glutamate (Figure 1.2 B). The thiol group of cysteine is the key feature for biological activities of GSH, and the γ-peptide bond is importance for not being degraded by most peptidases in the cell, with the exception of GGTs (Ohkama-Ohtsu et al., 2008). In bacteria, yeast and animals, GSH synthesis takes place only in the cytosol (Bachhawat et al., 2013; Lu, 2013; Stout et al., 2012). In contrast, glutathione biosynthesis in model plant *Arabidopsis thaliana* takes place in two different cell compartments. Here, GSH1 has been shown to be localise exclusively in plastids, whereas GSH2 localise, predominantly in the cytosol but also in the plastids (Wachter et al., 2005). Thus, the glutathione biosynthesis occurs in both plastids and cytosol and it requires an export of γ-EC from plastids to the cytosol (Pasternak et al., 2008).

The relevance of the cytosolic production of GSH was characterised by complementing mutant plants deficient in GSH2 with a wild–type GSH2 exclusively targeted to the cytosol. The complementation restored GSH biosynthesis and hence rescued the phenotype (Pasternak et al., 2008).

As mentioned before, GSH1 plays a key regulatory function in GSH biosynthesis, and feedback inhibition of GSH1 by glutathione plays as well an important role in glutathione homeostasis, both in plants and animals (Hell and Bergmann, 1990; Richman and Meister, 1975). In order to further study it, several genetic screens with mutagenised lines of Arabidopsis have been performed and resulted in the isolation of six mutants for GSH1: *rax1, pad2, cad2, nrc1, zir1* and *rml1*(Figure 1.3 A-B).

Due to mutation of GSH1, the amount of glutathione in these mutants varies between 5 and 50% compared to wild-type plants (Ball et al., 2004; Cobbett et al., 1998; Jobe et al., 2012; Parisy et al., 2007; Shanmugam et al., 2012). Clear indications of the importance of

3

GSH in Arabidopsis are visible in *rml1* mutants. This line in fact contains less than 5% of glutathione compare to a wild–type plant, which is related to a more severe phenotype, where the seedlings are not viable after ~3 weeks (Vernoux et al., 2000).
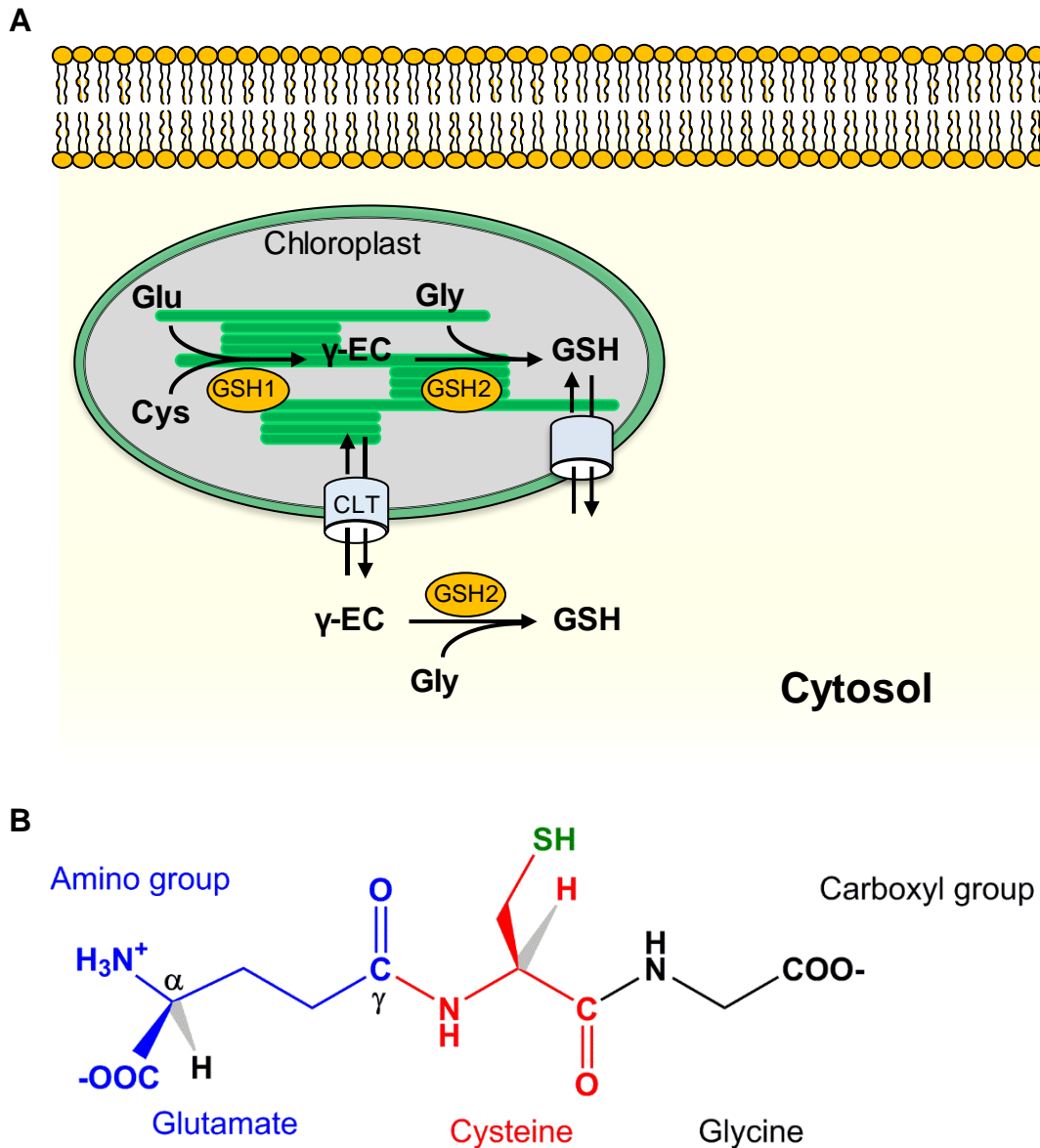
Figure 1.2: Glutathione biosynthesis and structure. (A) Glutathione biosynthesis pathway in Arabidopsis. The first step exclusively takes place in plastids while the second step takes place both in plastids and in the cytosol. Glutamate-cysteine ligase (GSH1) and glutathione synthase (GSH2) **(B)** Structure of tripeptide glutathione consists of glutamate (Glu), cysteine (Cys) and glycine (Gly).
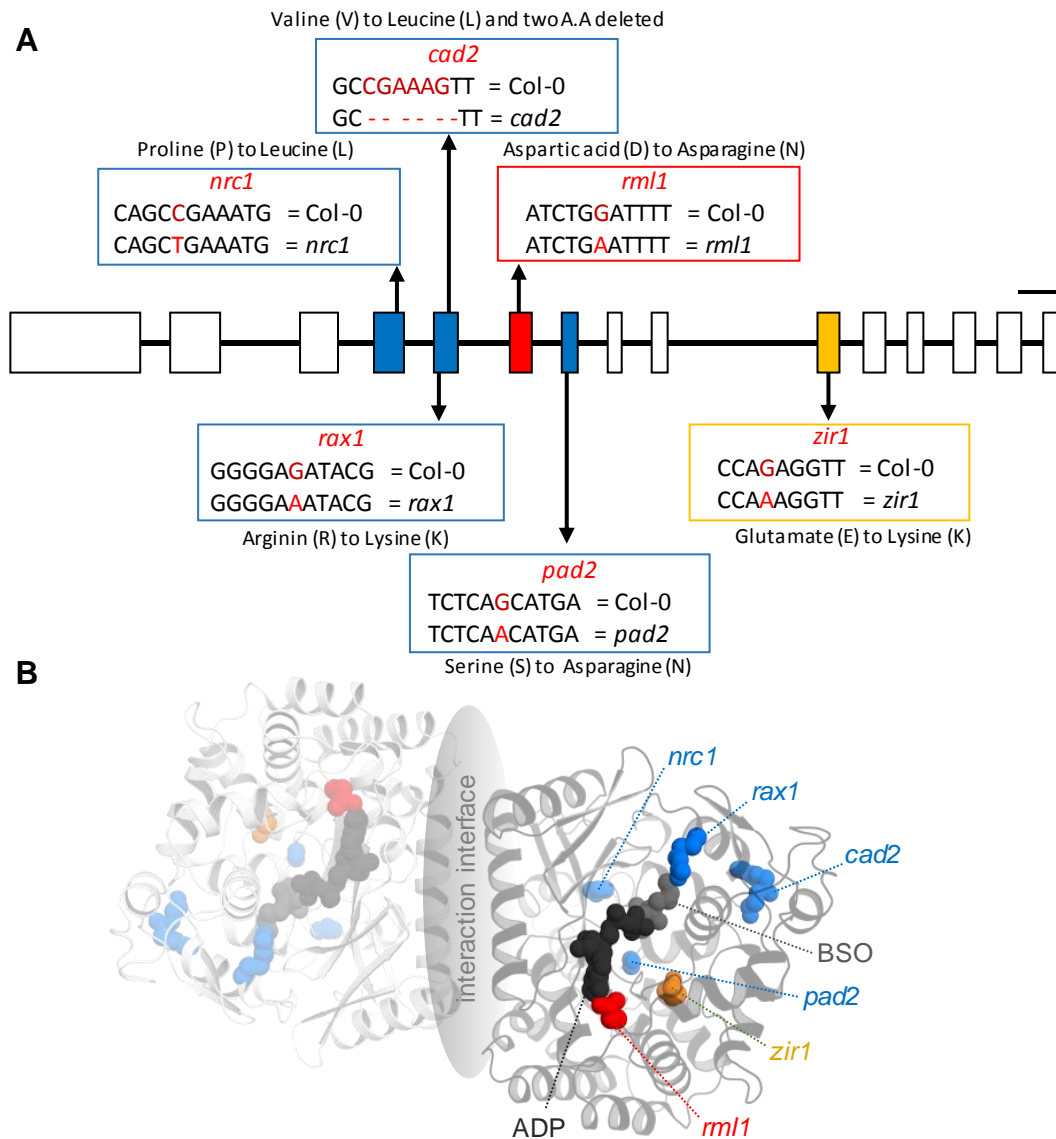
Figure 1.3: Arabidopsis *GSH1* gene and protein model (A) Gene model of Arabidopsis *GSH1* gene (*AT4G23100*) represents the positions and types of mutations of independent *gsh1* allelic series mutants. Exons and introns are illustrated as boxes and lines, respectively. **(B)** Protein homology model of *At*GSH1 depicting mutation for each *gsh1* mutants, BSO (L-Buthionine sulfoximine) a transition state analogue, inhibits glutathione biosynthesis by inhibiting GSH1 enzyme, ADP (Adenosine diphosphate) is a cofactor. Scale bar = 200 bp.

1.2.2 Glutathione functions

Glutathione has many critical functions in living organisms (Figure 1.4). In plants, it serves as electron donor for ascorbate recovery, storage and long-distance transport of reduced sulfur and posttranslational modifications of proteins through reversible glutathionylation of thiol residues (Cairns et al., 2006; Grzam et al., 2007). Furthermore, it also works in scavenging of reactive oxygen species (ROS) via the glutathione-ascorbate cycle (Foyer and Noctor, 2005) and detoxification of heavy metals (Cobbett and

Goldsbrough, 2002; Xu et al., 2014; Yadav, 2010) and xenobiotic compounds (Dixon et al., 1998).
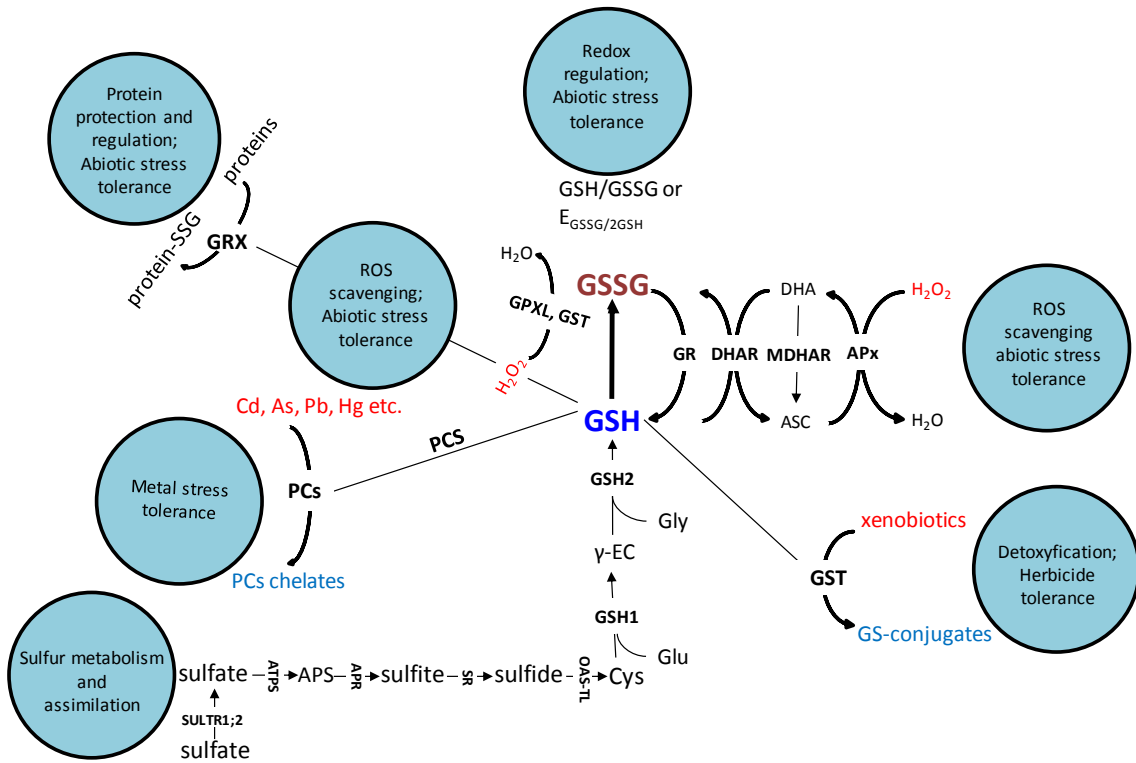
Figure 1.4: Overview of glutathione functions in Arabidopsis. Potential roles of glutathione and its significance against abiotic stress are illustrated in circles. Potential deleterious compounds are shown in red. Multiple GSH molecules are polymerised by phytochelatin synthase (PCS) to form phytochelatins (PC). Several antioxidative defence pathways are interconnected with GSH in order to remove the excess hydrogen peroxide (H_2O_2). The first defence pathway represents a direct non-enzymatic GSH oxidation. Secondly, the ascorbate-glutathione (ASC-GSH) cycle is displayed in which ASC and GSH are successively oxidised and reduced to allow ASC peroxidase (APX) to neutralize H_2O_2. Thirdly, the two major thiol-redox enzymes glutaredoxin (GRX) and thioredoxin (TRX) are presented that complement the GSH system in redox signalling. Abbreviations: Cysteine (Cys); Glutathione-S-transferase (GST); Glutathione peroxidase like enzyme (GPXL); Glutathione reductase (GR); Dehydroascorbate reductase (DHAR); Monodehydroascorbate reductase (MDHAR); Dehydroascorbate (DHA); ATP sulfurylase (ATPS); Adenosine 5'-phosphosulfate reductase (APR); O-acetylserine (thiol)lyase (OASTL) Sulfite reductase (SR). Modified from Zagorchev et al. (2013).

Glutathione is involved in the regulation of developmental processes, e.g. cell division (Vernoux et al., 2000) and flowering (Ogawa et al., 2004) and it acts as co-factor in coordination with iron-sulfur cluster transfer (Berndt et al., 2007).

Considering the broad range of functions linked to glutathione, it is not surprising that glutathione was found to be essential in plants (Cairns et al., 2006; Vernoux et al., 2000). Null mutants of glutathione biosynthesis resulting from T-DNA insertions in the gene *GSH1* result in an embryonic lethal phenotype (Cairns et al., 2006). Similarly, null mutants of *GSH2* are early seedling lethal (Pasternak et al., 2008a).

1.3 Subcellular glutathione compartmentation

Biochemically, compartmentation refers to the separation of metabolic processes that together constitute a metabolic cycle (van Gelder, 1982). The compartmentation of metabolites both inter and intracellular is a distinctive feature of eukaryotic cells, which is crucial for various physiological processes and metabolic regulation (Bowsher and Tobin, 2001; Hartmann et al., 2003). Glutathione is important for diverse functions in different subcellular compartments in plant cells. Alterations in GSH/GSSG is directly linked with cell proliferation, growth arrest or cell death (Circu and Yee Aw, 2008). Furthermore, combined changes in the levels of ROS and glutathione buffer can control cell proliferation in the nuclei and drive senescence in chloroplasts, mitochondria and peroxisomes (del Río et al., 2006; Galvez-Valdivieso and Mullineaux, 2010; Vianello et al., 2007; Vivancos et al., 2010). In response to severe oxidative stress, vacuoles accumulate ROS and GSSG (Queval et al., 2011). Therefore, subcellular distribution of antioxidants like glutathione and ascorbate together with their redox state can play an important role in plant growth and development (Kocsy et al., 2013).

Glutathione was found being differentially distributed between various subcellular compartments (cytosol, nucleus, mitochondria, and endoplasmic reticulum) in both plant and animal cells, giving rise to distinct subcellular redox pools (Figure 1.5). The amount of glutathione in the intracellular compartments depends on the relative volume occupied by each organelle of the cells. Under normal circumstances the cytosolic pool is considered to account for over 70 % of the total cellular glutathione, while the nuclear and mitochondrial compartments account for the remaining 10-30 % of the glutathione pool (Li et al., 2012; Lluis et al., 2005). Since, glutathione biosynthesis is highly compartment specific and biotic and abiotic stress situations affect each subcellular compartment differently, that results in fluctuations of subcellular glutathione contents (Zechmann, 2014). These intracellular fluctuations can be used as a stress indicator in order to elucidate the importance of the protective roles of glutathione at subcellular levels (Smith et al., 1996; Zechmann and Müller, 2010). Till now, detection of this tripeptide at subcellular level has been technically very challenging. Different approaches have been used to investigate the subcellular glutathione distributions such as high performance liquid chromatography (HPLC), enzyme assays and different microscopic based techniques. The first most used approached is the biochemical one, by using HPLC that allows to measured glutathione content after the isolation or fractionation of organelles such as chloroplasts, apoplast, mitochondria, peroxisomes and vacuoles. This technique allows to detect glutathione at millimolar concentrations and to discriminate between reduced and oxidised form(Jimenez et al., 1997; Krueger et al., 2009; Kuzniak and Sklodowska, 2005).

7
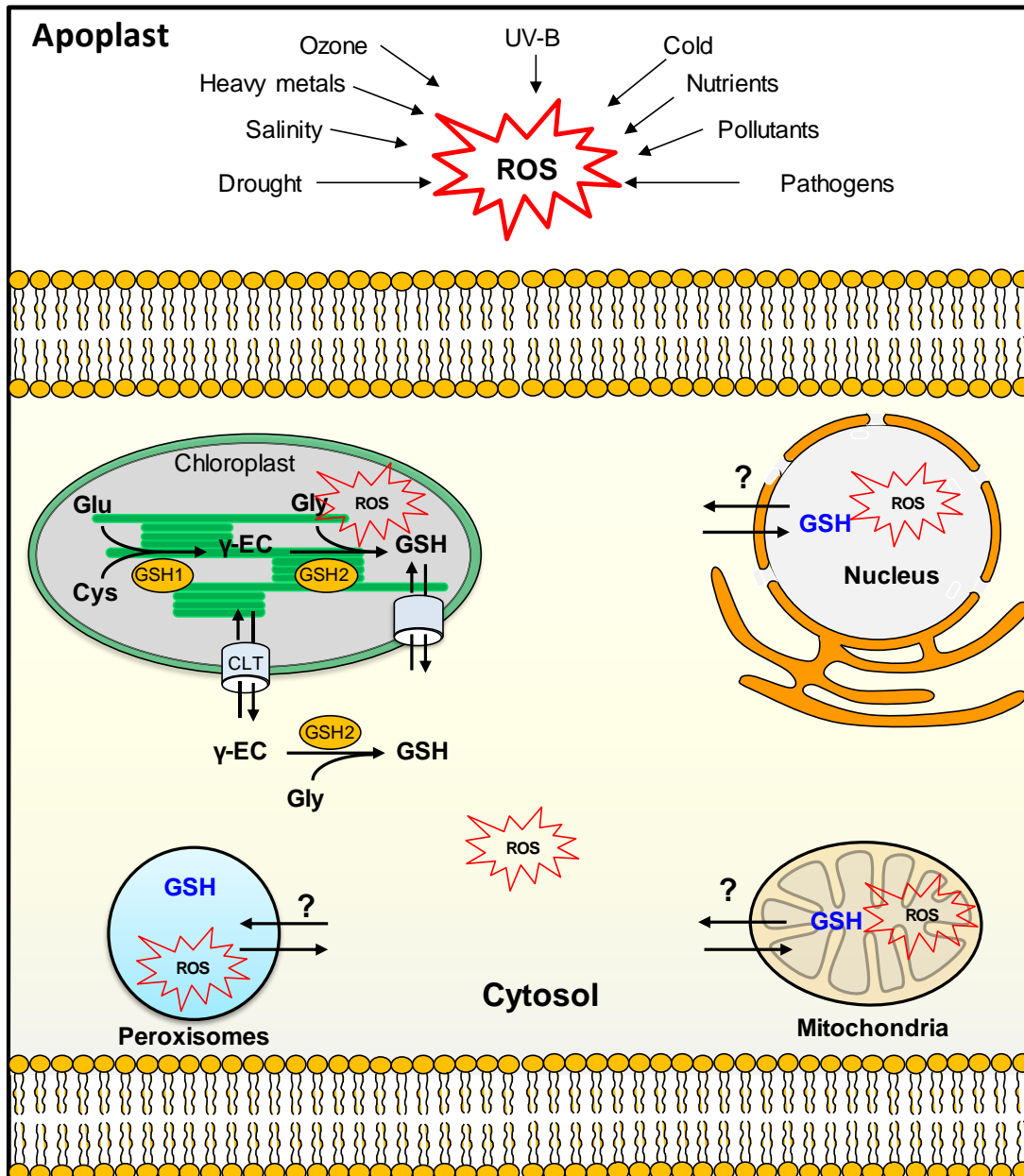
Figure 1.5: Compartmentation of glutathione in plant cell. Unfavorable environmental conditions result in formation of reactive oxygen species (ROS) in different subcellular compartments, which may intracellularly activate anti-oxidative and defense responses leading to plant acclimation.

As a downfall, the resolution of the redox state determination is conditioned to the quality of the isolation of the different compartments, where the pools may be contaminated, or even the redox state might change due to the extraction procedure.

The second common approach is the microscopical methods, based on the use of antibodies (Zechmann and Müller, 2010) and the fluorescent chemical dye monochlorobimane (MCB), which specifically labels glutathione *in vivo* and is used for the estimation of the total glutathione concentrations in plants (Meyer et al., 2001). This technique is, however, unable to discriminate between subcellular pools and the oxidised and reduced form.

A strong limitations of glutathione quantification in different compartments is the impossibility to measure glutathione in some organelles such as nucleus, endoplasmic reticulum (ER) and dictysomes (Noctor et al., 2002; Zechmann and Müller, 2010). Genetically encoded biosensors are the uprising method designed to overcome the limitations of conventional redox measurements (Gutscher et al., 2008). The genetically encoded redox sensitive green fluorescent protein (roGFP2) is a well-characterised sensor for redox measurement in Arabidopsis. It can be targeted to different subcellular compartments and it allows indirect visualisation of glutathione pool in subcellular compartments (Meyer et al., 2007). However, nowadays no further information is available whether and how cells are able to maintain different concentrations and redox state of glutathione in subcellular compartments under glutathione deficient situations. *In vivo* detection of the E_{GSH} by using roGFP2 sensor imaging will further resolve the dynamics of the glutathione redox buffer.

1.4 Glutathione degradation and turnover

Glutathione homeostasis is regulated by the γ-glutamyl cycle which in turn is based on glutathione synthesis, degradation and recycling of its components. The γ-peptide bond between glutamate and cysteine provides extra stability to glutathione against normal peptidases; nevertheless it is degraded by a special type of peptidases, γ-glutamyl-transferase (GGT) and γ -glutamyl-cyclotransferase (GGCT) which lead to two pathways of degradation (Meister, 1974; Ohkama-Ohtsu et al., 2008; Paulose et al., 2013). These two pathways operate in different compartments with distinct physiological significance and regulation (Figure 1.6). The GGT pathway operates extra cytosolic (apoplastic and vacuolar), while the GGCT pathway is restricted to the cytosol (Masi et al., 2015). There are four isoforms of GGT in Arabidopsis (GGT1, GGT2, GGT3 and GGT4) (Grzam et al., 2007; Storozhenko et al., 2002). The GGT1 and GGT2 are apoplastic localised, where GGT1 is bound to the cell wall and GGT2 is associated with the plasma membrane (Ferretti et al., 2009). These two isoforms of GGT recycle apoplastic glutathione by degrading both, GSH and GSSG into glutamate and cysteinyl-glycine (Cys-Gly). Degradation of Cys-Gly by dipeptidases yields the free amino acids. GGT3 is considered a pseudogene with an unusually truncated sequence and it lacks catalytic activity; GGT4 is vacuole–localised and involved in degradation of xenobiotic compounds conjugated with glutathione (Grzam et al., 2007). GGCT degrades the γ-glutamyl dipeptide, generated by GGTs, and releases amino acid from its γ-glutamyl carrier. During this reaction, the 5-oxoproline (5-OP) generated is converted into glutamate by the action of S-oxoprolinase, which can be reused for glutathione biosynthesis (Meister, 1974). In mice, the ChaC protein family functions as γ-glutamyl-cyclotranferases, acting specifically on glutathione (Kumar et al., 2012). The ChaC homologue in Arabidopsis grants heavy metal
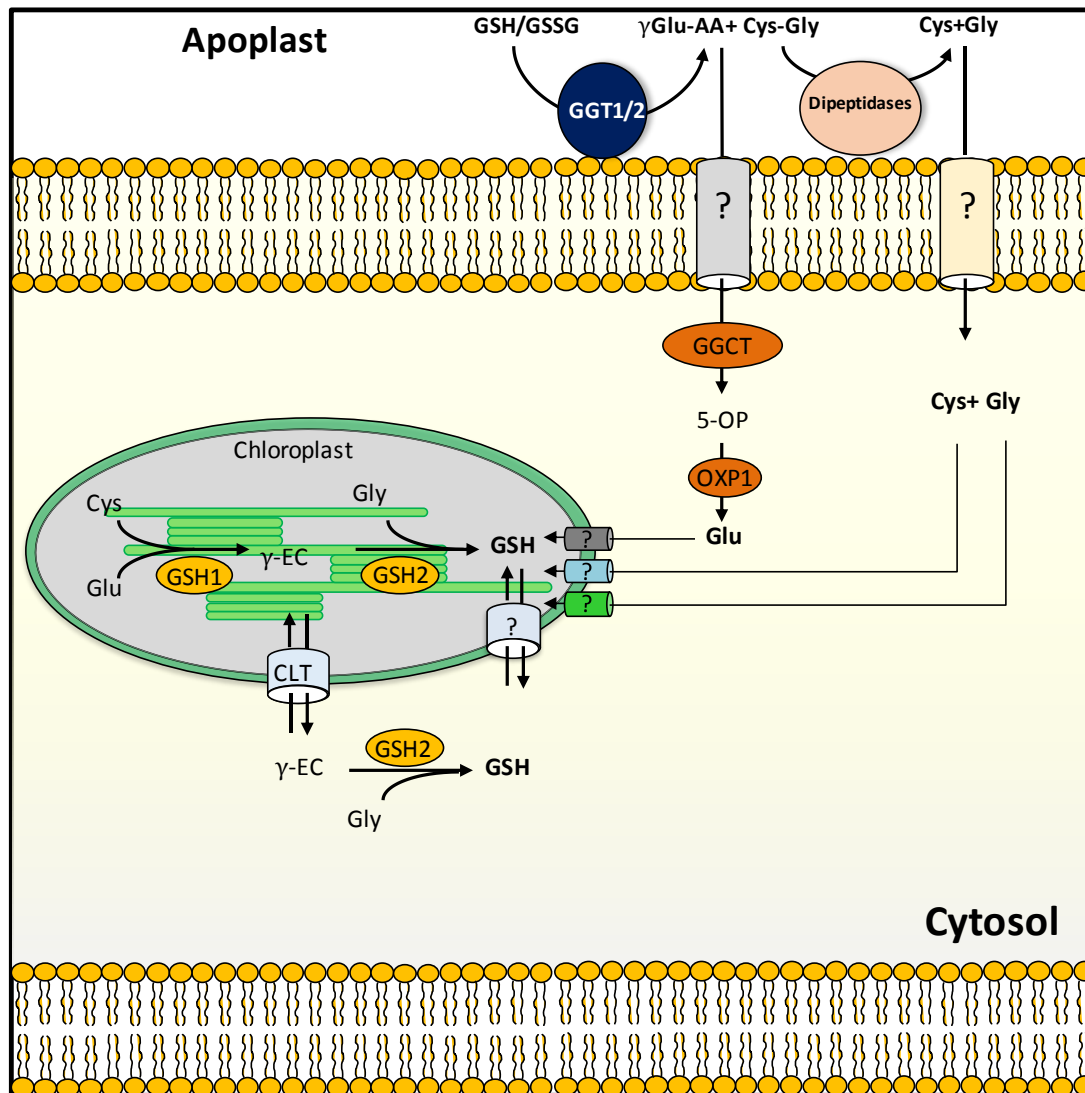
Figure 1.6: Model depicting predicted pathways of the γ-glutamyl cycle in plants. Glutathione is synthesised intracellularly and its export is mediated by as yet uncharacterised transporter/s. Apoplastic glutathione is hydrolysed to γGlu-AA (γGlutamyl dipeptide) and Cys-Gly by a gamma-glutamyl transferases(GGTs) bounded to the cell wall. Cys-Gly is further degraded by extracellular dipeptidases (DP) to individual amino acids and transported to the cell. γGlu-AA is converted to 5-Oxoproline (5-OP) by γ -glutamyl-cyclotransferase (GGCT) then to Glu by Oxoprolinase 1 (OXP1) and made available for *de novo* intracellular GSH synthesis. Adapted from Paulose et al. (2013).

tolerance by efficient glutamate recycling. Most eukaryotes have two ChaC homologues (ChaC1 and 2), while in Arabidopsis there are three ChaC homologues: GGCT2;1 (At5G26220), GGCT2;2 (At4G31290) and GGCT2;3 (At1G44790) (Kumar et al., 2015; Paulose et al., 2013).

Under sulfur deficiency, GGCT2;1 expression is strongly upregulated in root tips (Iyer-Pascuzzi et al., 2011), suggesting that plants start mobilizing sulfur by degrading glutathione (Figure 1.7). Two mutant lines for GGCT2;1 have been already generated by T-DNA insertion in Arabidopsis (*ggct2;1-1* and *ggct2;1-2*) (Paulose et al., 2013). However,

the significance of the GGCT pathway for cellular glutathione metabolism is still not fully understood yet.
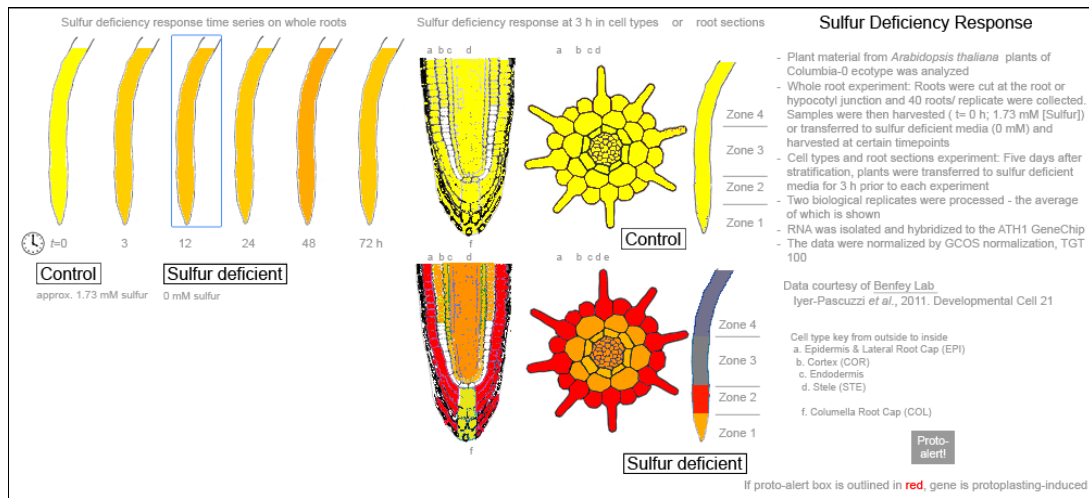
Figure 1.7: Sulfur deficiency leads to expression of the GGCT2;1 gene in Arabidopsis root tips. Output image from the electronic fluorescent pictographic (eFP) (Winter et al., 2007), that shows the expression pattern of GGCT2;1 under sulfur deficiency response in roots. The original data have been generated by the Benfey Lab (Iyer-Pascuzzi et al., 2011).

1.5   Glutathione transport

Plants are the primary producers of organic sulfur (Leustek et al., 2000), that has to be transported over long distances through the phloem in shoots and roots (Gigolashvili and Kopriva, 2014; Herschbach and Rennenberg, 1995). Glutathione is one of the major forms of reduce sulfur in plants (Leustek et al., 2000; Noctor et al., 2002). In Arabidopsis, glutathione synthesis is restricted to two compartments of cells, the cytosol and the plastids. Glutathione is, however, transported between organelles, cells and organs either via the apoplast, symplast or both (Noctor et al., 2012; Wachter et al., 2005). The transport of glutathione is not merely a passive transport, but it is part of a systemic signal transducing system, which senses sulfur status and mediates inter-organ regulation of sulfur nutrition (Lappartient and Touraine, 1996). Glutathione synthesis, degradation, use and inter- and intracellular transport equilibrate its concentration in different organelles, cells and tissues. Thus glutathione transport, along with compartmentation, are key regulators of glutathione homeostasis of living cells (Zhang et al., 2004).

 Long distance glutathione transport has been studied in maize (Rauser et al., 1991), spruce (Schneider et al., 1994), *Ricinus* (Bonas et al., 1982), grape berries (Adams and Liyanage, 1993) and poplar (Foyer and Noctor, 2001). Systemic glutathione transport in phloem and xylem is well established (Foyer et al., 2001; Rennenberg et al., 1979). Moreover, transport of glutathione has been biochemically characterised across species

(Bachhawat et al., 2013; Bourbouloux et al., 2000; Brechbuhl et al., 2010) but the molecular identity of the transporters has been elucidated in only few cases (Bachhawat et al., 2013). The multidrug resistance associated proteins (MRP), a subclass of ATP-binding cassette (ABC) transporter superfamily, was the first identified glutathione transporter in both yeast and mammalian cells. MRP was shown to be involved in glutathione efflux at the tonoplast in plants and yeast cells and at the plasma membrane of mammalian cells (Ballatori et al., 2009; Li et al., 1998; Rebbeor et al., 1998a, b). Increased amounts of glutathione have been reported in mammalian cancer cells that overexpress the gene for the apoptosis regulator BCL-2 (Voehringer et al., 1998), this is explained by the BH-3-domain present in BCL-2 proteins, which is able to bind glutathione (García-Giménez et al., 2013). In yeast, two ABC transporters, the bile pigment transporter 1 (Bpt1) and the yeast cadmium factor 1 (Ycf1p), transport glutathione from the cytosol into the vacuole (Ballatori et al., 2005). In plants, only a chloroquine-resistance transporter like transporters (CLTs) have been identified as plastid-located glutathione transporters (Maughan et al., 2010). Transport systems across other membranes still await to be discovered.

1.5.1 Bidirectional GSH transport by CLTs between plastids and cytosol

As mentioned earlier in this chapter, glutathione synthesis in Arabidopsis takes place in plastids and cytosol. Studies on radiolabelled wheat chloroplasts (Noctor et al., 2002) had postulated that GSH can be imported from the cytosol into the plastids. CLTs are the first functionally characterised members of the plant drug/metabolite exporter family. Arabidopsis has three genes identified to code for CLTs (*CLT1*, *CLT2* and *CLT3*) and the respective proteins are all localised in the inner envelope membrane of plastids, where they mediate the efflux of glutathione from the plastids to the cytosol (Maughan et al., 2010). However, it is still elusive whether CLTs are also involved in GSH transport from cytosol into plastids (Figure 1.8). Moreover, the fact that *clt* triple mutant under non-stress conditions shows no phenotype indicates that an additional, albeit less-efficient, pathway for export of γ-EC and/or GSH from plastids exists.
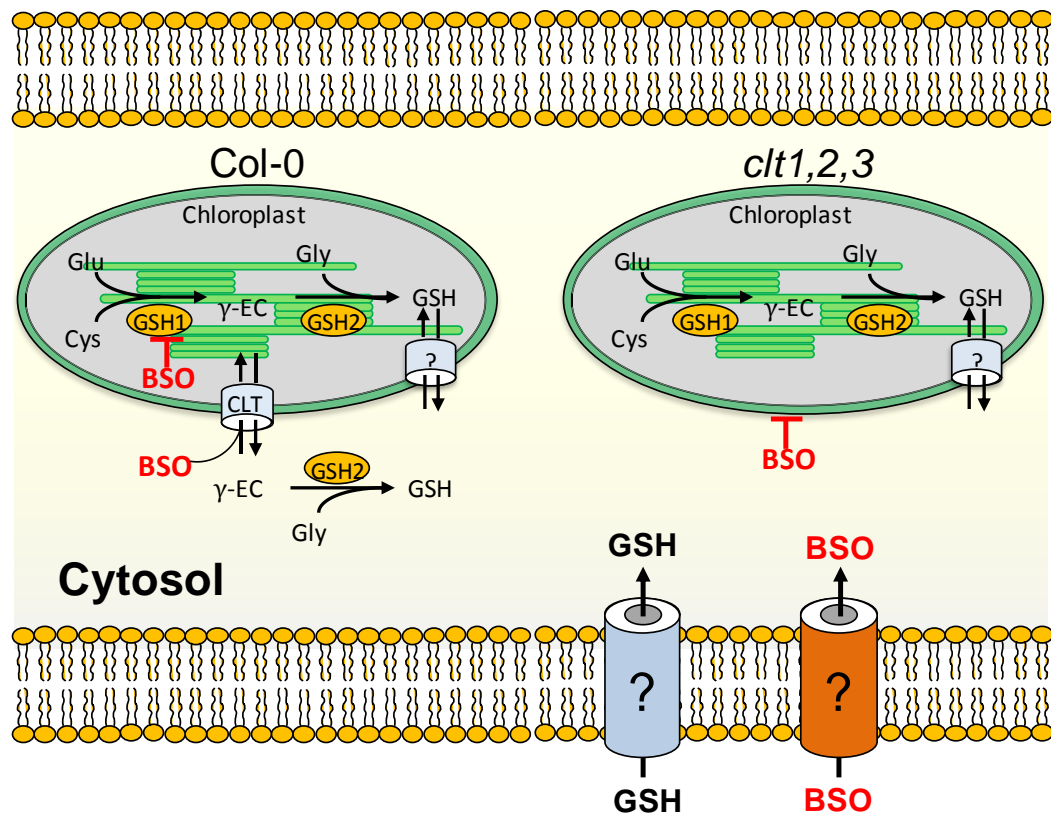
Figure 1.8: GSH transport across the plastidic membrane. GSH1 is exclusively localised in plastids and GSH2 mainly in cytosol (90% activity) and to a less extent in plastids (10% activity). Export of γ-EC/GSH from the plastids to cytosol is mediated by CLTs. Uptake of GSH into plastids is unknown and possibly also mediated by the CLTs.

1.5.2 Transport of GSH across the plasma membrane

Transport of GSH and GSSG across the plasma membrane plays a major role in maintaining the defensive capabilities of the apoplast. As a result of oxidative stress, GSSG is generated in the apoplast, and it must returned to the cytosol for re-reduction to GSH, since no NADH or NADPH and glutathione reductases has yet been detected in the extracellular space (Vanacker et al., 1998). The first transporter with high specificity and affinity for glutathione (Hgt1p) was discovered in yeast (Bourbouloux et al., 2000) and it belongs to the oligopeptide transporter (OPT) family. Hgt1p has homologues in plants, fungi and prokaryotes, but not in mammals (Yen et al., 2001). Nine OPTs have been described in plants (AtOPT1- AtOPT9), with 61-85% of sequence similarity among themselves and 49-53% sequence similarity to yeast Hgt1p (Koh et al., 2002). Several studies suggested a glycosyltransferase in rice (OsGT1), *Brassica juncea* (BjGT1) and AtOPT6 in Arabidopsis transport glutathione. A mutant yeast line (*Δhgt1p*) lacking the functional Hgt1p has been used as a platform for characterisation of glutathione transporters. Using this strain it has been shown that the complementation with neither

13

of the GTs mentioned nor any of the Arabidopsis OPTs recovers the capability of using GSH as the sole source of sulfur (Cagnac et al., 2004).

The characterisation of most of glutathione transporters is, however, still in its infancy due to their low affinities, multiple members and tissue specificity. In many cases proteins mediating glutathione transport across the organelle membranes as well as across the plasma membrane are still unknown or have been reported with some contradictory results (Bachhawat et al., 2013). Therefore, the transport systems for GSH and GSSG in plant cells still need to be explored. It has been already demonstrated that external glutathione supply rescued *rml1* root growth (Vernoux et al., 2000). For this reason, *rml1* mutant represents a good system to investigate glutathione transport in Arabidopsis (Figure 1.9).
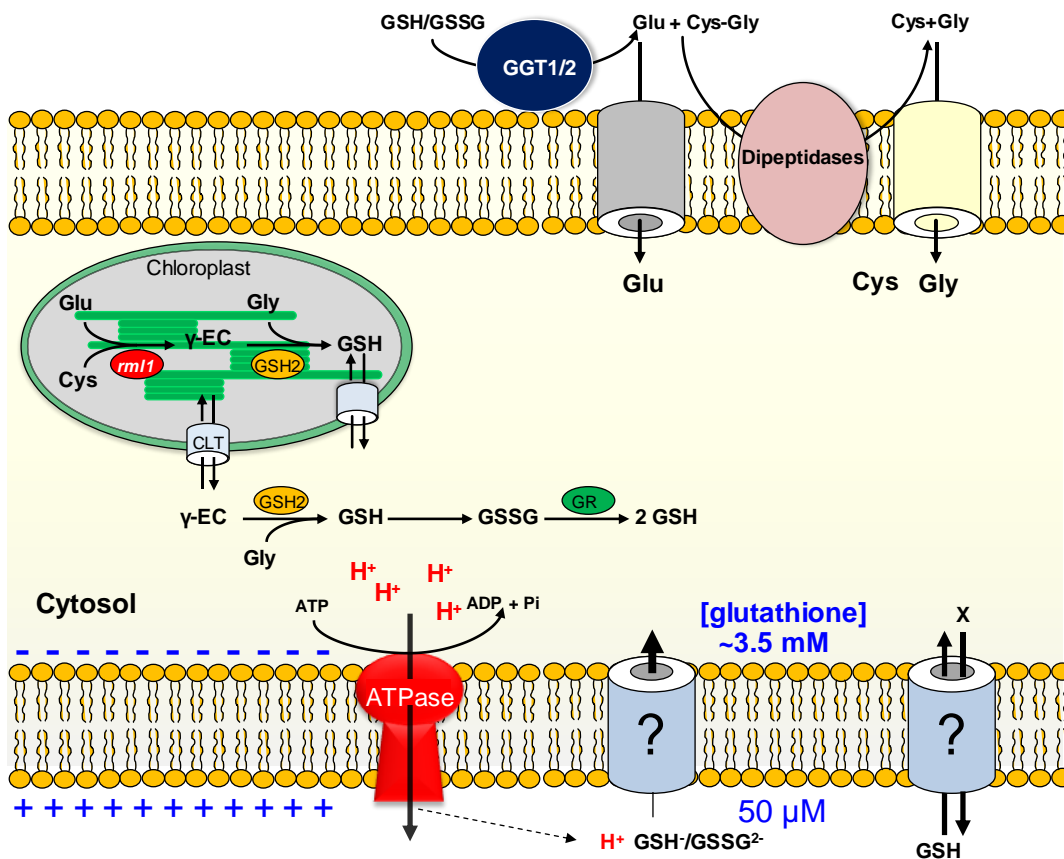
Figure 1.9: Model for glutathione uptake across the plasma membrane of *rml1* mutant roots. The GSH-deficient mutant *rml1* is exploited as an experimental system to study GSH transport. Glutathione can possibly be taken up as GSH, GSSG or as individual amino acids after the degradation by GGT1/2. The transport can potentially be mediated by uniporters, symporters or antiporters.

1.6 The roGFP2 sensor for exploring glutathione homeostasis in *planta*

To date, variety of approaches have been reported for evaluating the redox status of thiols (mainly glutathione) in biological samples (Comini, 2016; Rudyk and Eaton, 2014; Xu et al., 2011). Together with the direct assessment of the glutathione redox pair (GSH/GSSG) there are also indirect methods that measure production rates of ROS via oxidation sensitive dyes (Chen et al., 2010) or protein oxidation (England et al., 2006). However, these approaches have several limitations. Glutathione detection at subcellular level is technically very challenging. In fact, it can be easily washed out, redistributed or can be affected by stress during cell disruption and sample preparation (Hafer et al., 2008; Lee and Britz-McKibbin, 2009; Zechmann, 2014). Another critical part is the unspecific reactivity of ROS dyes and the fact that protein oxidation reflects accumulated damages instead of current redox status (Bonini et al., 2006). These issues have raised many doubts on how accurate the respective measurements reflect the *in vivo* situation, and therefore challenges to find better approaches (Xu et al., 2011; Zechmann, 2014). The development of redox-active variants of green fluorescent protein (GFP) and specifically the redox-sensitive green fluorescent proteins (roGFPs) provides a new system for measuring cellular redox status (Dooley et al., 2004; Jiang et al., 2006; Meyer and Dick, 2010; Remington, 2011). These genetically encoded biosensors were developed to overcome the limitations of conventional redox measurements (Gutscher et al., 2008) and they offer the advantage that they can be targeted to different subcellular compartments and allow indirect visualisation of glutathione pool in subcellular compartments (Meyer et al., 2007).

The major differences between GFP and roGFPs are two cysteines that were introduced into the β-barrel structure at positions 147 and 204 (Hanson et al., 2004). These cysteines are either reduced or forming an intra-molecular disulfide bond in equilibrium with the local glutathione redox status. Increased levels of oxidised roGFP indicate a shift in cellular redox status, monitored by following the ratio of fluorescence emission after excitation at 405 and 488 nm (Dooley et al., 2004; Hanson et al., 2004; Meyer and Dick, 2010; Schwarzländer et al., 2008) (Figure 1.10 A-B). There are six different variants of roGFP (roGFP1- roGFP6) and most commonly used are roGFP1 and roGFP2 (Hanson et al., 2004). Both roGFP1 and roGFP2 sensors exhibit a ratiometric change in their fluorescence spectra in response to alterations in the redox environment. Whereas roGFP1 (C48S/Q80R/S147C/Q204C) derived from the wild-type chromophore with S65 displays a dominant excitation peak around 400 nm, in contrast, roGFP2 (C48S/T65S/Q80R/S147C/Q204C), derived from EGFP containing the S65T mutation shows a predominant excitation peak at 490 nm. Moreover, roGFP1 and roGFP2 have different spectral properties due to a slight difference in the type of chromophore, which lead to a different degree of protonation of the chromophore (Hanson et al., 2004).

Maintaining of a reducing redox balance is a critical physiologic function of plant cells, that can be perturbed with a variety of biotic and abiotic stress (Foyer and Noctor, 2005; Scandalios, 2005). The fusion of the human GRX1 to roGFP2 via a 31 amino acid linker resulted in a redox active sensor that responds faster and in a more comparable manner than roGFP2 on its own (Gutscher et al., 2008). Plants carrying GRX1-roGFP2 (e.g. in the cytosol, plastids and peroxisomes) or roGFP2-GRX1 (in mitochondria) show ratiometric and reversible shifts in fluorescence on exposure to oxidants and reductants like DPS and DTT and they can be used to monitor the glutathione redox status during treatments (Figure 1.10 C). Thus, roGFPs (e.g. roGFP2) expressed in plants is a new and versatile tool that can be used to investigate how plants redox status responds during biotic and abiotic stresses at cellular and subcellular level.
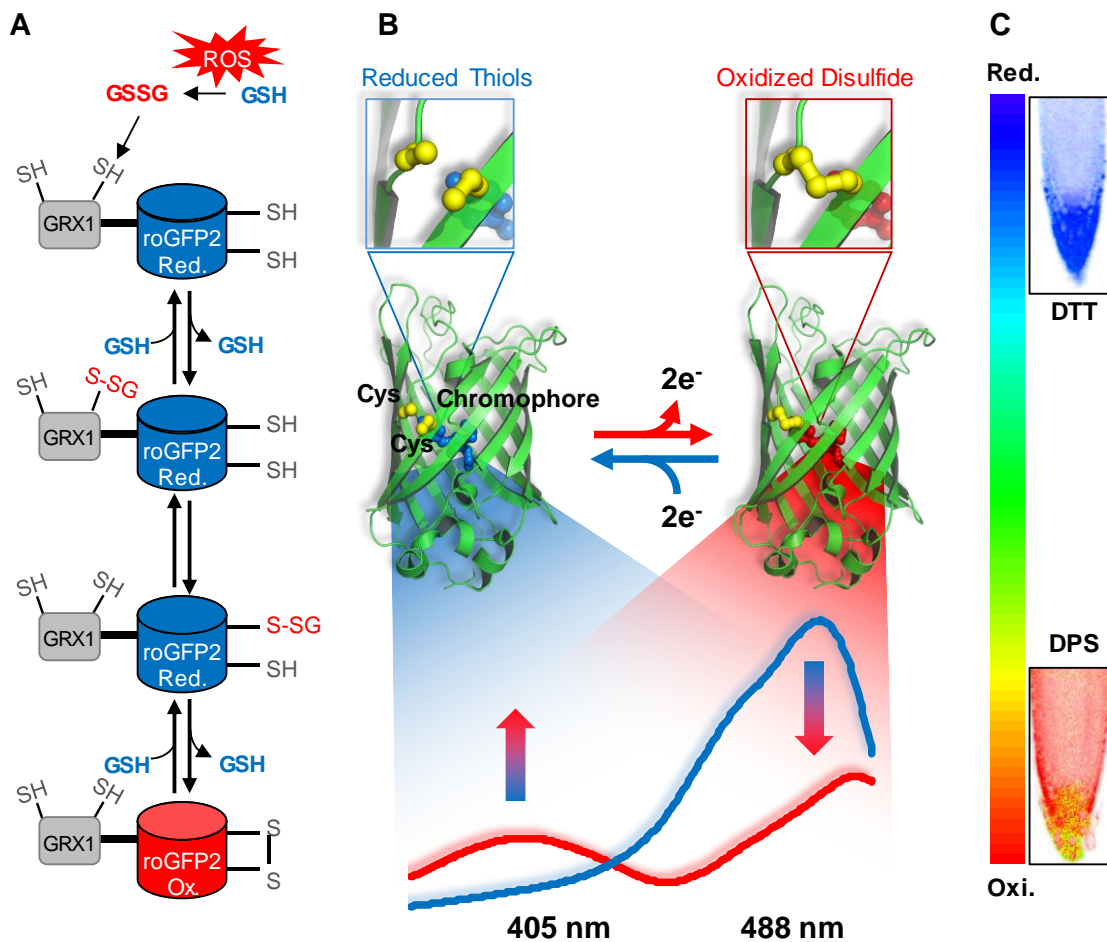
Figure 1.10: Molecular mechanism of the GRX1-roGFP2 biosensor. (A) Interactions of GRX1-roGFP2 with the glutathione system. Modified from Meyer and Dick (2010). Each three individual step of the thiol-disulfide exchange cascade is fully reversible. **(B)** Intramolecular conformational changes affect the roGFP2 spectra. Modified from Morgan and Schwarzländer (2016). **(C)** *In vivo* calibration of GRX1-roGFP2 in Arabidopsis root tips with 10 mM DTT and 5 mM DPS, for a maximum reduction and oxidation of roGFP2, respectively.

1.7 Project aims

The aim of this project was to understand glutathione homeostasis in Arabidopsis, with a specific focus on subcellular compartmentation, degradation, functionality and transport of glutathione. While the biosynthesis pathway of glutathione is well understood in respect of the participating enzymes, its compartmentation, degradation, functions and transport across the different membranes is still largely unknown. This work aims to investigate the implications of changes in glutathione levels in different subcellular compartments in mutants impaired either in glutathione synthesis or glutathione-related enzymes. Additionally, subcellular compartmentation was tested by blocking GSH1, by its inhibitor BSO in wild-type seedlings. Furthermore, to contribute to the understanding of intracellular transport capabilities, the glutathione biosynthetic pathway was mislocalised. The working hypothesis was based partly on complementation of GSH1 and GSH2 enzymes in T-DNA mutants impaired in GSH1 and GSH2 function. Furthermore, the glutathione degradation pathway via GGCT was investigated. In addition, characterisation and identification of new glutathione transporter across the plasma membrane was studied. Finally, the characterisation of CLT transporters for bidirectional transport of glutathione between plastids and cytosol was explored through compartment-specific reconstitution of the glutathione biosynthetic pathway in wild-type and mutant background by blocking the GSH1, by its inhibitor L-Buthionine-sulfoximine (BSO) (Figure 1.8).

The key aims of the project were to:

- test the role of glutathione during stress conditions (i.e. drought stress).

- evaluate the link between glutathione biosynthesis and subcellular redox homeostasis and how an altered glutathione biosynthesis could affect subcellular glutathione redox states.

- evaluate the impact of altered glutathione compartmentation by GSH1 and GSH2 mislocalisation.

- test whether the amount of glutathione or it redox potential could restrict plant growth.

- further explore the pathway of glutathione degradation via GGCT.

- investigate GSH bidirectional transport by CLTs across the plastidic membrane.

17

- explore how glutathione is transported across the plasma membrane and investigate whether glutathione is taken up as GSH, GSSG or degraded to amino acids prior to its uptake.

These aims were addressed with different approaches, including genetic analysis of Arabidopsis and yeast mutants in combination with live cell imaging approaches for *in vivo* analysis of glutathione homeostasis using confocal imaging. In addition, these data were supported by a biochemical analysis via HPLC.

2. RESULTS

2.1 Subcellular compartmentation and functionality of GSH

2.1.1 Effect of glutathione homeostasis on plant phenotype

Mutations in the *GSH1* gene have been shown to adversely affect the amount of glutathione. Independent mutations at various positions in *GSH1* have been identified (section 1.2.1). The *gsh1* allelic series mutants display between 5 and 50% of wild-type glutathione level (Ball et al., 2004; Cobbett et al., 1998; Jobe et al., 2012; Parisy et al., 2007; Shanmugam et al., 2012; Vernoux et al., 2000). The severe glutathione deficient mutant *rml1* with ~5% of glutathione pool is lethal after 2–3 weeks, which highlights the biological importance of glutathione in plants. Studying the entire series of *gsh1* mutants is a perfect system to explore the link between glutathione biosynthesis and plant development, as well as cellular and subcellular glutathione redox homeostasis.

2.1.1.1 Root phenotyping of *gsh1* allelic series mutants

To further investigate the effect of mutation on plant growth, root phenotyping of the *gsh1* allelic series mutants was undertaken. Under normal physiological conditions, some of the *gsh1* allelic series mutants showed restricted root growth (Figure 2.1).
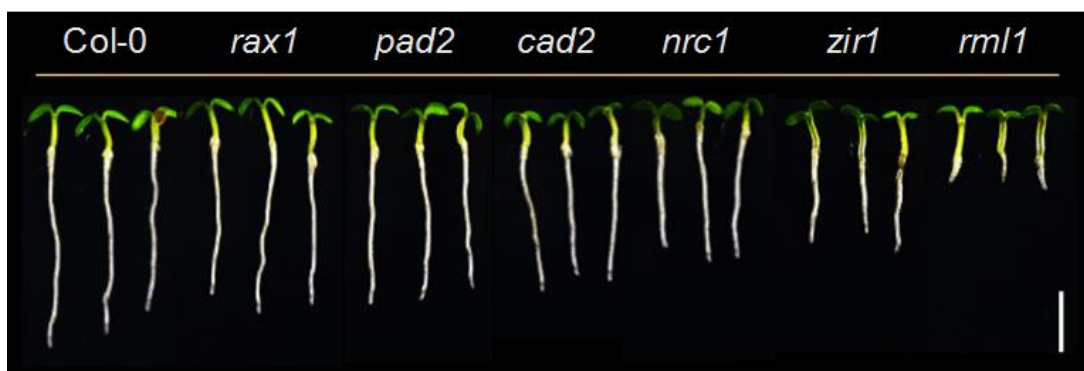
Figure 2.1: Root growth of *gsh1* allelic mutants correlates with GSH content. Phenotypes of five-day-old seedlings of *gsh1* allelic mutants on ½ MS media under long day condition. Scale bar = 5 mm

The total root length, length of lateral roots, number of lateral roots of *gsh1* allelic series mutants and wild-type were analysed. Statistical analysis of root phenotyping data revealed that the total and lateral roots length of *gsh1* allelic series mutants were significantly shorter in most of the cases (except for total root of *rax1*) compared to wild-type (Figure 2.2 A-B). The number of lateral roots was significantly lower in *nrc1* and *zir1*

(Figure 2.2 C). No significant differences were observed for root system depth, root system width and branching angle (data not shown).
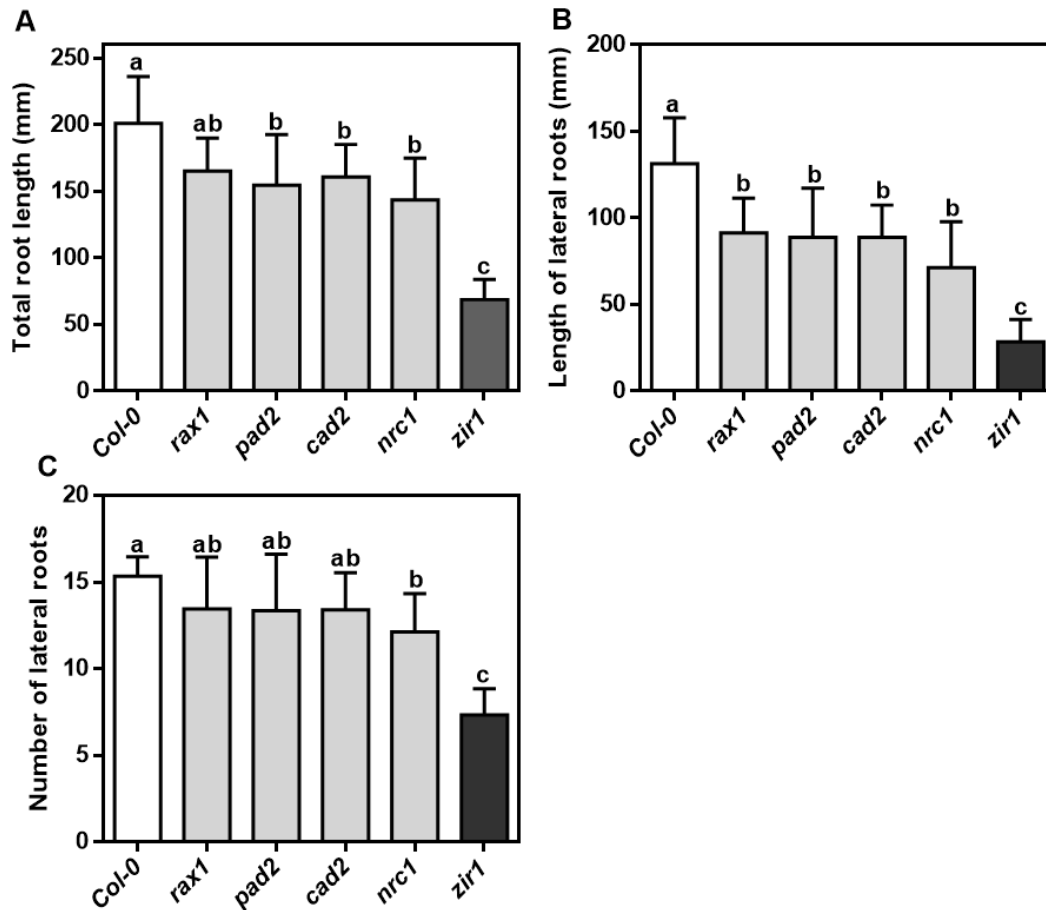
Figure 2.2: Root system architecture of *gsh1* allelic series mutants. (A) Total root length. **(B)** Length of lateral roots. **(C)** Number of lateral roots of wild-type and *gsh1* allelic series mutants after 20 days under short day conditions. Bars indicate means of biological replicates; $n \geq 10$; error bars = SD. Letters indicate significant differences (One-way ANOVA with Tukey's multiple comparisons test; *p*-value ≤ 0.05).

2.1.1.2 Shoot phenotyping of *gsh1* mutants

The results from roots phenotyping revealed that decrease in the amount of glutathione adversely affects primary and lateral root growth. To further explore the effect of *GSH1* mutation on shoot growth, shoot phenotyping of *gsh1* allelic series mutants in comparison to wild-type was investigated. Under short day condition some *gsh1* allelic series mutant showed a dwarf phenotype (Figure 2.3).

Figure 2.3: Shoot growth of *gsh1* allelic mutants correlates with GSH content. Shoot phenotype of four-week-old *gsh1* allelic series mutants and wild-type under short day condition.

2.1.1.2.1 GSH1 mutants show no obvious phenotypes under drought stress

The results of the different shoot phenotyping parameters monitored during, an automated high-throughput drought stress experiment are summarised in Table 2.1. While under non-stress condition shoot fresh weight of *rax1*, *pad2*, *nrc1* and *zir1* was significantly lower than wild-type, under drought condition, the shoot fresh weight was lower only in *zir1* mutants. Similarly, in control condition, all *gsh1* mutants had lower shoot dry weight compared to wild-type. In drought condition the shoot dry weight resembles the pattern observed for the fresh weight with only *zir1* being lighter than the other mutants and the wild-type. In addition, the differences in shoot water content (SWC%) were not significant. Furthermore, potential quantum yield of PII (Fv/Fm) measurement confirmed that there is no difference between mutants and wild-type under control and drought condition, with the exception of *zir1* which was significantly different under both conditions in comparison to wild-type. Photosynthetic leaf area (PLA) and area by circumference under control condition were significantly less than wild-type in all *gsh1* mutants except *cad2*. However, under drought condition only *rax1* and *zir1* were significantly lower than wild-type. Moreover, *nrc1* and *zir1* were specifically different for shoot stockiness under both control and drought conditions. In case of shoot compactness only *zir1* was significantly lower than wild-type under control condition. However, there were no difference under drought stress. Rosette diameter was only different in case of *zir1* under both control and drought conditions. Furthermore, drought stress did not affect surface coverage and eccentricity in *gsh1* mutants. Further details of individual parameters are given in Appendix I.

Table 2.1: Comparison of all parameters of shoot phenotyping. Values are mean from ≥ 10 biological replicates. Different letters indicate significant differences of *gsh1* allelic series mutant compared to wild-type (One-way ANOVA with Tukey's multiple comparisons test; *p*-value ≤0.05).

Genotypes		Col-0		rax1		pad2		cad2		nrc1		zir1	
Parameters	Conditions	Mean	SD	Mean	SD	Mean	SD	Mean	SD	Mean	SD	Mean	SD
Shoot fresh weight	Control	0.83^a	0.14	0.55^b	0.10	0.56^b	0.15	0.72^b	0.12	0.5^b	0.14	0.16^c	0.04
	Drought	0.42^a	0.09	0.36^a	0.10	0.39^a	0.09	0.42^a	0.07	0.34^a	0.08	0.1^b	0.03
Shoot dry weight	Control	0.073^a	0.013	0.046^b	0.008	0.052^b	0.013	0.052^b	0.013	0.046^b	0.008	0.014^c	0.004
	Drought	0.035^a	0.010	0.026^b	0.009	0.032^{ab}	0.008	0.032^{ab}	0.008	0.026^b	0.009	0.009^c	0.003
SWC(%)	Control	91.21^{ac}	0.90	91.6^a	0.91	90.65^c	0.91	92.77^b	0.89	90.8^{ac}	0.94	91.21^{ac}	0.91
	Drought	91.63^a	0.89	92.72^b	0.91	91.78^a	0.91	92.41^{ab}	0.89	92.19^{ab}	0.89	91.09^{ac}	0.90
Fv/Fm	Control	0.725^a	0.003	0.726^a	0.005	0.723^a	0.006	0.728^a	0.005	0.729^a	0.004	0.718^b	0.005
	Drought	0.730^a	0.006	0.726^a	0.007	0.725^a	0.005	0.735^a	0.006	0.731^a	0.004	0.715^b	0.003
Compactness	Control	0.65^a	0.06	0.59^a	0.11	0.66^a	0.08	0.64^a	0.07	0.58^a	0.14	0.51^b	0.24
	Drought	0.61^a	0.06	0.59^a	0.09	0.65^a	0.11	0.64^a	0.10	0.59^a	0.12	0.66^a	0.24
Stockiness	Control	0.04^a	0.01	0.05^a	0.01	0.04^a	0.00	0.04^a	0.01	0.05^a	0.01	0.08^b	0.02
	Drought	0.04^a	0.00	0.05^a	0.01	0.05^a	0.01	0.05^a	0.01	0.05^a	0.01	0.10^b	0.02
Surface coverage	Control	0.62^a	0.04	0.55^a	0.07	0.60^a	0.07	0.62^a	0.06	0.55^a	0.09	0.52^a	0.16
	Drought	0.55^a	0.06	0.53^a	0.10	0.60^a	0.08	0.56^a	0.09	0.55^a	0.11	0.63^a	0.15
Diameter	Control	8.77^a	0.92	7.38^a	1.71	7.58^a	0.96	8.79^a	0.91	7.78^a	1.29	5.49^b	2.15
	Drought	7.15^a	1.03	6.2^a	1.61	5.97^a	1.05	7.03^a	1.28	6.54^a	1.42	3.38^b	1.47
Eccentricity	Control	0.65^a	0.14	0.67^a	0.17	0.55^a	0.18	0.71^a	0.21	0.71^a	0.21	0.73^a	0.26
	Drought	0.57^a	0.18	0.59^a	0.22	0.54^a	0.2	0.59^a	0.21	0.58^a	0.23	0.5^a	0.25
PLA	Control	28.54^a	5.41	17.8^b	5.72	21.54^b	5.66	27.61^a	5.63	21.27^b	6.31	7.75^c	3.5
	Drought	16.44^a	2.97	11.51^c	3.78	13.34^{bc}	3.11	15.59^{ab}	1.79	13.33^{bc}	3.01	3.88^d	1.56
Circumference	Control	17.71^a	1.92	14.13^a	2.25	15.72^a	1.97	17.1^a	1.95	15.76^a	2.54	11.73^b	1.95
	Drought	13.64^a	1.32	11.84^a	1.4	13.32^a	1.51	13.87^a	1.11	13.54^a	1.26	10^b	1.43

2.1.2 Compartmentation of glutathione in GSH1 mutants

To further explore the effect of these mutations on the biosynthesis and distribution of glutathione on the cellular and subcellular level in the allelic series mutants, three different approaches were used: HPLC (High Performance Liquid Chromatography) analysis of low molecular weight thiols, *in situ* labelling of GSH with the thiol-specific dye monochlorobimane (MCB) (Meyer et al., 2001) and roGFP2-based redox measurement (Meyer et al., 2007).

2.1.3 Total glutathione pool in *gsh1* mutants

2.1.3.1 HPLC analysis reveals reduced glutathione levels in the *gsh1* mutants

To determine the total amount of glutathione in *gsh1* mutants in comparison with wild-type, five-day-old seedlings were used. The glutathione pool of wild-type seedlings was 273.40 ± 38.84 nmol g^{-1} FW^{-1}. In contrast, the *gsh1* allelic series mutants displayed a significant decrease in their GSH pool; *rax1* 142 ± 46.36, *pad2* 73.17 ± 22.6, *cad2* 66.0 ± 44.39, *nrc1* 60.84 ± 22.75, *zir1* 45.01 ± 19.53 and *rml1* 9.30 ± 5.88 nmol g^{-1} FW^{-1}, respectively (Figure 2.4 A). In contrast, cysteine levels determined by HPLC were significantly higher in the *gsh1* allelic series mutants than in the wild-type (Figure 2.4 B). These results are in line with levels previously described (Hernández et al., 2015).
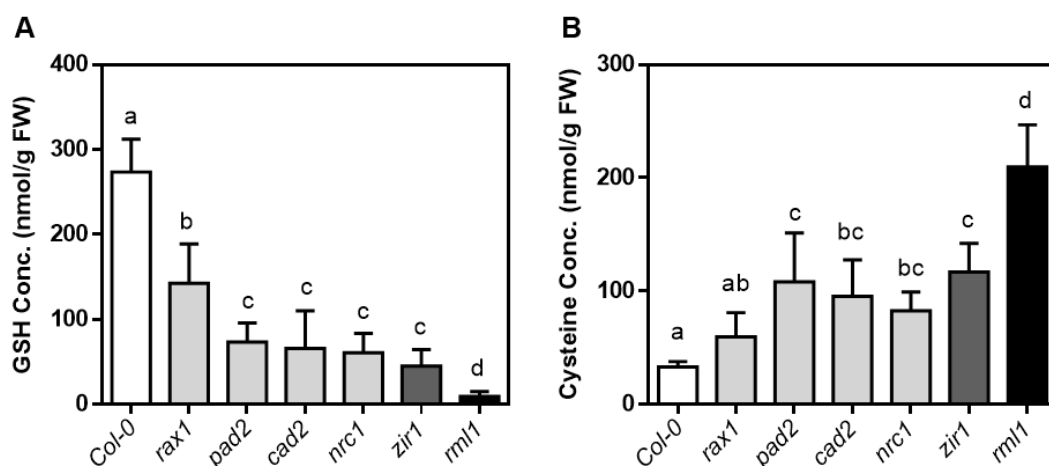
Figure 2.4: Measurement of the cellular glutathione pool by HPLC. (A) Total glutathione pool in five-day-old seedlings of wild-type and *gsh1* allelic series mutants **(B)** Total cysteine pool in *gsh1* allelic series mutants and wild-type. Bars indicate mean of biological replicates; $n \geq 10$, error bars = SD. Letters in each graph indicate significant differences (One-way ANOVA with Tukey's multiple comparisons test; *p*-value ≤ 0.05).

2.1.3.2 MCB visualises the decrease in glutathione pool of *gsh1* mutants *in vivo*

To analyse the decrease in glutathione pool of the *gsh1* mutants *in vivo*, GSH was visualised by MCB staining. MCB specifically labels glutathione *in vivo* and can thus be used for the estimation of total glutathione concentrations in plants (Meyer et al., 2001). MCB labelling of GSH was conducted on root tips of five-day-old seedlings grown vertically on agar plates under long day conditions. MCB labelling was less intense throughout the *gsh1* allelic series mutants than in the wild-type, while *zir1* and *rml1* showed the strongest reduction in GSH levels. Parallel propidium iodide (PI) staining of cell walls confirmed cell integrity (Figure 2.5 B). Together these data were in line with the HPLC measurements (Figure 2.4 A).
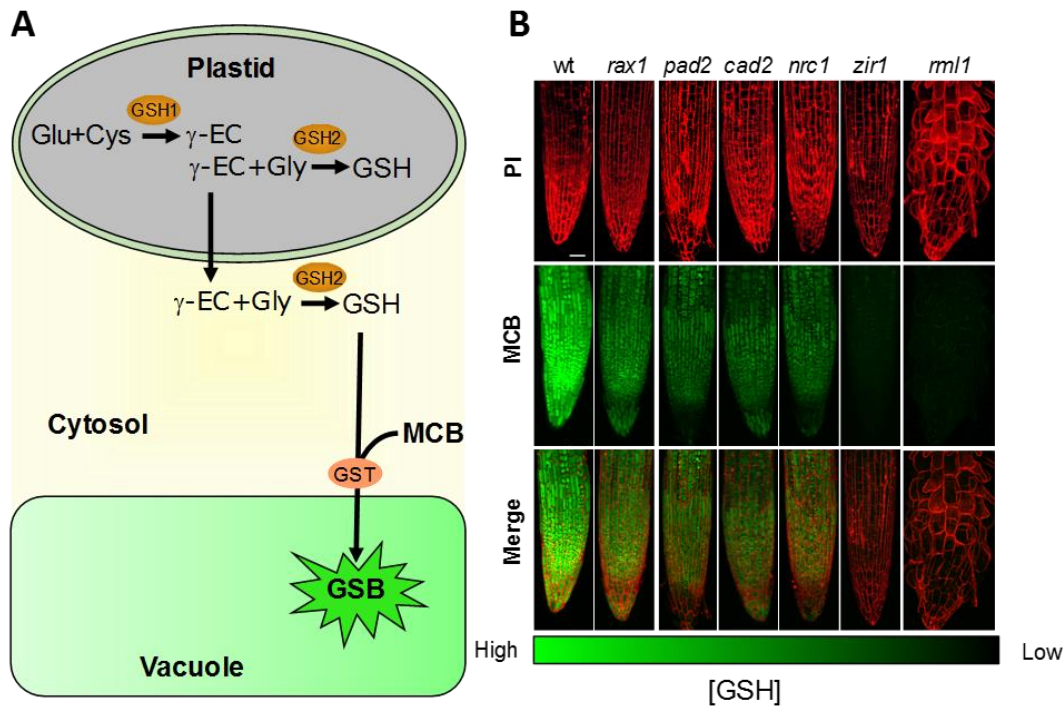
Figure 2.5: Visualisation of total glutathione in root tips of wild-type and *gsh1* allelic series mutants. (A) Mechanism of MCB labelling showing the conjugation of GSH to MCB which converts the non-fluorescent MCB into a highly fluorescent GSH-MCB (GSB) conjugated by GST (Glutathione S-transferase) that is subsequently sequestered in the vacuole via ABC transporters. **(B)** Maximum intensity projection of confocal z-stacks: Propidium iodide (PI) staining verified cellular integrity (upper panel), Monochlorobimane (MCB) labelling assesses the cellular glutathione pool (middle panel) and merge of PI and MCB (lower panel). Scale bar = 20 µm.

2.1.4 Glutathione redox homeostasis in *gsh1* mutants

To further explore the effect of GSH1 mutation at the subcellular level in *gsh1* mutants, roGFP2, a genetically encoded and well characterised sensor for redox measurement in Arabidopsis, was used (Meyer et al., 2007). Wild-type and *gsh1* mutant plants were transformed with roGFP2 fused to human glutaredoxin 1 (GRX1). The fusion of GRX1 to roGFP2 facilitates rapid and specific equilibration of the sensor protein with the glutathione pool (Gutscher et al., 2008). The GRX1 fused roGFP2 construct was targeted to the cytosol, plastids and mitochondria (Figure 2.6). For plastidic and mitochondrial targeting roGFP2 was fused behind the transketolase transit peptide (TKTP) and serine hydroxymethyltransferase (SHMT) signal peptides respectively. The sensor localisation was confirmed via CLSM according to Schwarzländer et al (2008). Co-localisation of roGFP2 targeted to plastid was confirmed with reference to chlorophyll autofluorescence (Figure 2.6 B). Mitochondrially localised roGFP2 was confirmed by MitoTracker labelling followed by co-localisation with roGFP2 signal (Figure 2.6 C).
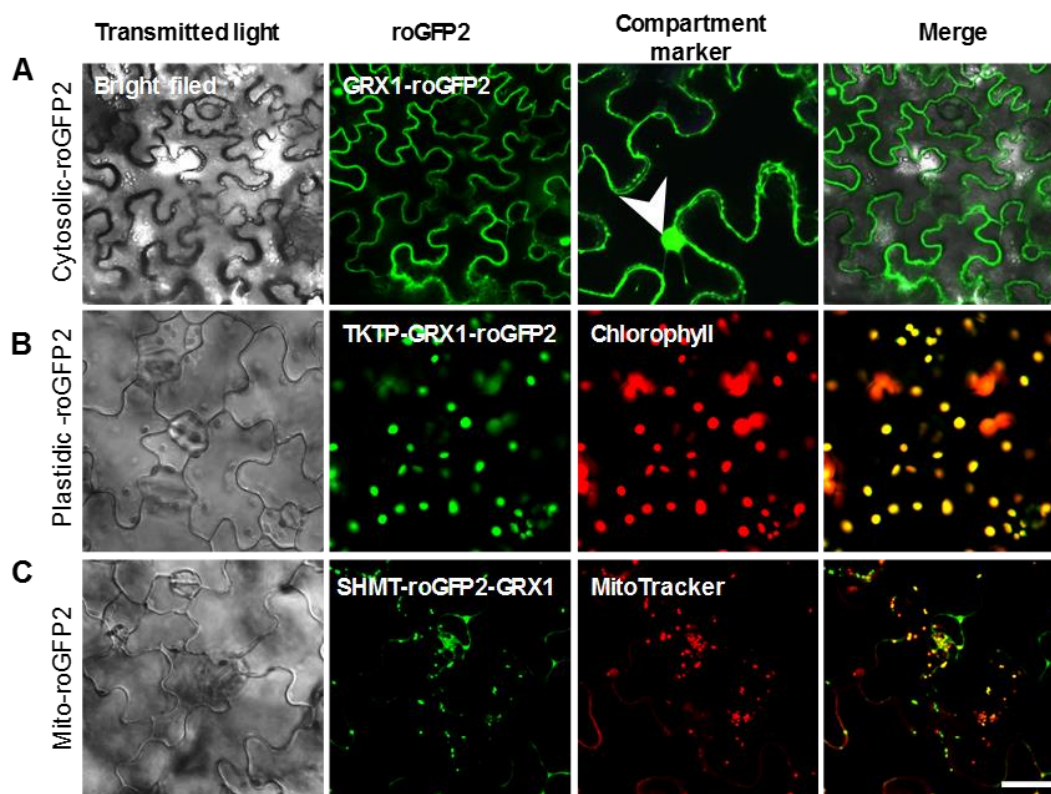
Figure 2.6: Subcellular localisation of different roGFP2 constructs in leaf cells of five-day-old Arabidopsis seedlings. (A) Cytosolic GRX1-roGFP2 at 488 nm (Green) arrow head points to clear GFP signal in the nucleus. (B) Plastidic TKTP-GRX1-roGFP2 at 488 nm (green) with chlorophyll autofluorescence at 633 nm (red). (C) SHMT-roGFP2-GRX1 in mitochondria at 488 nm (green) along with the mitochondrial marker MitoTracker at 543 nm (red). Scale bar = 20 µm.

2.1.4.1 Changes in the subcellular glutathione redox environment can be visualised with roGFP2

2.1.4.1.1 Mutation in *GSH1* gene affects the cytosolic redox environment

In order to determine the glutathione redox status in the cytosol, redox measurement in the cytosol of root tip cells was performed in the *gsh1* allelic series mutants via CLSM imaging. To assess the full dynamic range of roGFP2 *in vivo*, wild-type seedlings were incubated in 10 mM DTT to estimate the maximum reduction of roGFP2 and in 5 mM DPS to estimate the maximum oxidation, respectively. Followed by calibration of roGFP2, redox measurement was done in the *gsh1* allelic series mutants. Compared to wild-type, the redox state in the cytosol was oxidised in all *gsh1* allelic series mutants. Pseudo-colour coded ratiometric images revealed that roGFP2 targeted to the cytosol of *rax1*, *pad2*, *cad2* and *nrc1* was partially oxidised, while the oxidation of roGFP2 was significantly higher than the wild-type. RoGFP2 in the *zir1* mutants was clearly more oxidised than *rax1*, *pad2*, *cad2* and *nrc1* as illustrated by the lower ratio. In the severely GSH-deficient mutant *rml1*, roGFP2 was completely oxidised (Figure 2.7). These results

reveal that with a decrease of glutathione concentration the degree of roGFP2 oxidation increased.

Figure 2.7: Quantitative analysis of the glutathione redox status in roots of *gsh1* mutants and wild-type using GRX1-roGFP2 in the cytosol. (A) Pseudo-colour coded ratiometric images of root tips of wild-type treated with 10 mM DTT and 5 mM DPS for roGFP2 calibration. **(B)** Pseudo-colour coded ratiometric images of root tips (upper panel). Bars indicate means of biological replicates; $n \geq 10$, error bars = SD. Blue line indicates full reduction of roGFP2 upon DTT treatment while the red line indicates the complete oxidation of roGFP2 upon DPS treatment (lower panel). Letters indicate significantly different values (One-way ANOVA with Tukey's multiple comparisons test; p-value ≤ 0.05). Scale bar = 20 µm.

2.1.4.1.2 Mutation in *GSH1* gene affects plastidic redox environment only in roots of *gsh1* mutants

Since mutation in the *GSH1* gene affected cytosolic redox homeostasis of *gsh1* mutants, the effect of mutated GSH1 was further investigated on the redox homeostasis in plastids. Thus, redox imaging was performed on *gsh1* mutants expressing plastid targeted roGFP2. Pseudo-colour coded ratiometric images of root tips revealed that roGFP2 targeted to plastids of *rax1*, *pad2*, *cad2* and *nrc1* was partially oxidised. The roGFP2 targeted to plastids in *zir1* mutants was more oxidised than *rax1*, *pad2*, *cad2* and *nrc1*, while *rml1* plastidic roGFP2 was completely oxidised (Figure 2.8 A). These results indicate that

mutations in GSH1 affect the redox homeostasis in root plastids similarly to the observations in the cytosol (Figure 2.7). However, the redox state of roGFP2 targeted to leaf plastids of *rax1*, *pad2*, *cad2* and *nrc1* were similar to the redox state of roGFP2 in leaf plastids of wild-type. Only in *zir1*, roGFP2 targeted to leaf plastids was partially oxidised and in *rml1* plastids roGFP2 was completely oxidised (Figure 2.8 B).

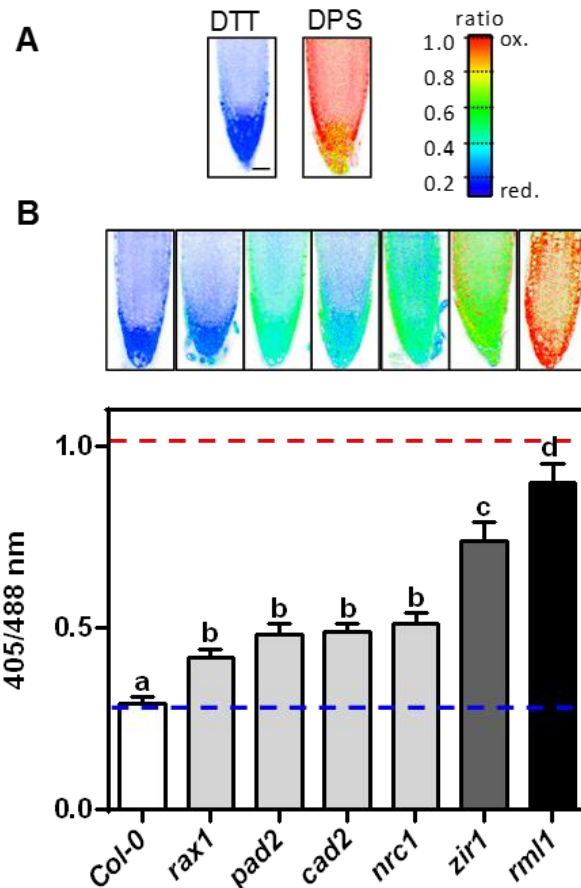**Figure 2.8: Quantitative analysis of the glutathione redox status in roots and leaves of *gsh1* mutants and wild-type using GRX1-roGFP2 targeted to the plastids. (A)** Redox imaging in root tips. **(B)** Redox imaging in leaf cells. Bars indicate means of biological replicates; n ≥ 10; error bars = SD. Letters indicate significant differences (One-way ANOVA with Tukey's multiple comparisons test; *p*-value ≤0.05). Scale bar = 20 µm

2.1.4.1.3 Mitochondria retained glutathione in *gsh1* mutants

To further investigate the effect of GSH1 mutation on mitochondrial glutathione redox status, redox imaging was pursued in *gsh1* mutants expressing roGFP2 in mitochondria. Pseudo-colour coded ratiometric images revealed that in roots, roGFP2 targeted to mitochondria of *rax1*, *pad2*, *cad2*, *nrc1* and *zir1* was less oxidised than the cytosolic and plastidic targeted roGFP2. Furthermore, in *rml1* mitochondrial targeted roGFP2 was highly oxidised compared to the other *gsh1* mutants (Figure 2.9). These data indicate that mutations in *GSH1* have a stronger effect on cytosolic and plastidial glutathione homeostasis than on mitochondrial glutathione homeostasis.
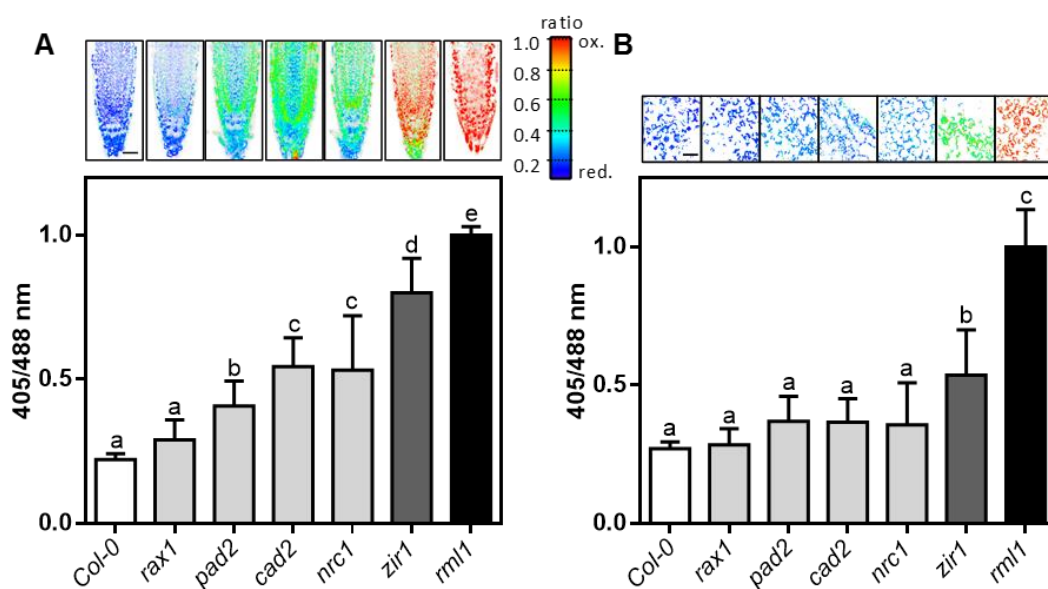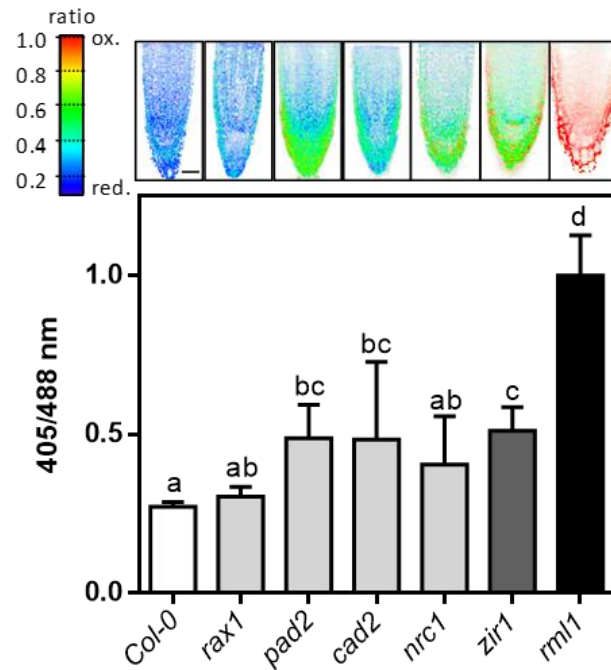
Figure 2.9: Quantitative analysis of the glutathione redox status in roots of *gsh1* mutants and wild-type using roGFP2-GRX1 targeted to the mitochondria. Redox imaging in root tips (upper panel). Bars indicate means of biological replicates; n ≥ 8; error bars = SD. Letters indicate significant differences (One-way ANOVA with Tukey's multiple comparisons test; *p*-value ≤0.05). Scale bar = 20 µm.

2.1.5 Mislocalisation of GSH1 and GSH2

Both proteins responsible for glutathione biosynthesis in Arabidopsis, GSH1 and GSH2, are encoded by single copy genes (Wachter et al., 2005). To study the importance of both GSH1 and GSH2 in plants, T-DNA insertion mutant lines for *AtGSH1* (At4g23100) and *AtGSH2* (At5g27380) were used. An Arabidopsis line containing a T-DNA insertion in the second intron of *GSH1* was designated as *gsh1-1* (Cairns et al., 2006), whereas a second T-DNA line containing a T-DNA insertion in the 7th exon of *GSH2* was designated as *gsh2-1* (Sessions et al., 2002) (Figure 2.10). To study the transport of glutathione and γ-EC across the intracellular membranes, GSH1 and GSH2 were re-localised to different subcellular compartments. The two T-DNA lines, *gsh1-1* and *gsh2-1,* were complemented with GSH1 and GSH2, targeted to different subcellular compartments.
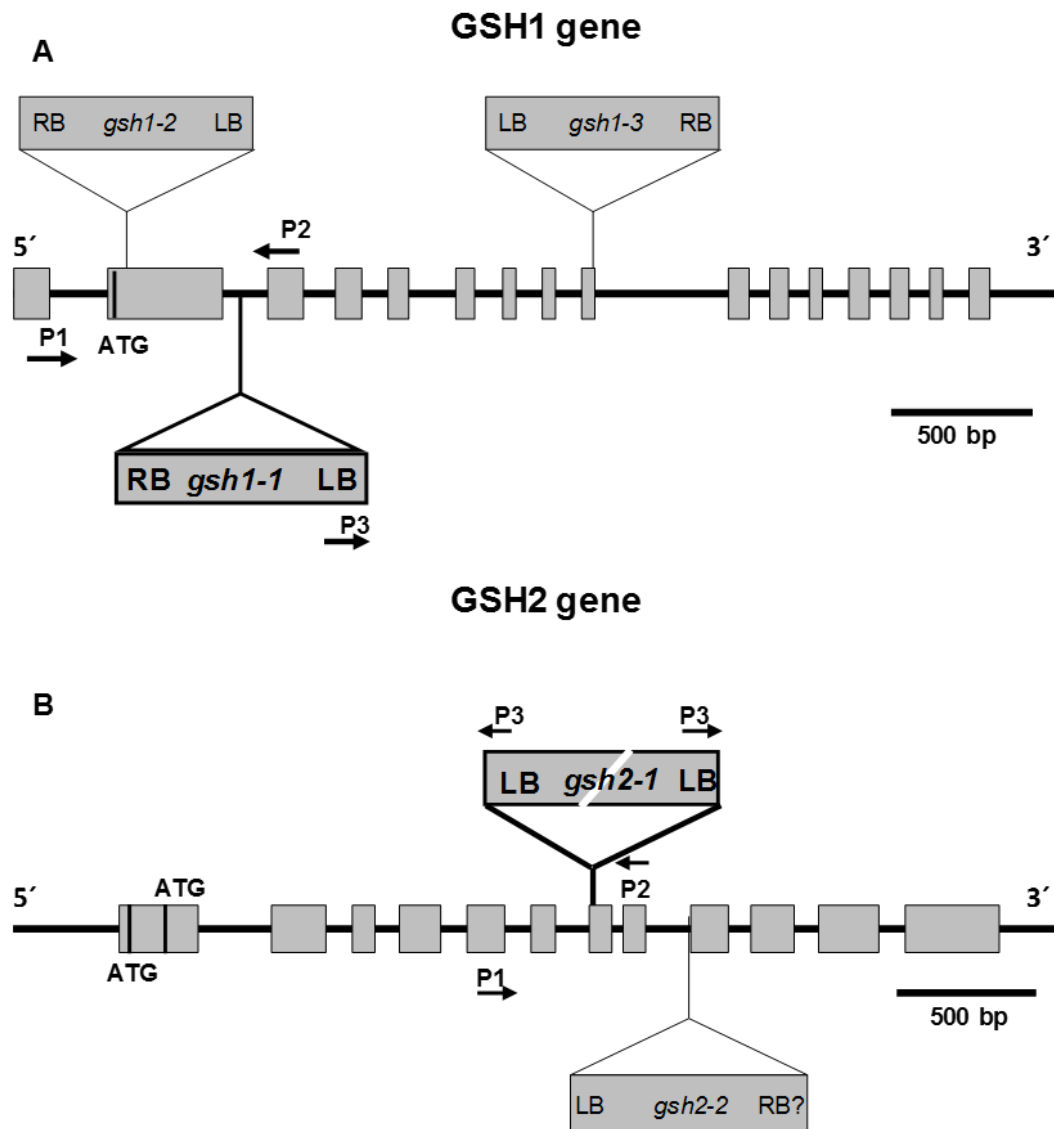
Figure 2.10: T-DNA insertion alleles of Arabidopsis *GSH1* and *GSH2* genes. (A) Gene model of *GSH1* with the T-DNA insertion for *gsh1-1*. **(B)** Gene model of *GSH2* with the T-DNA insertion for *gsh2-1*. Exons are represented as boxes and introns as lines. Vertical lines in the exons indicate the start codons ATG. Positions of primers used for genotyping of *gsh1-1* and *gsh2-1* lines are indicated by arrows. P1 (forward primer) and P2 (reverse primer) are genomic, while P3 (left border primer) are T-DNA primers.

2.1.5.1 Selection of heterozygous *gsh1-1 and gsh2-1* mutants

For complementing of GSH1 and GSH2, a selection of heterozygous *gsh1-1* null mutants was performed by genotyping PCR using gene specific genomic and T-DNA primers (Figure 2.11 A). Loss of the GSH1 gene leads to an embryonic lethal phenotype (Cairns et al., 2006) (Figure 2.11 B-C). Similarly, GSH2 null mutants are seedling-lethal (Pasternak et al., 2008b).
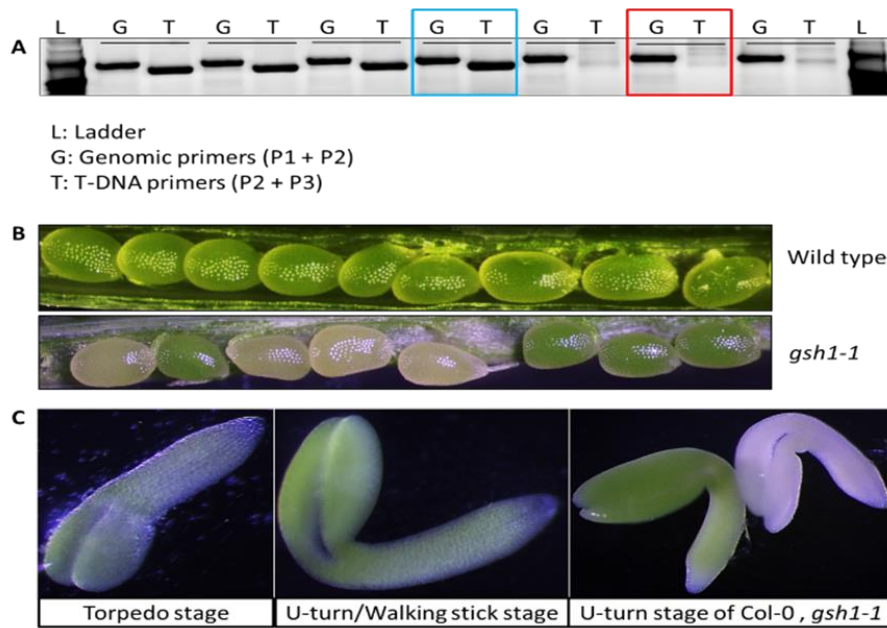
Figure 2.11: Genotyping PCR and open silique and embryo of *gsh1-1* knockouts. (A) The blue box on PCR gel indicates a heterozygous *gsh1-1* null mutants and the red box indicates a wild-type. **(B)** Opened siliques of wild-type and a heterozygous *gsh1-1* null mutant. (C) Different stages of embryo development of wild-type and *gsh1-1* heterozygous plants. Homozygous *gsh1-1* embryos (white) from torpedo stage onwards and can be distinguished from wild-type embryos (green).

The selection of *gsh2-1⁺ᐟ⁻* mutants was carried using BASTA for the screening. Heterozygous *gsh2-1* carries the bar-gene, conferring BASTA® resistance. Wild-type plants lacking the bar-gene could not survive (Figure 2.12).
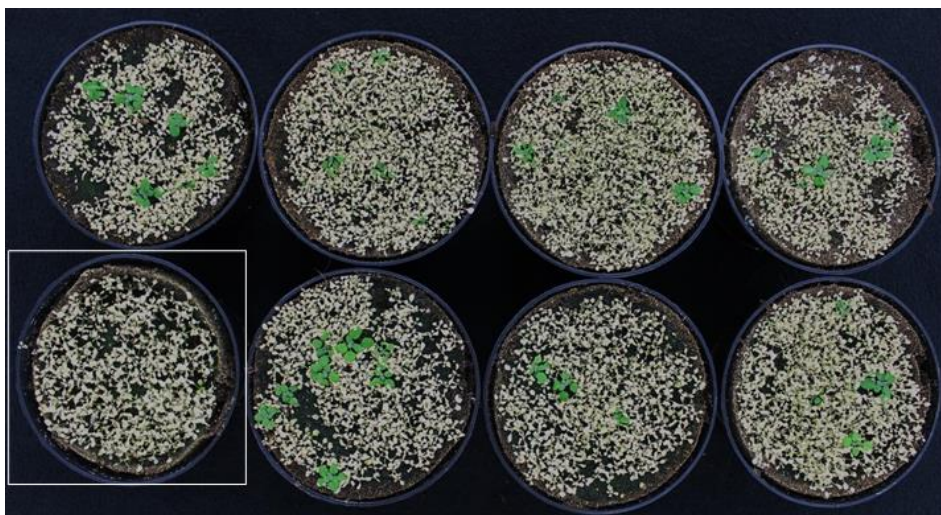
Figure 2.12: BASTA screening of *gsh2-1* mutants. The *ghs2-1⁺ᐟ⁻* mutants survive after BASTA screening due to resistance gene, while the wild-type (shown in white box) died due to the lack of BASTA® resistance.

2.1.5.2 Complementation of heterozygous *gsh1-1 and gsh2-1* mutants

Heterozygous *gsh1-1* and *gsh2-1* were complemented with nine different constructs (Figure 2.13).
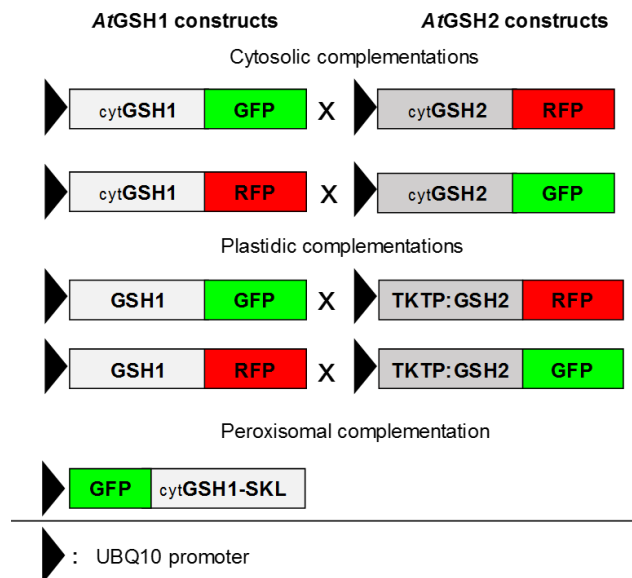
Figure 2.13: *At*GSH1 and *At*GSH2 constructs tagged with GFP and RFP. Cytosolic and plastidic targeted GSH1 and GSH2 were fused with C-terminal GFP and RFP (Cloning of cytosolic and plastidic constructs were performed in collaboration with Dr. Daniela Bausewein). Peroxisomal targeted GSH1 was fused with N-terminal GFP fusion. Expression of all construct is under control of the ubiquitin 10 promoter (pUBQ10).

Constructs for the cytosolic and plastidic complementation of GSH1 and GSH2 had a C-terminal fusion of GFP and RFP, while the construct for the peroxisomal complementation of GSH1 had an N-terminal GFP fusion. Furthermore, for both the cytosolic and peroxisomal complementation, truncated GSH1 and GSH2 constructs were used. In addition, for peroxisomal complementation of GSH1 construct, the tripeptide SKL, a targeting signal to peroxisomes (Reumann et al., 2007), was fused to the C-terminal.

2.1.5.3 Re-localisation of glutathione biosynthetic enzymes to the cytosol, plastids and peroxisomes

Complemented *gsh1-1* knockouts plants were identified by BASTA® screening, followed by genotyping PCR. The localisation and functionality of the fused proteins were confirmed initially by expressing constructs transiently in tobacco leaves and subsequently by stable transformation of Arabidopsis. Localisation of the constructs was confirmed via CLSM imaging. The plastidic localisation of the constructs were confirmed

with reference to chlorophyll autofluorescence (Figure 2.14 B, D and E). All constructs were localised to their expected compartments, except cytosolic cytoGSH1-RFP, which showed weak and patchy signal (Figure 2.14 C).
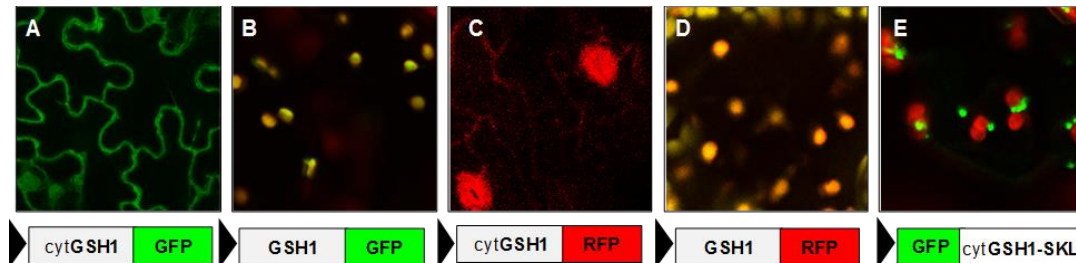
Figure 2.14: Localisation of fusion proteins for complemented *gsh1-1* homozygous Arabidopsis plant leaves. (A) Cytosolic GSH1-GFP. **(B)** Plastidic GSH1-GFP (green) merged with chlorophyll autofluorescence (red) results in yellow colour. **(C)** Cytosolic GSH1-RFP. **(D)** Plastidic GSH1-RFP (red) co-localised with chlorophyll autofluorescence (green). (E) Peroxisomal GFP-GSH1 (green) merged with chlorophyll autofluorescence (red).

All GSH1 complemented plants were viable, indicating that the C- and N-terminal fusion of GFP and RFP with GSH1 did not completely abolish GSH1 activity. However, cytosolic complemented GSH1-GFP and GSH1-RFP plants showed a small and compact rosette compared to wild-type (Figure 2.15 B and D).
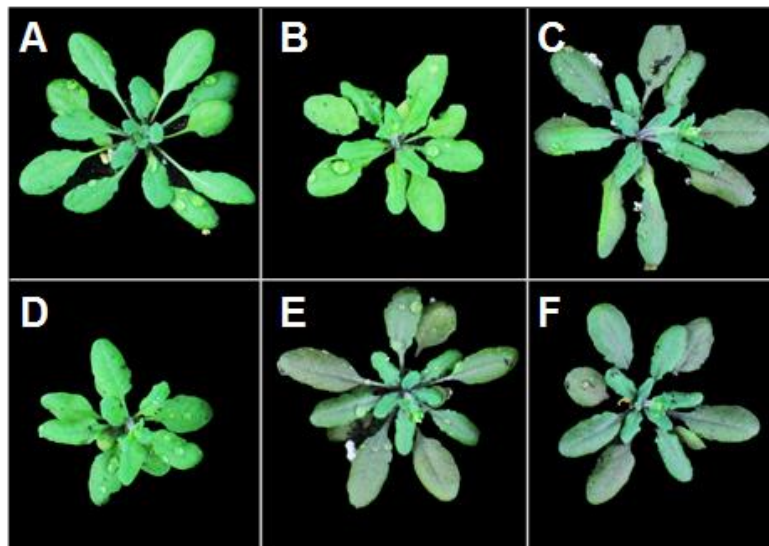
Figure 2.15: Phenotype of GSH1 complemented plants. (A) Wild-type control. (B-F) Plants complemented with cytosolic GSH1-GFP **(B)**, plastidic TKTP-GSH1-GFP **(C)**, cytosolic GSH1-RFP **(D)**, plastidic TKTP-GSH1-RFP **(E)**, and peroxisomal GFP-GSH1-SKL **(F)**.

2.1.5.4 Double mutants with mislocalised GSH1 and GSH2 are viable

The single mutants of mislocalised GSH2 (Pasternak et al., 2008b) and GSH1 without tagged fluorescent protein were viable (Figure 2.16). The double mutants of mislocalised GSH1 and GSH2 mutants were produced by crossing mislocalised GSH1 and GSH2 single mutants.
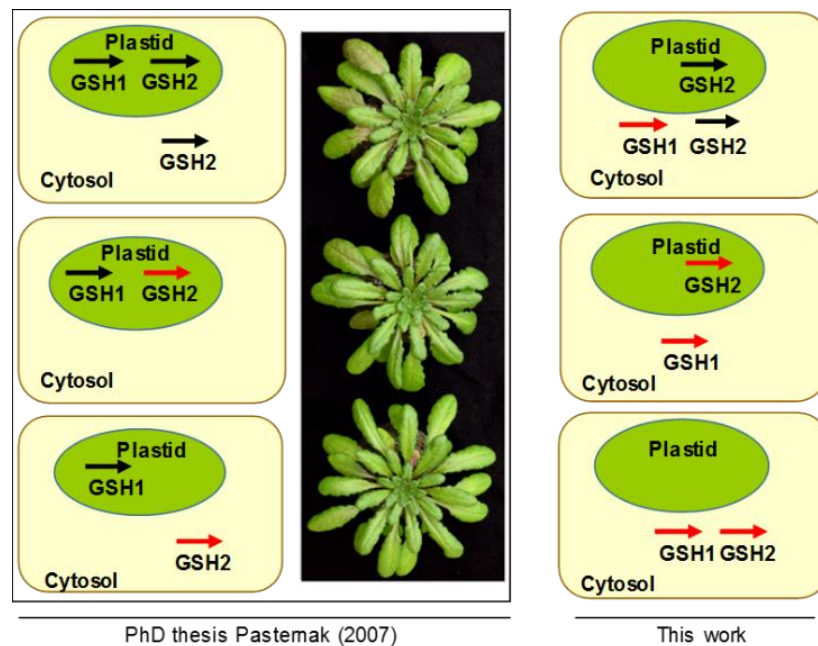
Figure 2.16: Model for mislocalisation of GSH1 and GSH2. Complemented GSH1 and GSH2 indicated with red arrows, and endogenous GSH1 and GSH2 indicated with black arrow.

Double homozygous plants of complemented GSH1 and GSH2 were selected in F3 generation via genotyping PCR for both *gsh1* and *gsh2* knockout mutant (Figure 2.17).
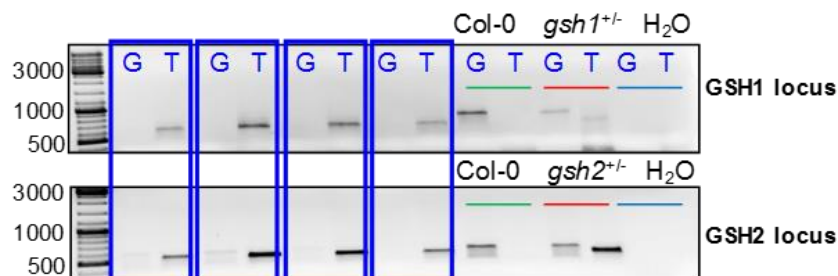
Figure 2.17: Genotyping PCR of *gsh1gsh2* double mutants in F3. Agarose gel of genotyping PCR. "G" indicates wild-type locus, T indicates the respective T-DNA loci. The blue boxes indicate viable GSH1, GSH2 complemented plants homozygous for both *gsh1* (upper panel) and *gsh2* (lower panel). Green lines indicate wild-type controls, red lines indicate *gsh1* and *gsh2* heterozygous control and blue lines indicate water control.

The double homozygous plants of *gsh1gsh2* with cytoGSH1pGSH2 and cytoGSH1cytoGSH2 complementation were viable and displayed compact rosettes in the early stage of development and showed anthocyanin accumulation; however, in later developmental stage plants were similar to wild-type (Figure 2.18).

Figure 2.18: Phenotypes of double homozygous of complemented GSH1 and GSH2 plants. Four-week-old plants (left panel) and eight-week-old plants (right panel) of wild-type control **(A)**, double homozygous plants of *gsh1gsh2* with cytosolic GSH1 and GSH2 complementation **(B)**, double homozygous of plants of *gsh1gsh2* with cytosolic GSH1 and plastidic GSH2 complementation **(C)**.

Furthermore, MCB labelling was pursued to assess the amount of glutathione in the complemented *gsh1gsh2* double mutants in comparison to wild-type and the partially glutathione deficient mutant *cad2*. Compared to the wild-type the complemented double mutants showed a low MCB labelling intensity which was similar to the labelling intensity in *cad2* (Figure 2.19 A).

2.1.5.5 Cadmium sensitivity of mislocalised GSH1GSH2 double mutants

Cadmium (Cd) is one of the most toxic elements and can be accumulated in plants easily. Further, the glutathione dependent phytochelatin synthesis pathway is one of the most important systems contributing to Cd tolerance (Chen et al., 2016). The GSH1GSH2 complemented mutants showed lower glutathione levels, were further tested for their susceptibility to Cd toxicity. The GSH1GSH2 double mutants, wild-type, and *cad2* plants were grown for two weeks on ½ MS media supplemented with different concentrations of $CdCl_2$. Upon Cd stress the GSH1GSH2 double mutants has significantly shorter root than the wild-type and the *cad2* mutant.The results showed that the GSH1GSH2

complemented mutants were more sensitive to Cd toxicity, compared to wild-type and *cad2* (Figure 2.19 B).
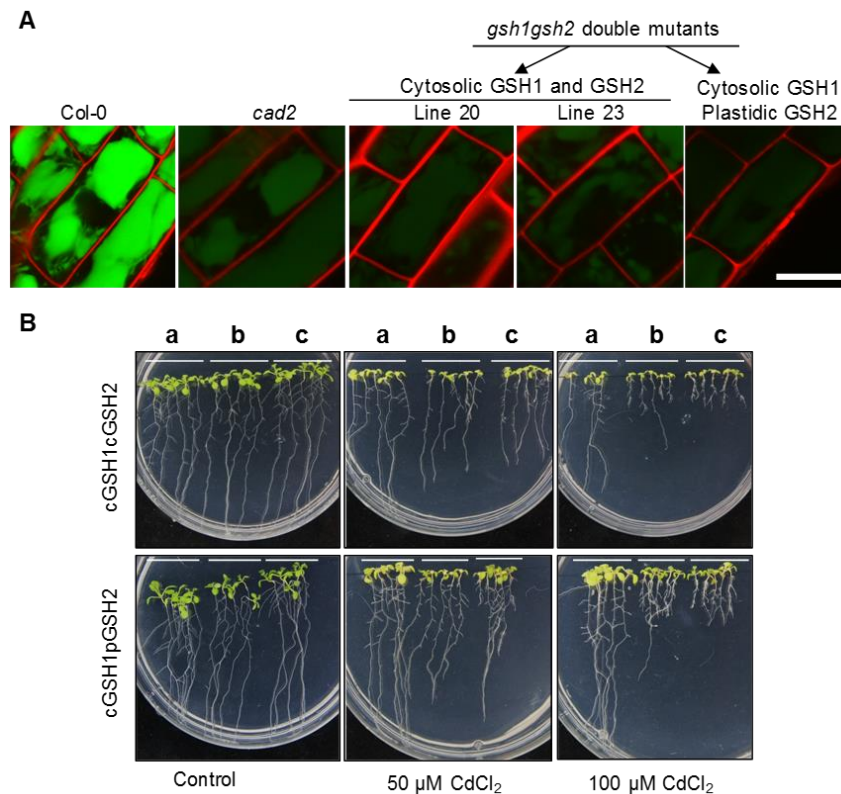
Figure 2.19: Visualisation of total glutathione and Cd toxicity of mislocalised GSH1GSH2 double mutants. (A) Representative images of root tips of five-day-old seedlings of wild-type, *cad2*, and GSH1GSH2 complemented mutants stained with MCB (green) to assess cellular glutathione pools in cells of the root elongation zone by CLSM. Propidium iodide (PI, red) staining verified cellular integrity. Scale bar = 20m µM. **(B)** Fourteen-day-old seedlings of a) wild-type, b) *cad2*, and c) GSH1GSH2 double complemented mutants.

2.1.6 Pharmacologically induced glutathione depletion in subcellular compartments

2.1.6.1 BSO induced glutathione depletion in roots and shoots

Buthionine sulfoximine (BSO) is well-known to specifically inhibit GSH1 activity in plastids and thus to deplete the entire glutathione pool after extended incubation (Griffith and Meister, 1979). Wild-type plants germinated on 1 mM BSO show pronounced growth retardation, leading to a phenocopy of the *rml1* phenotype (Figure 2.20). To further address glutathione homeostasis at subcellular level, pharmacologically induced glutathione depletion with BSO was performed on wild-type seedlings expressing GRX1-roGFP2 in the cytosol, plastids, peroxisome, mitochondria, and ER. Seedlings were

germinated on 1 mM BSO for five days and their redox state was assessed via CLSM in roots and leaves.
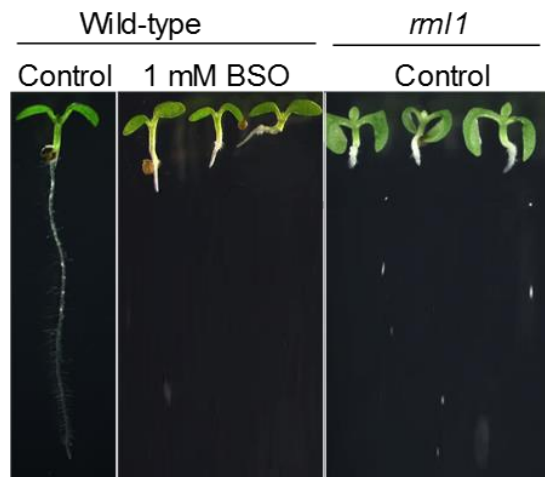
Figure 2.20: Wild-type germinated on 1 mM BSO shows pronounced growth retardation. Six-day-old seedlings of Arabidopsis grown on ½ MS supplemented with and without 1 mM BSO. From left to right, wild-type control, wild-type on 1 mM BSO and *rml1* control.

Pseudo-colour coded ratiometric images showed that roGFP2 was oxidised in all subcellular compartments in roots. In contrast to roots, roGFP2 remained partially reduced in leaves. These data indicate that the glutathione pool was depleted in all subcellular compartments in roots but less efficiently in leaves (Figure 2.21). Moreover, leaf plastids in different cell layers showed diversity in oxidation state, while epidermal plastids were more oxidised than mesophyll and plastids in guard cells were completely reduced.
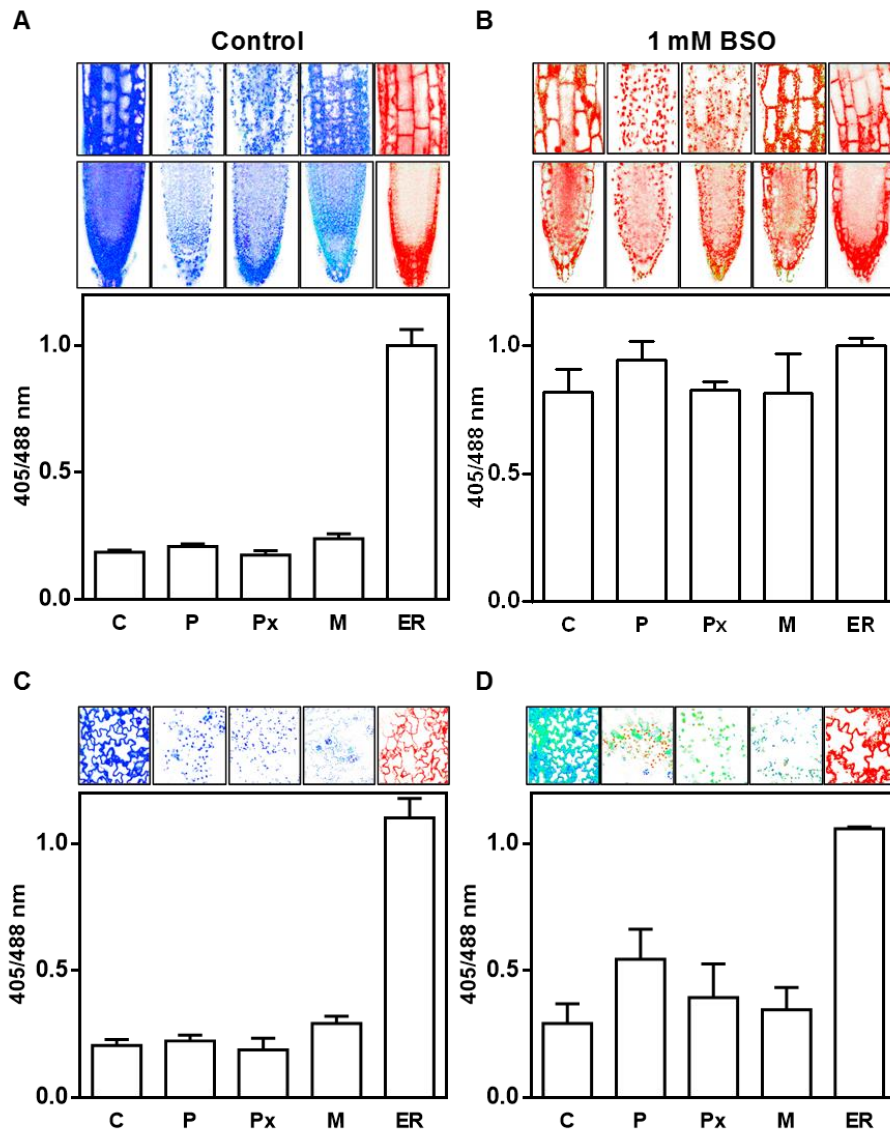
Figure 2.21: Redox imaging of wild-type seedlings with roGFP2 targeted in different subcellular compartments. Cytosol (C), Plastids (P), Peroxisomes (Px), Mitochondria (M), and endoplasmic reticulum (ER). Redox imaging in root tips of five-day-old seedlings grown on ½ MS medium **(A)** and ½ MS supplemented with 1 mM BSO **(B)** Redox imaging in leaves of five-day-od seedlings grown on ½ MS medium **(C)** and ½ MS supplemented with 1 mM BSO **(D)** Bars indicate means of biological replicates; $n \geq 10$; error bars = SD.

2.1.6.2 Depletion of glutathione pool in subcellular compartments upon BSO treatment

To investigate glutathione homeostasis in different subcellular compartments, five-day-old wild-type seedlings were transferred to ½ MS medium supplemented with 1 mM BSO for three days. Different tissues of BSO-treated seedlings were examined; and the pseudo-colour coded ratiometric images showed that roGFP2 was oxidised in the root tips (Figure 2.22 A), in the junction between roots and shoots (Figure 2.22 B) and in hypocotyl (Figure

2.22 C). Different oxidation levels of roGFP2 indicate that the glutathione depletion induced by BSO varies among the different tissues.
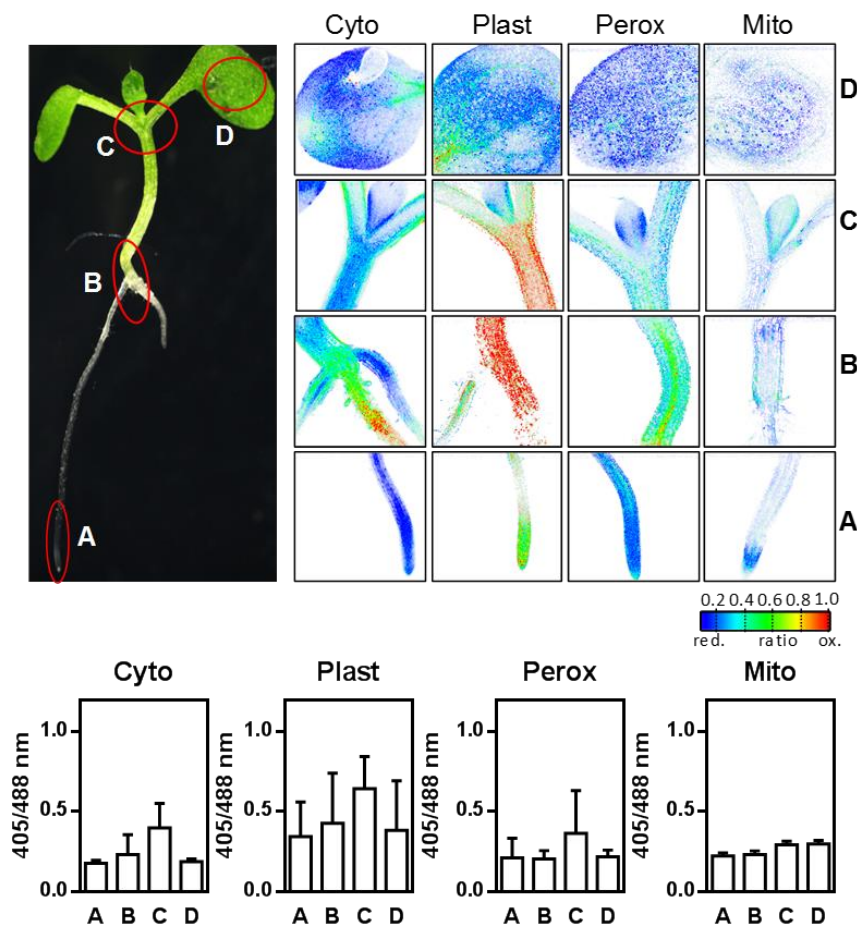
Figure 2.22: Glutathione pool upon BSO treatment in the cytosol, plastids, peroxisomes and mitochondria. Redox measurement of eight-day-old wild-type seedlings transferred for three days to ½ MS with 1 mM BSO. Upper panel: Pseudo-colour coded ratiometric images of different tissues **(A)** root tips, **(B)** Root-shoot junction, **(C)** Hypocotyl, black arrow point at reduced stomata, and **(D)** Cotyledons. Bars indicate means of biological replicates; $n \geq 12$; error bars = SD.

The partially reduced roGFP2 in leaves indicates that glutathione depletion was significantly lower than in other tissues. Interestingly, guard cells were completely reduced and surrounded by completely oxidised cells in the hypocotyl (Figure 2.22). Surprisingly, the higher oxidation of plastidic roGFP2 in root tips indicates that the plastidic glutathione pool in root tips depleted faster than cytosol, peroxisomes and mitochondria (Figure 2.22).

2.1.6.3 Recovery of glutathione pool in subcellular compartments after BSO removal

Glutathione recovery after BSO removal was as well investigated in different subcellular compartments. Wild-type seedlings germinated on ½ MS supplemented with 1 mM BSO

for five days were transferred to BSO free medium for two days. The pseudo-colour coded ratiometric images showed that roGFP2 in cytosol, peroxisomes, and mitochondria was completely reduced, while in plastids roGFP2 was still partially oxidised. The partially oxidised roGFP2 in plastids indicates that the recovery of glutathione pool was slower in plastids than in cytosol, peroxisomes, and mitochondria (Figure 2.23 A). Furthermore, BSO induced adventitious root formation and the inhibition of primary root growth that was not recovered after the plants were transferred to a BSO free medium (Figure 2.23 B).
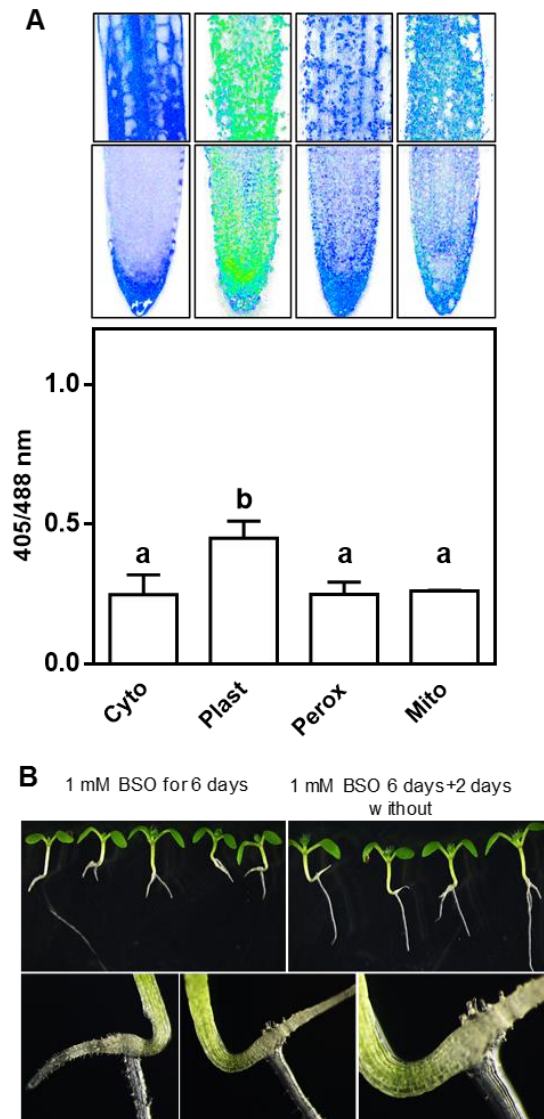
Figure 2.23: Glutathione recovery and root growth after BSO removal. Wild-type seedlings grown five days on 1 mM BSO then transferred for two days on control media. **(A)** Pseudo-colour coded ratio images of wild-type adventitious root tips expressing roGFP2 in cytosol, plastids, mitochondria, and peroxisomes. **(B)** Adventitious root formation after BSO treatment, primary root growth is inhibited by BSO. Bars indicate means of biological replicates; $n \geq 10$; error bars = SD. Letters indicate significant differences (One-way ANOVA with Tukey's multiple comparisons test; p-value ≤0.05).

Furthermore, pseudo-colour coded ratiometric images indicated that after BSO removal glutathione recovery varies among different tissue. Unlike glutathione depletion,

glutathione recovery was slower in the hypocotyl, in the junction between roots and shoots and in root tip (Figure 2.24).
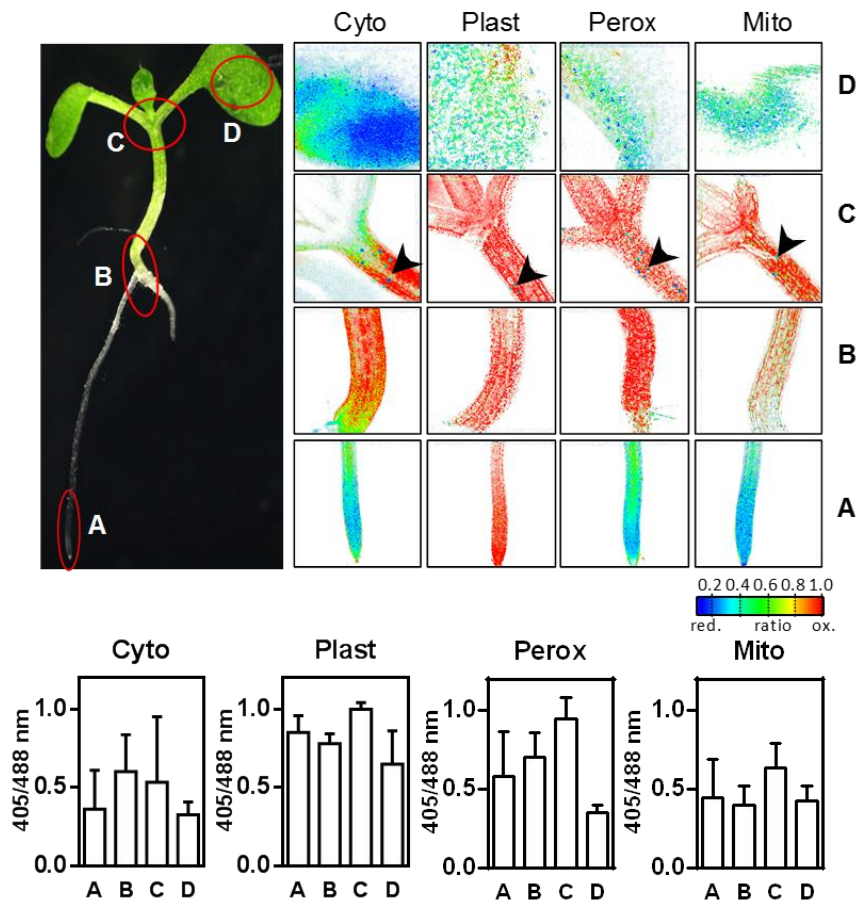
Figure 2.24: Recovery of glutathione pool in the cytosol, plastids, peroxisomes and mitochondria after BSO removal. Redox measurement of seven-day-old wild-type seedlings grown for five days on 1 mM BSO then transferred to BSO free media for two days. Upper panel: Pseudo-colour coded ratiometric images of different tissues **(A)** root tips, **(B)** root-shoot junction, **(C)** hypocotyl and **(D)** cotyledons. Bars indicate means of biological replicates; *n* = 8–12; error bars = SD.

2.1.7 Absolute amount of glutathione and plant growth

External glutathione supply rescues the *rml1* lethal phenotype (Vernoux et al., 2000) (Figure 2.25). To investigate whether the *rml1* lethal phenotype is due to low glutathione pool or due to oxidised redox state, two glutathione deficient mutants, *zir1* and *rml1* were crossed with *BSO insensitive roots 6* (*bir6)* and *glutathione reductase I* (*gr1)* mutants.
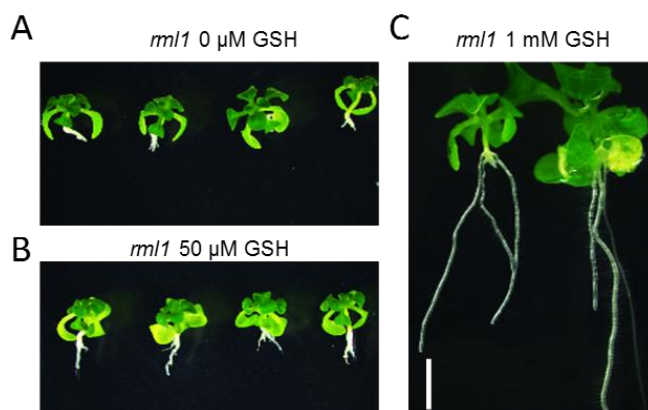
Figure 2.25: GSH feeding and root growth in *rml1*. Fourteen-day-old *rml1* seedlings grown under long day condition and transferred for eight days to liquid ½ MS supplemented with and without GSH. (A) Control (B) Supplemented with 50 µM GSH. (C) Supplemented with 1 mM GSH. Scale bar= 5 mm

The *bir6* mutant was isolated during a BSO screening by Koprivova et al. (2010). BIR6 belongs to the PPR (pentatricopeptide repeat) protein family, and it is involved in the splicing of intron 1 of the mitochondrial nad7 transcript which codes for a subunit of Complex I. Loss of function mutation in BIR6 affects the assembly of Complex I and results in a moderate growth retardation. Furthermore, *bir6* plants grown on BSO retained significantly higher level glutathione than wild-type (Figure 2.26) and the results were similar to what assessed by Koprivova et al. (2010). The *gr1* mutant exhibits a partially oxidised glutathione pool in the cytosol, without any obvious phenotype.
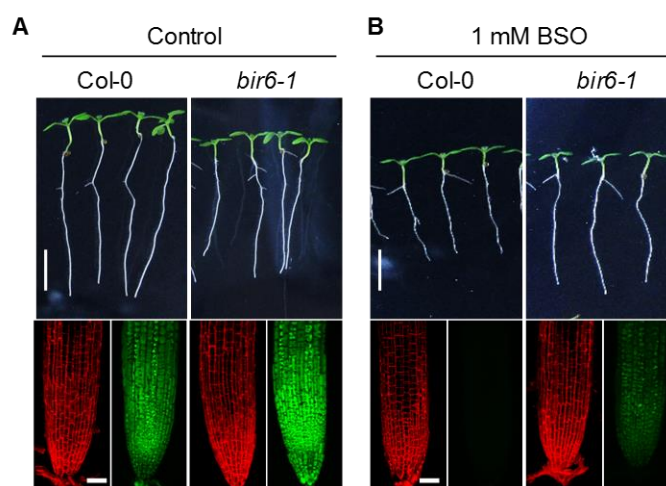
Figure 2.26: *bir6* mutant resistance to BSO treatment compared to the wild-type. (A) Upper panel: seven-day-old seedlings of wild-type and *bir6-1* grown on ½ MS. Scale bar = 5 mm. Lower panel: MCB labelling of root tips of seven-day-old wild-type and *bir6* under control condition (scale bar = 20 µm). **(B)** Upper panel: seven-day-old seedlings of *bir6* and wild-type transferred for 4 days to ½ MS supplemented with 1 mM BSO. MCB labelling of root tips of *bir6* and wild-type after BSO treatment.

Loss of GR1 was already proven to do not affect the glutathione pool (Marty et al., 2009). The confirmation of double mutants was done by genotyping PCR with gene specific

primers (Figure 2.27 A). The double mutants of *bir6zir1* and *bir6rml1* partially suppressed the *zir1* and *rml1* growth phenotype (Figure 2.27 B-C). However, double mutants of *gr1zir1* and *gr1rml1* had no effect on growth phenotype (Figure 2.27 B-C). Furthermore, the amount of total glutathione pool was assessed in double mutants with MCB labelling. The *bir6zir1* and *bir6rml1* double mutants showed more intense fluorescence of MCB labelling than *zir1* and *rml1* single mutants, indicating that these seedlings have more glutathione. In contrast, the *gr1zir1* and *gr1rml1* double mutants showed a similar fluorescence intensity of MCB labelling to *zir1* and *rml1* single mutants and no growth defects were observed (Figure 2.27 B-C). These results suggest that the absolute amount of glutathione rather than its redox potential restricts plant growth.
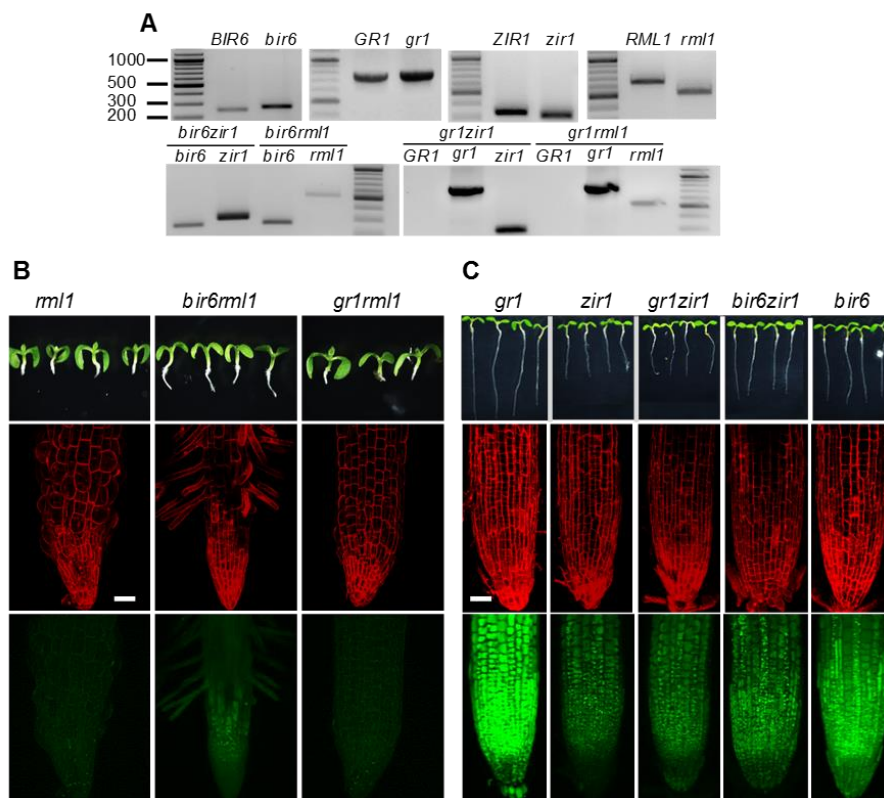
Figure 2.27: Phenotype and MCB labelling of single and double mutants of *bir6, gr1, zir1* and *rml1.* (A) Molecular confirmation of double homozygous mutants for *gr1, bir6, zir1* and *rml1* locus. **(B)** Phenotypes of *rml1, gr1rml1* and *bir6rml1* double homozygous mutants (upper panel). Representative CLSM images of single and double homozygous mutants root tips labelled with PI (50 µM) red and MCB (100 µM) green, Scale bar = 20 µm (lower panel). **(C)** Phenotypes of *gr1, bir6, zir1, gr1zir1* and *bir6zir1* double homozygous mutants (upper panel). Representative images of single and double homozygous mutants root tips labelled with PI (50 µM, red) and MCB (100 µM, green), Scale bar = 20 µm (lower panel).

2.1.8   GSSG export from plastids to cytosol is limited

To address the export of GSSG from plastids to the cytosol, the *gr2* mutant *miao* (Yu et al., 2013) was used. The *miao* mutant displays a strong inhibition of root growth and it

accumulates high levels of GSSG (Yu et al., 2013). Redox imaging in roots and leaves of wild-type and *miao* expressing plastid-localised and cytosol-localised roGFP2 revealed that roGFP2 was reduced in the cytosol to wild-type levels in roots and in leaves of the *miao* mutants (Figure 2.28 A). However, plastidic roGFP2 was highly oxidised in root- and leaf- epidermal cells of *miao*, but not in wild-type. Surprisingly, in leaf mesophyll, plastids roGFP2 was partially reduced in the *miao* (Figure 2.28 B). The oxidised roGFP2 in *miao* plastids in epidermal cells suggests that plastids cannot sufficiently export GSSG to cytosol.
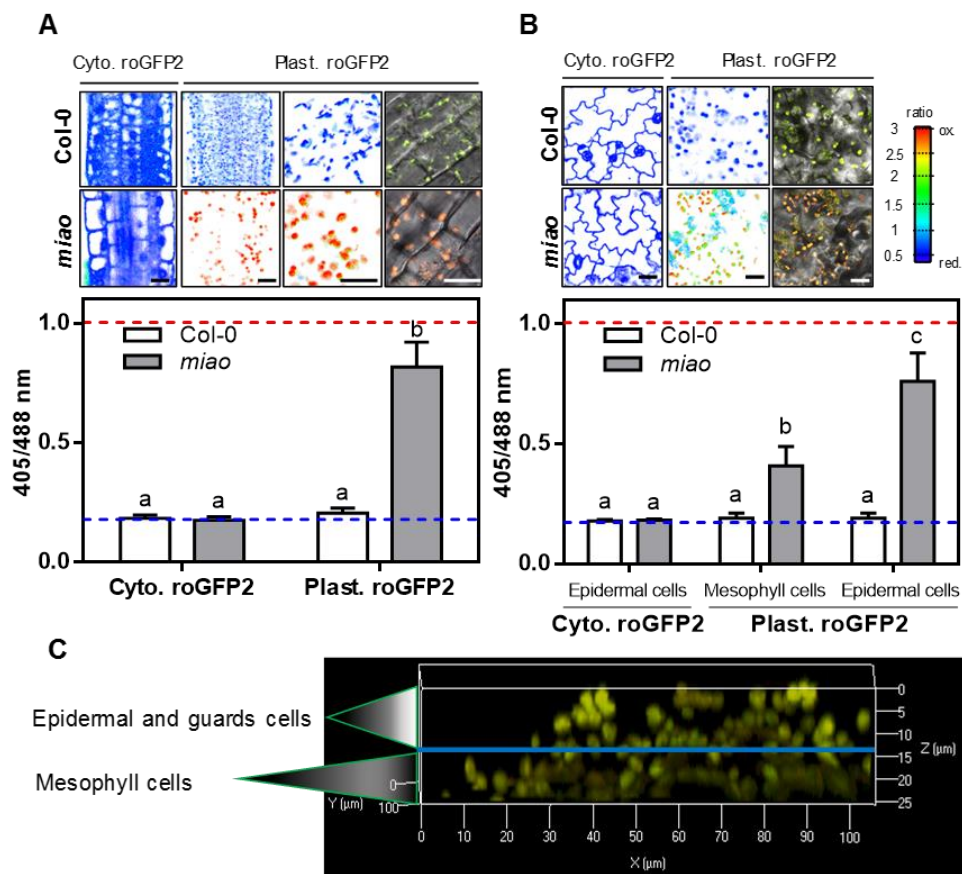
Figure 2.28: Comparison of redox state in the cytosol and plastids of *miao* with wild-type. (A) Redox measurement in the cytosol and plastids of root cells of five-day-old seedlings of wild-type and *miao* grown on ½ MS under long day condition. **(B)** Redox measurement in the cytosol and plastids of leaf cells of five-day-old seedlings of wild-type and *miao* grown on ½ MS under long day condition. Blue and red dash line on the graphs indicates the maximum reduction and oxidation of roGFP2 with 10 mM DTT and 25 mM H_2O_2, respectively. Bars represent average ratio of 405/488 nm of biological replicates; $n \geq 10$; error bars = SD. Letters indicate significant differences (Two-way ANOVA with Tukey's multiple comparisons test; *p*-value ≤0.05). Scale bar = 20 µm. **(C)** Confocal images indicating the position of plastids in epidermal and mesophyll cells layer in leaf.

2.1.8.1 Reduced mesophyll plastids in *miao* mutants is linked to light-dependent thioredoxin backup system

Mesophyll plastids were partially reduced in *miao* seedlings. To further investigate, whether the partial reduction of mesophyll plastids was light dependent, wild-type and *miao* seedlings were grown in darkness for five days. Redox measurement revealed that mesophyll plastids were oxidised in etiolated seedlings of mutants, while wild-type plastids were still reduced (Figure 2.29 B). The oxidation of mesophyll plastids in *miao* in darkness indicates that partial reduction of mesophyll plastids in light is light dependent and may be linked with the thioredoxin backup system. In addition, the number of plastids in the roots of *miao* mutants was significantly lower, however, plastids were bigger in the *miao* mutants than in wild-type (Figure 2.29 C-D).
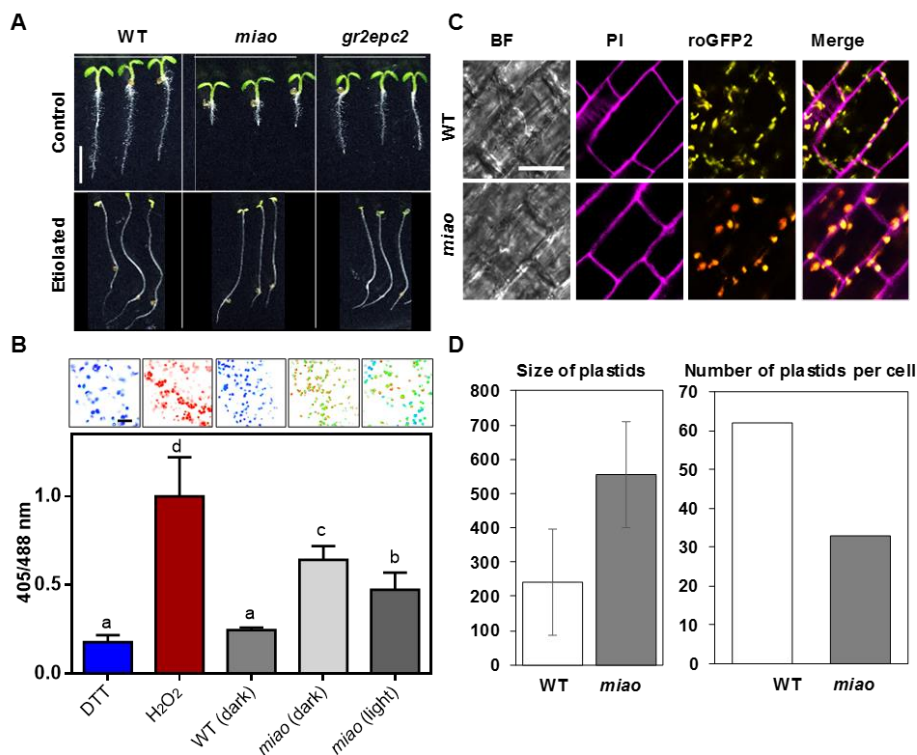
Figure 2.29: Partial reduction of mesophyll plastids is light-dependent. (A) Five-day-old seedlings of wild-type, *miao*, and *gr2epc2* mutants under dark and light conditions (scale bar = 5 mm). (B) Pseudo-colour coded images of the cotyledons of etiolated seedlings of wild-type, *miao*, and *gr2epc2* (upper panel). Bars represent mean of biological replicates; $n \geq 10$; error bars = SD. Letters indicate significant differences (Two-way ANOVA with Tukey's multiple comparisons test; p-value ≤0.05). Scale bar = 20 µm (lower panel). (C) PI labelling of wild-type and *miao* mutants expressing plastidic roGFP2. Scale bar = 20 µm. (D) Size and number of plastids per cell in wild-type and *miao* mutants.

2.1.9 Role of the ATP-binding cassette transporter of the mitochondrion 3 (ATM3) in GSSG export from mitochondria

It has been shown that the mitochondrial ATM3 transporter exports glutathione polysulfide (Schaedler et al., 2014). To further explore the role of ATM3 in the GSSG export from mitochondria to cytosol, double mutants of *atm3-4gr2epc2* were produced. Primary root length of *atm3-4gr2epc2* double mutant was significantly shorter than the wild-type and single mutants (Figure 2.30 A-B). Furthermore, the double mutant was stunted in growth and showed leaf chlorosis compared to wild-type and single mutants (Figure 2.30 C). In addition, the Fv/Fm ratio was significantly lower in *atm3-4gr2epc2* double mutants than in wild-type and single mutants (Figure 2.30 D). The dwarf and chlorotic phenotype of *atm3-4gr2epc2* was due to lack of ATM3 and GR2, thus these results provide genetic evidence that ATM3 may involve in the GSSG export from mitochondria to the cytosol.
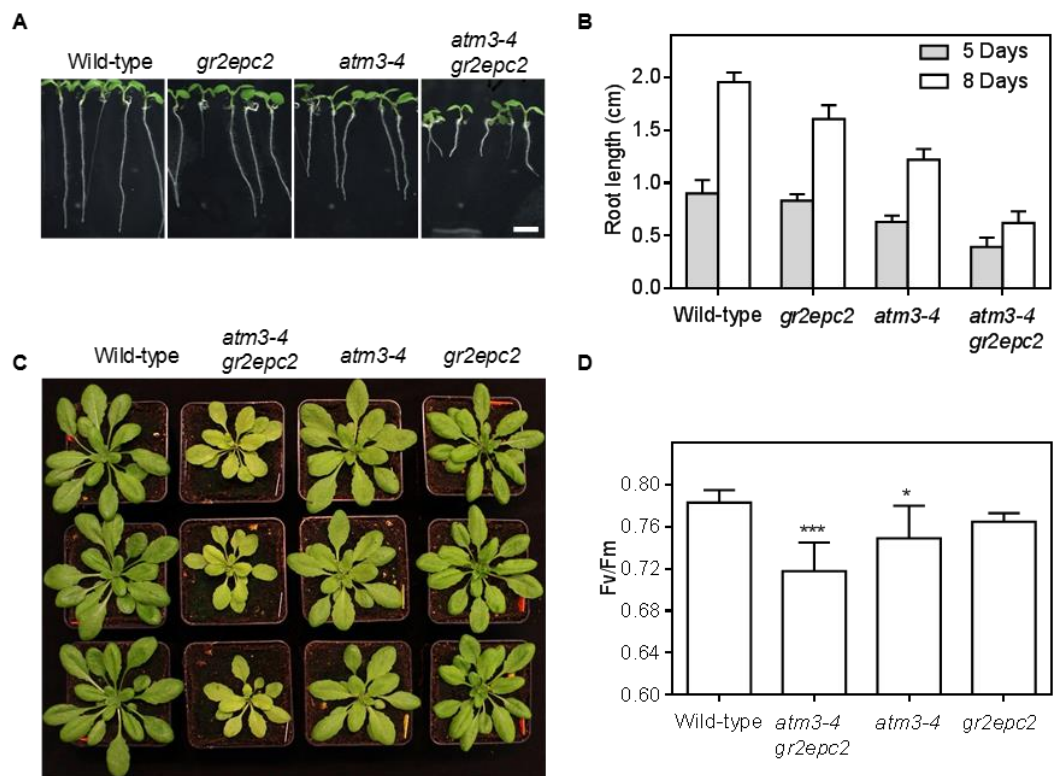
Figure 2.30: The *atm3-4gr2epc2* double mutant showed an enhanced dwarfed and chlorotic phenotype compared to wild-type and single mutants. (A) Eight-day-old seedlings of the double mutant *atm3-4gr2epc2* compared to wild-type and single mutants. Scale bar = 5 mm **(B)** Primary root length of the mutants compared to wild-type. Plants were grown on ½ MS medium for 5–8 days under long day conditions after 2–days stratification (*n* = 5-12). **(C)** Plants were grown under long day conditions for 4 weeks. **(D)** Pulse-amplitude modulated (PAM) fluorimetry of 4 week old plants grown in soil under long day conditions (*n* = 7). Bars indicate means of biological replicates; error bars = SD. The statistical analysis (one-way ANOVA with post hoc Holm-Sidak comparisons for wild-type vs. mutant) indicated significant changes; * *p*-value ≤0.05; ***p*-value ≤0.001. Data set was generated together with Anna Moseler.

2.1.10 GSSG export from mitochondria to cytosol is limited

In addition, the export of GSSG from mitochondria into the cytosol was tested with *gr2epc2* mutant expressing dual targeted roGFP2 to the cytosol and mitochondria. The knockout of GR2 mutant is lethal in early embryonic developmental stage (Tzafrir et al., 2004), While the *gr2epc2* mutant had complemented plastidic GR2 and are fully viable. Redox imaging was collected in wild-type and the *gr2epc2* mutant with regions of interest (ROIs) in cytosol and mitochondria to estimate the compartment specific glutathione redox status. While in wild-type both cytosol and mitochondria were reduced, in the *gr2epc2* mutant mitochondria, were more oxidised than the wild-type. No differences in the redox state in the cytosol were detected between wild-type and the *gr2epc2* mutant (Figure 2.31). The partially oxidised roGFP2 in mitochondria indicates that GSSG is not sufficiently exported from mitochondria into the cytosol.
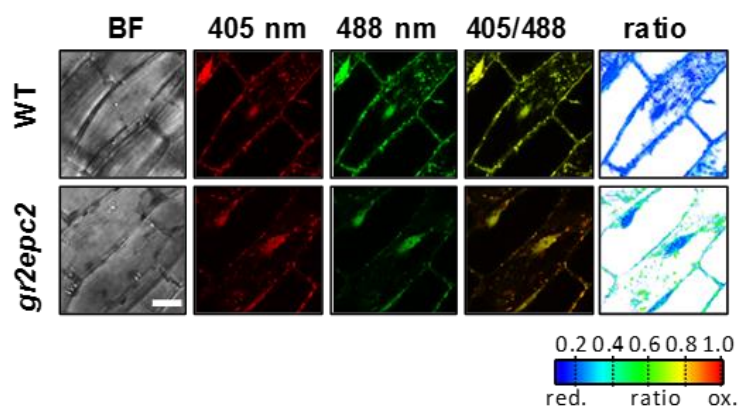
Figure 2.31: Redox imaging of the local glutathione redox state in mitochondria and cytosol. Redox imaging in hypocotyl of five-day-old seedlings of wild-type (upper panel) and *gr2epc2* (lower panel) mutants expressing dual targeted roGFP2-GRX1. From left to right, bright field pseduo-colour coded images from 405 nm (red) and 488 nm (green) roGFP2 excitation channels, merge of 405/488 nm and ratio images calculated from 405 and 488 nm. Scale bar = 20 µm.

2.2 Gamma-glutamyl cycle: glutathione degradation and transport

Glutathione homeostasis is regulated by the γ-glutamyl cycle, which is based on glutathione synthesis, degradation and transport. Gamma-glutamyl cycle was suggested as a classical pathway for glutathione transport across the plasma membrane (Ballatori et al., 2009). As introduced in section (1.4), that GGTs are involved in the degradation of extra cytosolic glutathione while GGCTs take part in controlling cytosolic glutathione homeostasis (Noctor et al., 2011; Ohkama-Ohtsu et al., 2008). GGCT degrades the γ-glutamyl dipeptide, generated by GGTs, and releases amino acid from its γ-glutamyl carrier (Meister, 1974). However, the cytosolic pathway of glutathione in plant still need further characterisation.

2.2.1 *In situ* detection of glutathione in root tips of *ggct2;1* mutants

It has been shown that γ-Glutamyl cyclotranferase (GGCT2;1), was up-regulated during arsenic stress and found to be involve in the degradation of glutathione (Paulose et al., 2013). In mammals, it has been reported, that the ChaC proteins family in functions as γ-glutamyl-cyclotranferases, acting specifically on glutathione (Kumar et al., 2012). In contrast, in plants, γ-glutamyl dipeptides suggested as a substrate for GGCT (Paulose et al., 2013). In the present study substrate specificity of GGCTs towards GSH was explored in two T-DNA insertion Arabidopsis mutant lines: *AtGGCT2;1-1* and *AtGGCT2;1-1* (Figure 2.32). It has been already shown that under sulfur deficiency GGCT2;1 expression is up regulated in root tips (Iyer-Pascuzzi et al., 2011), suggesting that plants start to mobilise sulfur by degrading glutathione. To further test the substrate specificity of GGCT towards GSH, the GGCT mutants were subjected to sulfur deprivation followed by MCB labelling.
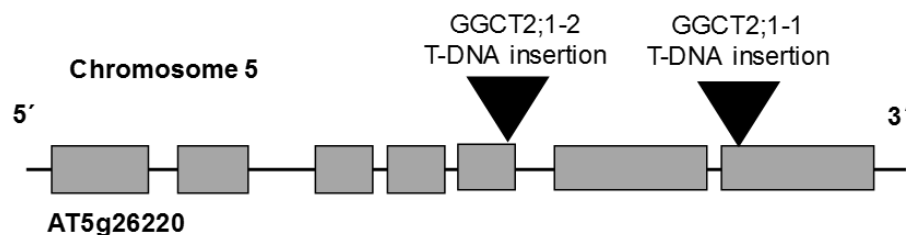
Figure 2.32: T-DNA insertion alleles of Arabidopsis GGCT2 genes. Gene model of GGCT2;1 (AT5g26220) depicting the two T-DNA insertion sites. Exons are represented as boxes and introns as lines. Modified from Paulose et al. (2013).

MCB labelling was done on five-day-old seedlings grown on ½ MS supplemented with or without sulfur. The results showed that after five-days there were no differences in the MCB fluorescent intensity of wild-type and *ggct2;1* mutant under both control and sulfur

deficient conditions (Figure 2.33). However, MCB of seven-day-old seedlings grown on ½ MS supplemented with or without sulfur showed a clear suppression of MCB fluorescence in wild-type compared to *ggct2;1-1* and *ggct2;1-2* mutants (Figure 2.33). Surprisingly, the complemented line *ggct2;1-ox4* showed similar labelling intensity to *ggct2;1-1* and *ggct2;1-2* (Figure 2.33). Intense MCB fluorescence in *ggct2;1-1* and *ggct2;1-2* mutants and suppression of MCB fluorescence in wild-type suggests that GGCTs specifically degrading GSH in the cytosol.
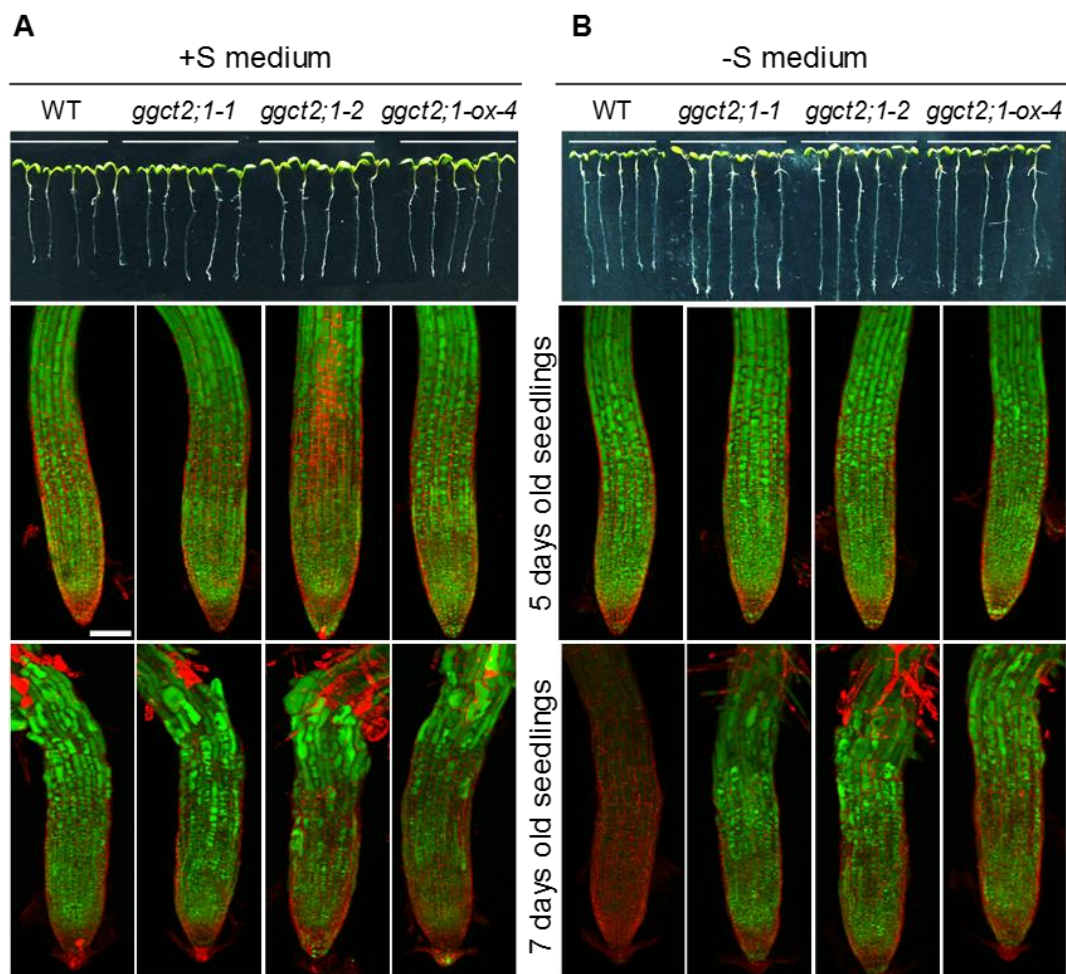
Figure 2.33: MCB based detection of GSH degradation under sulfur deficiency. Upper panel: phenotype of seven-day-old seedlings grown on ½ MS **(A)** in the presence of sulfur (+S) and **(B)** In the absence of sulfur (-S). Middle panel: MCB and PI labelling of five-day-old seedlings. Lower panel: MCB and PI labelling of seven-day-old seedlings. $n \geq 5$. Scale bar = 100 µM.

Additionally, MCB labelling was pursued in seven-day-old seedlings of glutathione deficient mutants, *cad2* and *rml1* grown on ½ MS supplemented with and without sulfur. Under control condition (+S) *cad2*, which has 30 % of wild-type glutathione showed a less intense MCB fluorescence compare to wild-type, *ggct2;1-1* and *ggct2;1-2* mutants (Figure 2.34). In contrast, in the absence of sulfur (-S) no MCB labelling was detected in

cad2, while in *rml1* both in presence and absence of sulfur no MCB labelling was detected (Figure 2.34).
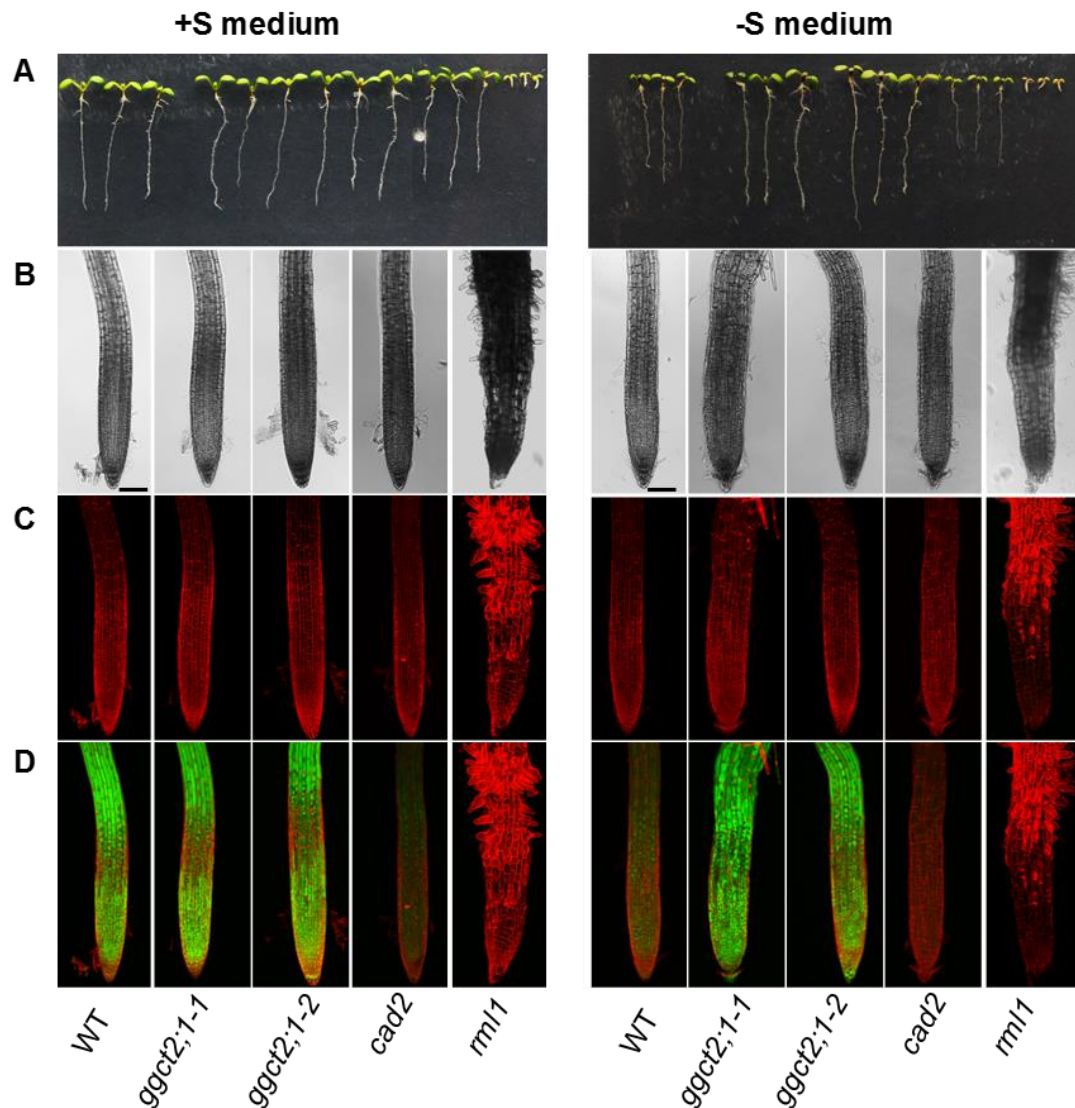
Figure 2.34: MCB based detection of GSH degradation under sulfur deficiency. Seven-day-old seedlings of wild-type, *ggct2;1-1*, *ggct2;1-2*, *cad2* and *rml1* grown on ½ MS supplemented with sulfur (left panel) and without sulfur (right panel). **(A)** Phenotype of seven-day-old seedlings **(B)** Bright field images of root tips. **(C)** PI labelling of root tips. **(D)** Merge of PI and MCB of root tips of wild-type and mutants. *n* ≥ 5. Scale bar = 100 µM.

2.2.1.1 Sulfate starvation and primary roots growth of *ggct2;1* mutants

Furthermore, length of primary root of seven-day-old seedlings of wild-type, *ggct2;1-1*, *ggct2;1-2, cad2* and *rml1* was measured. Under control condition (+S) no difference in primary root of wild-type compared to *ggct2;1-1* and *ggct2;1-2* mutants were observed. In contrast, the primary root of wild-type seedlings grown on –S was significantly shorter

compared to *ggct2;1-1* and *ggct2;1-2* mutants (Figure 2.35). Furthermore, primary roots of *cad2* and *rml1*, both in presence and absence of sulfur, were significantly shorter compared to wild-type and *ggct2;1-1* and *ggct2;1-2* mutants (Figure 2.35).
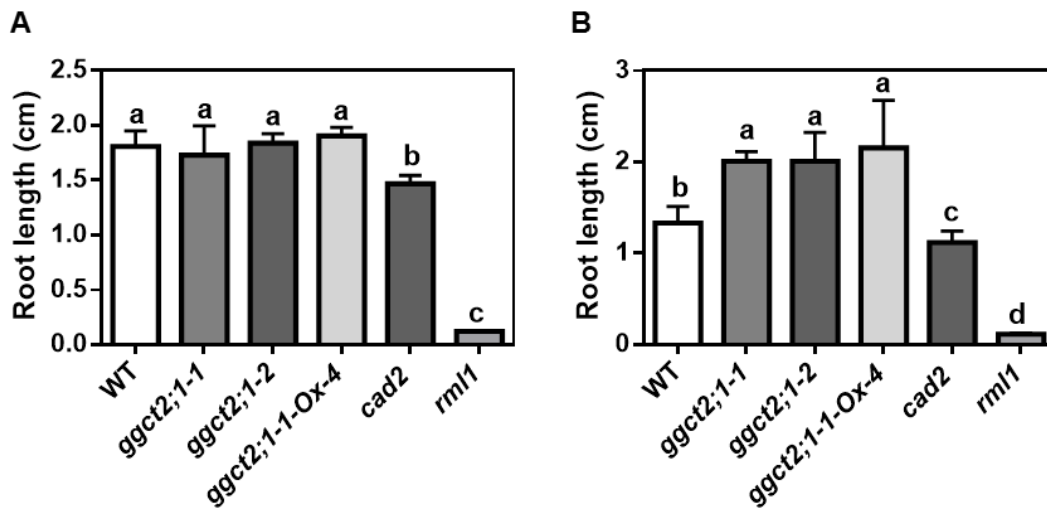
Figure 2.35: Effect of sulfur deficiency on length of primary root. Length of primary root of seven-day-old seedlings of wild-type, *ggct2;1-1, ggct2;1-2, cad2* and *rml1* grown on ½ MS supplemented A) with sulfur B) without sulfur. Bars indicate means of biological replicate; $n \geq 4$; error bars = SD. Letters indicate significant differences (One-way ANOVA with Tukey´s multiple comparisons test; *p*-value ≤0.05).

2.2.1.2 Molecular confirmation of double mutants

To further investigate the role of GGCTs in glutathione degradation, both GCCTs mutants were crossed with two glutathione deficient mutants, *zir1* and *rml1*. The confirmation of double mutants was done by genotyping PCR with gene specific primers (Figure 2.36).
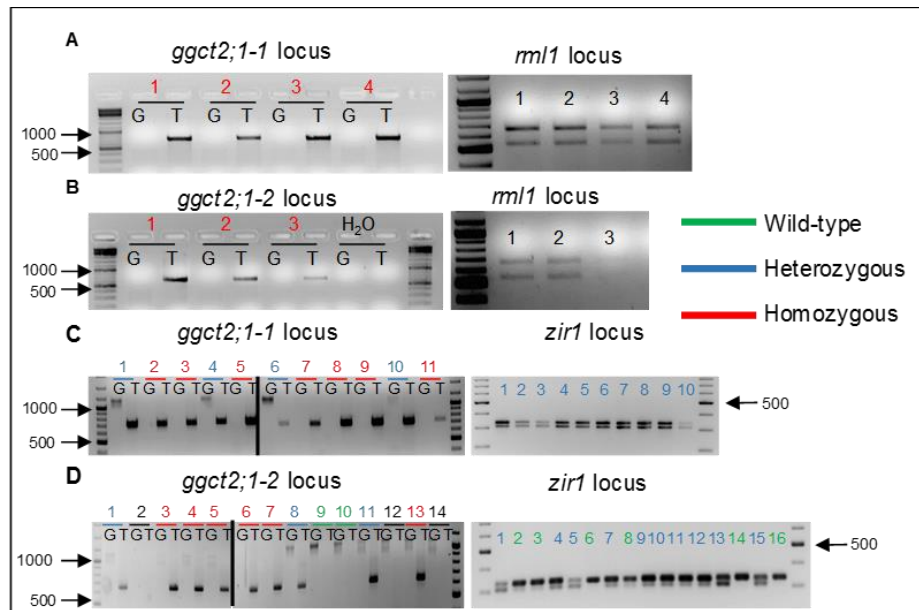
Figure 2.36: Genotyping PCR of *ggct* and *gsh1* double mutants. Agarose gel of genotyping PCR with gene and T-DNA specific primers of double mutants **(A)** *ggct2;1-1rml1*. **(B)** *ggct2;1-2rml1*. **(C)** *ggct2;1-1zir1*. **(D)** *ggct2;1-2zir1*. "G" indicates wild-type locus, T indicates the respective T-DNA locus. PCR product of *zir1* and *rml1* was digested with HindIII and ApoI restriction enzyme respectively. Green lines indicate wild-type controls, red lines indicate homozygous for *ggct2* locus and blue indicates all heterozygous for the respective locus.

2.2.1.3 Redox measurement of *ggct2;1* mutants grown on +S and –S medium

To investigate the redox status of glutathione pool of GGCTs mutants under sulfur deprivation, GGCTs mutants were stably transformed with the cytosolic GRX1-roGFP2 (Figure 2.37).
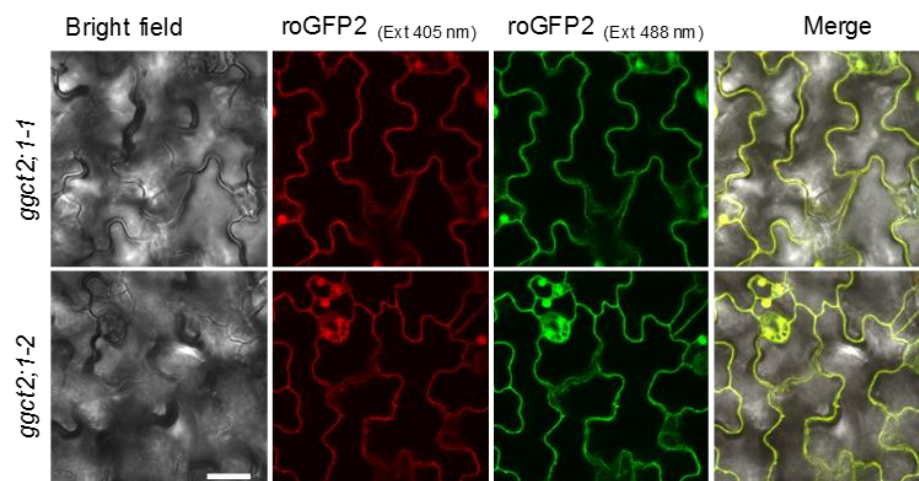
Figure 2.37: Confirmation of *ggct2* mutants expressing cytosolic GRX1-roGFP2. Localisation of GRX1roGFP2 in leaf cells of five-day-old of g*ggct2;1-1*(upper panel) and *ggct2;1-2* (lower panel) Arabidopsis mutants. Left to right bright field, roGFP2 excitation at 405 nm, roGFP2 excitation at 488 nm and merge of all. Scale bar = 20 μm.

2.2.2   Transport of GSH across the plasma membrane

In plants, glutathione is synthesised in two compartments: the plastids and the cytosol (Wachter et al., 2005). Thus, transport of GSH into other organelles and export into the apoplast requires specific glutathione transporters (Bachhawat et al., 2013). While transport of glutathione has been biochemically characterised in several species (Bachhawat et al., 2013; Bourbouloux et al., 2000; Brechbuhl et al., 2010), the molecular identity of the transporters have been elucidated in only few cases (Bachhawat et al., 2013). The Hgt1p/Opt1p was the first high affinity and high specificity plasma membrane GSH transporter found in yeast (*Saccharomyces cerevisiae*) (Bourbouloux et al., 2000). In plants, only CLTs (chloroquine-resistance transporter like transporters) have been identified as plastid-located glutathione transporters (Maughan et al., 2010). Transport systems across other membranes, however, still await molecular identification and functional characterisation.

2.2.2.1   External GSH, but not GSSG restore growth in *rml1* seedlings

As shown earlier, external GSH rescues *rml1* growth (Figure 2.25). To further test whether both GSH and GSSG can rescue *rml1*, five-day-old *rml1* seedlings were supplied with micromolar concentrations of GSH and GSSG. GSH supplement rescued the *rml1* growth phenotype in a concentration-dependent manner, suggesting that GSH can be transported across the plasma membrane. Unlike GSH, equimolar concentrations of oxidised glutathione (GSSG) did not suppress the *rml1* lethal phenotype (Figure 2.38 A). In addition, the *rml1* seedlings showed intense MCB labelling after one day on ½ MS supplemented with different GSH concentrations (0-250 µM). In contrast, *rml1* seedlings grown on ½ MS supplemented with different concentration of GSSG (0-125 µM) did not show MCB labelling (Figure 2.38 B).
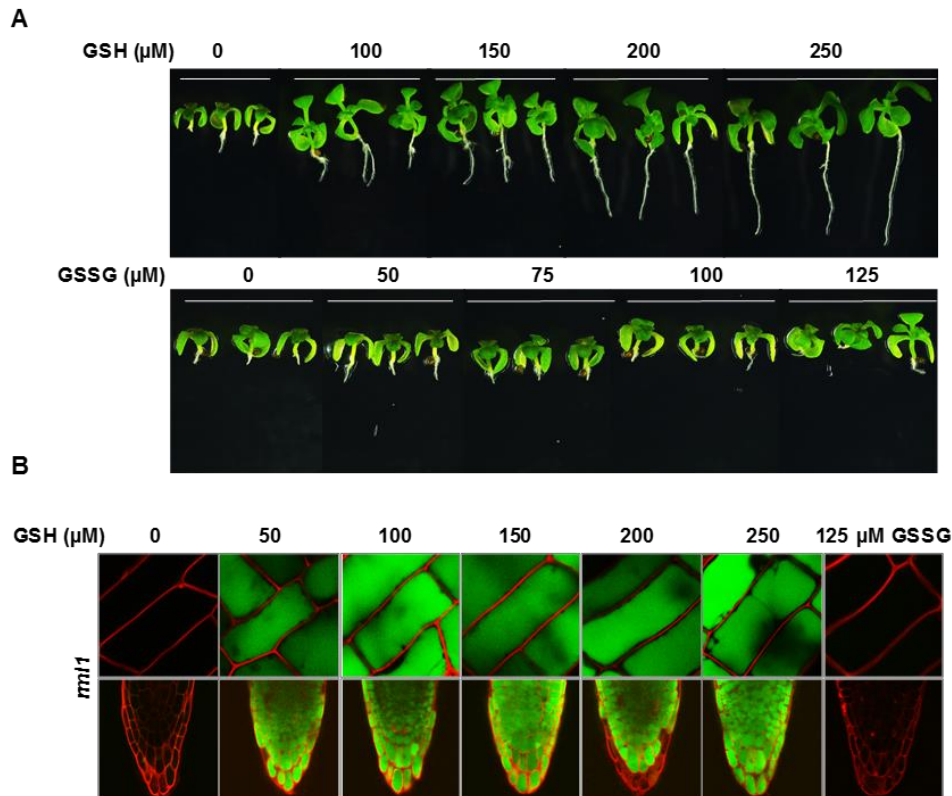
Figure 2.38: Growth and MCB labelling of *rml1* mutants supplied with glutathione. (A) Sixteen-day-old *rml1* seedlings grown for ten days on ½ MS with 0.8% phytagel supplemented with different concentrations of GSH (0–250 µM) or GSSG (0–125 µM); B). Representative images of *rml1* seedling root tips stained with MCB to assess cellular glutathione pools by confocal microscopy. Propidium iodide (PI) staining verified cellular integrity.

2.2.2.2 External GSH supply and *rml1* cytosolic roGFP2 reduction

The uptake of glutathione was verified with roGFP2 that, in contrast to MCB labelling, is able to distinguish between subcellular glutathione pools and the oxidised and reduced form. To further investigate whether glutathione is taken up only as GSH or also as GSSG, *rml1* seedlings expressing GRX1-roGFP2 in the cytosol were supplied with both GSH and GSSG. If taken up, GSSG should be converted to GSH through the glutathione reductase (GR) and hence lead to an increase of the E_{GSH} in the cytosol towards more negative values. The *rml1* seedlings expressing roGFP2 were transferred to liquid ½ MS supplemented with either 50 µM GSH or GSSG for 2–20 h. Seedlings were imaged after 2, 4, 6, 8, 16 and 20 h. The oxidised cytosolic roGFP2 in *rml1* seedlings was gradually reduced from 2–20 h in the presence of GSH, reaching wild-type level of reduction after 20 h, confirming GSH uptake (Figure 2.39 A). Unlike GSH, lower concentrations of GSSG (50 µM) did not reduce roGFP2, indicating that GSSG supplied at equimolar concentration was not transported across the plasma membrane (Figure 2.39 B). Furthermore, at 200 µM and 500 µM GSSG a partial reduction of roGFP2 was observed, and only with 1 mM GSSG roGFP2 was almost completely reduced (Figure 2.39 C).
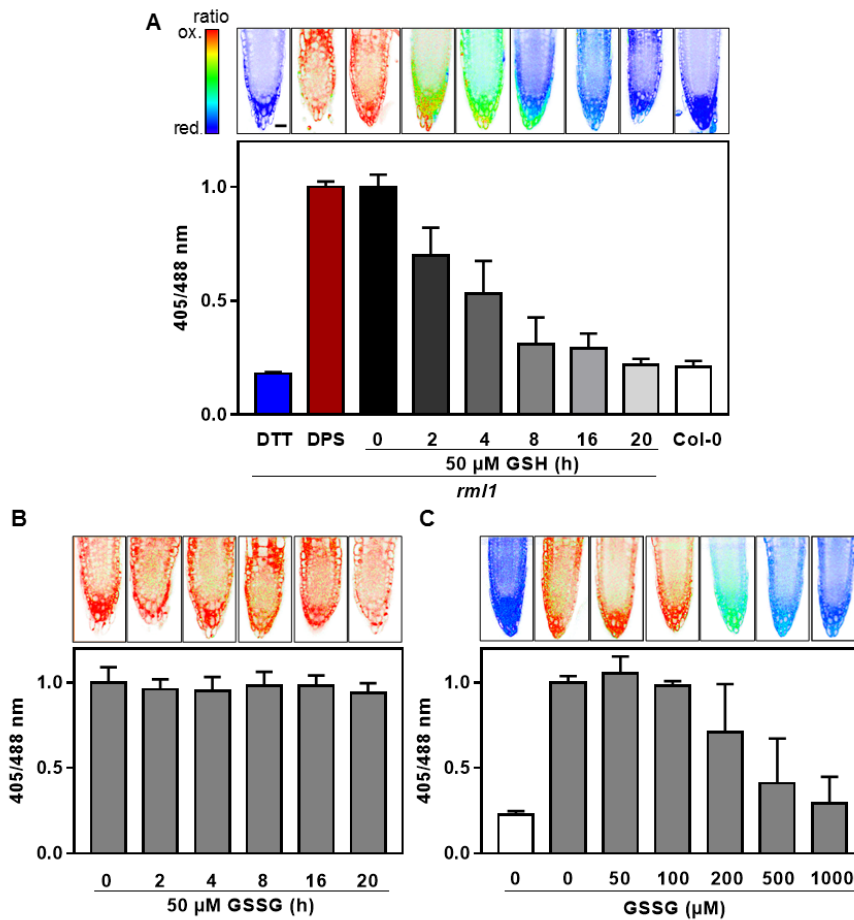
Figure 2.39: Redox imaging of *rml1* mutants grown on ½ MS supplemented with GSH or GSSG. A) Upper panel: pseudo-colour coded ratiometric images of the root tips of five-day-old *rml1* seedlings (grey–black bars) grown for 0–20 h in liquid ½ MS supplemented with 50 μM GSH along with untreated wild-type (white bar) as a control. Lower panel: ratiometric analysis of root tips indicating the average ratio of 405/488 nm. $n \geq 10$. Treatment of *rml1* seedlings with 10 mM DTT (blue bar) and 5 mM DPS (red bar) resulted in full reduction and oxidation of roGFP2, respectively. B) Upper panel: pseudo-colour coded ratiometric images of the root tips of five-days-old *rml1* seedlings (grey bars) grown for 0–20 h in liquid ½ MS supplemented with 50 μM GSSG. Lower panel: ratiometric analysis of root tips indicating the average ratio of 405/488 nm. $n = 10$-12. C) Upper panel: pseudo-colour coded ratiometric images of the *rml1* root tips (grey bars) treated with 0, 50, 100, 200, 500 and 1000 μM GSSG along with untreated wild-type (white bar) control. Lower panel: ratiometric analysis of root tips indicating the average ratio of 405/488 nm. $n \geq 10$. Scale bar = 20 μm. Data are shown as mean ± SD.

The reduction of roGFP2 with higher concentration (500-1000 μM) of GSSG, confirmed the residual transport of GSSG across the plasma membrane. The reduction of roGFP2 with 50 μM GSH to wild-type level, further support active GSH uptake against a concentration gradient and accumulation to low millimolar levels.

2.2.2.3 External GSH, but not amino acids lead to a reduction of cytosolic roGFP2

The GGT1/2 enzymes on the outer surface of the plasma membrane have been shown to degrade both GSH and GSSG into its amino acids (Ohkama-Ohtsu et al., 2008). Moreover, glutamate, glycine and cysteine are transported across the plasma membrane

via amino acid transporters (Lee et al., 2014; Rentsch et al., 2007). In the present work it was tested, whether feeding of these individual amino acids was sufficient to reduce roGFP2. Five-day-old *rml1* seedlings were supplied with 1 mM cysteine, glutamate or glycine for 20 h. The data from pseudo-colour coded ratiometric images and quantitative data analysis showed that cysteine, glutamate and glycine did not reduce roGFP2, confirming that these amino acids did not interact with roGFP2 (Figure 2.40 A). Additionally, five-day-old *rml1* seedlings were grown in ½ MS supplemented for 2–20 h with 50 µM N-Acetyl-L-cysteine (NAC), a precursor of glutathione biosynthesis. Unlike GSH, the oxidised cytosolic roGFP2 in *rml1* seedlings did not reduce in 20 h in the presence of NAC (Figure 2.40 B). In summary, the amino acids feeding revealed that these amino acids did not reduce the roGFP2 and suggest that they are not interacting with roGFP2.
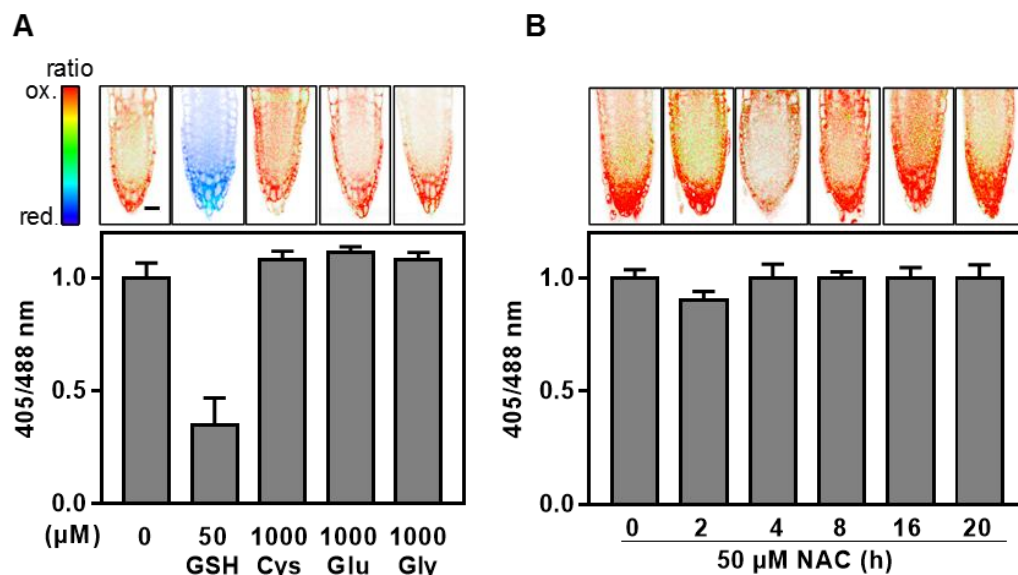
Figure 2.40: Effect of externally supplied amino acids on cytosolic roGFP2 redox state in *rml1*. (A) Upper panel: pseudo-colour coded ratiometric images of the root tips treated with 50 µM GSH and 1 mM Cys, Glu or Gly. Lower panel: ratiometric analysis of root tips indicating the average ratio of 405/488 nm. **(B)** Upper panel: pseudo-colour coded ratiometric images of the root tips of five-days-old *rml1* seedlings grown for 0–20 h in liquid ½ MS supplemented with 50 µM NAC. Lower panel: ratiometric analysis of root tips indicating the average ratio of 405/488 nm. $n \geq 8$. Data are shown as mean ± SD. Scale bar = 20 µm.

2.2.3 Active uptake of GSH depends on a proton gradient across the plasma membrane

Taking into consideration that the fast reduction of roGFP2 by efficient uptake of GSH, against a concentration gradient, indicates an active transport, feeding of GSH at lower temperature may give some indication to elucidate the way of transport. If metabolic and

catabolic processes slow down at lower temperatures, active transport would be expected to slow down as well.

To investigate the effect of cold treatment on GSH transport, GSH was supplied to five-day-old *rml1* seedlings at 4°C and 25°C for 20 h along with wild-type control. GSH supply to *rml1* seedlings at 25°C reduced cytosolic redox status. In contrast, GSH supply at 4°C did not reduce the *rml1* redox state. The oxidised redox status of *rml1* seedlings at 4°C in the presence of GSH indicated that there was no uptake of GSH and thus further supports the hypothesis of active transport. Wild-type seedlings confirmed that low temperature did not affect the roGFP2 redox status (Figure 2.41).
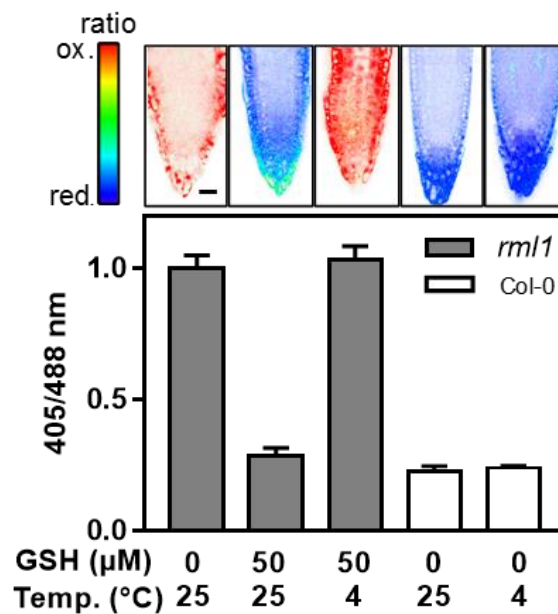
Figure 2.41: Effect of temperature on GSH uptake and roGFP2 redox state. Upper panel: pseudo-colour coded ratiometric images of the root tips of five-days-old seedlings of wild-type and *rml1* grown for 20 h in liquid ½ MS supplemented with and without GSH 50 µM GSH at 4°C and 25°C. Lower panel: ratiometric analysis of root tips indicating the average ratio of 405/488 nm. $n \geq 8$. Data are shown as means ± SD. Scale bar = 20 µm.

The net charge of GSH is negative and the negative membrane potential may prevent efficient GSH transport without an appropriate driving force. At the plasma membrane, P-type ATPases pump H^+ out of the cell and establish a pronounced H^+-gradient across the plasma membrane (Yan et al., 2002). Therefore, it was assumed that these H^+ neutralise the negative charge of GSH, allowing its transport across the plasma membrane via an unknown transporter. To assess the pH dependency of GSH transport, *rml1* seedlings were supplied with GSH at different external pH. GSH supply at pH 4.5, 5 and 5.6 completely reduced *rml1* redox status, indicating GSH uptake. In contrast, GSH feeding at pH 6.5 did not reduce the redox status of *rml1*. These data showed that at lower

pH GSH is efficiently taken up and suggest that uptake is proton dependent (Figure 2.42). As shown before, transport of GSH across the plasma membrane is pH dependent. To further explore that GSH transport is a proton dependent co-transport, vanadate, a well-known inhibitor of P-type ATPases (Bowman and Slayman, 1979), was used to inhibit proton flow at the plasma membrane.
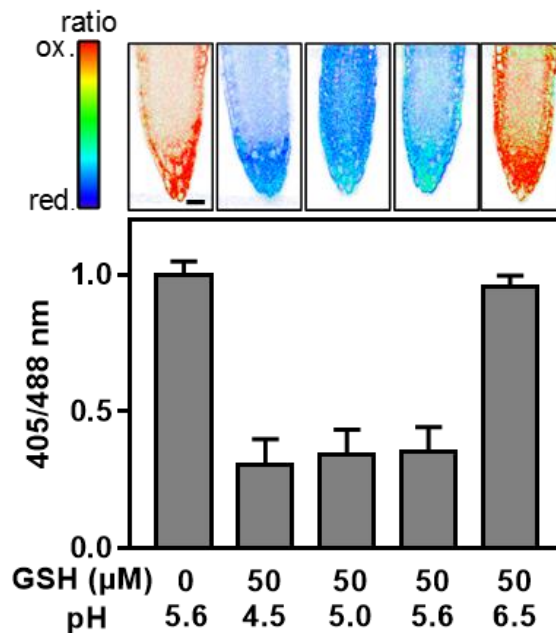
Figure 2.42: Effect of externally supplied GSH at different pH on roGFP2 redox state. Upper panel: pseudo-colour coded ratiometric images of the root tips of five-day-old rml1 seedlings grown for 20 h in liquid ½ MS supplemented with and without 50 µM GSH at different pH (4.5–6.5). Lower panel: ratiometric analysis of root tips indicating the average ratio of 405/488 nm. $n \geq 10$. Data are shown as means ± SD. Scale bar = 20 µm.

Five-day-old *rml1* seedlings were incubated for 20 h in ½ MS supplemented with 50 µM GSH or with 50 µM GSH and four different concentrations of vanadate (100, 200, 500 and 1000 µM). While GSH supply in the presence of 100 µM and 200 µM vanadate still partially reduced the redox state of roGFP2 in *rml1*, supply of GSH in the presence of 500 µM and 1000 µM vanadate did not reduce *rml1* cytosolic roGFP2 (Figure 2.43). The oxidised cytosolic roGFP2 in *rml1* in presence of GSH and vanadate suggests that vanadate inhibits ATPases and therefore abolishes the proton gradient required for GSH transport. Together, these data provide evidence that GSH uptake is a secondary active transport. To ensure that the inhibitory effect of vanadate on GSH uptake is specific and not caused by non-specific deleterious effects, the interference of vanadate with roGFP2 and cell integrity was tested. For this, redox measurement and PI labelling were

performed on five-day-old seedlings of *rml1* and wild-type grown for 20 h in ½ MS supplemented with 1 mM vanadate.
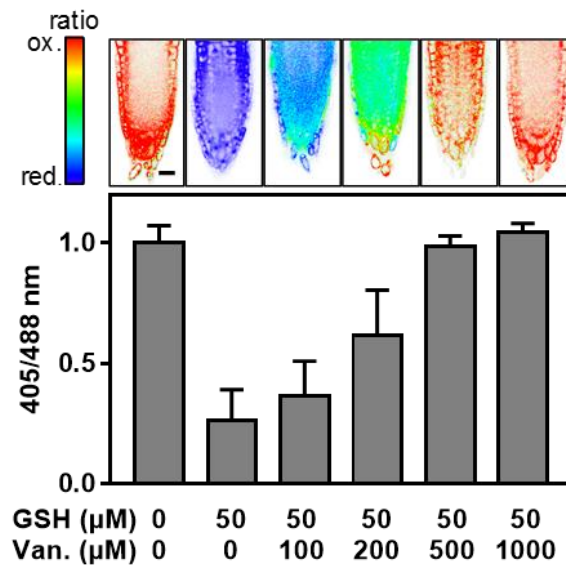
Figure 2.43: Effect of vanadate on GSH uptake. Upper panel: pseudo-colour coded ratiometric images of the root tips of five-day-old *rml1* seedlings grown for 20 h in liquid ½ MS supplemented with and without 50 µM GSH and 50 µM GSH with 100–1000 µM vanadate. Scale bar = 20 µm. Lower panel: ratiometric analysis of total images indicating the average ratio of 405/488 nm. $n \geq 10$. Data are shown as mean ± SD.

The pseudo-colour coded ratiometric images from roGFP2 redox measurements confirmed that vanadate did not affect roGFP2 fluorescence. Furthermore, PI staining verified that vanadate did not affect cellular integrity (Figure 2.44).
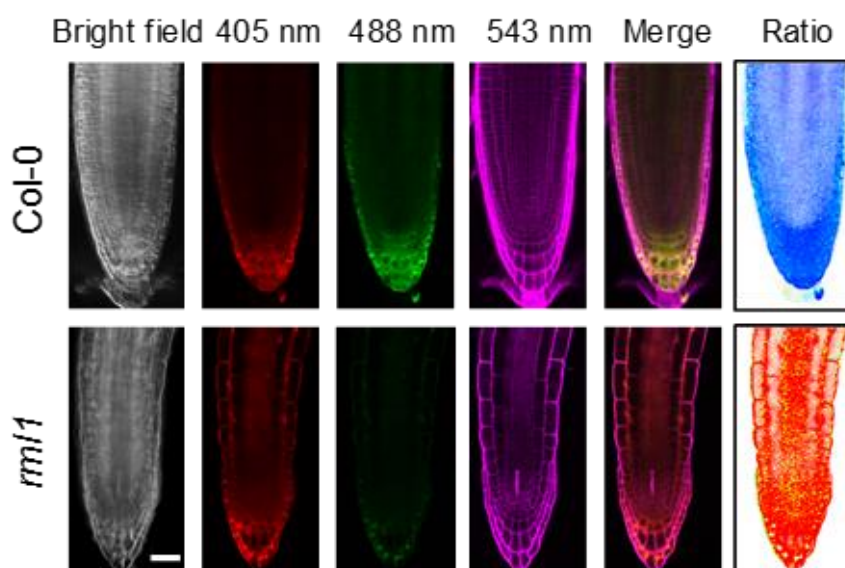
Figure 2.44: Effect of vanadate on roGFP2 and cell integrity. CLSM images showing bright field, 405 and 488 nm channels of roGFP2, 543 nm of PI, merge of 405, 488 and 543nm, and ratio image of 405/488 nm of roGFP2. Upper panel shows wild-type and lower panel shows *rml1* root tips. Scale bar = 20 µm.

2.2.4   Competitive inhibition of GSH uptake

In order to characterise the properties of the GSH transporter and ultimately identify the transporter, the first approach was to perform a competition assays of GSH with different substrates/chemicals. These competition assays might give some indications for the structure recognition by the transporter and could lead to the family of transporters.

2.2.4.1   Cysteine is a competitive inhibitor of GSH uptake

The tripeptide GSH is composed of amino acids, cysteine, glutamate and glycine. Therefore, the competition experiments of GSH with cysteine, glutamate, glycine and GSSG may give some indication for structure recognition by GSH transporter. To test whether individual amino acid residues of GSH and its oxidised form GSSG inhibit GSH uptake, five-day-old *rml1* seedlings were grown in ½ MS containing 50 µM GSH or 50 µM GSH plus 1 mM cysteine, glutamate, glycine or GSSG for 20 hours. The pseudo-colour coded ratiometric images showed that *rml1* seedlings grown on medium containing GSH and cysteine remained oxidised. In contrast, *rml1* seedlings grown on medium containing GSH and glycine, or GSH and GSSG were reduced. The *rml1* seedlings grown on GSH and glutamate remained partially oxidised (Figure 2.45).
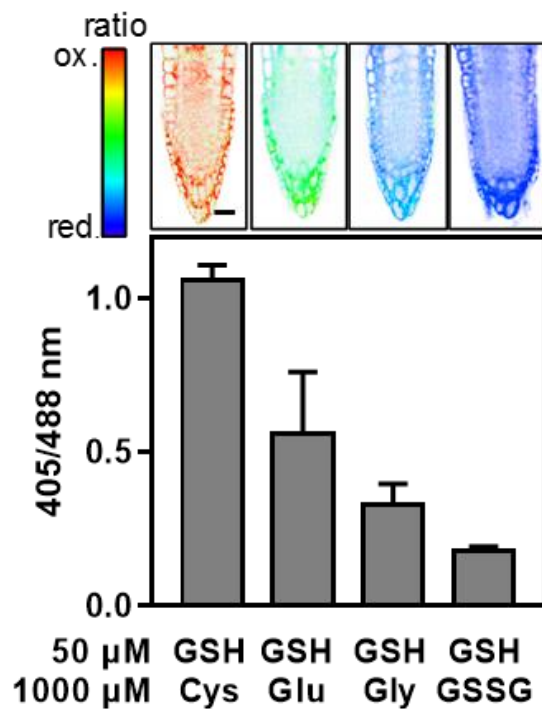
Figure 2.45: Redox imaging of GSH uptake in presence of Cys, Glu, Gly or GSSG. Upper panel: pseudo-colour coded ratiometric images of the root tips of five-day-old *rml1* seedlings grown for 20 h in liquid ½ MS supplemented with 50 µM GSH with 1 mM of Cys, Glu, Gly and GSSG. $n \geq 10$. Data are shown as means ± SD. Scale bar = 20 µm.

In summary, these results suggest that glutamate partially and cysteine very efficiently prevent GSH uptake.

2.2.4.2 BSO is a competitive inhibitor of GSH uptake

Since glutamate partially prevented GSH uptake in the competition assay, BSO that mimic of the γ-glutamylcysteine adduct, was used in a competition assays. BSO is a well-known inhibitor of GSH1 and has been extensively used for glutathione depletion in cell culture and *in vivo* model systems (Biterova and Barycki, 2010). BSO binds with its S-butyl group to the L-cysteine-binding site of GSH1 (Campbell et al., 1991). Furthermore, the glutathione transporters at plastidic membrane: CLTs also mediate transport of BSO to plastids (Maughan et al., 2010). Based on the structural similarities one can speculate that BSO and GSH might be transported by the same transporter across the plasma membrane. To test whether GSH uptake is inhibited by BSO, five-day-old seedlings of *rml1* were transferred to liquid ½ MS containing 50 µM GSH or 50 µM GSH and 100, 500 and 1000 µM BSO. The data from redox imaging revealed that redox state of *rml1* was only reduced on media supplemented with 50 µM GSH but was not reduced on media contain 50 µM GSH with different concentration of BSO. The oxidised redox state of *rml1* on media containing both GSH and BSO indicate that BSO completely inhibits GSH uptake and suggest that, similar to cysteine, BSO is also a competitive inhibitor of GSH (Figure 2.46).

Figure 2.46: GSH uptake in the presence of BSO. Upper panel: pseudo-colour coded ratiometric images of the root tips of five-days-old *rml1* seedlings grown for 20 h in liquid ½ MS supplemented with 50 µM GSH and different concentration of BSO (100–1000 µM). Lower panel: ratiometric analysis of root tips indicating the average ratio of 405/488 nm. $n \geq 8$. Data are shown as mean ± SD. Scale bar = 20 µm.

2.2.4.3 BSO did not prevent uptake of high concentrations of GSSG

To test whether BSO competes also with GSSG uptake at the plasma membrane, five-day-old *rml1* seedlings were transferred to liquid ½ MS containing different concentrations of GSSG with and without 1 mM BSO along with wild-type control. The data from pseudo-colour coded ratiometric images indicate that wild-type seedlings grown on ½ MS were reduced and *rml1* were oxidised. Moreover, *rml1* seedlings transferred for 20 h to ½ MS containing GSSG or GSSG plus 1 mM BSO were reduced (Figure 2.47). These data confirm that BSO did not compete with GSSG uptake.
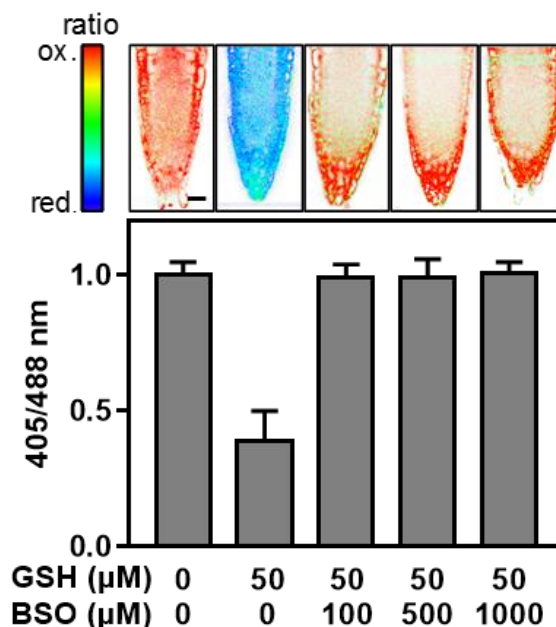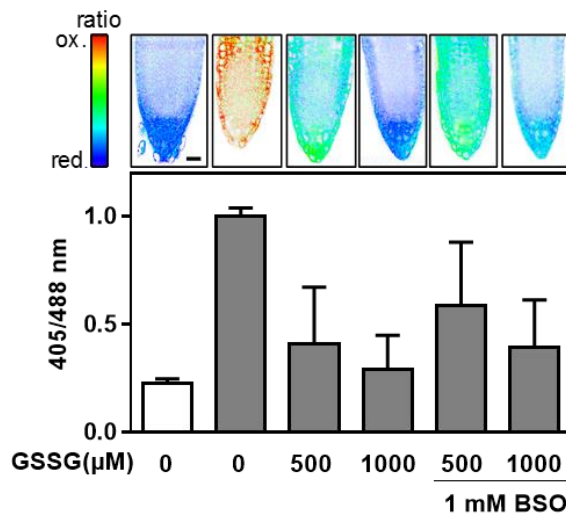

Figure 2.47: GSSG uptake in the presence of BSO. Upper panel: pseudo-colour coded ratiometric images of the root tips of five-days-old of wild-type control (white) and *rml1* (grey) seedlings grown for 20 h in liquid ½ MS supplemented with and without 500 and 1000 µM GSSG in absence and presence of 1 mM BSO. Lower panel: ratiometric analysis of root tips indicating the average ratio of 405/488 nm. $n \geq 8$. Data are shown as means ± SD. Scale bar = 20 µm.

2.2.4.4 S-hexyl-GSH is a competitive inhibitor of GSH uptake

For further studies along the line of GSH transport competition, analogues of GSH, BSO and glutamate were tested for GSH uptake competition. Glutathione sulfonic acid (GSA) and S-hexyl-glutathione (S-hexyl-GSH) were used as analogues for GSH, glutamine (Gln) and aspartate (Asp) as analogues for glutamate and methionine sulfoximine (MSO) as analogues for BSO. Furthermore, KNO_3 was used in the competition assay, as many several members of nitrate transporter 1/peptide transporter (NPF) family transport transports di- and tripeptides (Léran et al., 2014). To investigate these substrates for GSH uptake competition, five-day-old *rml1* and wild-type seedlings were transferred to ½ MS supplemented with and without 50 µM GSH or with 50 µM GSH and 1 mM of GSA, S-hexyl-GSH, Gln, Asp or KNO_3. First, these substrates were tested independently for interference with roGFP2. The redox state of wild-type seedlings on ½ MS supplied with 1 mM of GSA, S-hexyl-GSH, Gln, Asp or KNO_3 was reduced, whereas *rml1* seedlings were

oxidised. The pseudo-colour coded ratiometric images of wild-type and *rml1* seedlings root tips showed that none of these substrates affected the roGFP2 redox state in 20 h (Figure 2.48 A–B). Subsequently, GSH competition assays were performed in ½ MS containing 50 μM GSH alone or with 1 mM of MSO, GSA, S-hexyl-GSH, Gln, Asp or KNO₃. The pseudo-colour coded ratiometric images indicate that roGFP2 were reduced in *rml1* seedlings treated with GSA, Asp and KNO₃ in presence of GSH, suggesting that these substrates did not inhibit GSH uptake.
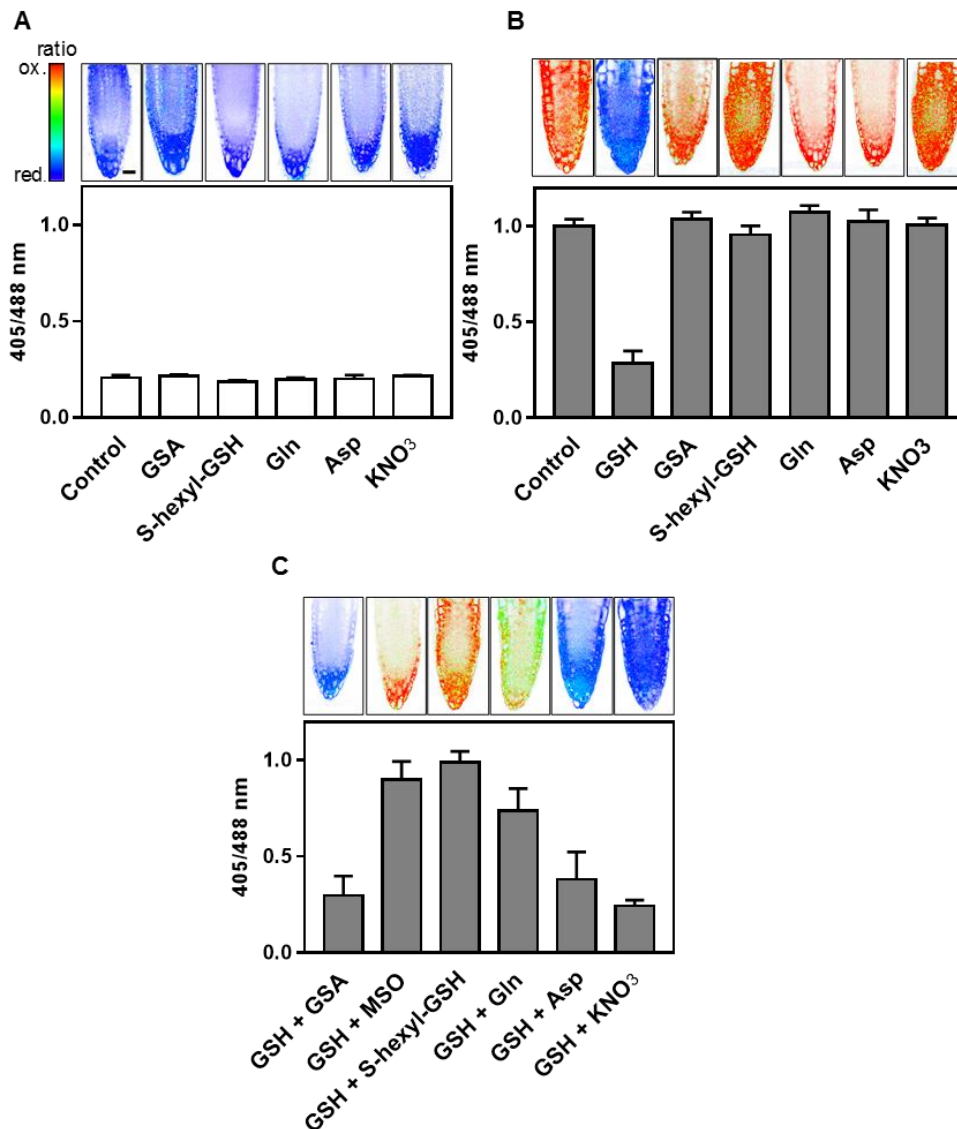
Figure 2.48: RoGFP2 based competition assay of different substrate with GSH uptake. Five-day-old seedling were grown for 20 h in ½ MS with different substrates. **(A)** Upper panel: pseudo-colour coded ratiometric images of the root tips of wild-type treated with 1 mM of GSA, S-hexyl-GSH, Gln, Asp and KNO₃ along with untreated wild-type control. Lower panel: ratiometric analysis of root tips indicating the average 405/488 nm ratio. **(B)** Upper panel: pseudo-colour coded ratiometric images of the root tips of *rml1* treated with 1 mM of GSA, S-hexyl-GSH, Gln, Asp and KNO₃ along with untreated *rml1* control. Lower panel: ratiometric analysis of total images indicating the average 405/488 nm ratio. **(C)** Upper panel: pseudo-colour coded ratiometric images of the root tips of *rml1* treated with 50 μM GSH along with 1 mM of GSA, S-hexyl-GSH, Gln, Asp and KNO₃. Lower panel: ratiometric analysis of root tips indicating the average 405/488 nm ratio. $n \geq 8$. Data are shown as means ± SD. Scale bar = 20 μm.

In contrast, Gln and MSO treated *rml1* seedlings in presence of GSH, roGFP2 were partially oxidised, indicating that Gln and MSO both partially inhibit the GSH uptake. Furthermore, *rml1* seedlings supplied with S-hexyl-GSH in presence of GSH were completely oxidised, suggesting that S-hexyl-GSH also inhibits GSH uptake (Figure 2.48 C).

2.2.5 Auxin effect on external GSH uptake

It has been reported that the Nitrate transporter 1/peptide transporter (NPF) family in plants transport a wide variety of substrates such as nitrate, peptides, amino acids, dicarboxylates, glucosinolates, indole-3-acetic acid (IAA), abscisic acid (ABA) (Léran et al., 2014). Since some NPFs transport peptides, the assumption made was if a member of NPF family may also be involved in GSH transport. Because AtNPF6.3 (old name NRT1.1) has been reported to transport IAA (Krouk et al., 2010), a competition assay for GSH and IAA was performed. Both natural auxin (IAA) and the synthetic auxins, 1-naphthaleneacetic acid (NAA) and 2,4-diclorophenoxyacetic acid (2,4-D) were tested for their ability to inhibit the uptake of GSH. Five-day-old wild-type and *rml1* seedlings were transferred to ½ MS supplemented with 100 μM IAA, NAA or 2,4-D with and without 50 μM GSH. RoGFP2 in the cytosol of wild-type seedlings supplied with 100 μM IAA and 50 μM GSH were reduced while in *rml1* seedlings were oxidised. The pseudo-colour coded ratiometric images of wild-type and *rml1* root tips revealed that GSH supply in presence of all three different types of auxin did not affect roGFP2 redox status, suggesting that auxins inhibit GSH uptake (Figure 2.49 A–B). Furthermore, the effect of NaOH and EtOH on roGFP2 redox state were tested, as auxin solution was prepared in these solvents. Both, NaOH and EtOH, did not interfere with roGFP2 redox state in the wild-type seedlings and nor in the *rml1* mutant seedlings (Figure 2.49 C). Alternatively, the inhibition of GSH uptake by auxins was tested with MCB and PI labelling on five-day-old *rml1* seedlings supplied with auxin and GSH.
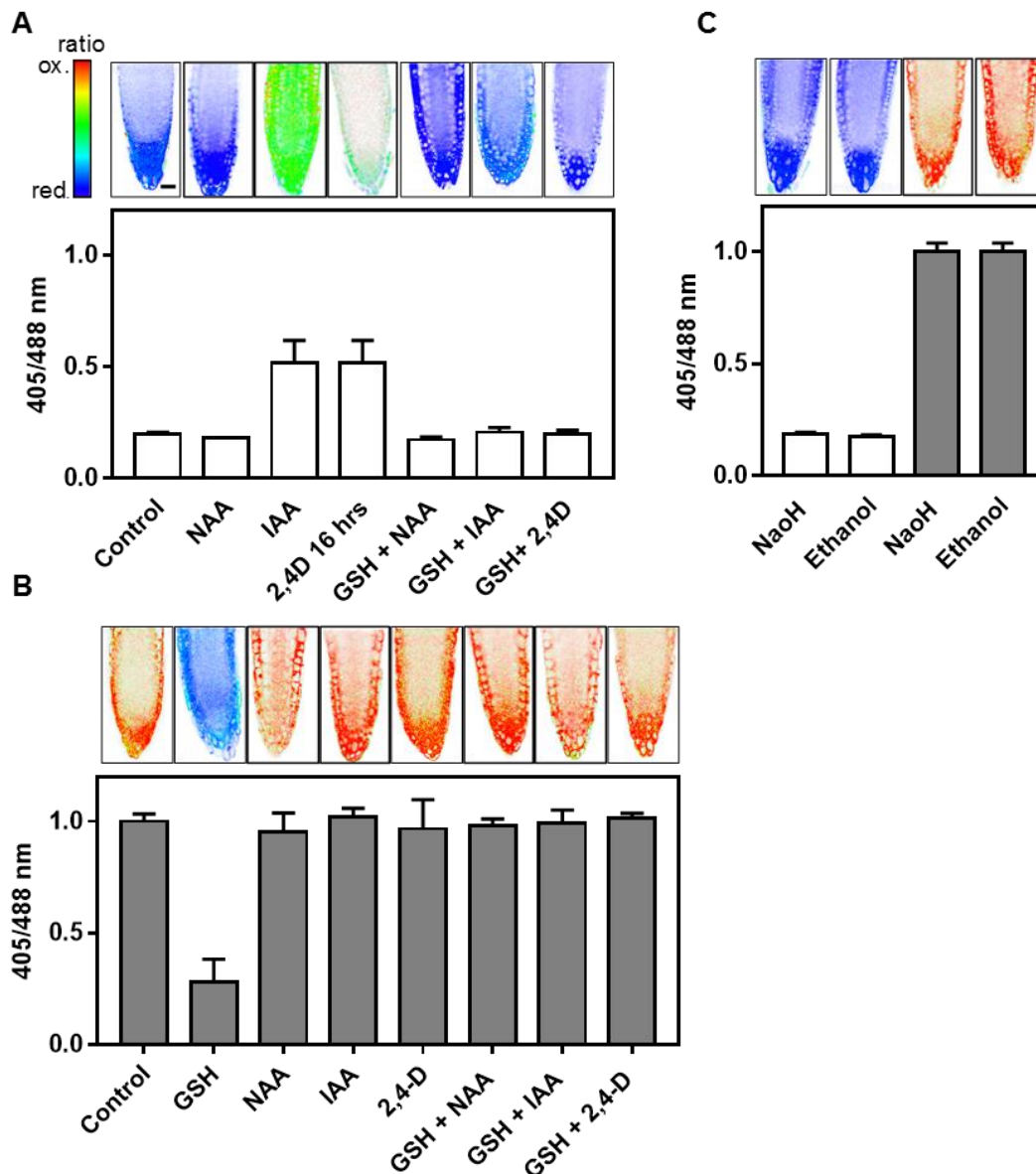
Figure 2.49: RoGFP2 based competition assay of GSH uptake in presence of IAA, NAA and 2,4D.
Five-day-old seedling grown for 20 h in ½ MS with different substrates **(A)** Upper panel: pseudo-colour coded ratiometric images of the root tips of wild-type treated with 50 µM GSH and 100 µM of IAA, NAA and 2,4D along with untreated wild-type control. Lower panel: ratiometric analysis of root tips indicating the average 405/488 nm ratio (white bar). **(B)** Upper panel: pseudo-colour coded ratiometric images of the root tips of *rml1* treated with 50 µM GSH and 100 µM of IAA, NAA and 2,4D along with untreated *rml1* control. Lower panel: ratiometric analysis of root tips indicating the average 405/488 nm ratio (grey bar). **(C)** Upper panel: pseudo-colour coded ratiometric images of the root tips of wild-type (white bar) and *rml1* (grey bar) treated with 1 N NaOH and absolute EtOH. Lower panel: ratiometric analysis of root tips indicating the average 405/488 nm ratio of wild-type (white bar) and *rml1* (grey bar). $n \geq 10$. Data are shown as means ± SD. Scale bar = 20 µm.

The *rml1* seedlings supplied with 50 µM GSH showed intense MCB labelling, while *rml1* seedlings supplied with 50 µM GSH in presence of 100 µM IAA or 100 µM NAA showed very little or even no MCB labelling. PI staining verified cellular integrity (Figure 2.50). These results are in line with roGFP2-based redox measurements in which auxins

prevented the reduction of roGFP2 by externally supplied GSH (Figure 2.49 B). Hence, MCB and PI labelling further confirmed the inhibition of GSH uptake by auxin.
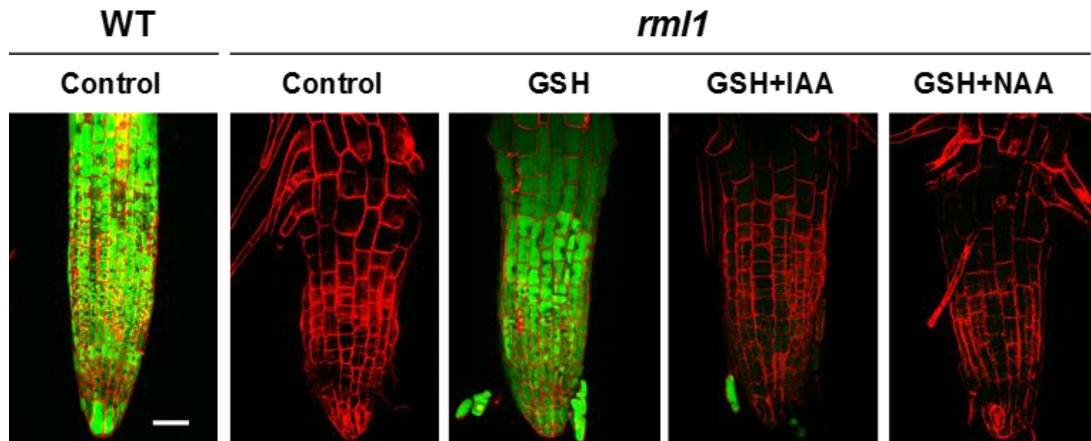
Figure 2.50: MCB labelling of GSH, IAA and NAA treated seedlings. Five-day-old *rml1* seedlings grown on ½ MS supplemented with and without 50 µM GSH and 100 µM IAA or NAA along with untreated wild-type seedlings as a control. Representative images of *rml1* and wild-type root tips stained with MCB to assess the cellular glutathione pools by CLSM (green). Propidium iodide (PI) staining of *rml1* root tips confirmed cell integrity (red). Scale bar = 20 µm.

2.2.5.1 GSH and the auxin-dependent gravity response

It has been reported that auxin transport controls a number of important growth and developmental processes, including the gravity response. In roots, IAA is transported with two different polarities, acropetally (*i.e.* from shoot to root apex) via the central cylinder and basipetally (i.e. from apex toward the base) along the outer cell layers. The acropetal transport of IAA has been implicated in control of lateral root development, whereas the basipetal movement of IAA has been linked to gravity response (Rashotte et al., 2001). Given that auxin inhibits GSH uptake, it was further hypothesised that GSH may vice versa also interfere with the normal gravity response of roots. To test this hypothesis, four-day-old wild-type seedlings were grown on ½ MS with or without GSH. On day four, plates were rotated 135° for two days (Figure 2.51 A-B). The seedlings were documented, using binocular microscopy and bending angles were measured using Adobe© Illustrator. The gravity response of GSH-treated seedlings was significantly less pronounced than in untreated seedlings, indicated by bending angles (Figure 2.51 C-D). These results showed that GSH interfere with gravity response. This might be due to auxin transport inhibition by GSH. Hence, GSH interference with the normal gravity response provides some further evidence for a functional link between IAA signalling and GSH transport.
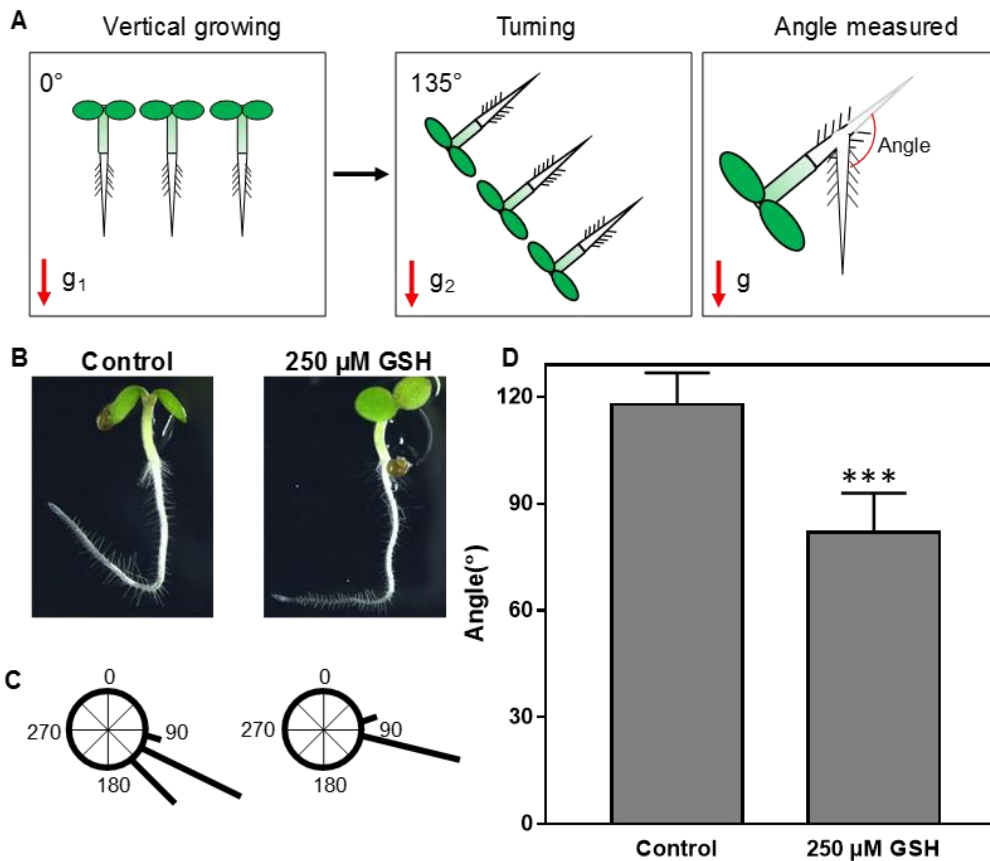
Figure 2.51: GSH interferes with the gravity response of roots. (A) Cartoon illustrating the gravity experiment; **(B)** Root gravity response of four-day-old wild-type seedlings germinated with and without 250 µM GSH at 0° (g₁) and rotated at 135° (g₂) for two days; **(C)** Circular histogram indicating the bending angle of different seedlings grown on control medium without GSH and medium supplemented with 250 mM GSH; **(D)** Quantitative analysis of the gravity response. Values are means of bending angles from ≥ 14 biological replicates; error bars = SD. Asterisks indicate significant differences (Student t-test; p-value ≤0.05).

2.2.5.2 External supply of GSH inhibits auxin accumulation in root tips

Taking into consideration the partial inhibition of the gravity response by GSH, the GSH-auxin cross-talk was further tested by using Col-0 seedlings expressing auxin responsive construct DR5:GUS (Chen et al., 2013). To test whether external GSH supply inhibits IAA transport, five-day-old Col-0 seedlings expressing DR5:GUS were supplied with 100 µM IAA in the presence and absence of 100 µM GSH. Results from this experiment indicate that external GSH supply suppresses GUS expression in the absence of external IAA (Figure 2.52 A). However, the suppression of the GUS expression was only partial in the presence of external IAA (Figure 2.52 B).
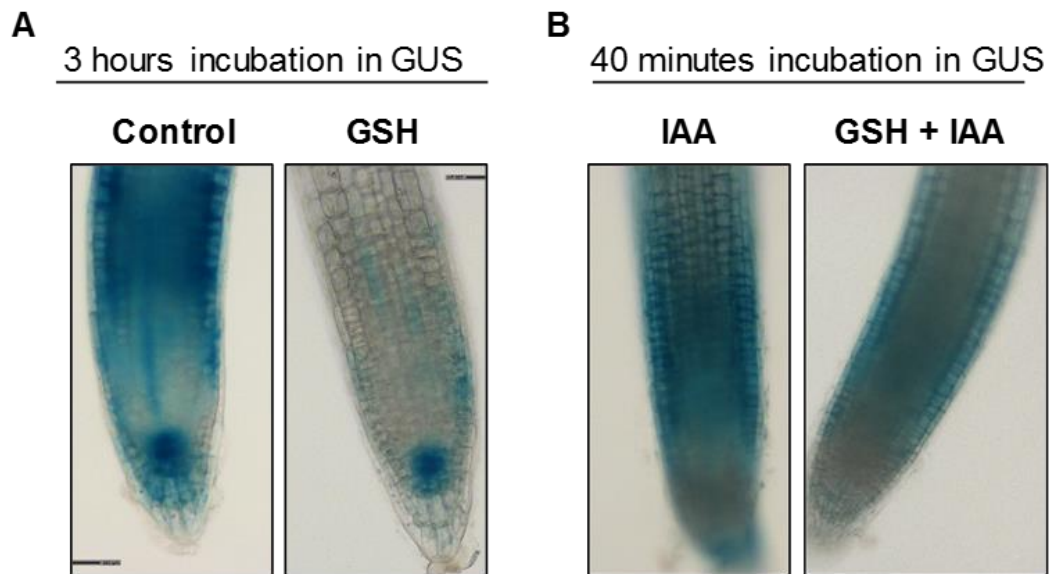
Figure 2.52: Effect of externally supplied GSH on DR5:GUS expression in root tips. Representative images of five-day-old seedling roots of wild-type expressing DR5:GUS grown for 20 h in ½ MS supplemented **(A)** with or without 100 µM GSH and incubated for three hours in GUS staining solution. **(B)** Roots grown in medium with 100 µM IAA in the absence and presence of 100 µM GSH and incubated for 40 min for GUS staining solution.

2.2.5.3 Impaired auxin transport did not affect GSH levels in roots

Inhibition of GSH uptake by IAA may indicate that auxin and GSH are transported through the same or related transport systems. For auxin transport, AUX1 has been identified as a high affinity auxin transporter in the plasma membrane responsible for uptake of IAA from the apoplast (Yang et al., 2006). To test whether genetically impaired auxin transport affects the cellular glutathione pool, two AUX1 mutants, *aux1-21* and *aux1-22*, were tested for their glutathione pool and cellular integrity through labelling with MCB and PI, respectively. The MCB labelling was very similar for the wild-type and both auxin mutants and PI labelling verified cellular integrity in all lines (Figure 2.53). These results suggest that deletion of AUX1 did not affect the steady state glutathione pool.
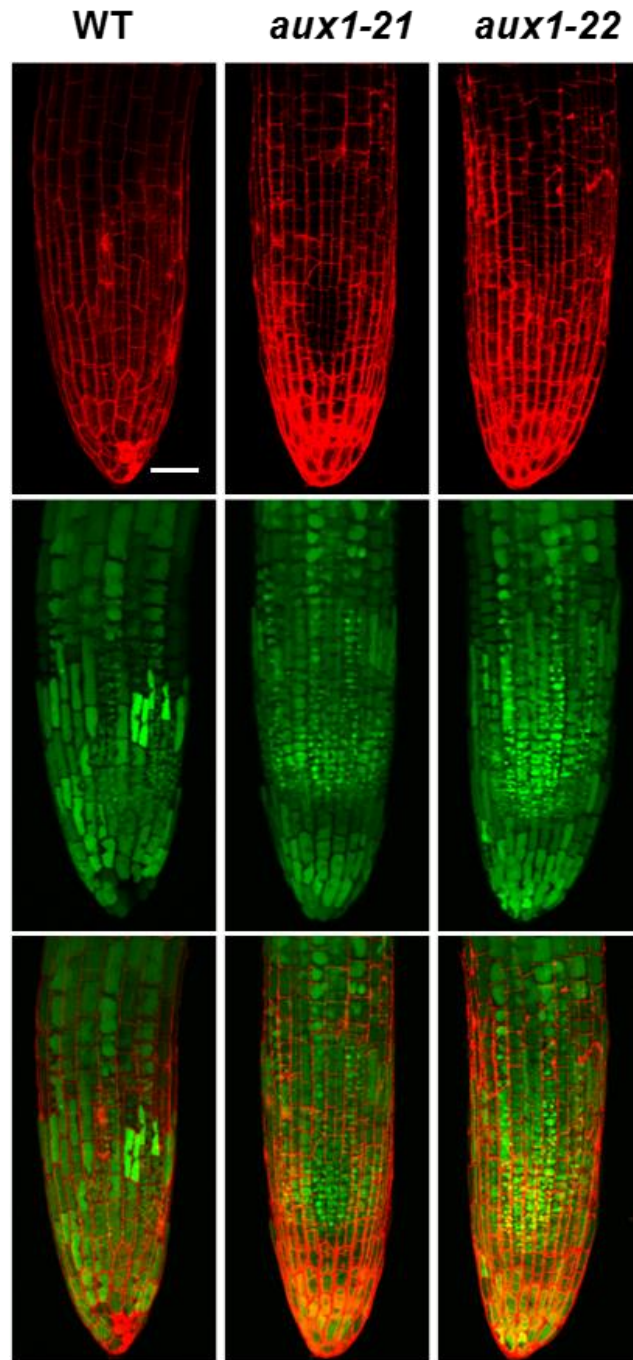
Figure 2.53: MCB labelling of auxin transport mutants. MCB labelling of five-day-old seedlings of wild-type, *aux1-21 and aux1-22* mutants grown on ½ MS solidified with 0.8% phytagel. Representative images of wild-type, *aux1-21 and aux1-22* seedling root tips stained with MCB to assess the cellular glutathione pool by CLSM. Propidium iodide (PI) staining verified cellular integrity. From top to bottom, PI labelling (exc. 543 nm), MCB labelling (exc. 405 nm) and merge of PI and MCB. Scale bar = 20 μm.

2.2.5.4 *aux1-21* null mutants show increased resistance to BSO

Since BSO inhibits GSH uptake, the *aux1-21* mutant was tested for its BSO sensitivity. Wild-type and *aux1-21* seeds grown on ½ MS supplemented with different concentration of BSO (0, 0.2 and 0.5 mM). The data from BSO treatment showed that the root length of

wild-type seedlings decreased with increased BSO concentrations. While there was also partial growth inhibition by BSO in *aux1-21* seedlings, the inhibition was far less pronounced. The effect of BSO on the cellular glutathione pool was further assessed by MCB staining of root tips grown on different concentrations of BSO. The MCB fluorescence in wild-type seedlings grown on 0.5 mM BSO was significantly less intense than *aux1-21*, suggesting that upon BSO treatment the glutathione pool depleted faster in wild-type than *aux1-21* (Figure 2.54 A-B). These results indicate that *aux1-21* was resistant to BSO and retained glutathione pool in presence of BSO. Resistance of *aux1-21* to BSO provided some further evidence that AUX1 may also transport GSH.
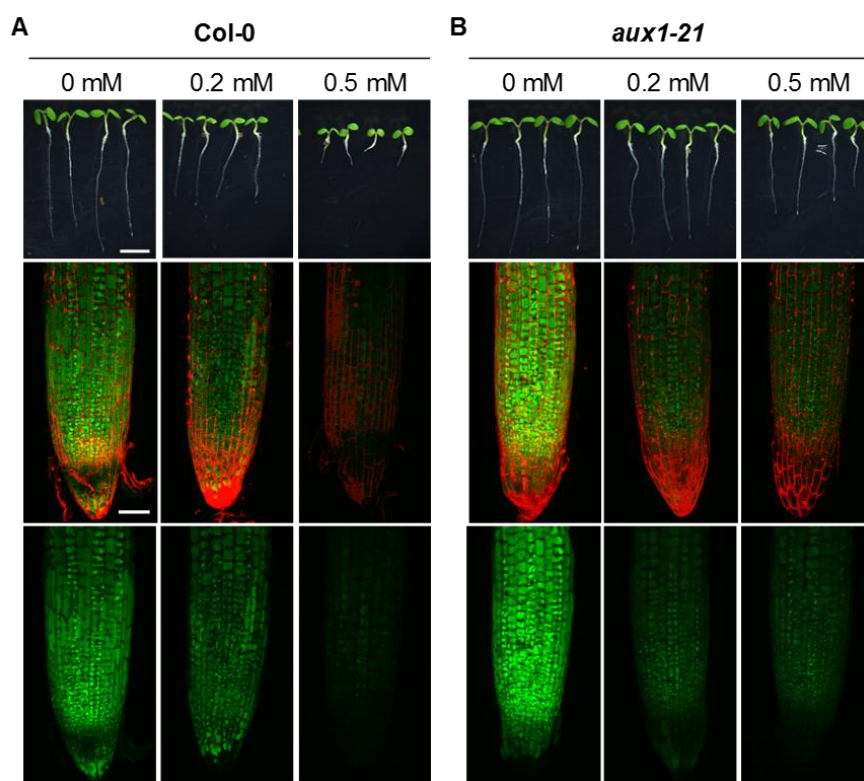
Figure 2.54: MCB labelling of *aux1-21* and wild-type root tips. Wild-type and *aux1-21* seedlings were grown on ½ MS with 0.8% phytagel supplemented with different concentration of BSO (0, 0.2 and 0.5 mM) for five days. **(A)** Phenotype of wild-type seedlings with and without BSO (upper panel). Representative images of root tips stained with MCB and PI displayed as maximum projections for MCB plus PI (second row) or only MCB (bottom row), respectively. **(B)** Phenotype of *aux1-21* seedlings with and without BSO (upper panel). Representative images of root tips stained with MCB and PI (lower panels). Scale bar = 20 μm.

2.2.5.5 Auxin transport is impaired by GSH

DII-VENUS is a Aux/IAA-based auxin signalling sensor that consists of a fast maturing yellow fluorescent protein fused in frame to Aux/IAA auxin-interaction domain (termed domain II; DII) and expressed under a constitutive promoter. This sensor provides a map of relative auxin distribution in different tissues. Auxin sensing is dependent on the rapid

degradation of the probe in response to exogenous auxin (Brunoud et al., 2012). To test inhibition of IAA transport by GSH, five-day-old seedlings expressing DII-VENUS were transferred to liquid ½ MS supplemented with or without 200 nM IAA and 100 µM GSH. The data from confocal images showed a strong fluorescence of sensor in control seedlings. Incubation of seedlings with only IAA resulted in an almost complete degradation of the sensor within 25 min. The incomplete degradation of sensor in seedlings treated with IAA in the presence of GSH suggest that GSH inhibits the IAA uptake (Figure 2.55 A). Furthermore, seedlings were incubated in PI for testing cellular integrity, upon treatment with IAA, but surprisingly the PI signal vanished completely; a possible explanation is that IAA somehow quenches the PI signal by an unknown mechanism (Figure 2.55 B).
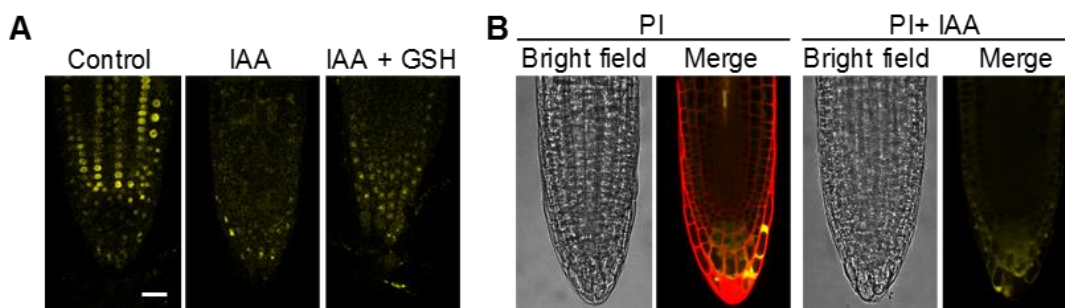
Figure 2.55: GSH and IAA uptake in wild-type seedling expressing DII-VENUS. Five-day old wild-type seedlings expressing DII-VENUS were incubated for 25 min in ½ MS supplemented with 200 nM IAA or 200 nM IAA + 100 µM GSH. **(A)** Representative images of root tips incubated in IAA with or without GSH. **(B)** Representative images of wild-type root tips stained with 50 µM PI in the absence and presence of 200 nM IAA. Scale bar = 20 µm.

2.2.6 High external GSH concentrations effect on root growth

As described previously, supply of different concentration of external GSH rescue the *rml1* growth phenotype. Furthermore, *rml1* seeds germinated on 250 µM, 1 mM and 2 mM GSH showed a similar recovery without any apparent inhibitory effect on root growth (Figure 2.56 A). However, wild-type seedlings germinated on 1 mM GSH showed a significantly shorter primary roots length (almost 30 % shorter) compared to the untreated wild-type seedlings (Figure 2.56 B–C).
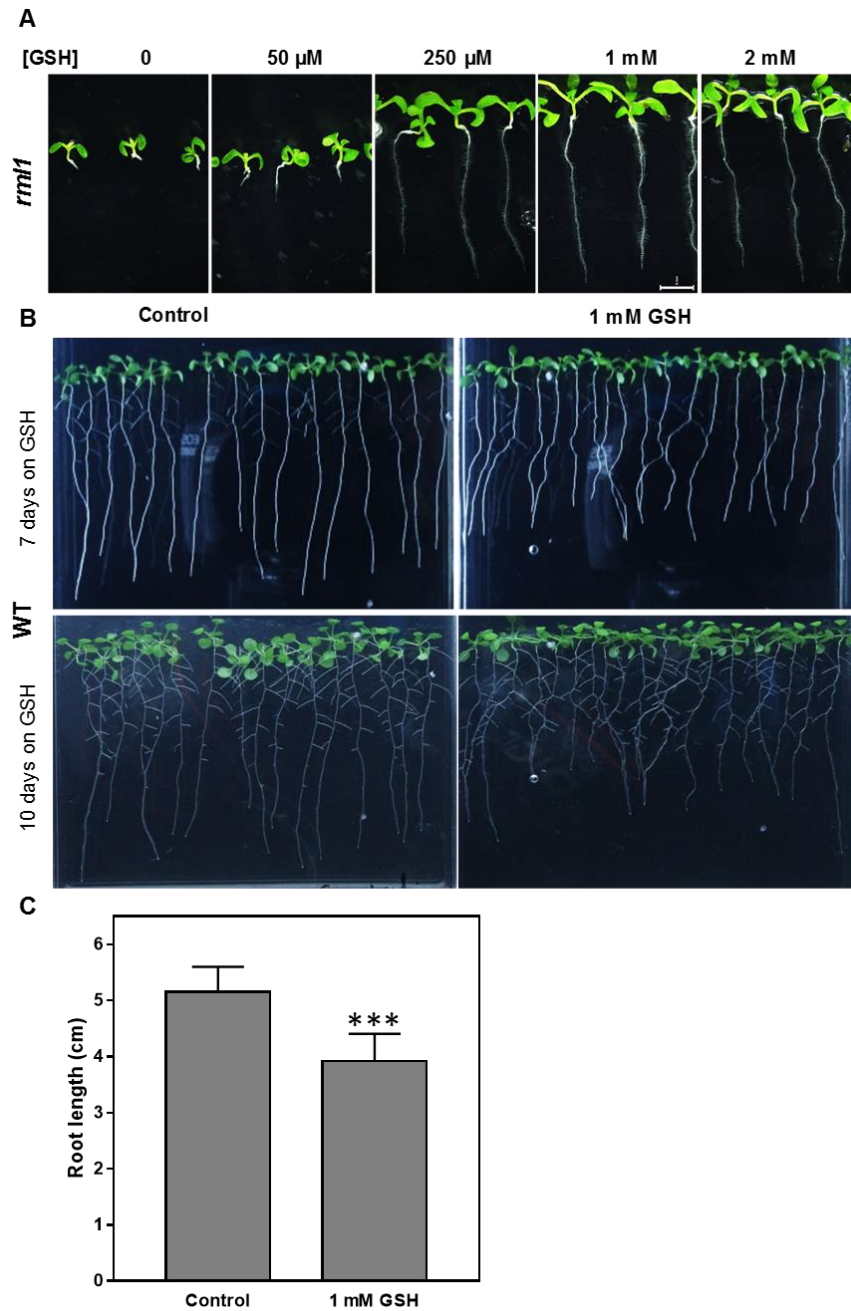
Figure 2.56: Effect of externally supplied GSH on root growth of *rml1* and wild-type. (A) Five-day-old *rml1* seedling grown on ½ MS supplemented with 0, 50, 250, 1000 and 2000 µM GSH for ten days. **(B)** Wild-type seedling grown for seven and ten days on ½ MS supplemented with and without 1 mM GSH. C) Values are mean of $n \geq 16$ biological replicates; error bars = SD of biological replicates. Strick indicate significant differences (Student t-test; *p*-value ≤0.05).

2.2.7 Rescuing of the growth phenotype of grafted *rml1* shoots by wild-type roots

To investigate the root to shoot long-distance GSH transport, a grafting was performed on five-day-old *rml1* and wild-type seedlings. Grafting was attempted with the *rml1* shoot grafted on wild-type roots and *vice versa*. The grafting from *rml1* shoots on wild-type

71

roots was successful and led to partial recovery of growth of the *rml1* shoot, and these grafted seedlings reached to flowering and produced small siliques, but did not produce seeds (Figure 2.57). However, the wild-type shoot grafted on *rml1* roots was not successful due to the very short root of this mutant. The rescue of grafted *rml1* shoots on wild-type roots provides evidence for long-distance transport of glutathione from root to shoot.
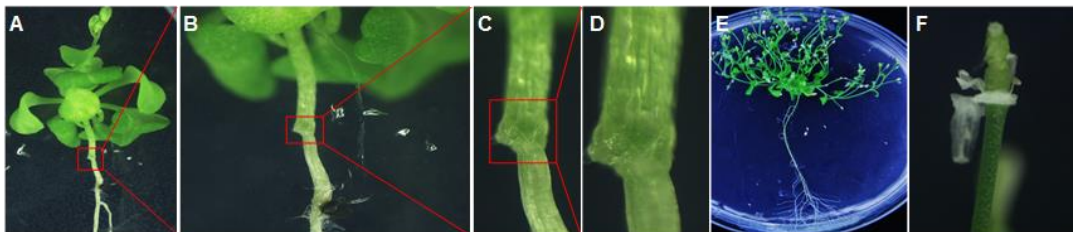
Figure 2.57: Grafting of *rml1* shoot on wild-type root. Five-day-old wild-type and *rml1* grown on ½ MS with 0.8% phytagel were used for grafting. **(A-D)** Red squares indicates the two weeks old grafted area of *rml1* shoot on wild-type root. **(E)** Six-week-old grafted plant. **(F)** Small seedless silique of six-week-old grafted plants.

2.2.7.1 *At*OPT4 is not the only transporter at plasma membrane

It has been reported that OPT4 is low affinity glutathione transporter. To also test that OPT4 is not the only transporter for GSH transport at plasma membrane, double mutant of *opt4* with *rml1* and *gsh1* were generated. Furthermore, to prove that AUX1 is the high affinity glutathione transporter, double mutants of *aux1* with *rml1* and *gsh1* were as well generated. The confirmation of the double mutants was done by genotyping PCR with gene specific primers (Figure 2.58).
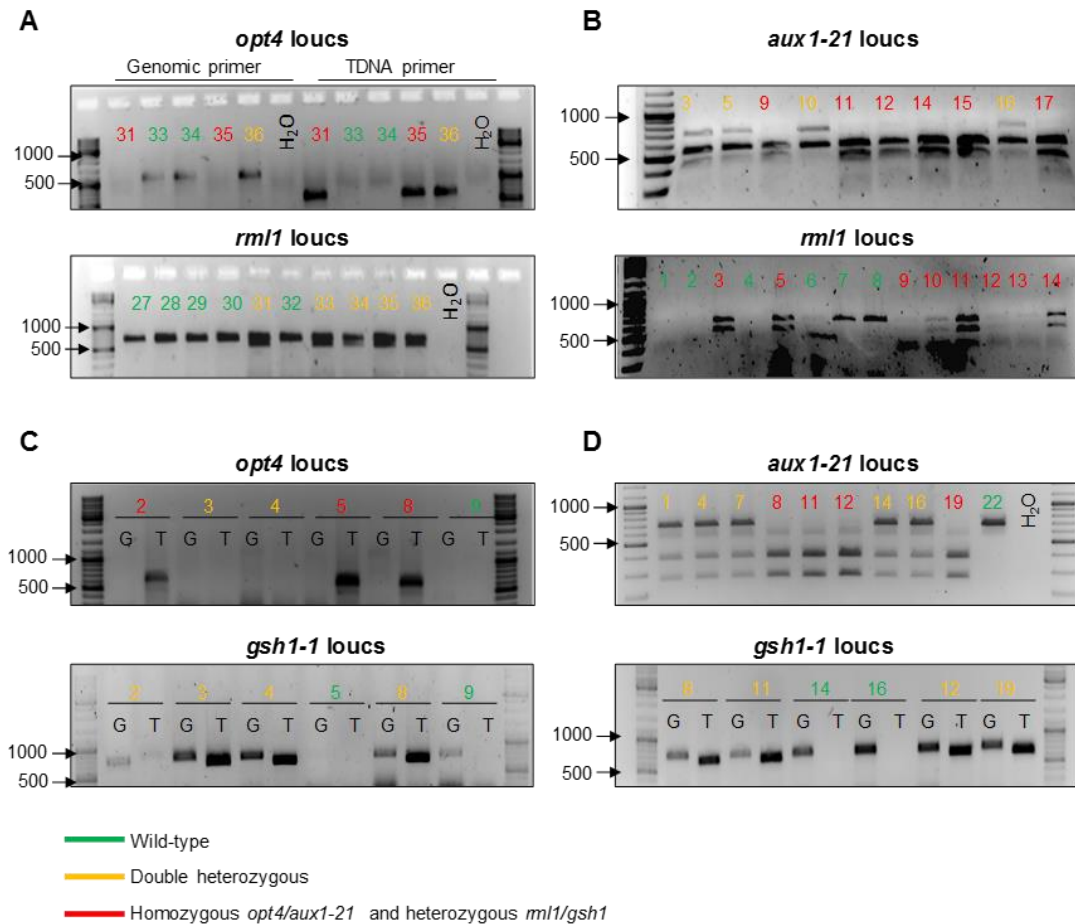
Figure 2.58: Genotyping PCR of *aux1, opt4, rml1* and *gsh1* double mutants. Agarose gel of genotyping PCR with gene and T-DNA specific primers of double mutants **(A)** *opt4rml1*. **(B)** *aux1-21rml1*. C) *opt4gsh1-1*. D) *aux1-21gsh1-1*. "G" indicates wild-type locus, T indicates the respective T-DNA locus. PCR product of *aux2-1* and *rml1* was digested with APaL1 and ApoI restriction enzymes, respectively.

Five-day-old seedlings of *rml1* and *opt4rml1* expressing cytosolic roGFP2 were grown in ½ MS supplemented with or without 50 µM GSH for 20 hours along with untreated wild-type control. The pseudo-colour coded ratiometric images showed that roGFP2 was remained oxidised in *rml1* and *opt4rml1* seedlings grown on ½ MS medium. In contrast, *rml1* and *opt4rml1* seedlings grown on ½ MS medium containing GSH showed fully reduced roGFP2 to wild-type level (Figure 2.59). In summary, these results prove that *At*OPT4 is not the only transporter at plasma membrane and suggests the presence of another high affinity GSH transporter.
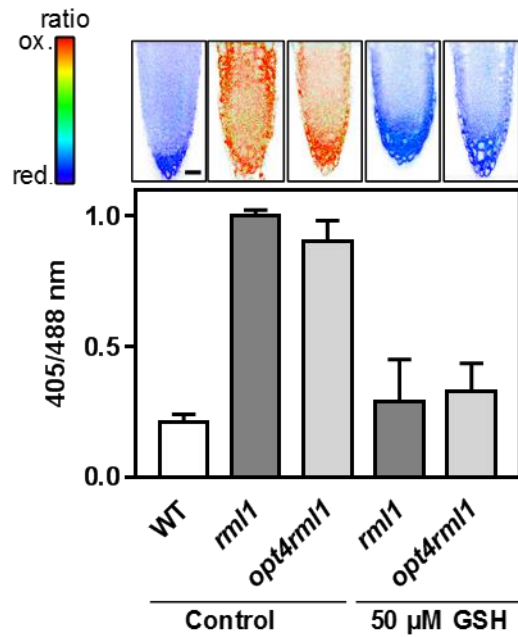
Figure 2.59: Redox imaging of WT, *rml1* and *opt4rml1* double mutants grown on ½ MS supplemented with GSH. Upper panel: pseudo-colour coded ratiometric images of the root tips of five-day-old *rml1* and *opt4rml1* seedlings grown for 20 h in liquid ½ MS supplemented with and without 50 µM GSH along with untreated wild-type as a control. Lower panel: ratiometric analysis of root tips of wild-type (white bar), *rml1* (dark grey bars) and *opt4rml1*(light grey bars) indicating the average ratio of 405/488 nm. $n \geq 10$. Data are shown as mean ± SD. Scale bar = 20 µm.

2.2.8 Glutathione transport analysis in yeast cells

Glutathione transport has been extensively studied in yeast and has led to the discovery of a high affinity glutathione transporter (Hgt1p) (Bourbouloux et al., 2000). In section 2.2.4.2, inhibition of GSH uptake by BSO in Arabidopsis roots suggests that both GSH and BSO might be taken up into the cell by the same transporter. To test whether Hgt1p in yeast might have similar properties, it was investigated whether BSO would also interfere with GSH uptake in yeast cells and with yeast GSH homeostasis in general.

2.2.8.1 Effect of BSO on yeast growth

As BSO inhibits GSH transport in Arabidopsis, it was hypothesised that Hgt1P in yeast may also transport BSO. To test this hypothesis, wild-type yeast (BY4742) cells were first grown on different concentration of BSO (1–10 mM). The results from spotting assay showed that surprisingly wild-type yeast strain were growing normally even on 10 mM BSO (Figure 2.60).
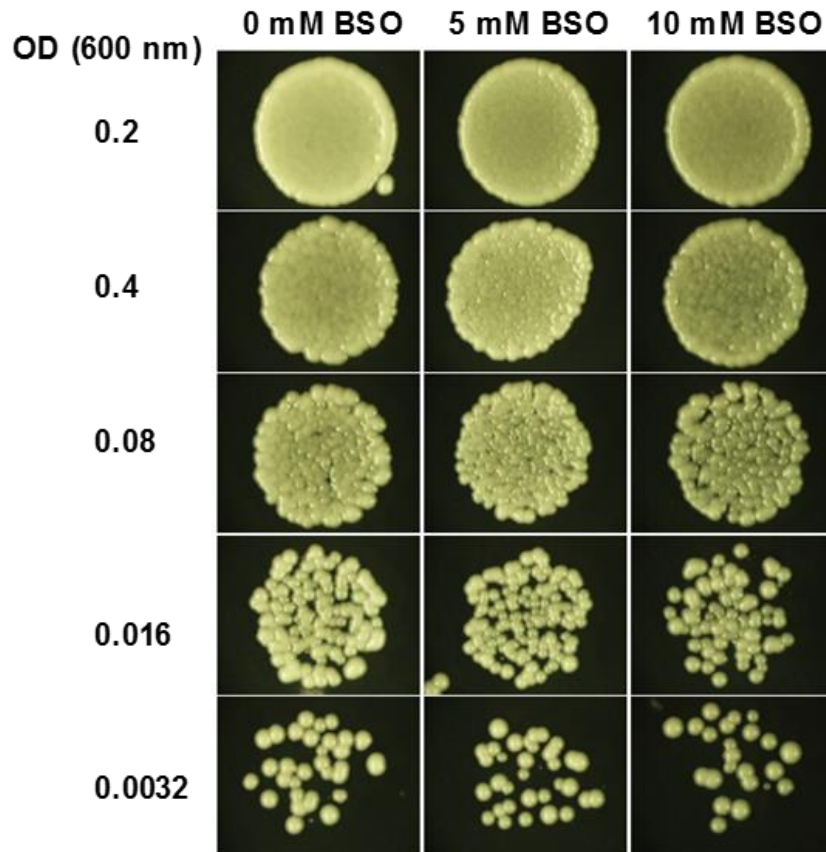
Figure 2.60: BSO does not inhibit the growth of yeast cells. Wild-type yeast was grown for spotting assay on YPD media supplemented with different concentration of BSO (0, 5 and 10 mM) for three days.

Furthermore, yeast growth sensitivity to BSO was also tested in yeast *gsh1* and *hgt1* mutants by performing growth and spotting assay in presence and absence of BSO. There were no differences in the growth of yeast cells grown on YPD media supplemented with or without BSO. The results from both growth and spotting assay indicate that unlike in plants BSO did not affect yeast growth (Figure 2.61 A-C). The results from growth and spotting assays suggest that either BSO is not taken up or that yeast cells are resistant to it.
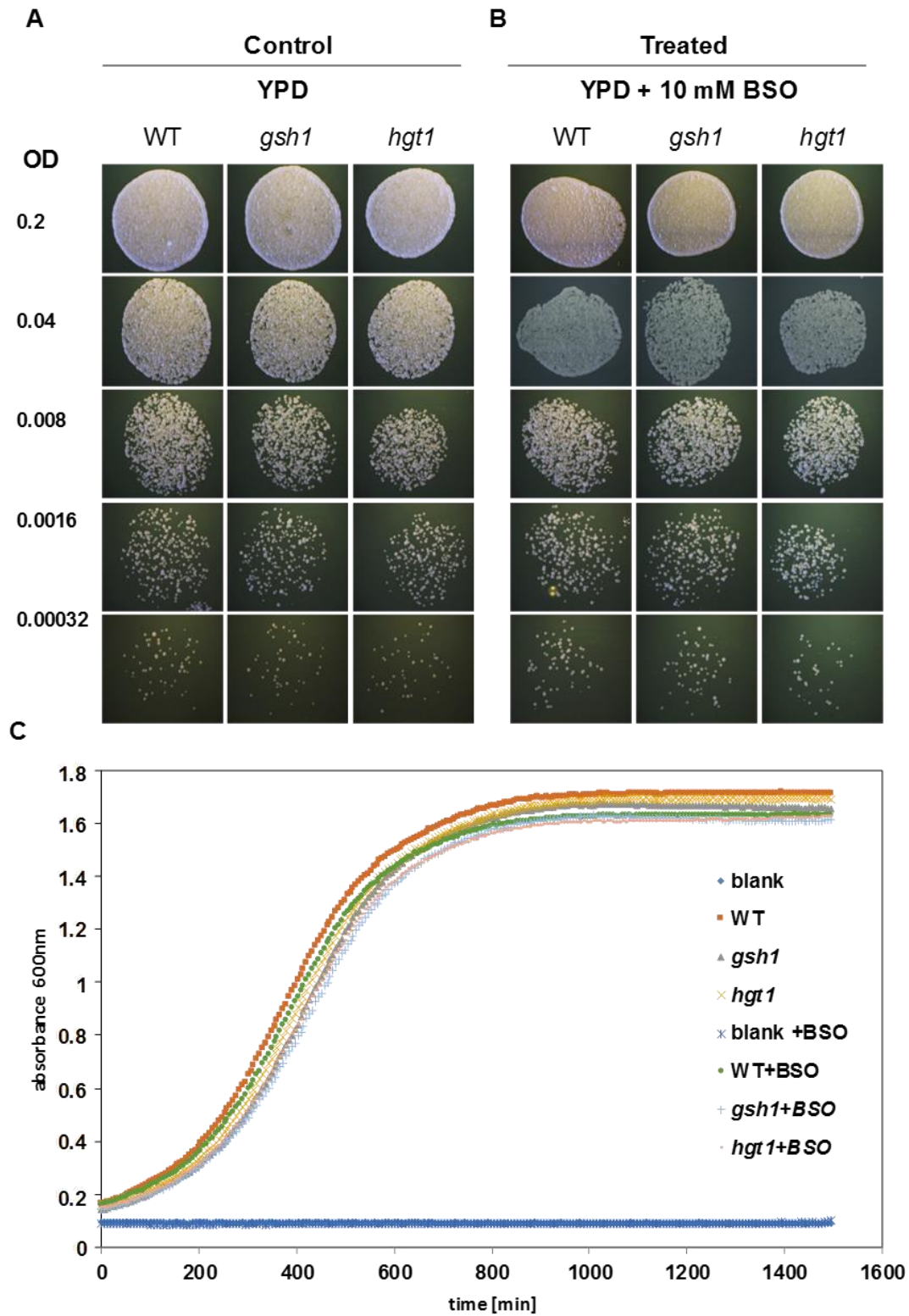
Figure 2.61: BSO does not inhibit growth of *gsh1* and *hgt1* yeast mutants. Wild-type, *gsh1* and *hgt1* yeast cells were grown on YPD media supplemented with or without 10 mM BSO for three days. **(A)** Control cells grown in the absence of BSO. **(B)** Cells treated with 10 mM BSO. **(C)** Overnight growth assay on a plate reader. $n = 3$. Data are shown as mean.

2.2.8.2 Depletion of glutathione pool by BSO in yeast

To test whether BSO is taken up by yeast and if it inhibits GSH biosynthesis, wild-type yeast was transformed with cytosolic GRX1-roGFP2. A selection of transformed colonies was carried on SD-leu media followed by an optical screen on a stereomicroscope using a GFP filter. Transformed colonies were highly fluorescent (Figure 2.62 A). Positively transformed yeast colonies were selected and grown overnight on SD-leu media supplemented with and without 5 and 10 mM BSO and subsequently subjected to ratiometric redox imaging on a confocal microscope. Calibration of roGFP2 was pursued with DTT and H_2O_2 for maximum reduction and oxidation, respectively. The pseudo-colour coded ratiometric images indicate that yeast cells grown on SD-leu showed reduced roGFP2, whereas yeast cells grown on SD-leu media supplemented with 5 mM BSO showed partially oxidised roGFP2. Moreover, yeast cells grown on SD-leu media supplemented with 10 mM BSO showed a completely oxidised roGFP2 (Figure 2.62 B-C). The oxidation of roGFP2 in the presence of BSO in yeast confirmed that BSO is efficiently taken up by yeast and it depletes the glutathione pool, but not affects yeast growth. In addition to wild-type, *hgt1* and *gsh1* yeast mutants were also transformed with cytosolic GRX1-roGFP2 and subjected to ratiometric redox imaging after growth on SD-leu medium with or without GSH and BSO. The ratiometric images reveal that wild-type and *hgt1* and yeast cells grown on SD-leu supplemented with 5 mM BSO showed oxidised roGFP2. In contrast *gsh1* yeast cells cannot synthesis glutathione and did not grow on media without GSH therefore was not included in the experiment. Only wild-type and *gsh1* yeast cells grown on SD-leu supplemented with and without BSO plus GSH showed reduced roGFP2. In contrast, *hgt1* yeast cells showed oxidised roGFP2 in presence of BSO plus GSH. The reduced roGFP2 in wild-type and *gsh1* yeast cells, supplied with GSH and in the presence of BSO, suggested that unlike in plants BSO did not inhibit GSH uptake in yeast. Moreover, oxidised roGFP2 in *hgt1* yeast cells grown on SD-leu supplemented with BSO plus GSH suggests that HGT1p is not transporting BSO (Figure 2.63). These results indicate that in yeast a separate transport system for GSH and BSO exists.
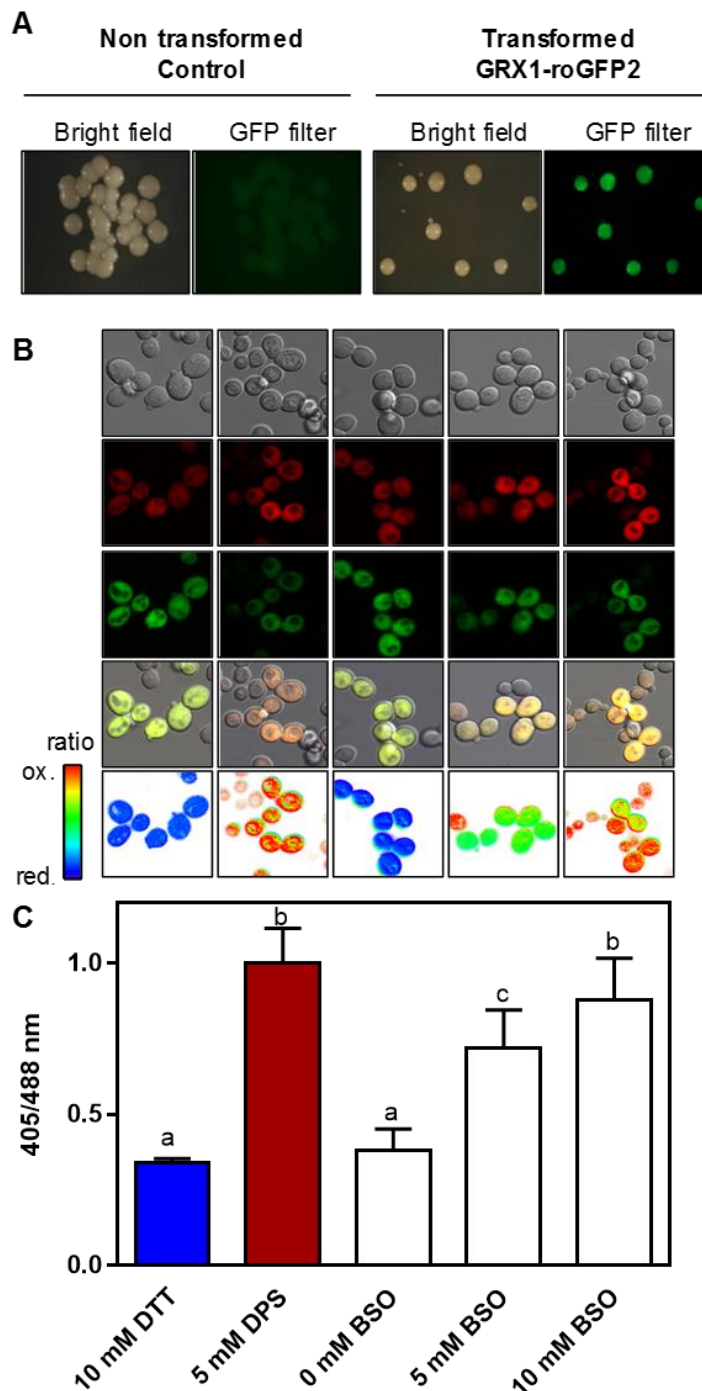
Figure 2.62: Effect of BSO on the redox status of yeast cells. (A) Transformed colonies of wild-type (BY4742) yeast with GRX1-roGFP2. Binocular microscopic images of non-transformed yeast colonies (left panel), yeast colonies transformed with GRX1-roGFP2 (right panel). **(B)** Confocal laser scanning microscopy of yeast cells grown on SD-leu supplemented with different concentration of BSO (0, 5 and 10 mM). From top to bottom bright field, 405 nm, 488 nm, merge and 405/488 nm ratio images. **(C)** Ratiometric analysis of total images indicating the average ratio of 405/488 nm. $n \geq 10$ images. Data are shown as mean ± SD. Letters indicate significant differences (One-way ANOVA with Tukey's multiple comparisons test; p-value ≤0.05).
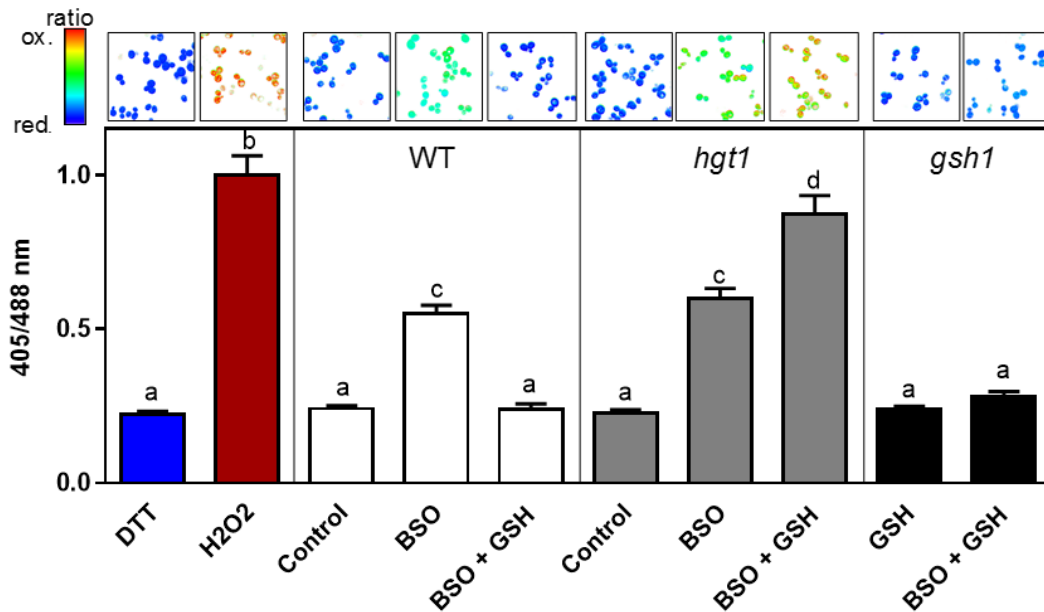
Figure 2.63: Effect of BSO on GSH uptake in yeast. Pseudo-colour coded ratiometric images of wild-type, *hgt1* and *gsh1* yeast cells grown overnight on SD-leu media supplemented with or without 50 µM GSH and 5 mM BSO (upper panel). Ratiometric analysis of yeast cell indicating the average ratio of 405/488 nm (lower panel). $n \geq 10$ images. Data are shown as mean ± SD. Letters indicate significant differences (One-way ANOVA with Tukey's multiple comparisons test; *p*-value ≤0.05).

2.2.8.3 Yeast *gsh1* mutant rescue by GSH and GSSG

Similar to plants (section 2.2.4), the competition assay of GSH with GSSG and BSO was also performed in yeast. A spotting assay was done with wild-type and *gsh1* yeast strains on SD media with and without GSH or GSSG. The yeast *gsh1* mutant cannot synthesise γ-EC and hence no GSH, requiring an external glutathione source. For this reason, *gsh1* mutants spotted on SD medium without glutathione did not grow. Supplementation of the medium with GSH or GSSG rescued the growth of the *gsh1* mutant. Furthermore, yeast *gsh1* mutant spotted on SD medium supplemented with GSH plus GSSG were also rescued, indicating that GSSG did not inhibit GSH uptake. In contrast to plants, low amount of GSSG also rescue yeast *gsh1* mutants (Figure 2.64). Summarised, these results further confirmed that, like in plants, GSSG did not inhibit GSH transport in yeast.
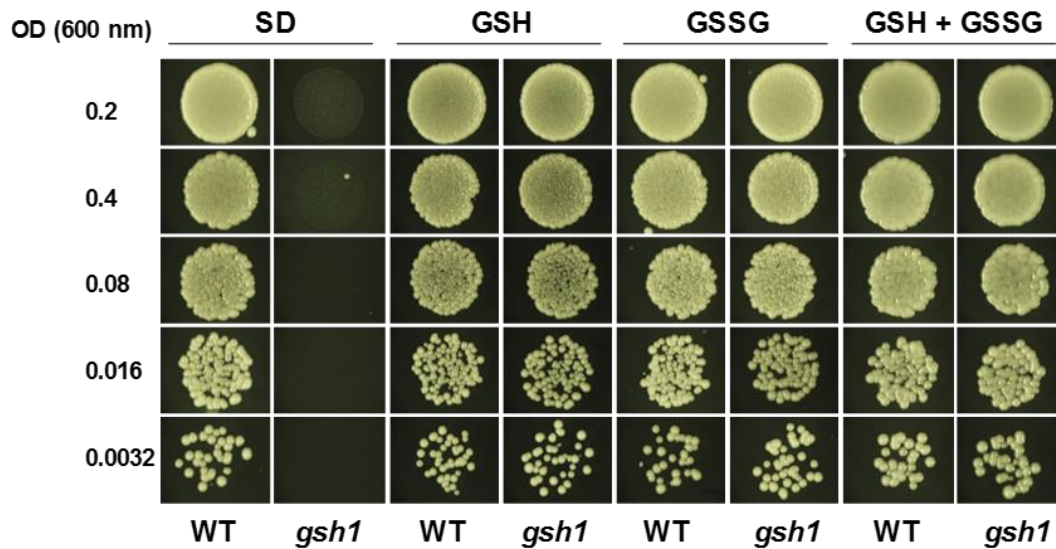
Figure 2.64: Rescue of *gsh1* yeast mutant with GSH or GSSG. Wild-type and *gsh1* yeast cells were grown on SD media supplemented with 50 µM GSH or GSSG, or both for three days. Non-supplemented cells are shown as controls on SD medium.

2.2.9 Bidirectional transport of CLTs between plastids and cytosol or CLTs export glutathione from plastids to cytosol

In *Arabidopsis thaliana*, the link between cytosolic and plastidic glutathione pools is facilitated by chloroquine-resistance transporter like transporters (CLTs). CLTs are the first functionally characterised members of the plant drug/metabolite exporter family (Maughan et al, 2010). The *in vivo* function of CLTs for bidirectional transport of glutathione between plastids and cytosol was analysed by inhibition of GSH biosynthesis with BSO. To test the bidirectional function of CLTs, wild-type and *clt1,2,3* mutants were transformed with plastidic and cytosolic roGFP2 sensor. Six-day-old wild-type and *clt1,2,3* mutant seedlings expressing plastidic and cytosolic roGFP2 were grown on ½ MS supplemented with or without BSO. Both treated and untreated seedlings were transferred for one day to liquid ½ MS supplemented with and without BSO and recovery of GSH was observed in wild-type and clt*1,2,3* base on roGFP2 redox state in both plastids and cytosol. The pseudo-colour coded ratiometric images of root tips indicate that under control condition cytosolic and plastic roGFP2 were reduced in both wild-type and *clt1,2,3*. Wild-type and *clt1,2,3* seedlings treated with BSO showed completely oxidised cytosolic roGFP2; however, plastic roGFP2 were completely oxidised only in wild-type but partially oxidised in *clt1,2,3*. After BSO removal plastidic roGFP2 in wild-type reduced slower than *clt1,2,3* while cytosolic roGFP2 reduced faster than *clt1,2,3* (Figure 2.65). The faster oxidation of wild-type plastidic roGFP2 on BSO treatment and the faster recovery of cytosolic roGFP2 after BSO removal suggested that CLTs are responsible for export of glutathione from plastids to cytosol.
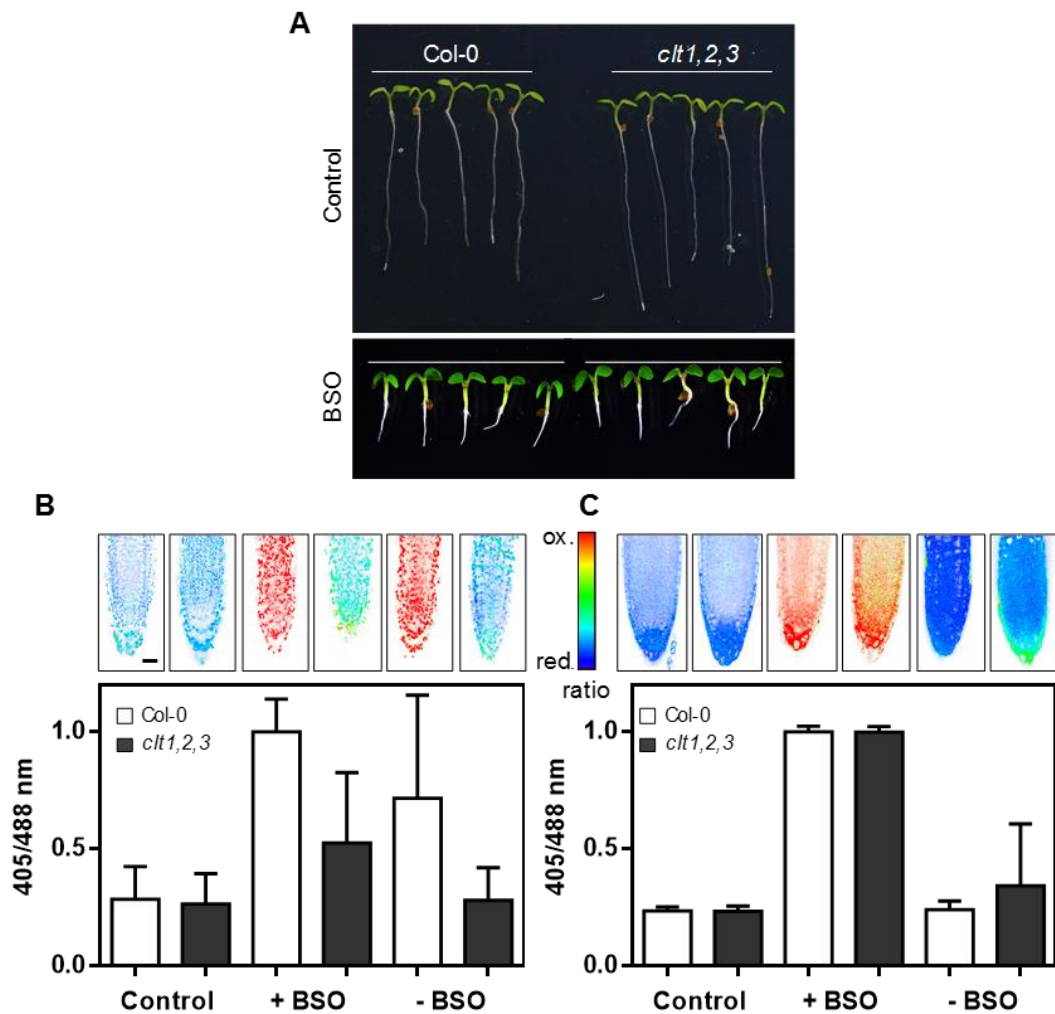
Figure 2.65: Effect of BSO on cytosolic and plastidic glutathione pool in *clt1,2,3* mutant and wild-type. (A) Seven-day-old seedlings of wild-type and *clt1,2,3* mutants grown on ½ MS supplemented with and without BSO, wild-type were supplied with 1 mM BSO and *clt1,2,3* with 2 mM BSO **(B)** Pseudo-colour coded ratiometric images of root tips of wild-type and *clt1,2,3* expressing plastidic roGFP2 grown on ½ MS supplemented with or without BSO (upper panel). Ratiometric analysis of root tips indicating the average 405/488 nm ratio (lower panel). **(C)** Pseudo-colour coded ratiometric images of root tips of wild-type and *clt1,2,3* expressing cytosolic roGFP2 grown on ½ MS supplemented with or without BSO (upper panel). Ratiometric analysis of root tips indicating the average 405/488 nm ratio (lower panel). $n \geq 10$. Data are shown as mean ± SD. Scale bar = 20 µm.

2.2.10 Glutathione accumulation in mitochondria under glutathione deficiency

High amounts of glutathione have been reported for mitochondria compared to other compartments (Zechmann et al., 2008). To further test this hypothesis, five-day-old *rml1* seedlings expressing mitochondrial roGFP2 were transferred for 20 h to ½ MS supplemented with or without GSH followed by cell imaging via CLSM. The results from pseudo-colour coded ratiometric images revealed that upon external GSH supply mitochondrial roGFP2 reduced faster than cytosolic roGFP2 (Figure 2.66). The faster

reduction of mitochondrial roGFP2 suggested that mitochondria accumulate glutathione if the cellular glutathione is far below the normal steady state.

Figure 2.66: Accumulation of GSH in mitochondria. Pseudo-colour coded ratiometric images of single cells in roots elongation zone of five-day-old *rml1* seedlings grown on ½ MS supplemented with and without GSH along with untreated wild-type control.

3. DISCUSSION

3.1 Low glutathione mutants display growth-deficiency phenotypes and insensitivity to drought stress
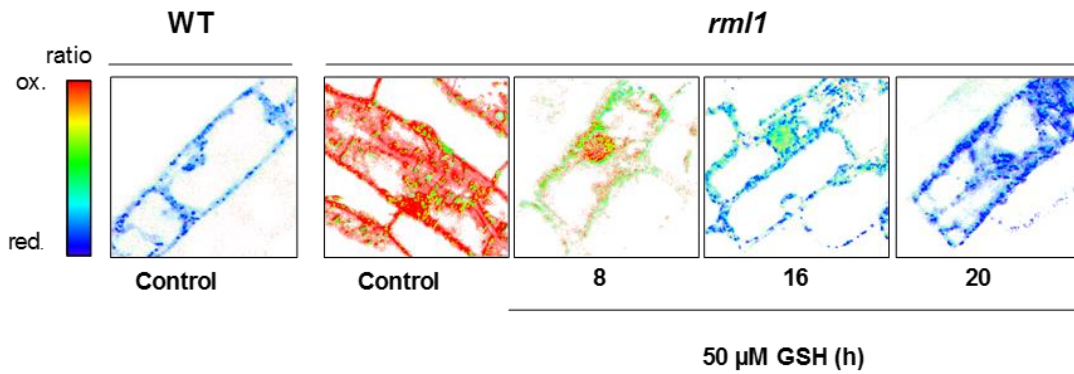
Environmental stresses, such as drought, high salinity and cold, adversely affect plant development and performance (Nahar et al., 2015; Plessis et al., 2011). The non-enzymatic antioxidant glutathione is an important part of redox homeostasis and is required for normal plant growth (Kim et al., 2005; Noctor et al., 2012). Changes in the total pool of glutathione or in its oxidation levels have been reported in diverse plant species as a response of long term exposure to abiotic stresses (Ball et al., 2004). Consequently, it has been shown that both exogenously and endogenously increased glutathione level conferred tolerance to drought and salt stress in Arabidopsis plants (Chen et al., 2012; Cheng et al., 2015). In this study it has been observed that under normal physiological environment, the length of lateral roots and the total root length of mutants with defects in GSH1 and thus impaired in glutathione synthesis were significantly shorter in most of the cases, compared to wild–type and with the only exception of *rax1*. Additionally, the number of lateral roots was decreased only in case of *nrc1* and *zir1*. The severe glutathione deficient mutant *rml1*, which has less than 5% glutathione compared to the wild-type, showed restricted root growth (Vernoux et al., 2000). Likewise, pharmacological inhibition of GSH synthesis in wild-type seedling also leads to depletion of glutathione and to the arrest of root growth (Koprivova et al., 2010; Vernoux et al., 2000). The genetic analysis of different Arabidopsis mutants suggest that a threshold in glutathione concentration is essential for root and shoot development (Bashandy et al., 2010; Vernoux et al., 2000). Being evident the relation between glutathione and root growth, the response of *gsh1* mutants to drought stress was investigated using an automated phenotyping system. The glutathione-deficient mutants showed no or minor drought susceptible phenotype. This result indicates that glutathione does not seem to be critical for the establishment of a drought tolerance. Therefore, the results in this study clearly contrasts the lower survival rate of *pad2* compared to wild-type under drought stress, suggesting that endogenously increased GSH conferred tolerance to drought stress in Arabidopsis, as reported by Cheng et al (2015). Similar to this study, it has been shown that a depletion of the glutathione pool does not impair plant response to mild water stress in *pad2* mutant (Jubany-Marí et al., 2016). It has been reported that mutants with low glutathione pool develop mechanisms of acclimation to water stress by reducing plant biomass and increasing the endogenous concentrations of glutathione and ascorbate. In contrast, wild–type plants need an initial response phase before reaching acclimation which is marked by a decrease in antioxidants (Jubany-Marí et al., 2016). The automated phenotyping system used in the present study is far more robust than conventional

phenotyping because multiple genotypes with a number of different phenotyping parameter can be measured in parallel and without interference by the experimentalist, minimising at the same time potential sources of error.

3.2 Glutathione compartmentation

3.2.1 Altered glutathione biosynthesis effects differently subcellular compartmentation of glutathione

Glutathione biosynthesis is restricted to the cytosol and plastids (Wachter et al., 2005), from where it is distributed to the different subcellular compartments by an unknown transport mechanisms (Zechmann et al., 2008). Compartmentation of metabolites in diverse organelle, tissues and organs is essential for various physiological processes and for metabolic regulation (Bowsher and Tobin, 2001; Hartmann et al., 2003). Different methods are already suggested in literature to measure the subcellular glutathione pool. Glutathione concentration calculated from HPLC measurement is assumed to be in a millimolar range in different subcellular plant compartments (Hartmann et al., 2003; Jimenez et al., 1997; Krueger et al., 2009; Kuźniak and Skłodowska, 2004; Vanacker et al., 1998). Biochemical methods reports glutathione concentration from 0.5 to 5 mM in chloroplasts (Foyer and Halliwell, 1976; Krueger et al., 2009; Noctor et al., 2002), between 1 and 3.52 mM in the cytosol (Krueger et al., 2009; Noctor et al., 2002) and 0.73 mM in the vacuole (Krueger et al., 2009). Moreover, with MCB as a GSH-specific fluorescent dye the glutathione concentration in the cytosol was estimated between 2.7 and 3.2 mM (Meyer et al., 2001).

All these methods nonetheless have limitation. While MCB labelling allows the quantification of glutathione *in vivo*, HPLC analysis can distinguish between subcellular glutathione pools and the oxidised and the reduced form. HPLC measurements provide subcellular resolution and assessment of the redox state but only if cell compartments are previously isolated and with the limitation that the redox state might change during the extraction procedure (Zechmann, 2014). Moreover, it is unclear how well the obtained results reflect the *in vivo* situation (Chew et al., 2003; Noctor et al., 2002). Furthermore, glutathione measured with electron microscopy in different subcellular organelles in Arabidopsis leaves indicated the highest concentrations in mitochondria (14.8 mM) followed by nuclei (6.4 mM), the cytosol (4.5 mM), peroxisomes (4.4 mM), chloroplasts (1.2 mM) and the lowest glutathione concentration in vacuoles (0.08 mM) (Koffler et al., 2013). The limitations of this approach are, that the tissue must be pre-fixed and that the used antibody do not discriminate between the reduced and oxidised form of glutathione (Zechmann, 2014).

In the present study a novel strategy was used to gain a deeper understanding about the subcellular compartmentation of glutathione. Genetically encoded biosensors overcome the limitations of other methods previously mentioned (Gutscher et al., 2008). Therefore, present study offers new insight into the compartmentation of glutathione. The roGFP2 sensor had been expressed in different subcellular compartments of *gsh1* allelic series mutants and glutathione redox potential was measured at steady state. The redox measurement in *gsh1* mutants showed that the cytosolic and plastidic glutathione pool were more affected, with impaired glutathione biosynthesis, while mitochondrial glutathione pool was less affected. Moreover, plastids in leaves of *gsh1* mutants were more reduced than root plastids, reinforcing the hypothesis that plastids from roots and leaves behave differently. The different behaviour of plastids in roots and leaves has been already previously reported (Whatley, 1983). In addition, the effect of impaired glutathione biosynthesis was tested by the inhibition of glutathione biosynthesis with BSO in wild-type expressing roGFP2 in different subcellular compartments. Upon the application of the inhibitor, the glutathione pool in root plastids depleted faster and recovered more slowly compared to the cytosol, peroxisome and mitochondria. In leaves, on the contrary, supply of BSO did not deplete the glutathione pool completely. This may be explained either by an inefficient transport of BSO to the shoot or by the fact that leaves have larger glutathione pool compared to roots. An higher concentration of glutathione in maize leaves compared to roots has been already reported by Ahmad et al. (2016). The differential response of leaves and roots towards Cd has been also reported with less effect on leaves than roots (Jozefczak et al., 2014). In future, time course measurements of glutathione depletion by BSO could further confirm the effect of this compound on different subcellular compartments. Moreover, quantification of the glutathione pool in roots and leaves separately may explain the diminished effect of BSO on leaves.

3.2.2 Mislocalisation of GSH1 and GSH2 enzymes to cytosol, plastids and peroxisomes

The fact that glutathione biosynthesis is taking part in different compartments is a unique feature of plants (Hell and Bergmann, 1988; Wachter et al., 2005). In Arabidopsis, GSH1 has been shown to localise exclusively in plastids, whereas GSH2 localise predominantly in the cytosol but also in plastids (Wachter et al., 2005). Restricting the GSH biosynthesis only to the cytosol or plastids has been shown to be sufficient for recovering normal plant development (Lim et al., 2014; Pasternak et al., 2008b). To test further the ability of GSH and its precursors to cross the membrane of respective organelle, TDNA mutants of *gsh1-1* and *gsh2-1* were complemented imitating the synthesis into different compartments. Double mutants of *gsh1gsh2* complemented with *EcGSH1* and *AtGSH2* exclusively in the cytosol showed an aberrant phenotype, with chlorotic leaves and reduced root growth and seedling lethality under normal conditions (Lim et al., 2014). In this work *gsh1gsh2*

double mutant were complemented with endogenous *AtGSH1* and *AtGSH2* and the complemented lines were viable and displayed compact rosettes in early stage of development, normal over in later stages of development. Under normal growth condition, complemented double mutants showed low MCB labelling intensity and higher sensitivity to CdCl₂, compared to wild–type and *cad2*. It has been reported that the quantitative RT-PCR of the double complemented mutants showed significantly lower cAtGSH2 expression compared to the parent cAtGSH2 transgenic line, suggesting silencing of transgene. This leads to hyperaccumulation of γ-EC and decreased GSH content in the double complemented mutant, suggesting that GSH biosynthesis is limited by GSH2 activity (Lim et al., 2014). The deleterious effect of hyperaccumulation of γ-EC has been already reported (Au et al., 2012; Creissen et al., 1999) and it might contribute to the lethality of the double mutant (Lim et al., 2014). A possible explanation for the low level of glutathione founded in double mutants could be that GSH1 activity is affected in cytosol or cytosolic environment, which is not favourable for GSH1 normal regulation of activity. Furthermore, MCB labelling confirmed that GSH levels remain low in double complemented mutants. However, it is not possible to tell yet whether this is due to interference with the catalytic process, expression levels or localisation. To further address these questions it would be necessary to test for GSH1 expression levels with available antibodies and search for putative regulatory interaction partners like TRXs or GRXs.

Compartmentation of glutathione biosynthesis was further characterised by expressing GSH1 and GSH2 fused with a GFP or RFP reporter tag. The *gsh1* mutant expressing GSH1 with N and C tag GFP/RFP in plastids, and in the cytosol were fully viable. The fusion of a FP tag to GSH1 did not completely abolish its activity. Similarly, it has been reported that transgenic line expressing functional GSH1-GFP were viable (Hiruma et al., 2013). Previously, it has been reported that AtGSH1 extracted from Arabidopsis chloroplasts in homodimeric configuration (Hothorn et al., 2006). So the two reasonable explanations would be that either GFP fusion to GSH1 does not affect its dimerisation or that GSH1 is active in an its monomeric form (Figure 3.1).
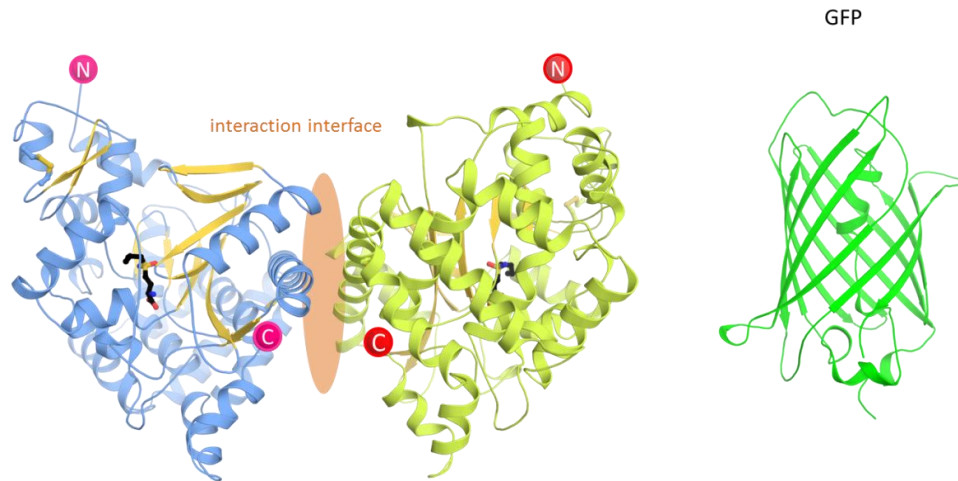
86

Figure 3.1: *At*GSH1 homology model (left) and green fluorescent protein (GFP) (right). AtGSH1 cartoon model depicting the two dimers with the N and C terminal. The structure is based on crystallisation model of *Brassica juncea* GSH1 (PDB: 2GWC). The model has 95.5 %. sequence identity with *Brassica juncea*.

In the future the glutathione pool of these mutants will be further analyses by HPLC. Additionally, mutants will be tested under different stresses, for example in the presence of heavy metal. Moreover, in the present study *At*GSH1 polyclonal antibodies were produced and tested on wild-type GSH1 (Figure 3.2) and they can be used in the future to test for the expression levels of AtGSH1 fused to GFP.
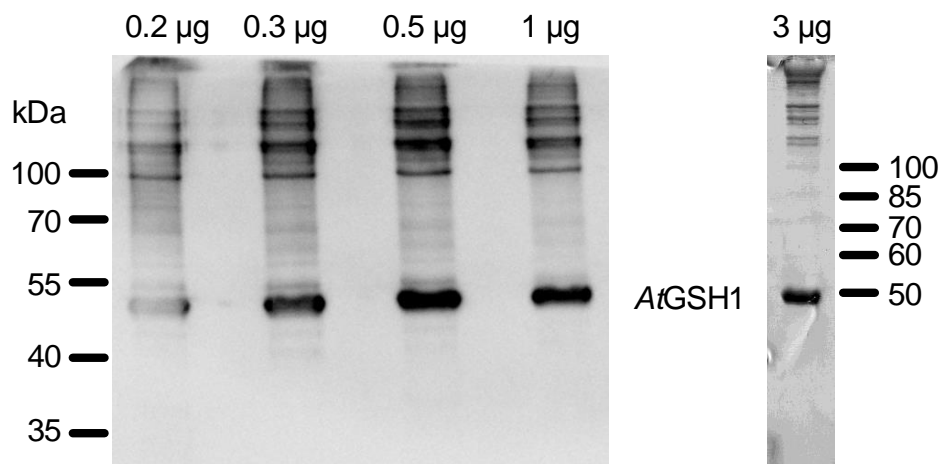

Figure 3.2. Protein blot analysis of *At*GSH1 with *At*GSH1 antibody. Total protein isolated from three-week-old wild-type Arabidopsis plant used for, left: Western blot of *aAt*GSH1 with dilatation of (1:500) and incubated for 2 h at RT with Pierce ECL Western Blotting Substrate. Exposure time of blot was 4 min. Right: Coomassie-stained gel (10 % SDS PAGE)

3.2.3 Growth restriction of *gsh1* mutants is limited by absolute amounts of glutathione

As reported and shown in this work, glutathione is critical in plant development. This metabolite plays pivotal functions in embryo and meristem development (Bashandy et al., 2010; Cairns et al., 2006; Frottin et al., 2009; Reichheld et al., 2007; Vernoux et al., 2000). The severely glutathione deficient mutant *rml1*, is unable to develop a mature root (Vernoux et al., 2000). Moreover, glutathione in Arabidopsis has been implicated in secondary metabolism and pathogen responses. Externally supplied GSH mimics fungal elicitors in activation of the expression of defence related genes (Dron et al., 1988; Gómez et al., 2004; Senda and Ogawa, 2004). The partial glutathione deficient mutants *rax1* and *cad2* has been already shown to increase the susceptibility to a virulent *Pseudomonas syringae* (Ball et al., 2004). Other *gsh1* mutants, such as *pad2-1* showed enhanced susceptibility to various fungal, bacterial and oomycete pathogens. This indicates that the decreased glutathione pool is the only factor responsible for the accumulation of defence compounds such as camalexin and for the resulting resistance against these pathogens (Parisy et al., 2006, 2007). The strong phenotype in glutathione deficient mutants raised the question whether the effect is due to a reduction in the total amount of glutathione or its redox potential. Crosses with *bir6* partially suppressed *zir1* and *rml1* growth phenotype in double mutants. In contrast, *gr1* did not show any effect in *gr1zir1* and *gr1rml1* double mutants (Figure 2.27). The recovery of *zir1* and *rml1* growth phenotype by *bir6* confirms that growth inhibition of *gsh1* mutants is caused by the amount of glutathione rather than its redox potential. Considering that glutathione is an important cofactor for many physiological processes (Berndt et al., 2007; Lillig et al., 2005; Lushchak, 2012; Wong et al., 1989), a reduction on the total amount of glutathione can explain the restriction in plant growth (Figure 3.3). To further confirm this hypothesis, the double mutants could be transformed with GRX1-roGFP2iL in order to further investigate the redox status of the double mutants.
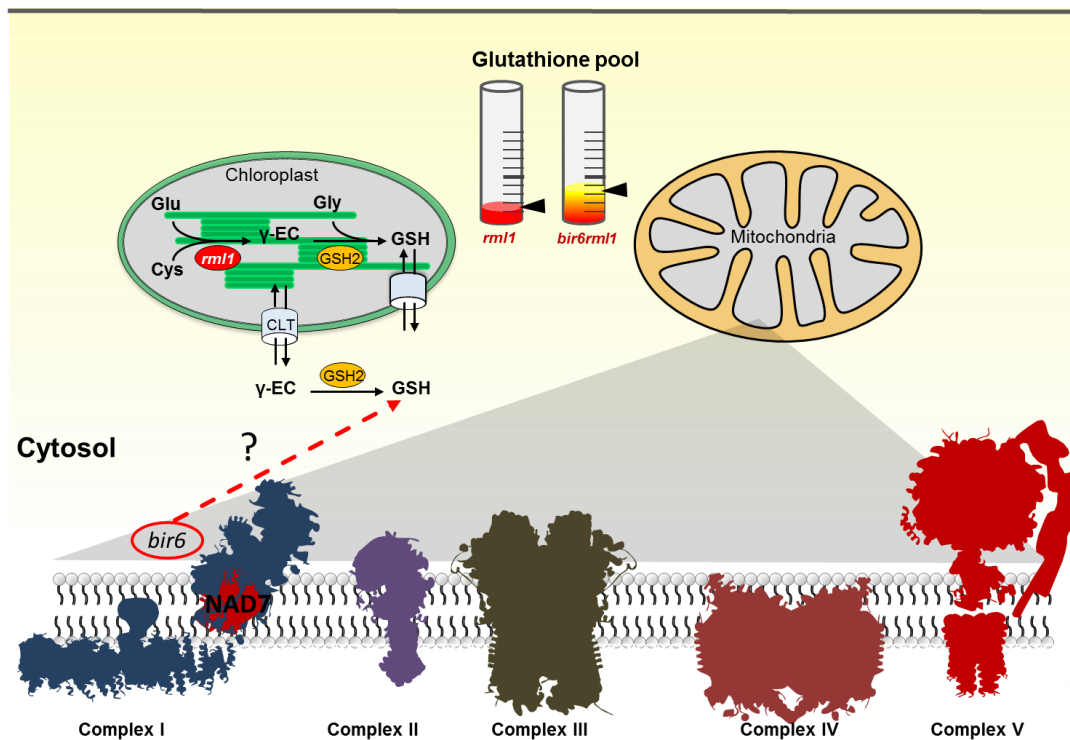
Figure 3.3: Model for glutathione and root growth.

3.3 Glutathione degradation and transport

3.3.1 Glutathione degradation

The glutathione exported from the cell is required for its normal turnover, metabolic pathways and disposition of glutathione adducts (Ballatori et al., 2009). The γ-glutamyl cycle has been reported to be important in both transport of glutathione across the plasma membrane and GSH degradation (Meister and Tate, 1976). This is initiated by the action of γ-glutamyl transpeptidase (GGT), which cleaves the γ-glutamyl bond in either reduced, oxidised or conjugated forms of GSH in the apoplast. A GGT-independent degradation pathway via the intermediate 5-oxoproline being produced by γ-glutamyl cyclotransferase (GGCT) has been proposed in Arabidopsis (Ohkama-Ohtsu et al., 2008). GGTs are involved in the degradation of extra cytosolic glutathione, while GGCTs would take part in controlling cytosolic glutathione homeostasis (Noctor et al., 2011; Ohkama-Ohtsu et al., 2008). In mice it has been reported that the ChaC protein family functions as γ-glutamyl-cyclotranferases, acting specifically on glutathione (Kumar et al., 2012). In contrast, in plants it was proposed that GGCTs accept only γ-glutamyl dipeptides as a substrate (Paulose et al., 2013). Therefore, in the present study, degradation of cytosolic glutathione via GGCTs was tested in Arabidopsis mutants lacking GGCT enzymes along with wild-type control. Moreover, it has been shown that under sulfur deficiency GGCT2;1 expression is up regulated in root tips (Iyer-Pascuzzi et al., 2011), suggesting

that plants start mobilising sulfur by degrading glutathione. The results presented in section (2.2.1) show that the mutants *ggct2;1-1* and *ggct2;1-2* grown on sulfur-deficient media showed more intense MCB labelling compared to wild-type. Additionally, mutants had longer roots compared to wild–type on sulfur-deficient media. This further supports the ideas that GGCT directly degrade glutathione into 5-oxoproline and the dipeptide Cys-Gly. The 5-oxoproline and Cys-Gly are then further degraded by oxoprolinase and dipeptidases, to Glu, Cys and Gly, and can be reuse for glutathione biosynthesis. Similar results have been generated through functional assays in yeast and biochemical characterisation of the purified recombinant enzymes GGCT2;2 and GGCT2;3, proving that these enzymes specifically degrade glutathione to yield 5-oxoproline and Cys-Gly and that they show no significant activity towards γ-glutamyl cysteine (Kumar et al., 2015). Furthermore, the *ggct2;1-1* and *ggct2;1-2* T-DNA lines were stable transformed and screened for cytosolic roGFP2 and double mutants of *ggct2;1-1* and *ggct2;1-2* with *zir1* and *rml1* were generated and selected, but could not be analysed anymore during the course of this thesis project for time reasons. These double mutants thus need to be analysed and characterised in future research.

3.3.2 Glutathione transport at the plasma membrane

Glutathione transport through the plasma membrane plays a pivotal role in maintaining the defensive antioxidant capacity of the apoplast (Vanacker et al., 1998). Initially, the first proteins associated to GSH transport were the Multidrug resistance associated proteins (MRP). MRP's belong to a subclass of the ATP binding cassette (ABC) protein superfamily involved in glutathione efflux at the plasma membrane in mammals and vacuolar membrane in yeast (Li et al., 1998; Rebbeor et al., 1998a, b). These transporters have broad substrate specificity and low affinity for glutathione and therefore it may indicate that these transporters would be primarily required for the efflux of glutathione conjugates, rather than for glutathione itself (Ballatori et al., 2005).

3.3.2.1 Existence of low and high affinity glutathione transporter at plasma membrane

The first high affinity and highly specific plasma membrane GSH transporter was found in yeast and named high affinity glutathione transporter 1 (Hgt1p) (Bourbouloux et al., 2000). Hgt1p belongs to the oligopeptide transporter (OPTs) family, which are present in yeast in three isoforms, while in Arabidopsis, a large family of nine OPTs (*At*OPT1 to *At*OPT9) has been described. They share 61-85% of sequence similarity among themselves and 49-53% sequence similarity to yeast Hgt1p (Koh et al., 2002). Different functions have been reported for these nine Arabidopsis OPTs. *At*OPT1 is likely to be involved in the transport of peptides from the surrounding maternal transmitting tract

tissues for use in nourishing pollen tube growth (Stacey et al., 2006); *At*OPT2 is not involved in iron transport, while it might be involved in transport of other metals (Lubkowitz, 2011); *At*OPT3 is a phloem-specific iron transporter that is essential for iron homeostasis in Arabidopsis and a misregulation of OPT3 leads to an over accumulation of cadmium in seeds (Mendoza-Cozatl et al., 2014; Zhai et al., 2014); *At*OPT4 function as proton-coupled oligopeptide transporters with broad but distinct substrate specificities (Osawa et al., 2006); *At*OPT5 possibly mediates heavy metal phytotoxicity and *At*OPT6 is able to transport glutathione derivatives, metal complexes, Cd-glutathione, etc. but not GSSG (Cagnac et al., 2004; Pike et al., 2009). Very little is known about the roles of *At*OPT7, *At*OPT8 and *At*OPT9 and the known information comes from a small number of expression studies (Lubkowitz, 2011). The characterisation of most of these transporters is still in its infancy due to their low affinities, multiple members and tissue specificity. Hgt1p mediated GSH uptake exhibits saturation kinetics (K_m=55 µM) (Bourbouloux et al., 2000) and GSH uptake kinetics also indicate the presence of low affinity (K_m= 6 mM) transporter system in yeast (Miyake et al., 1998). Likewise, in plants the presence of two different transport systems for GSH uptake reflected by the kinetic parameters have been reported. In tobacco leaves, both high affinity (K_m= 17 µM) and low affinity (apparent K_m=310 µM) GSH transport systems were detected (Schneider et al., 1992). It has been testified recently that from the Arabidopsis OPTs family, only AtOPT4 rescued the auxotrophic phenotype of the *met15 opt1* mutant in the presence of GSH as the sole sulfur source. Moreover, biochemical characterisation of AtOPT4 confirmed that it functions as a low-affinity glutathione transporter (Zhang et al., 2016). The molecular identification of the high affinity glutathione transporter, however, is still lacking in plants. Possible candidate for such a transport could be OPTs (Lubkowitz, 2011), amino transporters (Ortiz-Lopez et al., 2000; Tegeder, 2012), or peptide transporters (PTR) (Rubio-Aliaga and Daniel, 2008). All PTRs have been tested by others but no transport was observed. In this work, glutathione transport system was investigated by using severe glutathione deficient mutant *rml1* as model system. Rescuing of *rml1* on GSH but not GSSG indicates that only GSH is taken up across the plasma membrane (Figure 2.38). This was further confirmed by MCB labelling in seedlings supplemented with GSH. Additionally, GSH and GSSG feedings were examined in *rml1* seedlings expressing cytosolic roGFP2. After 20 h of GSH treatment, the seedlings showed reduction of glutathione pool to a wild–type level. In contrast to GSH, GSSG and amino acids components of GSH (Glu, Cys and Gly) did not showed a reduction of cytosolic roGFP2 (Figure 2.39 and Figure 2.40). These results confirmed that in a low concentrations range (50-250 µM), glutathione is taken up as GSH but not as GSSG. Likewise, in rat liver microsomal vesicles preferential transport of GSH but not GSSG was found indicating that microsomal membrane is impermeable toward GSSG (Banhegyi et al., 1999). On the other hand, *rml1* seedlings supplemented with 500 µM or 1000 µM of GSSG showed a

reduction of roGFP2 in the cytosol of *rml1*, suggesting that: higher concentration of GSSG may passively diffuses through the plasma membrane, the GSH transporter may have low affinity towards GSSG or there could be separate low affinity GSSG transporter. It has been already proved that in basal-lateral membrane vesicles from rat kidney that a comparison of the rate of uptake of equimolar concentration of GSSG with GSH, indicating that GSSG is transported at only 20% of the rate of GSH (Lash and Jones, 1984).

In yeast, GSH uptake is reported to be inhibited by GSSG but not by individual amino acids (Bourbouloux et al., 2000). In contrast to these results, the present study indicates that Arabidopsis seedlings treated with different GSSG concentrations did not inhibit GSH uptake. Higher concentration (1 mM) of glutamate seems to inhibit GSH uptake partially, while 1 mM of cysteine completely inhibits GSH transport. Additionally, it was shown that GSH uptake is inhibited by BSO, MSO, S-hexylglutathione. BSO inhibits GSH at plasma membrane, and it has been reported that it enters plastids via CLTs (Maughan et al., 2010). This unknown transporter at plasma membrane, along with GSH, could possibly transport also BSO. In contrast, BSO did not inhibit GSSG uptake, suggesting a separate transport system for GSSG. Since in yeast BSO did not inhibits GSH uptake, the possible explanations could be that, either HGT1p is not a transporter for BSO or it is immediately pumping out by Multiple-drug-resistance (MDR) present at the plasma (Figure 3.4). Recently it has been reported that *At*OPT4 is low affinity glutathione transporter (Zhang et al., 2016), and for this reason it was further investigated in this study by generating *opt4rml1* double mutant. External GSH feeding to an *opt4rml1* double mutant along with *rml1* showed GSH uptake and confirmed that *opt4* is not the only transporter of GSH at plasma membrane, but rather additional high affinity transporters exist.

Besides the already mentioned possible GSH transporters, several members of nitrate transporter 1/peptide transporter (NPF) had shown to transport a wide variety of substrates and for many of these peptide transporters the substrate is unknown. In particular, a member of NPF family, *At*NPF6.3, is involved in nitrate-regulated auxin (IAA) transport (Krouk et al., 2010; Léran et al., 2014). IAA inhibits GSH uptake; however, no inhibition was seen with KNO_3 (Figure 2.48). The GSH and auxin interaction was further investigated by checking the decrease of the expression of an auxin sensing line, DR5-GUS, in a wild–type genetic background and incubated in GSH (Figure 2.52).

Moreover, wild–type seedlings expressing DII-VENUS showed intense fluorescence of the sensor under control condition, followed by less intense fluorescence in seedlings incubated in GSH and IAA, while seedlings incubated with IAA showed a complete degradation of sensor, observable by a strong decrease of the fluorescence. Lower fluorescence in GSH and IAA treatments might be due to the diffusion of IAA through

the plasma membrane or through another low affinity transporter, something that may occur also in the DR5:GUS lines.
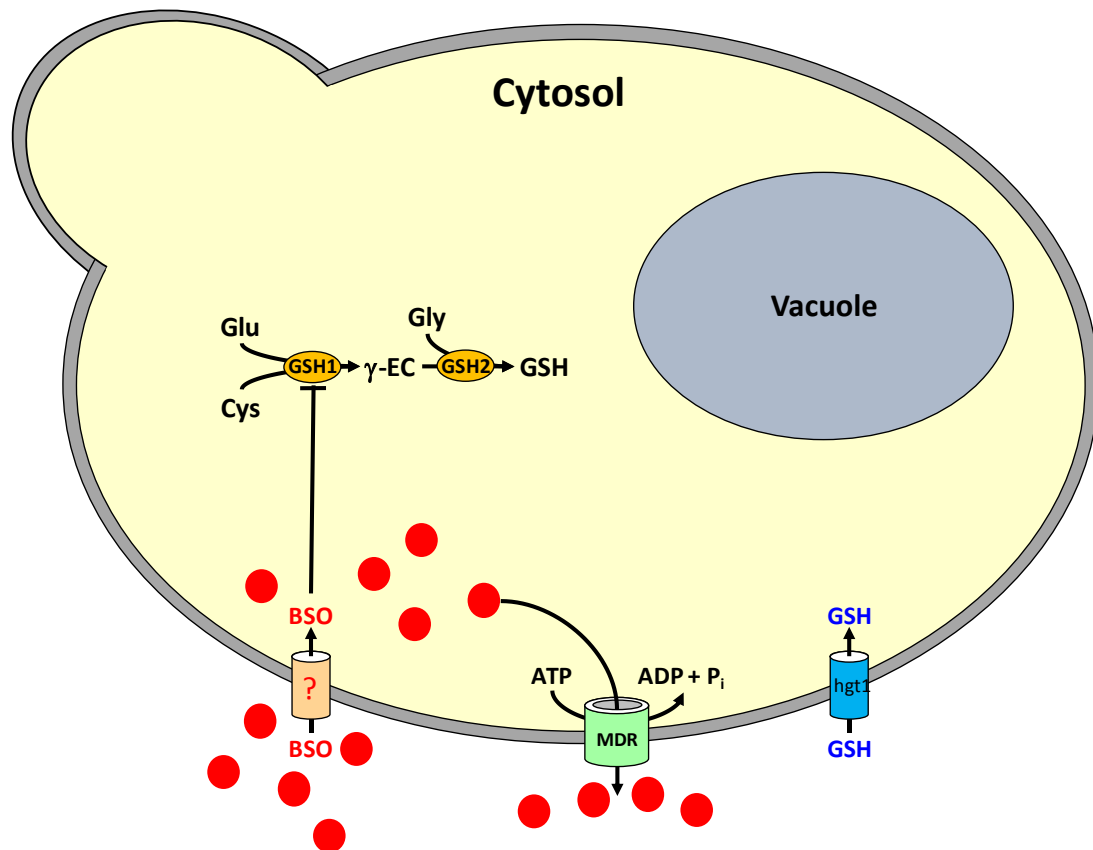

Figure 3.4: Putative model for BSO resistance caused by multidrug resistance transporters (MDR) in yeast.

Auxin plays an important role in the gravitropic response of the root (Rashotte et al., 2001), therefore the effect on the root response in a seedling grown in a GSH supplemented plate were explored (Figure 2.51). After two days of treatment, an impaired gravity response was observed. Based on this observation, the working hypothesis is that AUX1 might be the transporter for GSH. Additionally, mutants lacking auxin transporter, *aux1-21* showed partial resistance to BSO compared to wild–type. In order to confirm the hypothesis in the future, double mutants of *aux1* with *rml1* and *gsh1* were generated, for upcoming analysis glutathione transport.

A screening of competitive inhibitors (like di- and tri-peptides) on the plate reader might also lead to the respective transporter family. Followed by the expression of possible candidates in *Xenopus oocytes,* this combination of approaches might provide further information on the molecular identity of GSH transporters.

3.4 CLTs are established transporter of glutathione and BSO at plastidic membrane

In Arabidopsis, coupling of the plastidic and cytosolic glutathione pools is mediated by chloroquine resistance transporter like transporters (CLTs) (Maughan et al., 2010). In Arabidopsis, there are three isoforms of CLTs, involved in the export of γ-EC and GSH from plastids to cytosol. Arabidopsis mutants lacking all these transporters (*clt1clt2clt3*) are sensitive to Cd, but do not present a lethal phenotype (Maughan et al., 2010), which suggests that another transport system might be present at the plastidic membrane. Transport of glutathione across the chloroplast envelope has been shown in wheat using radioactive labelled GSH (^{35}S-labelled GSH), proving that at least two systems are able transport GSH across the chloroplast envelope (Noctor et al., 2002). The first member of CLTs, CLT1 was identified in a genetic screen on BSO, and only the *clt1* null mutant was resistant to BSO. Additionally, *clt1,3* double mutants show increased BSO resistance. It has been already reported that CLT1 and CLT3 transport BSO in to the plastids, where it inhibits GSH1 (Maughan et al., 2010). In this study bidirectional transport of GSH across the plastidic membrane was investigated by growing wild–type and *clt1,2,3* triple mutants on BSO. As a result, it was observed that, under controlled condition, cytosolic and plastic roGFP2 were reduced in root tips of both wild–type and in *clt1,2,3*. However, MCB labelling of *clt1,2,3* triple mutants was less intense compared to wild-type. In contrast, oxidised cytosolic glutathione pool has been reported in *clt1,2,3* triple mutants (Maughan et al., 2010). Seedlings treated with BSO showed completely oxidised cytosolic roGFP2 in root tips; however, plastidic roGFP2 were completely oxidised only in wild–type and only partially oxidised in *clt1,2,3*. After BSO removal, plastidic roGFP2 in root tips of wild–type reduces more slowly compared to *clt1,2,3*. On the other hand cytosolic roGFP2 in wild-type reduces faster than *clt1,2,3*. This result suggests, that CLTs are responsible only for export of glutathione from plastids to the cytosol, and did not support the hypothesis of CLTs mediate transport of GSH from the cytosol into the plastids. In contrast to wild-type plastids, which were completely oxidised with 1 mM BSO, *clt1,2,3* plastids were still not completely oxidised with 2 mM BSO. To further support the export of GSH via CLTs from plastids to the cytosol, time series redox measurement will be undertaken in the future. For which strong oxidation of *clt1,2,3* plastids similar to wild-type will be required, upon BSO treatment, a different setting for the experiement should be set. Wild–type plastids stay largely oxidised after incubation without BSO and the GSH pool does not immediately recover. This might be due to a newly syntethised GSH being exported to the cytosol and to other compartments. Optimisation of the minimal BSO concentration required for a better oxidization of the *clt1,2,3* plastids is currently in progress, together with a different the setup of the experiment that enable to check kinetically the response over time. As a final approach, isolated chloroplasts epressing roGFP2 can be fed with

GSH, and their redox state could be followed by fluoresence in a hightroughput system, such as the plate reader.

4. CONCLUSION

Based on the results presented and discussed in this study, a working model summarising the cellular and subcellular glutathione homeostasis is proposed (Figure 4.1). This model illustrates the effect of impaired glutathione biosynthesis on the redox status of different subcellular compartments, degradation and transport of glutathione across the plasma membrane.
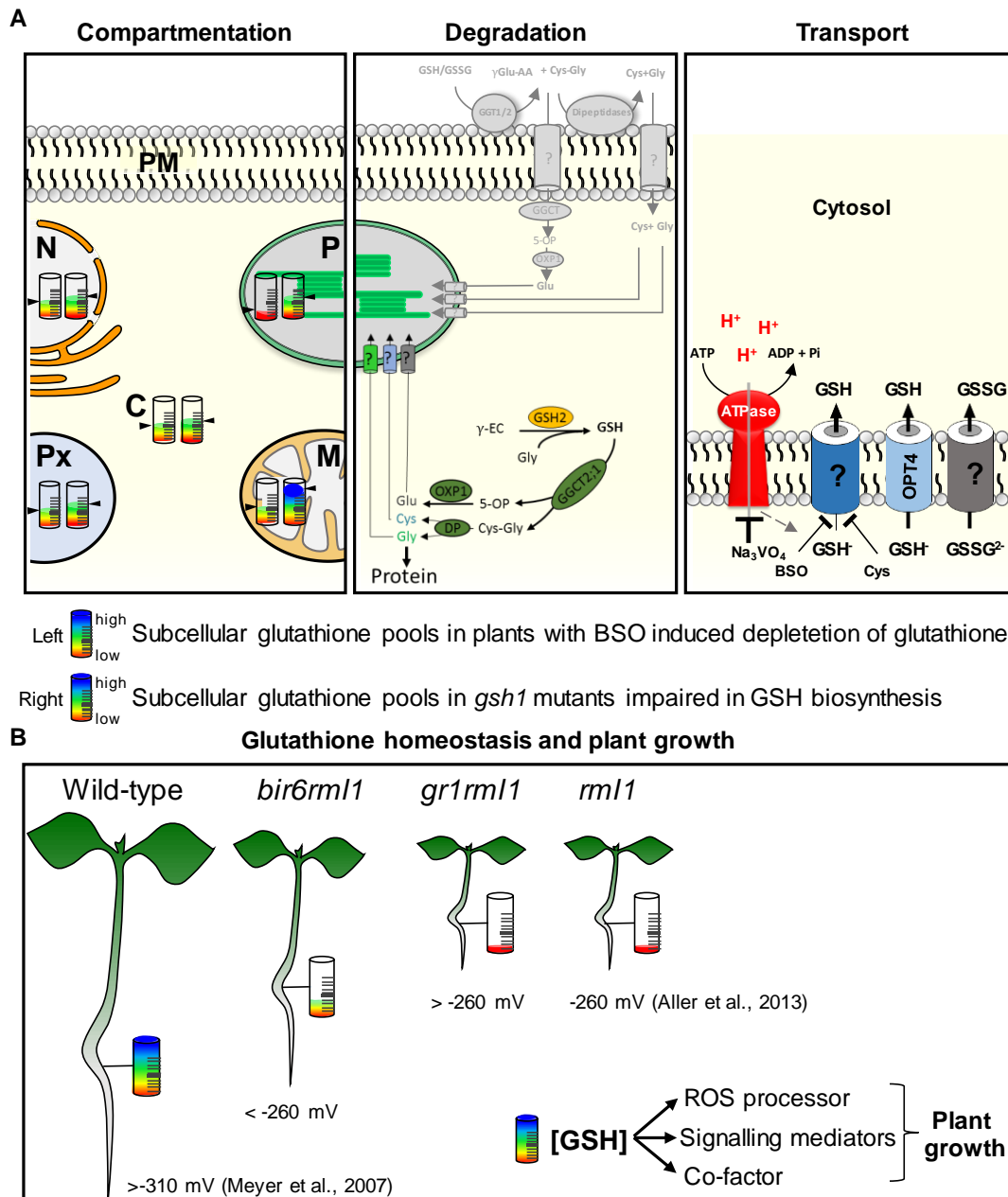

Figure 4.1: Working model for glutathione homeostasis and impact on plant growth.(A) The glutathione pool affected by depletion or by impaired glutathione biosynthesis in subcellular compartments (the cytosol (C), peroxisomes (Px), plastids (P) and mitochondria (M)) (left panel) and GSH degradation by GGCTs (middle panel). The grey coloured pathway for glutathione degradation has been suggested by Griffith et al. (1978). The right panel shows both low and high affinity GSH transporters at the plasma membrane (PM) including putative competitors. **(B)** Model depicting the impact of the amount of glutathione and glutathione redox potential in plant growth.

It is concluded that in case of impaired GSH biosynthesis the GSH pool in all compartments except the mitochondria is severly affected. All available data suggest that mitochondria maintain a slightly higher GSH concentration—either due to continuous active uptake of GSH, or due to less turnover. Furthermore, it was confirmed that upon pharmacological inhibition of glutathione biosynthesis via BSO, the plastidic glutathione pool depletes faster and recovers slower than in other subcellular compartments. This could be either due to effcient active uptake or the size of the compartments and turnover. In addition, the pathway for glutathione degradation via GGCTs in the cytosol is confirmed, and it was resolved that GGCTs specifically degrade glutathione in the cytosol similar to the model that had been proposed by Paulose et al (2013). Moreover, the characterisation of glutathione transport was done, which suggests the presence of a high affinity transporters at the plasma membrane besides the already reported low affinity GSH transporter *At*OPT4. Additionally, *opt4rml1* double mutant further confirmed that *At*OPT4 is not the only GSH transporter at the plasma membrane and there are inidications for high affinty transporter which is inhibited by BSO and Cys. Finally, the impact of the total amount of glutatione and glutathione redox status on plant growth was also presented, and it was discovered that the amount of glutathione in partially GSH depleted mutants rather than its redox potential restricts plant growth.

5. MATERIALS AND METHODS

5.1 Laboratory equipment and materials

5.1.1 Consumables and Chemicals

General chemicals were purchased from Sigma-Aldrich (www.sigmaaldrich.com/germany), Duchefa Biochemie (www.duchefa-biochemie.nl), Merck (www.merckmillipore.de), Roth (www.carlroth.com) or AppliChem (www.applichem.com). General plastic ware was purchased from Sarstedt (www.sarstedt.com/php/main.php) and VWR (de.vwr.com/store).

5.1.2 Kits and enzymes

NucleoSpin® Plasmid	Macherey-Nagel[1]
NucleoSpin® Gel and PCR Clean-up	Macherey-Nagel
Gateway® BP clonase II enzyme mix	Thermo Fisher Scientific[2]
Gateway® LR clonase II enzyme mix	Thermo Fisher Scientific
Phusion® High-Fidelity DNA Polymerase (2 U μL^{-1})	Thermo Fisher Scientific
Taq DNA Polymerase (5 U μL^{-1})	BioLabs
FastDigest ApoI(XapI)	Thermo Fisher Scientific
FastDigest NheI	Thermo Fisher Scientific
FastDigest HindIII	Thermo Fisher Scientific
FastDigest APaL1(Alw44I)	Thermo Fisher Scientific
FastDigest MfeI	Thermo Fisher Scientific

5.1.3 Antibiotics and herbicides — Working concentration

Ampicillin	100 $\mu g\,mL^{-1}$
Gentamycin	100 $\mu g\,mL^{-1}$
Kanamycin	50 $\mu g\,mL^{-1}$
Rifampicin	100 $\mu g\,mL^{-1}$
Spectinomycin	100 $\mu g\,mL^{-1}$
Sulfadiazine sodium salt	5.25 $mg\,L^{-1}$
BASTA®	240 $mg\,L^{-1}$
Hygromycin B	20 $\mu g\,mL^{-1}$
Geneticin	200–300 $\mu g\,mL^{-1}$

[1] www.sigmaaldrich.com/de
[2] https://www.thermofisher.com/de

98

5.2 Plant methods

5.2.1 Plant material

Arabidopsis thaliana (L.) Heynh ecotype Col-0 was used as wild-type. Additionally, the following mutants listed in Table 5.1 were used for this study.

Table 5.1: Arabidopsis mutant lines

Name	Locus	Line	Characteristics
rax1	*AT4G23100*	-	Point mutation in GSH1
cad2	*AT4G23100*	-	6 bp deletion in GSH1
pad2	*AT4G23100*	-	Point mutation in GSH1
nrc1	*AT4G23100*	-	Point mutation in GSH1
zir1	*AT4G23100*	-	Point mutation in GSH1
rml1	*AT4G23100*	-	Point mutation in GSH1
gr1	*AT3G24170*	SALK_105794	T-DNA insertion in GR1
bir6-1	*AT3G48250*	-	point mutation in BIR6
gsh1	*AT4G23100*	SALK_011665	T-DNA insertion in GSH1
gsh2	*AT5G27380*	SAIL_301_C06	T-DNA insertion in GSH2
ggct2;1-1	*AT5G2620*	SALK_117578	T-DNA insertion in GGCT
ggct2;1-2	*AT5G2620*	SALK_056007	T-DNA insertion in GGCT
opt4	*AT5G64410*	SALK_130258C	T-DNA insertion in OPT4
aux1-21	*AT2G38120*	-	Point mutation in AUX1-21
clt1,2,3	*AT5G19380, AT4G24460, AT5G12170*	SALK_008200 SALK_042635 SAIL_756_G07	T-DNA insertion in CLT
miao	*AT3G54660*		Point mutation in GR2

Seeds of *aux1-21* and *opt4* were obtained from Nottingham Arabidopsis Stock Centre. Seeds of the *bir6-1* were kindly provided by Stanislav Kopriva and *ggct2* lines were kindly provided by Thomas Leustek.

5.2.2 Growth conditions

5.2.2.1 Growth conditions for plants grown on sterile medium

Seeds were surface-sterilised with 70% (v/v) EtOH for 3–5 min and then washed 3–4 times with dH_2O prior to plating. Either nutrient medium (Somerville and Ogren, 1982) or half-strength Murashige & Skoog medium including vitamins (Duchefa, www.duchefa-biochemie.nl) was used with pH adjusted to 5.8 and solidified with 0.8% (w/v) phytagel (Sigma-Aldrich, www.sigmaaldrich.com). After stratification for 2 d at 4°C in darkness, the plates were transferred to growth cabinets for growth under long-day conditions (16 h light at 22°C and 8 h dark at 18°C) with light intensities of 75 $\mu mol\ m^{-2}\ s^{-1}$ and 50% relative air humidity.

5.2.2.2 Growth conditions for soil grown plants

Seeds placed in Eppendorf tubes were filled with water and stratified for 2 d at 4°C in darkness. Aftewards seeds were planted in pots containing a mixture of soil:sand:vermiculite (ratio of 10:1:1). The soil was obtained from Floragard, Oldenburg (Floradur° Anzuchtssubstrat). Pots were transferred to growth chambers and kept under long-day conditions (16 h light at 19°C and 8 h dark at 17°C) with the light intensities between 65–120 $\mu mol\ m^{-2}\ s^{-1}$ and 50% of relative air humidity.

5.2.3 Plant transformation

5.2.3.1 Transient transformation of tobacco plant

Agrobacteria containing the desired binary vector were inoculated in 5 ml LB medium (1 % (w/v) bacto tryptone, 0.5 % (w/v) bacto yeast extract and 1 % (w/v) NaCl, pH 7.0, for plates: 2 % agar, sterilize by autoclaving.) supplemented with the appropriate antibiotics and grown on a rotary shaker with 220 rpm at 28°C to an OD_{600} of 0.5–1. The cells were harvested by centrifugation at 5,000 g for 2 min and resuspended in dH_2O to an OD_{600} of 1–1.5. Tobacco plants were well-watered before infiltration to ensure high stomatal aperture, and facilitate the infiltration process. Subsequently, Agrobacterium suspension was infiltrated into the abaxial side of leaves using a needle-free 1 ml-syringe. After 2 d, the infiltrate leaves were analysed for transgene expression.

5.2.3.2 Stable transformation of Arabidopsis

Arabidopsis plants were stably transformed performing the floral dip transformation described by Clough and Bent (1998). Agrobacteria cells were grown in selective LB medium to an OD_{600} of ~1.0 under shaking conditions at 220 rpm at 28°C. The cell culture

with a final volume of 400 mL was inoculated with a 5 mL-starting culture grown overnight under the same conditions. The cells were harvested by centrifugation at 5,000 g for 10 min at 4°C and resuspended in the floral-dip medium containing 5% (w/v) sucrose and 0.02% (v/v) Silwet L-77 to an OD_{600} of 1–1.5. The floral plant part was dipped into the suspension for 5 s. Afterwards, plants were placed horizontally in a tray and cover with a plastic dome to ensure high relative humidity during the overnight incubation in the dark. On the next day, plants were re-erected and transferred to standard growth conditions in the growth cabinet. The dipping procedure was repeated after one week to increase the transformation rate.

5.2.3.3 Screening for transformed Arabidopsis

Screening of transformed plants was performed with different chemical and/or fluorescent selection markers. Transformants carrying the BAR gene as selection marker were grown on soil for 2 weeks under long-day conditions. After 2 and 3 weeks, the plants were sprayed with a 240 mg L^{-1} glufosinate ammonium solution (Basta˚).

Transformants carrying the kanamycin (npt), hygromycin (hpt) or sulfadiazine (sul) resistance genes as selection marker were screened on agar plates according to the protocol of Harrison et al (2006). Seeds were surface sterilised using the same procedure described in section 5.2.2.1, and grown on half-strength MS plates solidified with 0.8% (w/v) agar and 50 µg mL^{-1} kanamycin, 20 µg mL^{-1} hygromycin B or 5.25 mg L^{-1} of sulfadiazine sodium salt, respectively.

Transformants carrying fluorescent protein sensors were screened and documented with the stereomicroscope (Leica M165 FC) and attached camera (Leica DFC425 C). Fluorescent plants expressing GFP were excited at 470±40 nm and the emission collected at 525±50 nm using a GFP filter. Plants expressing RFP were excited at 545±30 nm and emission collected at 620±30 nm using a DsRed filter.

5.2.4 Automated and conventional phenotyping

Phenotyping experiments were carried out at the Institute IBG-2: Plant Sciences, Forschungszentrum Jülich GmbH as described previously (Caliandro et al., 2013; Nagel et al., 2009). For root phenotyping, plants were grown on agar-plates, allowing an easy accessing to the root system. Arabidopsis seeds were surface-sterilized with NaClO and then sown on sterile one-third-strength modified Hoagland solution solidified with 1% (w/w) agarose in Petri dishes (120 × 120 × 17 mm). Seeds were placed into holes drilled into the upper rim of the plates for the roots to develop under axenic conditions while the shoots grew outside the plates. Four seeds per Petri dish were placed on the upper side of the closed Petri dishes, sealed with fabric tape (Micropore, 3 M Health Care, Neuss,

Germany) and placed vertically in a plastic box to avoid light exposure of roots. During germination, the holes were covered with a film (Parafilm, Pechiney Plastic Packaging, Menasha, WI, USA) to keep the seeds moist. Seeds were stratified at 4 °C in the dark for 5 d before they were grown vertically in the plastic box on an 'root carousel' ('root carousel' set-up) in a climate chamber with illumination in 12/12 h light/dark cycles with a photon flux density of 90–100 μmol m^{-2} s^{-1} (PAR). At a distinct position on the root carousel, roots were automatically documented with a high-resolution CCD-camera (IPX-6 M3-TVM, Imperx Inc., Boca Raton, FL, USA) under infrared illumination. Root system architecture of each plant was analysed by the GROWSCREEN-ROOT method from Nagel et al. (2009). The image analysis was manually double-checked and edited in the cases where the software failed to recognize root structures due to insufficient contrast.

For shoot phenotyping in response to drought stress, plants were grown in pots filled with soil. Plants were well-watered until day 22 and thereafter half of plants were subjected to drought stress for 10 d before plants were re-watered (Figure 5.1)
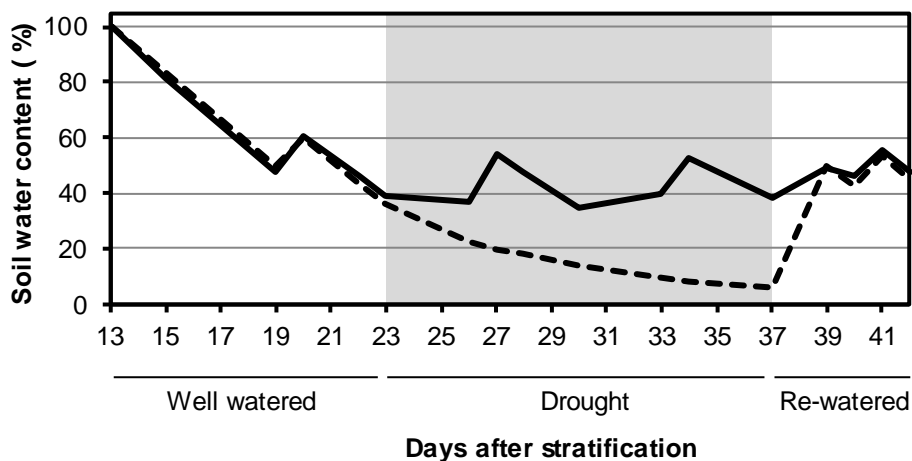
Figure 5.1: Model illustrating drought stress experiment regime. Model illustrating the watering regime and soil water content during the experiment for drought stressed plants (dashed line) and control plants (solid line).

Shoot growth was analysed automatically by using the GROWSCREEN FLUORO setup described earlier (Jansen et al., 2009; Barboza-Barquero et al., 2015). Seeds of wild-type and all *gsh1* mutant lines were place individually in pots, stratified for 3 days at 4 °C in the dark. Subsequently seeds were germinated and after seven days plants with similar germination time were transferred to larger pots (7 x 7 x 8 cm) and randomized on trays with 30 plants on each tray. All plants were then grown in growth chambers under fully controlled conditions at 22/18 °C, 170 μmol m^{-2} s^{-1} PAR, and 8/16 h day/night regime. The soil water content (SWC) was recorded gravimetrically. After an initial soaking, the SWC was decreased until a value of approx. 40 %. Subsequently the SWC was held through intermittent addition of water. Starting from day 15 after germination, all plants

were initially documented for the projected leaf area (PLA) and chlorophyll fluorescence every second day. During the second and third week, when the shoot size increased exponentially, all growth parameters were collected on a daily basis. All readings were taken around midday to ensure that the rosettes were oriented almost horizontally above the soil. The PLAs A_1 and A_2 of two consecutive days were used to calculate the relative leaf growth rate (RLGR) (% d^{-1}) according to the equation $RLGR = 100 \times 1/t \times \ln(A_2/A_1)$. Chlorophyll fluorescence was recorded after dark adaptation for at least 30 mins with a camera-based system to calculate colour coded images of F_v/F_m as a measure of the potential quantum yield of photosystem II. For further analysis, average values for F_v/F_m for whole rosettes were calculated.

For drought stress experiments the plants were split into two subpopulations in which the first population was well watered during the experiment and the second population from day 24 onwards was exposed to drought until growth ceased. Subsequently, plants were again watered to a soil water content of about 40 % and allowed to recover. All plants were harvested after 44 days to determine fresh and dry weight.

Leaf circumference, rosette compactness, rosette stockiness and excentricity were calculated from the PLA, as described earlier (Jansen et al., 2009).

For conventional root growth phenotyping, seedlings were grown vertically on plates containing 0.8% (w/v) phytagel and 0.1% (w/v) sucrose. Five and eight days after stratification, root length was documented. Effects of exogenously supplied GSH on root length was analysed by growing seedlings on plates containing half-strength MS nutrient plates (see section 5.2.2.1) with 0.5% (w/v) sucrose, with and without supplementation of 1 mM GSH. Roots were documented using the stereomicroscope (Leica M165 FC) and attached camera (Leica DFC425 C). Root lengths were measured using Adobe Illustrator CS5.1.

5.2.5 Gravity experiment

Four-day-old wild-type seedlings grown on 0.5-strength MS media supplemented with or without 250 µM GSH were rotated by 135° and kept for two days in darkness. The seedlings were documented on binocular and binding angles determined using Adobe Illustrator CS5.1.

5.2.6 Determination amino acid content via HPLC

5.2.6.1 Extraction of amino acids

Amino acids were extracted from 20–100 mg frozen plant tissue in 200–400 µL of 80% EtOH incubated on shaker for 15 min at 4°C and 600 rpm. After the incubation, the

extracts were centrifuged for 10 min at 4°C and 14000 rpm. The supernatants were transferred to fresh tubes and kept on ice. The pellets were extracted a second time with 200–400 µL of 80% EtOH, performing the same procedure for a total of three times. The supernatants of all three extractions were pooled and subjected to high performance liquid chromatography (HPLC) measurements or stored at -20°C until further use.

5.2.6.2 Quantification of amino acids

For the HPLC analysis of amino acids, 100 µL of EtOHic extracts (5.2.6.1) were diluted with 900 µL of dH$_2$O (1:10) in flat bottom vials before loading into the HPLC autosampler (Ultimate Autosampler 3000; Dionex). Before separation, the amino acids were derivatised in a separated reaction vial by pre-column derivatization, consisting of automatic mixing of 25 µL 1x OPA solution (Grace Davison Discovery Sciences), 5.5 µL 1M borat buffer pH 10.7 and a 25 µL sample prior the analysis. After 1.5 min of incubation, 20 µL of the derivatisation mixtures were injected into the HPLC system and separated onto HyperClone 3 µm ODS(C18)120 150x4.6 mm HPLC column (Phenomenex) by a discontinues gradient consisting of solvent A (8.8 mM NaPO$_4$ pH 7.5 and 0.2% (v/v) tetrahydrofuran (THF)) and increasing proportions of solvent B (18.7 mM NaPO$_4$ pH 7.5, 32.7% (v/v) MeOH and 20.6% (v/v) acetonitrile). Separated fluorescent derivatives were excited at 380 nm and detected at 480 nm using a RF 2000 flourescence detector (Dionex) in the "low" sensitivity mode. Data acquisition and analysis was executed with the Chromeleon software (6.80 SR7; Dionex). Proteinogenic amino acids (Sigma) were used as standards.

5.3 Molecular biological techniques

5.3.1 DNA extraction

DNA from Arabidopsis tissue was extracted according to Edwards et al. (1991). Plant tissue was homogenised in Eppendorf tubes containing 400 µL of Edwards buffer (200 mM Tris-HCl (pH 7.5), 250 mM NaCl, 25 mM EDTA and 0.5% (w/v) SDS). The homogenised samples were centrifuged at 20,000 g for 10 min before 350 µL of supernatant was transferred into a new Eppendorf tube. 350 µL isopropanol was added to the sample prior centrifugation at 20,000 g for 5 min. The supernatant was subsequently discarded and the pellet containing the DNA was washed with 300 µL of 70% (v/v) EtOH. After air-drying for 1 h at room temperature, DNA was resuspended in 30–50 µL dH2O and heated for 5 min at 95°C to facilitate dissolving process. DNA was quantified with the spectrophotometer NanoDrop 2000 (Thermo Scientific) and DNA samples were stored at -20°C.

5.3.2 Oligonucleotides

Primers were synthesised by MWG (www.eurofinsgenomics.eu). Salt-adjusted oligonucleotide-melting temperatures were calculated using an online oligonucleotide properties calculator (http://biotools.nubic.northwestern.edu/OligoCalc.html). Lyophilised oligonucleotides were resuspended in dH_2O to a working concentrations of 10 pmol μL^{-1}. Primer stocks and working solutions were stored at -20°C. The primers used in this study are shown in Table 5.4.

Table 5.2: List of genotyping and sequencing primers

No.	Primers	Sequence
463	GSH1_T1_N	TGTTTCGGGTGGCGTGAG
464	GSH1_T1_C	GCTTTCCCTGGTCAACAA
3053	SALK_LBb1.3	ATTTTGCCGATTTCGGAAC
641	*rml1*_g1472	GCCAATGCTCTCACCCTAAA
642	*rml1*_c2142	GGCAATGGTTAGTCAAAATCG
3026	*zir1* Fw. primer	GTTTGAGCAGTATGTTGACTACGCAC
3027	*zir1* Rev. primer	GAAAGACTCTTGAGGCAGATGATTAAGCT
747	*cad2*_L_wt	CAAGGGTACCAACTTTCG
748	*cad2*_L_mutant	AGACCAAGGGTACCAAGCA
749	*gsh1*	TTTGGATGTTTTGAGGAT
2985	*bir6* Fw. primer	TGAAAGCTTTGGCGTTTTTCAATT
2986	*bir6* Rev. primer	GGTTTGAACGGACCATCCATC
330	GR2_N	TCGTCTATGGAGCTACTTACGGTGG
331	GR2_C	CGCAAAAATATCCAATCTACTGAGCAC
315	GSH2_N1	TTCCACTTGTTTGCAGGTCATTGC
316	GSH2_C1	AATAAACCACTGCGACTGCTTGGC
321	SAIL_LB3	TAGCATCTGAATTTCATAACCAATCTCGATACAC
605	G_550A09_LP	TCTTTGATTAAGCATGAAACATTG
606	G_550A09_RP	AGGCGATTCAAAAAGCATCTC

1037	T-DNA sir1-2	ATATTGACCATCATACTCATTGC
3523	*atm3* Fw primer	ATTGCTACACTTGCGGGAGATGC
3524	*atm3* Rev primer	GATGGTGAGTTATCTGAGAGG
328	GR1_N	GCTACCCTTTCAGGACTTCCAGACC
329	GR1_C	CACAATGTTCTCCTGCAAACATGC
309	LBb1_neu	GACCGCTTGCTGCAACTCTCTCAGG
3242	*trxo1*-1 Fw primer	AATCATCATCGTTGACTTGCC
3243	*trxo1*-1 Rev primer	ACACATCCACTTAGCGTGAGG
3053	SALK_LBb1.3	ATTTTGCCGATTTCGGAAC
3244	*trxo1*-2 Fw primer	AAATCCCGCCCTACAGATATG
3245	*trxo1*-2 Rev primer	TCGAGTGATGAAGGGAAATTG
3675	3675_*ggct2;1-1*_L	TTTAAATTGAGCAGTGGGGTG
3676	3676 *ggct2;1-1* R	TGAGGGCTTCGAAAAGTATTG
3677	3677 *ggct2_1-2* L	CTGCTAGGACTTGTACGCTGG
3678	3678 *ggct2_1-2* R	TTCAACAATGCCTTCACTTCC
3856	AUX1-21 Fw primer	CAACAGTGGTTTGAAGTACTTG
3857	AUX1-21 Rev primer	TGAATGTTTCACACCTTCCGC
4120	OPT4_LP	TAAGTAACAAATGGCATCGCC
4121	OPT4_BP	TTCACGTCATAAGCAAGCATC
689	*pDONR*_Fw primer	TCGCGTTAACGCTAGCATGGATCTC
690	*pDONR*_Rev primer	GTAACATCAGAGATTTTGAGACAC

Table 5.3: List of cloning primers

No.	Primer	Sequence
2789	cGSH1 fw_gateway	GGGGACAAGTTTGTACAAAAAAGCAGGCTCAgcggcaagt
2790	cGSH1 rev_gateway	GGGGACCACTTTGTACAAGAAAGCTGGGTTCAAAGCTT

5.3.3 Polymerase chain reaction

Two different polymerase chain reactions (PCRs) protocols were used for cloning and genotyping. For the cloning PCR, 0.02 U μL^{-1} Phusion® High-Fidelity DNA Polymerase was used in a total volume of 50 μL containing 1x Phusion buffer, 200 μM dNTPs, 0.5 μM oligonucleotide A, 0.5 μM oligonucleotide B, and 0.5 μL template DNA. The thermocycling conditions described below were applied with the C1000™ thermal cycler from BIO-RAD (www.bio-rad.com).

Step	Temperature	Time	
Initial denaturation	98°C	180 s	
Denaturation	98°C	30 s	
Annealing	52–60°C	30 s	34x
Elongation	72°C	60 s per kbp	
Final extension	72°C	300 s	
Hold	12°C	∞	

For genotyping, the PCR reaction was executed in a total volume of 20 μL containing 0.025 U μL^{-1} *Taq* DNA polymerase (BioLabs), 1x Standard *Taq* Reaction Buffer, 200 μM dNTPs, 0.2 μM oligonucleotide A, 0.2 μM oligonucleotide B and 2 μL template DNA. Alternatively, genotyping PCR was performed with homemade *Taq* DNA polymerase as shown below.

Component	Taq (μL)	Final conc.
dH$_2$O	12.8–14.3	-
DNA template	0.5–2	-
Primer forward	0.4	2 μM
Primer reverse	0.4	2 μM
dNTPs	0.4	200 μM
Buffer	2	1x
Polymerase	2	2.5 units

Annealing temperatures shown below were adjusted to primer properties using the Oligonucleotide Properties Calculator (http://biotools.nubic.northwestern .edu/OligoCalc.html).

Step	Temperature	Time
Initial denaturation	95°C	120 s
Denaturation	95°C	30 s
Annealing	52–60°C	30 s
Elongation	72°C	60 s per kbp
Final extension	72°C	420 s
Hold	12°C	∞

(Denaturation/Annealing/Elongation repeated 20/30x)

5.3.4 Genotyping of Arabidopsis mutants

For genotyping, genomic DNA was extracted as described in section (5.3.1). The oligonucleotides were designed with the T-DNA Primer Designer from Signal Salk (http://signal.salk.edu/tdnaprimers.2.html) and listed in Table 5.2. Wild-type and T-DNA insertion alleles were identified with left and right genomic oligonucleotides or with the T-DNA oligonucleotide combined with a genomic oligonucleotide as specified in Table 5.4. PCR was performed according to section (5.3.3). To identify mutants with deletions or mutations, the PCR product was digested with enzymes described in section (5.3.5).

Table 5.4: Oligonucleotides used for genotyping of Arabidopsis mutants

Mutant name	Combination for wild-type allele	Combination for T-DNA insertion
gsh1-1	#463; #464	#464; #3053
gsh2-1	#415; #416	#416; #321
ggct2;1-1	#3675; #3676	#3676; #3053
ggct2;1-2	#3677; #3678	#3678; #3053
aux1-21	#3856; #3857: digestion with APaL1	
opt4	#4120; #4121	#4121; #3053
gr1	#330; #331	#331; #3053
bir6	#2985; #2986: digestion with MfeI	
zir1	#3026; #3027: digestion with HindIII	

sir2	#605; #606	#606; #1037
cad2	#747; #748	#748; #749
rml1	#641; #642: digestion with ApoI	
atm3-4	#3523; #3524; digestion with NheI	
gr2epc2	#328; #329	#329; #3053

5.3.5 Digestion of DNA with restriction endonucleases

For digestion of vectors or PCR products, restriction enzymes cutting double-stranded DNA from Fermentas or New England Biolabs were used. Digestion was performed in 20–30 μL final volume with 1–2 U enzyme per 1 μg DNA. Reaction conditions were applied according to manufacturer's recommendations.

5.3.6 DNA Gel electrophoresis

PCR or digested products were separated via agarose gel-electrophoresis. Depending on the size of the fragments, 0.8–2.5% (w/v) agarose was melted in 0.5x TBE-buffer (90 mM Tris-HCl [pH 8], 90 mM boric acid, 0.5 mM EDTA) before ethidium bromide was added to a final concentration of 0.5 μg mL^{-1}. DNA was mixed with loading buffer (0.025% (w/v) bromophenol blue, 0.025% (w/v) xylene cyanole and 4% (v/v) glycerol). GeneRuler™ DNA Ladder Mix (www.thermoscientificbio.com) was used as molecular mass standard. DNA was separated by applying a current of 100–120 V in 0.5x TBE running buffer. The gel was documented using MF-ChemiBIS 2.0 (DNR Bio-Imaging Systems).

5.3.7 PCR product purification from agarose gel

DNA fragments of interest were excised from agarose gels using a scalpel under UV lamp and purified with the NucleoSpin® Gel and PCR Clean-up kit (Macherey-Nagel) according to the manufacturer's recommendations. DNA was eluted in 20 μL dH$_2$O.

5.3.8 Gateway® cloning

Gateway® cloning was performed following the manufacturer's instructions (www.lifetechnologies.com/de/de/home/lifescience/cloning/gatewaycloning/protocols.html). For cloning, the sequence of interest was amplified with *att*B-flanking sites and cloned into an entry vector (pDONR) using the Gateway® BP clonase II enzyme mix. Empty Gateway® vectors used in this study are listed in Table 5.5.

Table 5.5: Vectors used for Gateway® cloning

Vector	Selectable Markers in Bacteria	Description
pDONR201	Kanamycin	entry clone for further Gateway® cloning (Invitrogen)
pDONR207	Gentamycin	entry clone for further Gateway® cloning (Invitrogen)
pUBN-GFP-DEST	Streptomycin	expression clone for further Gateway® cloning (Invitrogen)

The pDONR entry vectors were transformed into *E. coli* DH5α and selected on LB supplemented with antibiotics (5.4.3). The presence of the gene of interest was verified by Colony PCR prior to isolation of the plasmids. The integrity of the purified plasmid (5.4.4) was confirmed by sequencing (5.3.9).

The gene of interest was LR-recombined into a destination vector employing the Gateway® LR clonase II enzyme mix. *E. coli* DH5α were transformed with the recombined vector and subsequently the plasmid was purified and used for plant transformation. The entry and destination clones generated in this study are listed in Table 5.6.

Table 5.6: Donor and expression vectors generated

Entry clone	Expression clone	Usage	Finale organism
pDONR201-cGSH1-SKL	pUBN-cGSH1-SKL-GFP-DEST	Complementation	*A. thaliana gsh1*
pDONR207-cGSH1-SKL	pUBN-cGSH1-SKL-GFP-DEST	Complementation	*A. thaliana gsh1*

5.3.9 DNA sequencing

Donor vectors cloned with gene of interest (5.3.8) were verified by sequencing using the oligonucleotides #689 and #690 (reference table to primer!!!). DNA sequencing was done by StarSeq GmbH (www.starseq.de/com). Samples were prepared according to the company's guidelines.

5.4 Microbiological methods

5.4.1 Bacterial methods

Bacterial strains used in this study are listed in Table 5.7.

Table 5.7: Bacterial strains

Strain	Genotype
E. coli DH5α	F– Φ80*lacZ*ΔM15 Δ(*lacZYA-arg*F) U169 *recA*1 *end*A1 *hsd*R17 (rK–, mK+) *pho*A *sup*E44 λ– *thi*-1 *gyr*A96 *rel*A1
E. coli Origami (DE3)	Δ(ara-leu)7697 Δ lacX74 Δ phoA PvuII phoR ara Δ 139 ahpC gale galK rpsLF′[lac+ lacIq pro] (DE3)gor522::Tn10 trxB (KanR, StrR,TetR
A. tumefaciens C58C1	C58 background; T$_i$-plasmid cured (RifR, AmpR; Deblaere et al., 1985)
A. tumefaciens AGL-1	C58 (RifR), RecA, pTiBo542DT- (CarbR) (Lazo et al., 1991)

5.4.2 Growth conditions for bacteria

Bacteria strains were cultured overnight in LB medium (1% (w/v) tryptone, 0.5% (w/v) yeast extract, 1% (w/v) NaCl, pH 7 with NaOH). *E. coli* and *A. tumefaciens* cells were incubated at 37°C or 28°C, respectively. Selection of transformed bacteria was performed on LB plates containing 1% (w/v) agar and respective antibiotics. For an overnight-culture, a single colony was inoculated in 5 mL of LB medium.

5.4.3 Heat-Shock-Transformation of *E. coli*

One μL of the respective plasmid or 5 μL of the BP/LR reaction was added to 100 μL and incubated on ice for 10 min. The mix was heat-shocked for 50 s at 42°C prior adding 500 μL LB medium. The cells were incubated for 30–60 min at 37°C in a shaking incubator at 160 rpm. Subsequently, the cells were plated on LB-agar plates containing the appropriate antibiotics and incubated overnight at 37°C.

5.4.4 Isolation of plasmid DNA from *E. coli*

E. coli cells containing the plasmid were grown in 5 mL LB medium containing the appropriate antibiotics at 37°C overnight in a shaking incubator. The plasmids were isolated with the NucleoSpin® Plasmid kit (Macherey-Nagel) following the manufacturer's protocol. Eluted DNA was quantified with the spectrophotometer Nano Drop 2000.

5.4.5 Electropulse-Transformation of *A. tumefaciens*

Forty µL electrical competent *A. tumefaciens* cells were mixed with 1 µL of the respective plasmid on ice before transfer to pre-chilled electroporation cuvettes. Cells were pulsed with 2,500 V for approximately 5 ms, followed by addition of 500 µL LB medium. The cell suspension was incubated for 1–2 h at 28°C under shaking conditions. Afterwards, 50–100 µL of the culture was plated on LB-agar plates containing the appropriate antibiotics and incubated for 2 d at 28°C.

5.4.6 Glycerol stocks

Preparation of glycerol stocks was carried out by growing bacteria cultures in 5 mL selective LB medium overnight. Four hundreds µL of the bacterial culture was mixed with 600 µl of 80% (v/v) sterile glycerol in a 2 mL Eppendorf tube. The mixture was shock-frozen in liquid nitrogen and stored at -80°C.

5.4.7 Yeast methods

The yeast strains used in this study are listed in Table 5.8.

Table 5.8: Yeast strains

S. cerevisiae (BY4742) WT	*MATα; his3Δ1; leu2Δ0; lys2Δ0; ura3Δ0* **Wild-type, S288C derivative strain, EUROSCARF**
S. cerevisiae (BY4741) Δ*gsh1*	Mat a; his3Δ1; leu2Δ0; met15Δ0; ura3Δ0; YJL101c::kanMX4
S. cerevisiae Δ*hgt1*	

5.4.8 Growth conditions for *S. cerevisiae*

A single colony of the desired yeast strain was inoculated with microstreaker in YPD medium (1% (w/v) Bacto yeast extract, 2% (w/v) peptone from casein and 2% (w/v) glucose). For selection of transformed yeast cells, medium composed of 0.67% (w/v) yeast nitrogen base (YNB) without amino acids, 0.136% (w/v) yeast synthetic drop-out medium and 2% (w/v) glucose was used, lacking a specific amino acid (10 mg L^{-1} histidine, 10 mg L-tryptophane, 50 mg L-leucine or 10 mg uracil) depending on the used plasmid. Plates were solidified with 2% (w/v) Bacto Agar and cells were streaked and grown 2–3 d at 30°C. The liquid cultures were grown at 30°C over-night at 220 rpm. Growth and sensitivity to BSO was determined on SD plates, prepared as described above, by spotting 1:5 serial dilutions of exponential cultures and recording growth after 2 d of incubation at 30°C

with a stereomicroscope (Leica M165 FC) equipped with a camera (DFC 425 C). Growth rates were assessed in 96-well plates in a volume of 260 µL at 28°C using a plate reader (POLARstar Omega) to monitor the increase of absorbance at 600 nm.

For selection of *hgt1* yeast cells harbouring the Kan4MX selection cassette, geneticin (200-300 µg mL^{-1}) was added to the YPD medium.

5.4.9 Transformation of *S. cerevisiae*

The yeast transformation was performed according to the lithium acetate/single-stranded carrier DNA/PEG method described by Gietz and Schiestl (2007). A single colony of the yeast strain was inoculated with a microstreaker into 10 mL liquid YPD medium and incubated overnight on a rotary shaker at 190 rpm and 30°C. Afterwards, the culture was diluted to an OD_{600} of 0.1 and grown to an OD_{600} of 0.4–0.6. The cells were harvested by centrifugation at 3,000 *g* for 1 min. The pellet was resuspended in 1 mL sterile dH_2O and centrifuged and resuspended again as before. One hundred µL of the yeast cells were added to the transformation mix (240 µl PEG 4000 (50% (w/v)), 36 µL lithium acetate 1.0 M, 50 µL single-stranded carrier DNA (2 mg mL^{-1}; pre-heated for 5 min at 95°C) together with 34 µL plasmid DNA plus sterile dH_2O and vortexed for 1 min. The samples were heat-shocked for 30 min at 42°C before centrifugation at 10,000 *g* for 1 min. The supernatant was discarded and the pellet was resuspended in 100 µL sterile dH_2O. Selection was carried out on SD medium plates supplemented with the corresponding auxotrophic marker and incubated for 3–4 d at 30°C.

5.5 Protein methods and enzyme assays

5.5.1 Modelling of AtGSH1

A homology model of Arabidopsis GSH1 was built with MODELLER (http://salilab.org/modeller/) using *Brassica juncea* GSH1 (BjGSH1; PDB: 2GWC; 96% sequence identity) as a template. The transition state analogon and ADP molecules shown in the structure were modeled according to *E. coli* GCL (PDB: 2D33) after superimposition with the AtGSH1 model.

5.5.2 Affinity-based purification of recombinant roGFP2 protein

Recombinant roGFP2 protein was expressed in *E. coli* Origami DE3 cells and purified via hexa-histidine affinity chromatography using an N-terminal 6xHis-tag. Cells were grown at 37°C to an OD_{600} of ~0.8 in selective LB medium. Protein expression was induced by addition of IPTG (final concentration 1 mM) to the culture. The culture was harvested after induction for 18–24 h at 20°C by centrifugation at 13,000 *g* for 10 min and

resuspended in binding buffer (50 mM Tris-HCl, [pH 8], 250 mM NaCl, 20 mM imidazole and 0.5 mM PMSF). After sonicating the cells for 5 min, cell debris was pelleted by centrifugation at 13,000 g. The sterile-filtered (0.45 µm mesh width) supernatant was loaded on a 1 mL Ni^{2+} pre-loaded HisTrap™ HP affinity column (GE Healthcare) by cycling over the column for at least 30 min with a constant flow rate of 1 mL min^{-1}. The loaded column was washed with 4 mL of wash buffer (50 mM Tris-HCl, pH 8, 250 mM NaCl containing increasing concentrations of imidazole (20, 40, 60 and 80 mM). Finally, the protein was eluted with 250 mM imidazole.

5.5.3 Total protein extraction from Arabidopsis

Leaf tissue of 150–200 mg from 3-week-old plants was transferred to an Eppendorf tube and frozen in liquid nitrogen for grinding. 500 µL extraction buffer (50 mM HEPES KOH [pH 7.4], 10 mM KCl, 1 mM EDTA, 1 mM EGTA, 10% (v/v) glycerol) supplemented with 10 mM DTT and 0.5 mM PMSF were added and vortexed for 15 min. Samples were centrifuged for 10 min at 4°C at max speed to remove cell debris. The samples extracts were desalted via PD-Midi Trap G25 columns following the manufacturer's protocol (www.gelifesciences.com) and eluted in resuspension buffer (100 mM potassium phosphate buffer [pH 7.4], 1 mM EDTA). Extracts were stored at -80°C.

5.5.4 Determination of protein content

The protein concentration of was determined by Bradford assay (Bradford, 1976). Bovine serum albumin (BSA) standards (0, 0.1, 0.2, 0.4 and 0.8 µg µL^{-1}) were used to establish the standard curve. Ten µL of adequately diluted protein solution was mixed with 260 µL Bradford reagent in 96-well plates (Sarstedt, flat base, transparent) and incubated for 5 min at room temperature. Absorbance of the samples with three technical replicates was measured with a plate reader (POLARstar Omega; BMG) and protein concentrations were determined with reference to the absorbance of the standard curve.

5.5.5 SDS-PAGE

Individual proteins were separated by molecular weight on discontinuous gel system (Laemmli, 1970), applying a 4% stacking and 10% resolving gel. Before gel loading, protein samples were diluted to appropriate concentrations and boiled for 5 min at 95°C in 1x Laemmli buffer (2% (w/v) SDS, 20 mM Tris HCl [pH 6.8], 0.02% (w/v) bromophenol blue, 0.4 M DTT and 10% (v/v) glycerol). In addition to samples, molecular mass standards (PageRuler Unstained Protein Ladder; Thermo Scientific) were loaded and the electrophoretic run performed in running buffer (25 mM Tris-HCl [pH 8.3], 192

mM Glycine, 0.1% (v/v) SDS) at 110 V for approximately 120 min until the bromophenol running front reached the bottom of the gel.

5.5.6 Staining of protein gels

Proteins were visualised by incubating the gel for at least 1 h in staining solution (0.1% (w/v) Coomassie, 10% (v/v) acetic acid and 45% (v/v) MeOH) on a shaker. Gels were discoloured with destaining solution containing 10% (v/v) acetic acid and 30% (v/v) EtOH or in dH$_2$O overnight. Gels were documented with an office scanner.

5.5.7 Western blot and *At*GSH1 antibodies

Total cell extract was heated at 95 °C for 5 min and separated on standard SDS-PAGE gels. The wet blot sandwich was assembled in blotting buffer (1.44% glycine (w/v), 0.5% (w/v) Tris, 0.1% SDS (w/v), 20% MeOH (v/v)) and proteins were transferred to the PVDF membrane (BioTrace PVDF Transfer Membrane; Pall Corporation) in the Criterion™ Blotter at 40 mA and 4°C overnight. Afterwards, the membrane was blocked with 5% milk powder in TBS-T (20 mM Tris-HCl [pH 7.6], 137 mM NaCl, 0.1% Tween 20) for 1 h at room temprature. The membrane was washed three times with TBS-T and labeled with 1:500 and 1:5000 diluted primary antiserum overnight at 4°C. The membrane was washed three times with TBS-T for 5 min. Immunolabelling was detected by chemiluminescence using secondary horseradish peroxidase-conjugated antibodies (1:20,000 in 0.5% milk powder in TBS-T) and Pierce ECL Western Blotting Substrate (www.piercenet.com/cat/western-blotting-substrates). Chemiluminescence was detected with the MF-ChemiBIS 2.0 imaging system.

5.5.8 Aconitase and malate dehydrogenase assay

Two-week-old seedlings were homogenised in extraction buffer (50 mM Tris-HCl [pH 8.0], 50 mM KCl, 0.2% (v/v) Triton X-100, 2 mM sodium citrate, 1 mM DTT) and centrifuged for 10 min at 4°C to extract total proteins. Per biological replicate, three technical replicates were performed for the assays in 100 μL total volume.

Aconitase activity was analysed in a coupled assay of 100 μL volume measuring NADPH formation based on the increased absorbance at 340 nm using a plate reader (CLARIOstar; BMG) and 96-well plates (Sarstedt). The reaction mixture contained 50 mM HEPES pH 7.8, 2.5 mM NADP$^+$, 5 mM MnCl$_2$, 0.1% (v/v) Triton X-100 and 0.05 U isocitrate dehydrogenase. After addition of protein extracts from the seedlings, 8 mM cis-aconitic acid was added to start the reaction.

For measuring the malate dehydrogenase activity, absorbance was recorded as above in the following mixture: 0.1 M HEPES [pH 7.8], 0.5 mM NADH, 5 mM MgCl₂, 0.65% (v/v) Triton X-100. The reaction was started by the addition of 750 μM oxaloacetic acid.

5.5.9 Protein sensors subcellular localisation and Microscopy

Fluorescent seedlings and yeast colonies were selected based on fluorescence using the stereomicroscope (Leica M165 FC) equipped with a GFP or DsRed filter. Subsequently, sub-localisation of the protein sensor was assessed with a confocal laser scanning microscope (Zeiss LSM 780, attached to an Axio Observer.Z1 and equipped with different lenses: Plan-Apochromat 10x/0.3 M27, 25x LD LCI Plan-Apochromat 25x/0.8 Imm Korr DIC M27, 40× C-Apochromat 40×/1.2 W Korr and 63× Plan-Apochromat 63×/1.40 Oil DIC (Carl Zeiss Microscopy)) with the use of appropriate markers, *i.e.* chlorophyll fluorescence for plastidic localisation and MitoTracker Orange CM-H₂TMRos (0.5 μM; vacuum infiltration and incubation for >15 min) for mitochondria. Yeast cells were transferred to a slide and immobilised with 0.1% (w/v) agarose. The excitation and emission wave lengths of different sensors are shown in Table 5.9.

5.6 Glutathione measurement

5.6.1 HPLC

Approximately 20 mg plant material were homogenized and extracted in 10-fold volume of 0.1 N HCl. Samples were centrifuged at 4° C for 10 min. 25 μL from the supernatant were mixed with 20 μL 0.1 M NaOH and 1 μL 100 mM freshly prepared dithiothreitol for reduction of disulfides. Samples were vortexed, spin down and incubated at 37°C in darkness for 15 min. Afterwards, 10 μL 1 M Tris/HCl [pH 8.0], 35 μL dH₂O and 5 μL 100 mM monobromobimane in acetonitrile (Thiolyte® MB, Calbiochem) were mixed and added to the samples. The samples were again vortexed, spin down and incubated at 37°C in darkness for 15 min. Then, 100 μL 9% acetic acid were added, vortexed and centrifuged at full speed and 4°C for 15 min. Eventually, ~180 μL supernatant was transferred to HPLC vials. Thiol conjugates were separated by HPLC (SpherisorbTM ODS2, 250 x 4.6 mm, 5 μm, Waters) using two different buffers C (10% MeOH, 0.25% acetic acid, [pH 3,7]) and D (90% MeOH, 0.25% acetic acid, [pH 3,9]). A linear gradient elution from 4 to 20%buffer D added to buffer C within 20 min and a flow rate of 1 mL min⁻¹ was employed. Bimane derivates were detected fluorimetrically (474 detector, Waters) exciting at 390 nm and collecting emission at 480 nm.

5.6.2 Monochlorobimane (MCB) labelling

Five-day-old seedlings were incubated in 100 µM MCB for 30 min followed by 5 min incubation in 50 µM propidium iodide (PI). After washing with dH_2O and careful mounting on a glass slide in a drop of dH_2O (Meyer, 2001), Z-stacks of root tips were collected with a confocal laser scanning microscope (5.5.9). The excitation and emission of GSB (GSH conjugated to bimane) adduct and PI is shown in Table 5.9. The z-stack were projected in ZEN software and exported as single images.

5.6.3 roGFP2 based redox imaging

Five-day-old seedlings stably expressing GRX1 fused roGFP2 were mounted on a slide in a drop of dH_2O and immediately transferred to the confocal microscope imaged with different lenses (5.5.9). roGFP2 was excited in multi-track mode with line switching between 405 nm and 488 nm excitation (Table 5.9). Autofluorescence was excited at 405 nm and collected at 431–470 nm and integrated into image analysis as described previously by Schwarzländer et al. (2008). The intensity outputs of the 405 and 488 nm lasers were kept constant at a 1:3 ratio throughout the experiment. The ratio analysis was performed in a MATLAB software (Fricker, 2016).

5.7 Non-destructive GUS staining

Five-day-old seedlings expressing DR5:GUS were transferred for 20 h to liquid 0.5 MS with 100 µM IAA, either in the presence and absence of 100 µM GSH. Histochemical GUS assays were performed as described previously (Jefferson et al., 1987). In brief, seedlings were incubated in GUS solution (200 µg mL^{-1} X-GlcA (Duchefa Biochemie) in 20 mM sodium phosphate buffer, [pH 7.0]) in darkness at RT until blue tissue colourization became visible. Subsequently, GUS staining in root tips was analysed by bright field microscopy (Axio Observer.Z1, Carl Zeiss Microscopy) equipped with a 20x lens (LD Plan-Neofluar® 20x/0.4 Korr, Carl Zeiss Microscopy) and with a camera (Zeiss AxioCam MRc) using the software Palm Robo V4.5.

5.8 D-II VENUS assay

Five-day-old seedlings expressing DII-VENUS were incubated for 25 min at room temperature in liquid 0.5 MS supplemented with 200 nM IAA or 200 nM IAA and 100 µM GSH. After incubation, seedlings were analysed by confocal microscopy with 40x lens (5.5.9). Excitation and emission of D-II VENUS is shown in Table 5.9.

Table 5.9: Excitation and emission of different chemical and genetic sensors

Sensors	Excitation wave length (nm)	Emission wave length (nm)
GFP	488	504–530
RFP	543	560-640
roGFP2	405/488	504–530
Autoflourescence	405	431–470
Chlorophyll flourescence	488/543	647–745
MitoTracker	543	560–620
DII VENUS	488	500–540
MCB	405	449–613
PI	543	613–704
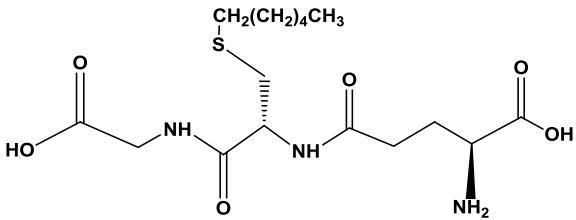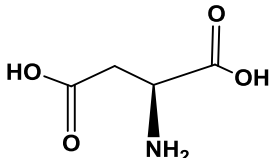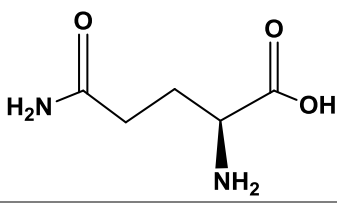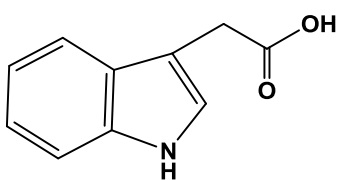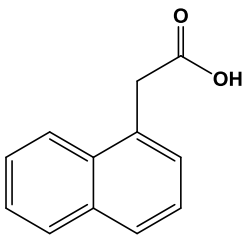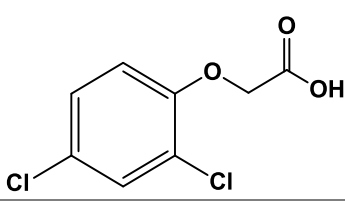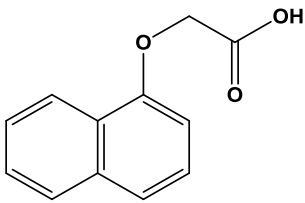
5.9 Feeding experiments and GSH competition assay

Five-day-old seedlings were transferred to liquid 0.5 MS medium supplemented with different substrates for 16-20 h (Table 5.10) and pH adjusted to 5.8.

Table 5.10: Different substrates used for feed experiments

Chemical	Structure	Concentration used
Reduced glutathione (GSH)		50, 100, 150, 200, 250 , 500 and 1000 µM
Cysteine		50 and 1000 µM
Glutamate		50 and 1000 µM
Glycine		50 and 1000 µM

Oxidised glutathione (GSSG)		50, 100, 125, 200, 500 and 1000 μM
N-acetylcysteine (NAC)		50 and 1000 μM
L-Buthionine-sulfoximine (L-BSO)		100, 500 and 1000 μM
MSO		1000 μM
Vanadate		100, 500 and 1000 μM
Glutathionesulfonic acid (GSA)		1000 μM

119
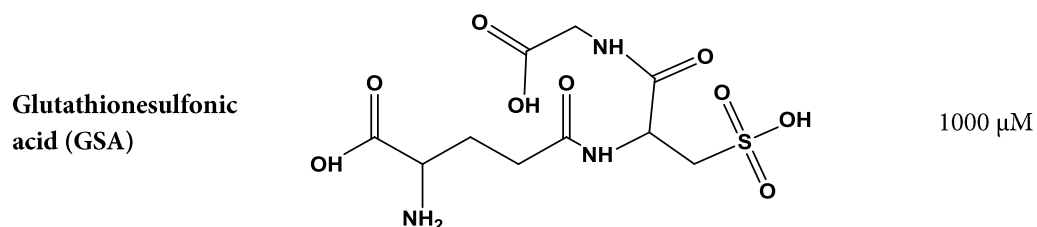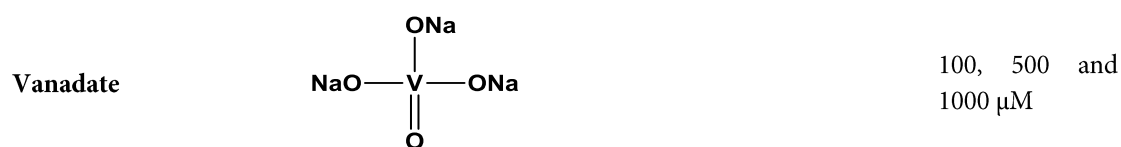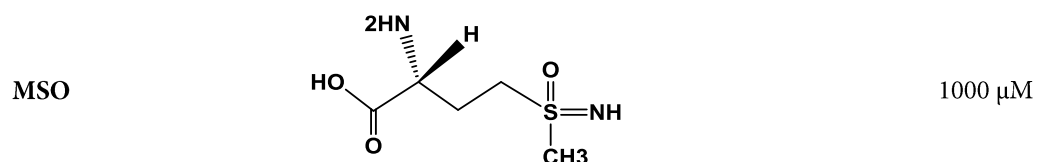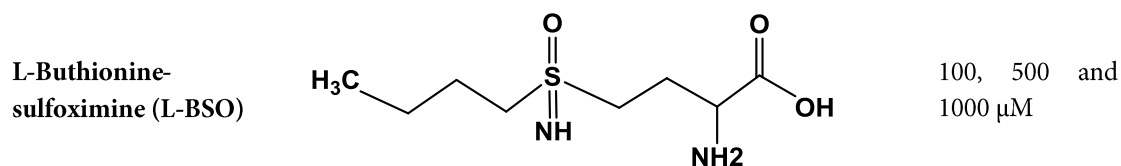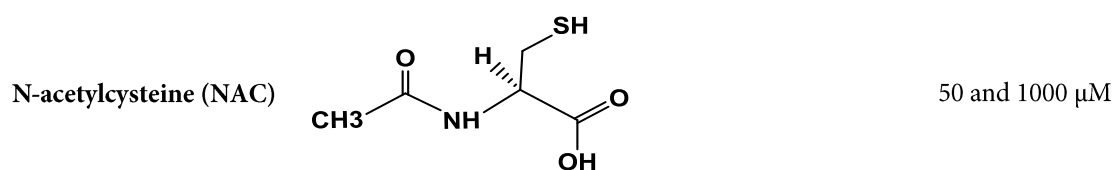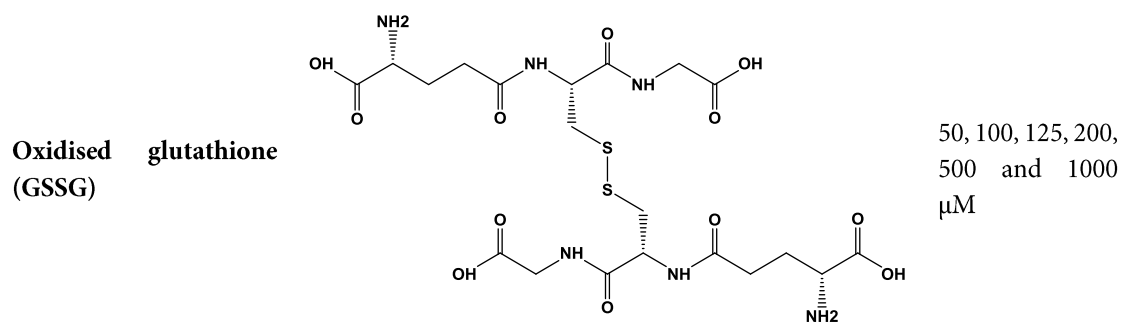
S-Hexylglutathione (S-hexyl-GSH)		1000 μM
Aspartate		1000 μM
Glutamine		1000 μM
Potassium nitrate	KNO3	1000 μM
Indole-3-acetic acid (IAA)		1, 10, 100 and 200 nM
1-Naphthaleneacetic acid (NAA)		100 and 200 nM
2,4-Dichlorophenoxyacetic acid (2, 4D)		100 and 200 nM
1-naphthoxyacetic acid (1 NOA)		100 and 200 nM

2-naphthoxyacetic acid (2 NOA)		100 and 200 nM
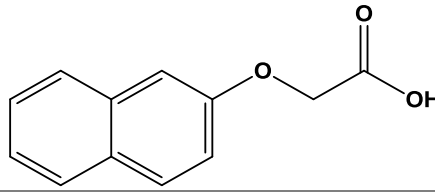
5.10 Grafting of Arabidopsis plants

Grafting was performed in 5-day-old wild-type and *rml1* seedlings grown on 0.5 MS with 1 % (w/v) phytagel. After stratification, seedlings were etiolated for 3 days under long day conditions by covering completely with aluminium foil followed by 2 days in long day condition. Subsequently, wild-type shoots were grafted on *rml1* roots and *vice versa* under a stereomicroscope by using fine scissors and forceps. Grafted seedlings were transferred back to long-day growth conditions.

5.11 Crossing of Arabidopsis plants

Mature siliques and open flowers from the inflorescence of the mother plants were removed, retaining 3–5 flower buds at shoot meristem. Flower buds were open by inserting the tip of fine forceps at bottom of the buds between petals and carpels. Next, all anthers were removed and the stigma was cross-pollinated by shedding pollen from mature flowers of father plants. Pollinated inflorescences were marked and success of pollination was verified by the formation of siliques after two days.

5.12 Statistical Analysis

Statistical analysis was performed with GraphPad Prism 7 (GraphPad Software).

6. REFERENCES

Adams, D.O., and Liyanage, C. (1993). Glutathione increases in Grape Berries at the onset of ripening. American Journal of Enology and Viticulture *44*, 333-338.

Ahmad, N., Malagoli, M., Wirtz, M., and Hell, R. (2016). Drought stress in Maize causes differential acclimation responses of glutathione and sulfur metabolism in leaves and roots. BMC Plant Biology *16*, 247.

Au, K.K.C., Pérez-Gómez, J., Neto, H., Müller, C., Meyer, A.J., Fricker, M.D., and Moore, I. (2012). A perturbation in glutathione biosynthesis disrupts endoplasmic reticulum morphology and secretory membrane traffic in *Arabidopsis thaliana*. Plant Journal *71*, 881-894.

Bachhawat, A.K., Thakur, A., Kaur, J., and Zulkifli, M. (2013). Glutathione transporters. Biochimica et Biophysica Acta *5*, 30.

Ball, L., Accotto, G.-P., Bechtold, U., Creissen, G., Funck, D., Jimenez, A., Kular, B., Leyland, N., Mejia-Carranza, J., and Reynolds, H. (2004). Evidence for a direct link between glutathione biosynthesis and stress defense gene expression in Arabidopsis. The Plant Cell *16*, 2448-2462.

Ballatori, N., Hammond, C.L., Cunningham, J.B., Krance, S.M., and Marchan, R. (2005). Molecular mechanisms of reduced glutathione transport: role of the MRP/CFTR/ABCC and OATP/SLC21A families of membrane proteins. Toxicology and Applied Pharmacology *204*, 238-255.

Ballatori, N., Krance, S.M., Marchan, R., and Hammond, C.L. (2009). Plasma membrane glutathione transporters and their roles in cell physiology and pathophysiology. Molecular Aspects of Medicine *30*, 13-28.

Banhegyi, G., Lusini, L., Puskas, F., Rossi, R., Fulceri, R., Braun, L., Mile, V., di Simplicio, P., Mandl, J., and Benedetti, A. (1999). Preferential transport of glutathione versus glutathione disulfide in rat liver microsomal vesicles. Journal of Biological Chemistry *274*, 12213-12216.

Bashandy, T., Guilleminot, J., Vernoux, T., Caparros-Ruiz, D., Ljung, K., Meyer, Y., and Reichheld, J.-P. (2010). Interplay between the NADP-linked thioredoxin and glutathione systems in Arabidopsis auxin signalling. The Plant Cell *22*, 376-391.

Berndt, C., Hudemann, C., Hanschmann, E.M., Axelsson, R., Holmgren, A., and Lillig, C.H. (2007). How does iron-sulfur cluster coordination regulate the activity of human glutaredoxin 2? Antioxidants & Redox Signalling *9*, 151-157.

Biterova, E.I., and Barycki, J.J. (2010). Structural basis for feedback and pharmacological inhibition of *Saccharomyces cerevisiae* glutamate cysteine ligase. The Journal of Biological Chemistry *285*, 14459-14466.

Bonas, U., Schmitz, K., Rennenberg, H., and Bergmann, L. (1982). Phloem transport of sulfur in Ricinus. Planta *155*, 82-88.

Bonini, M.G., Rota, C., Tomasi, A., and Mason, R.P. (2006). The oxidation of 2',7'-dichlorofluorescin to reactive oxygen species: A self-fulfilling prophesy? Free Radical Biology & Medicine *40*, 968-975.

Bourbouloux, A., Shahi, P., Chakladar, A., Delrot, S., and Bachhawat, A.K. (2000). Hgt1p, a high affinity glutathione transporter from the yeast *Saccharomyces cerevisiae*. Journal of Biological Chemistry *275*, 13259-13265.

Bowman, B.J., and Slayman, C.W. (1979). The effects of vanadate on the plasma membrane ATPase of *Neurospora crassa*. Journal of Biological Chemistry *254*, 2928-2934.

Bowsher, C.G., and Tobin, A.K. (2001). Compartmentation of metabolism within mitochondria and plastids. Journal of Experimental Botany *52*, 513-527.

Bradford, M.M. (1976). A rapid and sensitive method for the quantitation of microgram quantities of protein utilizing the principle of protein-dye binding. Anal Biochem *72*, 248-254.

Brandes, N., Schmitt, S., and Jakob, U. (2009). Thiol-based redox switches in Eukaryotic proteins. Antioxidants & Redox Signalling *11*, 997-1014.

Brechbuhl, H.M., Gould, N., Kachadourian, R., Riekhof, W.R., Voelker, D.R., and Day, B.J. (2010). Glutathione transport is a unique function of the ATP-binding cassette protein ABCG2. Journal of Biological Chemistry *285*, 16582-16587.

Brunoud, G., Wells, D.M., Oliva, M., Larrieu, A., Mirabet, V., Burrow, A.H., Beeckman, T., Kepinski, S., Traas, J., Bennett, M.J., *et al.* (2012). A novel sensor to map auxin response and distribution at high spatio-temporal resolution. Nature *482*, 103-106.

Buchanan, B.B., and Balmer, Y. (2005). Redox regulation: a broadening horizon. Annual Review of Plant Biology *56*, 187-220.

Cagnac, O., Bourbouloux, A., Chakrabarty, D., Zhang, M.-Y., and Delrot, S. (2004). AtOPT6 Transports Glutathione derivatives and is induced by primisulfuron. Plant Physiology *135*, 1378-1387.

Cairns, N.G., Pasternak, M., Wachter, A., Cobbett, C.S., and Meyer, A.J. (2006). Maturation of Arabidopsis seeds is dependent on glutathione biosynthesis within the embryo. Plant Physiology *141*, 446-455.

Caliandro, R., Nagel, K.A., Kastenholz, B., Bassi, R., Li, Z., Niyogi, K.K., Pogson, B.J., Schurr, U., and Matsubara, S. (2013). Effects of altered α- and β-branch carotenoid biosynthesis on photoprotection and whole-plant acclimation of Arabidopsis to photo-oxidative stress. Plant Cell & Environment *36*, 438-453.

Campbell, E.B., Hayward, M.L., and Griffith, O.W. (1991). Analytical and preparative separation of the diastereomers of L-buthionine (SR)-sulfoximine, a potent inhibitor of glutathione biosynthesis. Analytical Biochemistry *194*, 268-277.

Chen, J., Yang, L., Yan, X., Liu, Y., Wang, R., Fan, T., Ren, Y., Tang, X., Xiao, F., and Cao, S. (2016). Zinc-finger transcription factor zat6 positively regulates cadmium tolerance through the glutathione-dependent pathway in Arabidopsis. Plant Physiology *171*, 707-719.

Chen, J.H., Jiang, H.W., Hsieh, E.J., Chen, H.Y., Chien, C.T., Hsieh, H.L., and Lin, T.P. (2012). Drought and salt stress tolerance of an Arabidopsis glutathione S-

transferase U17 knockout mutant are attributed to the combined effect of glutathione and abscisic acid. Plant Physiology *158*, 340-351.

Chen, X., Zhong, Z., Xu, Z., Chen, L., and Wang, Y. (2010). 2',7'-Dichlorodihydrofluorescein as a fluorescent probe for reactive oxygen species measurement: Forty years of application and controversy. Free Radical Research *44*, 587-604.

Chen, Y., Yordanov, Y.S., Ma, C., Strauss, S., and Busov, V.B. (2013). DR5 as a reporter system to study auxin response in Populus. Plant Cell Reports *32*, 453-463.

Cheng, M.C., Ko, K., Chang, W.L., Kuo, W.C., Chen, G.H., and Lin, T.P. (2015). Increased glutathione contributes to stress tolerance and global translational changes in Arabidopsis. Plant Journal *83*, 926-939.

Chew, O., Whelan, J., and Millar, A.H. (2003). Molecular definition of the ascorbate-glutathione cycle in Arabidopsis mitochondria reveals dual targeting of antioxidant defenses in plants. Journal of Biological Chemistry *278*, 46869-46877.

Circu, M.L., and Yee Aw, T. (2008). Glutathione and apoptosis, Vol 42 (Free Radical Research).

Clough, S.J., and Bent, A.F. (1998). Floral dip: a simplified method for *Agrobacterium*-mediated transformation of *Arabidopsis thaliana*. Plant Journal *16*, 735-743.

Cobbett, C., and Goldsbrough, P. (2002). Phytochelatins and metallothioneins: roles in heavy metal detoxification and homeostasis. Annual Review of Plant Biology *53*, 159-182.

Cobbett, C.S., May, M.J., Howden, R., and Rolls, B. (1998). The glutathione-deficient, cadmium-sensitive mutant, *cad2–1*, of *Arabidopsis thalianais* deficient in γ-glutamylcysteine synthetase. Plant Journal *16*, 73-78.

Comini, M.A. (2016). Measurement and meaning of cellular thiol:disufhide redox status. Free Radical Research *50*, 246-271.

Creissen, G., Firmin, J., Fryer, M., Kular, B., Leyland, N., Reynolds, H., Pastori, G., Wellburn, F., Baker, N., Wellburn, A., *et al.* (1999). Elevated glutathione biosynthetic capacity in the chloroplasts of transgenic tobacco plants paradoxically causes increased oxidative stress. The Plant Cell *11*, 1277-1291.

del Río, L.A., Sandalio, L.M., Corpas, F.J., Palma, J.M., and Barroso, J.B. (2006). Reactive oxygen species and reactive nitrogen species in peroxisomes. production, scavenging, and role in cell signalling. Plant Physiology *141*, 330-335.

Dietz, K.J. (2003). Plant peroxiredoxins. Annual Review of Plant Biology *54*, 93-107.

Dietz, K.J., Jacob, S., Oelze, M.L., Laxa, M., Tognetti, V., de Miranda, S.M., Baier, M., and Finkemeier, I. (2006). The function of peroxiredoxins in plant organelle redox metabolism. Journal of Experimental Botany *57*, 1697-1709.

Dixon, D.P., Cummins, L., Cole, D.J., and Edwards, R. (1998). Glutathione-mediated detoxification systems in plants. Current Opinion in Plant Biology *1*, 258-266.

Dooley, C.T., Dore, T.M., Hanson, G.T., Jackson, W.C., Remington, S.J., and Tsien, R.Y. (2004). Imaging dynamic redox changes in mammalian cells with green fluorescent protein indicators. Journal of Biological Chemistry *279*, 22284-22293.

Dron, M., Clouse, S.D., Dixon, R.A., Lawton, M.A., and Lamb, C.J. (1988). Glutathione and fungal elicitor regulation of a plant defense gene promoter in electroporated protoplasts. Proceedings of the National Academy of Sciences *85*, 6738-6742.

Edwards, K., Johnstone, C., and Thompson, C. (1991). A simple and rapid method for the preparation of plant genomic DNA for PCR analysis. Nucleic acids research *19*, 1349.

England, K., Driscoll, C.O., and Cotter, T.G. (2006). ROS and protein oxidation in early stages of cytotoxic drug induced apoptosis. Free Radical Research *40*, 1124-1137.

Fairlamb, A.H., Blackburn, P., Ulrich, P., Chait, B.T., and Cerami, A. (1985). Trypanothione: a novel bis (glutathionyl) spermidine cofactor for glutathione reductase in trypanosomatids. Science *227*, 1485-1487.

Foyer, C.H., and Halliwell, B. (1976). The presence of glutathione and glutathione reductase in chloroplasts: A proposed role in ascorbic acid metabolism. Planta *133*, 21-25.

Foyer, C.H., and Noctor, G. (2001). The molecular biology and metabolism of glutathione. In significance of glutathione to plant adaptation to the environment (Springer), pp. 27-56.

Foyer, C.H., and Noctor, G. (2005). Redox homeostasis and antioxidant signalling: A metabolic interface between stress perception and physiological responses. The Plant Cell *17*, 1866-1875.

Foyer, C.H., Theodoulou, F.L., and Delrot, S. (2001). The functions of inter- and intracellular glutathione transport systems in plants. Trends in Plant Science *6*, 486-492.

Frand, A.R., Cuozzo, J.W., and Kaiser, C.A. (2000). Pathways for protein disulfide bond formation. Trends in Cell Biology *10*, 203-210.

Fricker, M.D. (2016). Quantitative redox imaging software. Antioxidants & Redox Signalling *24*, 752-762.

Frottin, F., Espagne, C., Traverso, J.A., Mauve, C., Valot, B., Lelarge-Trouverie, C., Zivy, M., Noctor, G., Meinnel, T., and Giglione, C. (2009). Cotranslational proteolysis dominates glutathione homeostasis to support proper growth and development. The Plant Cell *21*, 3296-3314.

Galvez-Valdivieso, G., and Mullineaux, P.M. (2010). The role of reactive oxygen species in signalling from chloroplasts to the nucleus. Physiologia Plantarum *138*, 430-439.

García-Giménez, J.L., Markovic, J., Dasí, F., Queval, G., Schnaubelt, D., Foyer, C.H., and Pallardó, F.V. (2013). Nuclear glutathione. Biochimica et Biophysica Acta *1830*, 3304-3316.

Gietz, R.D., and Schiestl, R.H. (2007). High-efficiency yeast transformation using the LiAc/SS carrier DNA/PEG method. Nature Protocols *2*, 31-34.

Gigolashvili, T., and Kopriva, S. (2014). Transporters in plant sulfur metabolism. Frontiers in Plant Science *5*.

Gómez, L.D., Vanacker, H., Buchner, P., Noctor, G., and Foyer, C.H. (2004). Intercellular distribution of glutathione synthesis in Maize leaves and its response to short-term chilling. Plant Physiology *134*, 1662-1671.

Griffith, O.W., Bridges, R.J., and Meister, A. (1978). Evidence that the gamma-glutamyl cycle functions *in vivo* using intracellular glutathione: effects of amino acids and selective inhibition of enzymes. Proceedings of the National Academy of Sciences *75*, 5405-5408.

Griffith, O.W., and Meister, A. (1979). Potent and specific inhibition of glutathione synthesis by buthionine sulfoximine (S-n-butyl homocysteine sulfoximine). Journal of Biological Chemistry *254*, 7558-7560.

Groitl, B., and Jakob, U. (2014). Thiol-based redox switches. Biochimica et Biophysica Acta *8*, 19.

Grzam, A., Martin, M.N., Hell, R., and Meyer, A.J. (2007). γ-Glutamyl transpeptidase GGT4 initiates vacuolar degradation of glutathione S-conjugates in Arabidopsis. FEBS Letters *581*, 3131-3138.

Gutscher, M., Pauleau, A.-L., Marty, L., Brach, T., Wabnitz, G.H., Samstag, Y., Meyer, A.J., and Dick, T.P. (2008). Real-time imaging of the intracellular glutathione redox potential. Nature Methods *5*, 553-559.

Hafer, K., Iwamoto, K.S., and Schiestl, R.H. (2008). Refinement of the dichlorofluorescein assay for flow cytometric measurement of reactive oxygen species in irradiated and bystander cell populations. Radiation Research *169*, 460-468.

Hanson, G.T., Aggeler, R., Oglesbee, D., Cannon, M., Capaldi, R.A., Tsien, R.Y., and Remington, S.J. (2004). Investigating mitochondrial redox potential with redox-sensitive green fluorescent protein indicators. Journal of Biological Chemistry *279*, 13044-13053.

Hartmann, T.N., Fricker, M.D., Rennenberg, H., and Meyer, A.J. (2003). Cell-specific measurement of cytosolic glutathione in poplar leaves. Plant Cell & Environment *26*, 965-975.

Hell, R., and Bergmann, L. (1988). Glutathione synthetase in tobacco suspension-cultures - catalytic properties and localisation. Physiologia Plantarum *72*, 70-76.

Hell, R., and Bergmann, L. (1990). Lambda-Glutamylcysteine synthetase in higher plants: catalytic properties and subcellular localisation. Planta *180*, 603-612.

Hernández, L.E., Sobrino-Plata, J., Montero-Palmero, M.B., Carrasco-Gil, S., Flores-Cáceres, M.L., Ortega-Villasante, C., and Escobar, C. (2015). Contribution of glutathione to the control of cellular redox homeostasis under toxic metal and metalloid stress. Journal of Experimental Botany.

Herschbach, C., and Rennenberg, H. (1995). Long-distance transport of 35S-sulfur in 3-year-old beech trees (*Fagus sylvatica*). Physiologia Plantarum *95*, 379-386.

Hiruma, K., Fukunaga, S., Bednarek, P., Piślewska-Bednarek, M., Watanabe, S., Narusaka, Y., Shirasu, K., and Takano, Y. (2013). Glutathione and tryptophan metabolism are required for Arabidopsis immunity during the hypersensitive response to hemibiotrophs. Proceedings of the National Academy of Sciences *110*, 9589-9594.

Hopkins, F.G.w.a.s.i.t.t.b.L.J.H. (1929). On glutathione: a reinvestigation. Journal of Biological Chemistry *84*, 269-320.

Hothorn, M., Wachter, A., Gromes, R., Stuwe, T., Rausch, T., and Scheffzek, K. (2006). Structural basis for the redox control of plant glutamate cysteine ligase. Journal of Biological Chemistry *281*, 27557-27565.

Iyer-Pascuzzi, A.S., Jackson, T., Cui, H., Petricka, J.J., Busch, W., Tsukagoshi, H., and Benfey, P.N. (2011). Cell identity regulators link development and stress responses in the Arabidopsis root. Developmental Cell *21*, 770-782.

Jefferson, R.A., Kavanagh, T.A., and Bevan, M.W. (1987). GUS fusions: beta-glucuronidase as a sensitive and versatile gene fusion marker in higher plants. EMBO Journal *6*, 3901-3907.

Jiang, K., Schwarzer, C., Lally, E., Zhang, S., Ruzin, S., Machen, T., Remington, S.J., and Feldman, L. (2006). Expression and characterisation of a redox-sensing green fluorescent protein (reduction-oxidation-sensitive green fluorescent protein) in Arabidopsis. Plant Physiology *141*, 397-403.

Jimenez, A., Hernandez, J.A., Del Rio, L.A., and Sevilla, F. (1997). Evidence for the presence of the ascorbate-glutathione cycle in mitochondria and peroxisomes of Pea leaves. Plant Physiology *114*, 275-284.

Jobe, T.O., Sung, D.Y., Akmakjian, G., Pham, A., Komives, E.A., Mendoza-Cózatl, D.G., and Schroeder, J.I. (2012). Feedback inhibition by thiols outranks glutathione depletion: a luciferase-based screen reveals glutathione-deficient γ-ECS and glutathione synthetase mutants impaired in cadmium-induced sulfate assimilation. Plant Journal *70*, 783-795.

Jozefczak, M., Keunen, E., Schat, H., Bliek, M., Hernández, L.E., Carleer, R., Remans, T., Bohler, S., Vangronsveld, J., and Cuypers, A. (2014). Differential response of Arabidopsis leaves and roots to cadmium: Glutathione-related chelating capacity vs antioxidant capacity. Plant Physiology and Biochemistry *83*, 1-9.

Jubany-Marí, T., Meehan, S., López-Carbonell, M., and Alegre, L. (2016). Water-deficit response is not affected by glutathione deficiency in *Arabidopsis thaliana pad2-1* plants. American Journal of Plant Sciences *7*, 2020.

Kim, B.-J., Choi, C.-H., Lee, C.-H., Jeong, S.-Y., Kim, J.-S., Kim, B.-Y., Yim, H.-S., and Kang, S.-O. (2005). Glutathione is required for growth and prespore cell differentiation in Dictyostelium. Developmental Biology *284*, 387-398.

Klapheck, S. (1988). Homoglutathione: isolation, quantification and occurrence in legumes. Physiologia Plantarum *74*, 727-732.

Klapheck, S., Chrost, B., Starke, J., and Zimmermann, H. (1992). γ-Glutamylcysteinylserine—a new homologue of glutathione in plants of the family Poaceae. Plant Biology *105*, 174-179.

Kocsy, G., Tari, I., Vanková, R., Zechmann, B., Gulyás, Z., Poór, P., and Galiba, G. (2013). Redox control of plant growth and development. Plant Science *211*, 77-91.

Koffler, B.E., Bloem, E., Zellnig, G., and Zechmann, B. (2013). High resolution imaging of subcellular glutathione concentrations by quantitative immunoelectron microscopy in different leaf areas of Arabidopsis. Micron *45*, 119-128.

Koh, S., Wiles, A.M., Sharp, J.S., Naider, F.R., Becker, J.M., and Stacey, G. (2002). An oligopeptide transporter gene family in Arabidopsis. Plant Physiology *128*, 21-29.

Koprivova, A., des Francs-Small, C.C., Calder, G., Mugford, S.T., Tanz, S., Lee, B.R., Zechmann, B., Small, I., and Kopriva, S. (2010). Identification of a pentatricopeptide repeat protein implicated in splicing of intron 1 of mitochondrial nad7 transcripts. Journal of Biological Chemistry *285*, 32192-32199.

Krouk, G., Lacombe, B., Bielach, A., Perrine-Walker, F., Malinska, K., Mounier, E., Hoyerova, K., Tillard, P., Leon, S., Ljung, K., *et al.* (2010). Nitrate-regulated auxin transport by NRT1.1 defines a mechanism for nutrient sensing in plants. Developmental Cell *18*, 927-937.

Krueger, S., Niehl, A., Lopez Martin, M.C., Steinhauser, D., Donath, A., Hildebrandt, T., Romero, L.C., Hoefgen, R., Gotor, C., and Hesse, H. (2009). Analysis of cytosolic and plastidic serine acetyltransferase mutants and subcellular metabolite distributions suggests interplay of the cellular compartments for cysteine biosynthesis in Arabidopsis. Plant Cell & Environment *32*, 349-367.

Kumar, A., Tikoo, S., Maity, S., Sengupta, S., Sengupta, S., Kaur, A., and Kumar Bachhawat, A. (2012). Mammalian proapoptotic factor ChaC1 and its homologues function as γ-glutamyl cyclotransferases acting specifically on glutathione. EMBO Reports *13*, 1095-1101.

Kumar, S., Kaur, A., Chattopadhyay, B., and Bachhawat, A.K. (2015). Defining the cytosolic pathway of glutathione degradation in *Arabidopsis thaliana*: Role of the ChaC/GCG family of gamma-glutamyl cyclotransferases as glutathione-degrading enzymes and AtLAP1 as the Cys-Gly peptidase. Biochemical Journal *468*, 73-85.

Kuźniak, E., and Skłodowska, M. (2004). Comparison of two methods for preparing mitochondria from Tomato leaves to study the ascorbate-glutathione cycle activity. Biologia Plantarum *48*, 537-542.

Laemmli, U.K. (1970). Cleavage of structural proteins during the assembly of the head of bacteriophage T4. Nature *227*, 680-685.

Lappartient, A.G., and Touraine, B. (1996). Demand-driven control of root ATP sulfurylase activity and SO42- uptake in intact Canola (The role of phloem-translocated glutathione). Plant Physiology *111*, 147-157.

Lash, L.H., and Jones, D.P. (1984). Renal glutathione transport. Characteristics of the sodium-dependent system in the basal-lateral membrane. Journal of Biological Chemistry *259*, 14508-14514.

Lee, C.P., Wirtz, M., and Hell, R. (2014). Evidence for Several cysteine transport mechanisms in the mitochondrial membranes of *Arabidopsis thaliana*. Plant and Cell Physiology *55*, 64-73.

Lee, R., and Britz-McKibbin, P. (2009). Differential rates of glutathione oxidation for assessment of cellular redox status and antioxidant capacity by capillary electrophoresis-mass spectrometry: an elusive biomarker of oxidative stress. Analytical Chemistry *81*, 7047-7056.

Léran, S., Varala, K., Boyer, J.-C., Chiurazzi, M., Crawford, N., Daniel-Vedele, F., David, L., Dickstein, R., Fernandez, E., and Forde, B. (2014). A unified nomenclature of nitrate transporter 1/peptide transporter family members in plants. Trends in Plant Science *19*, 5-9.

Leustek, T., Martin, M.N., Bick, J.A., and Davies, J.P. (2000). Pathways and regulation of sulfur metabolism revealed through molecular and genetic studies. Annual Review of Plant Physiology and Plant Molecular Biology *51*, 141-165.

Li, L., Lee, T.K., Meier, P.J., and Ballatori, N. (1998). Identification of glutathione as a driving force and leukotriene C4 as a substrate for oatp1, the hepatic sinusoidal organic solute transporter. Journal of Biological Chemistry *273*, 16184-16191.

Li, S. (2014). Redox Modulation Matters: Emerging Functions for Glutaredoxins in plant development and stress responses. Plants *3*, 559-582.

Li, W., Busu, C., Circu, M.L., and Aw, T.Y. (2012). Glutathione in cerebral microvascular endothelial biology and pathobiology: Implications for brain homeostasis. International Journal of Cell Biology *2012*, 434971.

Lillig, C.H., Berndt, C., Vergnolle, O., Lonn, M.E., Hudemann, C., Bill, E., and Holmgren, A. (2005). Characterisation of human glutaredoxin 2 as iron-sulfur protein: a possible role as redox sensor. Proceedings of the National Academy of Sciences *102*, 8168-8173.

Lim, B., Pasternak, M., Meyer, A.J., and Cobbett, C.S. (2014). Restricting glutamylcysteine synthetase activity to the cytosol or glutathione biosynthesis to the plastid is sufficient for normal plant development and stress tolerance. Plant Biology *16*, 58-67.

Lluis, J.M., Morales, A., Blasco, C., Colell, A., Mari, M., Garcia-Ruiz, C., and Fernandez-Checa, J.C. (2005). Critical role of mitochondrial glutathione in the survival of hepatocytes during hypoxia. Journal of Biological Chemistry *280*, 3224-3232.

Lu, S.C. (2013). Glutathione synthesis. Biochimica et Biophysica Acta *1830*, 3143-3153.

Lubkowitz, M. (2011). The oligopeptide transporters: A small gene family with a diverse group of substrates and functions? Molecular Plant *4*, 407-415.

Lushchak, V.I. (2012). Glutathione homeostasis and functions: Potential Targets for medical interventions. Journal of Amino Acids *2012*, 26.

Lyons, T.W., Reinhard, C.T., and Planavsky, N.J. (2014). The rise of oxygen in Earth/'s early ocean and atmosphere. Nature *506*, 307-315.

Marty, L., Siala, W., Schwarzländer, M., Fricker, M.D., Wirtz, M., Sweetlove, L.J., Meyer, Y., Meyer, A.J., Reichheld, J.-P., and Hell, R. (2009). The NADPH-dependent thioredoxin system constitutes a functional backup for cytosolic glutathione reductase in Arabidopsis. Proceedings of the National Academy of Sciences *106*, 9109-9114.

Masi, A., Trentin, A.R., Agrawal, G.K., and Rakwal, R. (2015). Gamma-glutamyl cycle in plants: a bridge connecting the environment to the plant cell? Frontiers in Plant Science *6*, 252.

Maughan, S.C., Pasternak, M., Cairns, N., Kiddle, G., Brach, T., Jarvis, R., Haas, F., Nieuwland, J., Lim, B., Müller, C., *et al.* (2010). Plant homologs of the *Plasmodium falciparum* chloroquine-resistance transporter, *PfCRT*, are required for glutathione homeostasis and stress responses. Proceedings of the National Academy of Sciences *107*, 2331-2336.

Meister, A. (1974). The gamma-glutamyl cycle. Diseases associated with specific enzyme deficiencies. Annals of Internal Medicine *81*, 247-253.

Meister, A. (1988a). Glutathione metabolism and its selective modification. Journal of Biological Chemistry *263*, 17205-17208.

Meister, A. (1988b). On the discovery of glutathione. Trends in Biochemical Sciences *13*, 185-188.

Meister, A., and Tate, S.S. (1976). Glutathione and related gamma-glutamyl compounds: biosynthesis and utilization. Annual Review of Biochemisty *45*, 559-604.

Mendoza-Cozatl, D.G., Xie, Q., Akmakjian, G.Z., Jobe, T.O., Patel, A., Stacey, M.G., Song, L., Demoin, D.W., Jurisson, S.S., Stacey, G., *et al.* (2014). OPT3 is a component of the iron-signalling network between leaves and roots and misregulation of OPT3 leads to an over-accumulation of cadmium in seeds. Molecular Plant *7*, 1455-1469.

Meuwly, P., Thibault, P., and Rauser, W.E. (1993). γ-Glutamylcysteinylglutamic acid-a new homologue of glutathione in maize seedlings exposed to cadmium. FEBS Letters *336*, 472-476.

Meyer, A.J. (2008). The integration of glutathione homeostasis and redox signalling. Journal of Plant Physiology *165*, 1390-1403.

Meyer, A.J., Brach, T., Marty, L., Kreye, S., Rouhier, N., Jacquot, J.P., and Hell, R. (2007). Redox-sensitive GFP in *Arabidopsis thaliana* is a quantitative biosensor for the redox potential of the cellular glutathione redox buffer. Plant Journal *52*, 973-986.

Meyer, A.J., and Dick, T.P. (2010). Fluorescent protein-based redox probes. Antioxidants & Redox Signalling *13*, 621-650.

Meyer, A.J., May, M.J., and Fricker, M. (2001). Quantitative *in vivo* measurement of glutathione in Arabidopsis cells. Plant Journal *27*, 67-78.

Miyake, T., Hazu, T., Yoshida, S., Kanayama, M., Tomochika, K., Shinoda, S., and Ono, B. (1998). Glutathione transport systems of the budding yeast *Saccharomyces cerevisiae*. Bioscience, Biotechnology, and Biochemistry *62*, 1858-1864.

Morgan, B., and Schwarzländer, M. (2016). Fluoreszierende Proteinsensoren für die redoxregulation in lebenden zellen. BIOspektrum *22*, 260-263.

Nagel, K.A., Kastenholz, B., Jahnke, S., van Dusschoten, D., Aach, T., Mühlich, M., Truhn, D., Scharr, H., Terjung, S., Walter, A., *et al.* (2009). Temperature responses of roots: impact on growth, root system architecture and implications for phenotyping. Functional Plant Biology *36*, 947-959.

Nahar, K., Hasanuzzaman, M., Alam, M.M., and Fujita, M. (2015). Glutathione-induced drought stress tolerance in mung bean: coordinated roles of the antioxidant defence and methylglyoxal detoxification systems. AoB Plants 7, plv069.

Newton, G.L., and Javor, B. (1985). Gamma-glutamylcysteine and thiosulfate are the major low-molecular-weight thiols in halobacteria. Journal of Bacteriology 161, 438-441.

Noctor, G., Gomez, L., Vanacker, H., and Foyer, C.H. (2002). Interactions between biosynthesis, compartmentation and transport in the control of glutathione homeostasis and signalling. Journal of Experimental Botany 53, 1283-1304.

Noctor, G., Mhamdi, A., Chaouch, S., Han, Y.I., Neukermans, J., Marquez-Garcia, B., Queval, G., and Foyer, C.H. (2012). Glutathione in plants: an integrated overview. Plant Cell & Environment 35, 454-484.

Noctor, G., Queval, G., Mhamdi, A., Chaouch, S., and Foyer, C.H. (2011). Glutathione. The Arabidopsis Book / American Society of Plant Biologists 9, e0142.

Ogawa, K., Hatano-Iwasaki, A., Yanagida, M., and Iwabuchi, M. (2004). Level of glutathione is regulated by ATP-dependent ligation of glutamate and cysteine through photosynthesis in Arabidopsis thaliana: mechanism of strong interaction of light intensity with flowering. Plant & Cell Physiology 45, 1-8.

Ohkama-Ohtsu, N., Oikawa, A., Zhao, P., Xiang, C., Saito, K., and Oliver, D.J. (2008). A gamma-glutamyl transpeptidase-independent pathway of glutathione catabolism to glutamate via 5-oxoproline in Arabidopsis. Plant Physiology 148, 1603-1613.

Okumura, R., Koizumi, Y., and Sekiya, J. (2003). Synthesis of hydroxymethylglutathione from glutathione and L-serine catalyzed by carboxypeptidase Y. Bioscience, Biotechnology, and Biochemistry 67, 434-437.

Ortiz-Lopez, A., Chang, H., and Bush, D.R. (2000). Amino acid transporters in plants. Biochimica et Biophysica Acta 1, 1-2.

Osawa, H., Stacey, G., and Gassmann, W. (2006). ScOPT1 and AtOPT4 function as proton-coupled oligopeptide transporters with broad but distinct substrate specificities. Biochemical Journal 393, 267-275.

Oven, M., Raith, K., Neubert, R.H., Kutchan, T.M., and Zenk, M.H. (2001). Homo-phytochelatins are synthesised in response to cadmium in azuki beans. Plant Physiology 126, 1275-1280.

Parakh, S., and Atkin, J.D. (2015). Novel roles for protein disulfide isomerase in disease states: a double edged sword? Frontiers in Cell and Developmental Biology 3.

Parisy, V., Poinssot, B., Owsianowski, L., Buchala, A., Glazebrook, J., and Mauch, F. (2007). Identification of PAD2 as a γ-glutamylcysteine synthetase highlights the importance of glutathione in disease resistance of Arabidopsis. Plant Journal 49, 159-172.

Park, J.W., Mieyal, J.J., Rhee, S.G., and Chock, P.B. (2009). Deglutathionylation of 2-Cys peroxiredoxin is specifically catalyzed by sulfiredoxin. Journal of Biological Chemistry 284, 23364-23374.

Pasternak, M., Lim, B., Wirtz, M., Hell, R., Cobbett, C.S., and Meyer, A.J. (2008a). Restricting glutathione biosynthesis to the cytosol is sufficient for normal plant development. The Plant Journal *53*, 999-1012.

Pasternak, M., Lim, B., Wirtz, M., Hell, R., Cobbett, C.S., and Meyer, A.J. (2008b). Restricting glutathione biosynthesis to the cytosol is sufficient for normal plant development. Plant Journal *53*, 999-1012.

Paulose, B., Chhikara, S., Coomey, J., Jung, H.-i., Vatamaniuk, O., and Dhankher, O.P. (2013). A γ-Glutamyl cyclotransferase protects Arabidopsis plants from heavy metal toxicity by recycling glutamate to maintain glutathione homeostasis. The Plant Cell *25*, 4580-4595.

Pike, S., Patel, A., Stacey, G., and Gassmann, W. (2009). Arabidopsis OPT6 is an oligopeptide transporter with exceptionally broad substrate specificity. Plant and Cell Physiology *50*, 1923-1932.

Plessis, A., Cournol, R., Effroy, D., Silva Pérez, V., Botran, L., Kraepiel, Y., Frey, A., Sotta, B., Cornic, G., Leung, J., *et al.* (2011). New aba-hypersensitive Arabidopsis mutants are affected in loci mediating responses to water deficit and dickeya dadantii infection. PLOS ONE *6*, e20243.

Poole, L.B. (2015). The Basics of thiols and cysteines in redox biology and chemistry. Free Radical Biology & Medicine *0*, 148-157.

Queval, G., Jaillard, D., Zechmann, B., and Noctor, G. (2011). Increased intracellular H_2O_2 availability preferentially drives glutathione accumulation in vacuoles and chloroplasts. Plant Cell & Environment *34*, 21-32.

Rashotte, A.M., DeLong, A., and Muday, G.K. (2001). Genetic and chemical reductions in protein phosphatase activity alter auxin transport, gravity response, and lateral root growth. The Plant Cell *13*, 1683-1697.

Rauser, W.E., Schupp, R., and Rennenberg, H. (1991). Cysteine, γ-glutamylcysteine, and glutathione levels in Maize seedlings: distribution and translocation in normal and cadmium-exposed plants. Plant Physiology *97*, 128-138.

Rebbeor, J.F., Connolly, G.C., Dumont, M.E., and Ballatori, N. (1998a). ATP-dependent transport of reduced glutathione in yeast secretory vesicles. Biochemical Journal *334*, 723-729.

Rebbeor, J.F., Connolly, G.C., Dumont, M.E., and Ballatori, N. (1998b). ATP-dependent transport of reduced glutathione on YCF1, the yeast orthologue of mammalian multidrug resistance associated proteins. Journal of Biological Chemistry *273*, 33449-33454.

Reichheld, J.-P., Khafif, M., Riondet, C., Droux, M., Bonnard, G., and Meyer, Y. (2007). Inactivation of thioredoxin reductases reveals a complex interplay between thioredoxin and glutathione pathways in Arabidopsis Development. The Plant Cell *19*, 1851-1865.

Remington, S.J. (2011). Green fluorescent protein: a perspective. Protein Science *20*, 1509-1519.

Rennenberg, H., Schmitz, K., and Bergmann, L. (1979). Long-distance transport of sulfur in *Nicotiana tabacum*. Planta *147*, 57-62.

Rentsch, D., Schmidt, S., and Tegeder, M. (2007). Transporters for uptake and allocation of organic nitrogen compounds in plants. FEBS Letters *581*, 2281-2289.

Reumann, S., Babujee, L., Ma, C., Wienkoop, S., Siemsen, T., Antonicelli, G.E., Rasche, N., Lüder, F., Weckwerth, W., and Jahn, O. (2007). Proteome analysis of Arabidopsis leaf peroxisomes reveals novel targeting peptides, metabolic pathways, and defense mechanisms. The Plant Cell *19*, 3170-3193.

Richman, P.G., and Meister, A. (1975). Regulation of gamma-glutamyl-cysteine synthetase by nonallosteric feedback inhibition by glutathione. Journal of Biological Chemistry *250*, 1422-1426.

Roos, G., and Messens, J. (2011). Protein sulfenic acid formation: from cellular damage to redox regulation. Free Radical Biology & Medicine *51*, 314-326.

Rubio-Aliaga, I., and Daniel, H. (2008). Peptide transporters and their roles in physiological processes and drug disposition. Xenobiotica *38*, 1022-1042.

Rudyk, O., and Eaton, P. (2014). Biochemical methods for monitoring protein thiol redox states in biological systems. Redox Biology *2*, 803-813.

Scandalios, J.G. (2005). Oxidative stress: molecular perception and transduction of signals triggering antioxidant gene defenses. Brazilian Journal of Medical and Biological Research *38*, 995-1014.

Schaedler, T.A., Thornton, J.D., Kruse, I., Schwarzländer, M., Meyer, A.J., van Veen, H.W., and Balk, J. (2014). A conserved mitochondrial atp-binding cassette transporter exports glutathione polysulfide for cytosolic metal cofactor assembly. Journal of Biological Chemistry *289*, 23264-23274.

Schneider, A., Martini, N., and Rennenberg, H. (1992). Reduced glutathione (GSH) transport into cultured tobacco cells. Plant Physiology and Biochemistry *30*, 29-38.

Schneider, A., Schatten, T., and Rennenberg, H. (1994). Exchange between phloem and xylem during long distance transport of glutathione in spruce trees [*Picea abies*[Karst.] L.). Journal of Experimental Botany *45*, 457-462.

Schwarzländer, M., Fricker, M.D., Muller, C., Marty, L., Brach, T., Novak, J., Sweetlove, L.J., Hell, R., and Meyer, A.J. (2008). Confocal imaging of glutathione redox potential in living plant cells. Journal of Microscopy *231*, 299-316.

Sen, C.K., and Packer, L. (2000). Thiol homeostasis and supplements in physical exercise. The American Journal of Clinical Nutrition *72*, 653S-669S.

Senda, K., and Ogawa, K.i. (2004). Induction of PR-1 accumulation accompanied by runaway cell death in the lsd1 mutant of Arabidopsis is dependent on glutathione levels but independent of the redox state of glutathione. Plant and Cell Physiology *45*, 1578-1585.

Sessions, A., Burke, E., Presting, G., Aux, G., McElver, J., Patton, D., Dietrich, B., Ho, P., Bacwaden, J., Ko, C., *et al.* (2002). A high-throughput Arabidopsis reverse genetics system. The Plant Cell *14*, 2985-2994.

Shanmugam, V., Tsednee, M., and Yeh, K.C. (2012). Zinc tolerance induced by iron 1 reveals the importance of glutathione in the cross-homeostasis between zinc and iron in *Arabidopsis thaliana*. Plant Journal *69*, 1006-1017.

Simoni, R.D., Hill, R.L., and Vaughan, M. (2002). The discovery of glutathione by F. Gowland Hopkins and the beginning of biochemistry at Cambridge University. Journal of Biological Chemistry *277*, e13.

Somerville, C., and Ogren, W. (1982). Isolation of photorespiration mutants in *Arabidopsis thaliana*. Methods in chloroplast molecular biology/M Edelman, RB Hallick, and NH Chua, editors.

Stacey, M.G., Osawa, H., Patel, A., Gassmann, W., and Stacey, G. (2006). Expression analyses of Arabidopsis oligopeptide transporters during seed germination, vegetative growth and reproduction. Planta *223*, 291-305.

Sthijns, M., Weseler, A., Bast, A., and Haenen, G. (2016). Time in Redox adaptation processes: from evolution to Hormesis. International Journal of Molecular Sciences *17*, 1649.

Stout, J., Vos, D.D., Vergauwen, B., and Savvides, S.N. (2012). Glutathione biosynthesis in bacteria by bifunctional GshF is driven by a modular structure featuring a novel hybrid ATP-grasp fold. Journal of Molecular Biology *416*, 486-494.

Tegeder, M. (2012). Transporters for amino acids in plant cells: some functions and many unknowns. Current Opinion in Plant Biology *15*, 315-321.

Tzafrir, I., Pena-Muralla, R., Dickerman, A., Berg, M., Rogers, R., Hutchens, S., Sweeney, T.C., McElver, J., Aux, G., Patton, D., *et al.* (2004). Identification of genes required for embryo development in Arabidopsis. Plant Physiology *135*, 1206-1220.

van Gelder, N. (1982). Principles of compartmentation. in experimental neurochemistry (Springer), pp. 183-206.

Van Laer, K., Hamilton, C.J., and Messens, J. (2013). Low-molecular-weight thiols in thiol-disulfide exchange. Antioxidants & Redox Signalling *18*, 1642-1653.

Vanacker, H., Harbinson, J., Ruisch, J., Carver, T.L.W., and Foyer, C.H. (1998). Antioxidant defences of the apoplast. Protoplasma *205*, 129-140.

Vernoux, T., Wilson, R.C., Seeley, K.A., Reichheld, J.-P., Muroy, S., Brown, S., Maughan, S.C., Cobbett, C.S., Van Montagu, M., and Inzé, D. (2000). The root meristemless1/cadmium sensitive2 gene defines a glutathione-dependent pathway involved in initiation and maintenance of cell division during postembryonic root development. The Plant Cell *12*, 97-109.

Vianello, A., Zancani, M., Peresson, C., Petrussa, E., Casolo, V., Krajňáková, J., Patui, S., Braidot, E., and Macrì, F. (2007). Plant mitochondrial pathway leading to programmed cell death. Physiologia Plantarum *129*, 242-252.

Vivancos, P.D., Dong, Y., Ziegler, K., Markovic, J., Pallardo, F.V., Pellny, T.K., Verrier, P.J., and Foyer, C.H. (2010). Recruitment of glutathione into the nucleus during cell proliferation adjusts whole-cell redox homeostasis in *Arabidopsis thaliana* and lowers the oxidative defence shield. Plant Journal *64*, 825-838.

Voehringer, D.W., McConkey, D.J., McDonnell, T.J., Brisbay, S., and Meyn, R.E. (1998). Bcl-2 expression causes redistribution of glutathione to the nucleus. Proceedings of the National Academy of Sciences *95*, 2956-2960.

Wachter, A., Wolf, S., Steininger, H., Bogs, J., and Rausch, T. (2005). Differential targeting of GSH1 and GSH2 is achieved by multiple transcription initiation: implications for the compartmentation of glutathione biosynthesis in the *Brassicaceae*. Plant Journal *41*, 15-30.

Whatley, J.M. (1983). The ultrastructure of plastids in roots. International Review of Cytology *85*, 175-220.

Winter, D., Vinegar, B., Nahal, H., Ammar, R., Wilson, G.V., and Provart, N.J. (2007). An "Electronic Fluorescent Pictograph" browser for exploring and analyzing large-scale biological data sets. PLOS ONE *2*, e718.

Wong, M., Helston, L.M., and Wells, P.G. (1989). Enhancement of murine phenytoin teratogenicity by the gamma-glutamylcysteine synthetase inhibitor L-buthionine-(S,R)-sulfoximine and by the glutathione depletor diethyl maleate. Teratology *40*, 127-141.

Xing, S., Lauri, A., and Zachgo, S. (2006). Redox regulation and flower development: a novel function for glutaredoxins. Plant Biology *8*, 547-555.

Xu, P., Liu, L., Zeng, G., Huang, D., Lai, C., Zhao, M., Huang, C., Li, N., Wei, Z., Wu, H., *et al.* (2014). Heavy metal-induced glutathione accumulation and its role in heavy metal detoxification in *Phanerochaete chrysosporium*. Applied Microbiology and Biotechnology *98*, 6409-6418.

Xu, X., von Löhneysen, K., Soldau, K., Noack, D., Vu, A., and Friedman, J.S. (2011). A novel approach for *in vivo* measurement of mouse red cell redox status. Blood *118*, 3694-3697.

Yadav, S.K. (2010). Heavy metals toxicity in plants: An overview on the role of glutathione and phytochelatins in heavy metal stress tolerance of plants. South African Journal of Botany *76*, 167-179.

Yan, F., Zhu, Y., Müller, C., Zörb, C., and Schubert, S. (2002). Adaptation of H(+)-pumping and plasma membrane H(+) ATPase activity in proteoid roots of white lupin under phosphate deficiency. Plant Physiology *129*, 50-63.

Yang, Y., Hammes, U.Z., Taylor, C.G., Schachtman, D.P., and Nielsen, E. (2006). High-affinity auxin transport by the aux1 influx carrier protein. Current Biology *16*, 1123-1127.

Yen, M.-R., Tseng, Y.-H., and Saier, M.H. (2001). Maize Yellow Stripe1, an iron-phytosiderophore uptake transporter, is a member of the oligopeptide transporter (OPT) family. Microbiology *147*, 2881-2883.

Yu, X., Pasternak, T., Eiblmeier, M., Ditengou, F., Kochersperger, P., Sun, J., Wang, H., Rennenberg, H., Teale, W., Paponov, I., *et al.* (2013). Plastid-localised glutathione reductase2–regulated glutathione redox status is essential for Arabidopsis root apical meristem maintenance. The Plant Cell *25*, 4451-4468.

Zagorchev, L., Seal, C., Kranner, I., and Odjakova, M. (2013). A central role for thiols in plant tolerance to abiotic stress. International Journal of Molecular Sciences *14*, 7405.

Zechmann, B. (2014). Compartment-specific importance of glutathione during abiotic and biotic stress. Frontiers in Plant Science *5*, 566.

Zechmann, B., Mauch, F., Sticher, L., and Muller, M. (2008). Subcellular immunocytochemical analysis detects the highest concentrations of glutathione in mitochondria and not in plastids. Journal of Experimental Botany *59*, 4017-4027.

Zechmann, B., and Müller, M. (2010). Subcellular compartmentation of glutathione in dicotyledonous plants. Protoplasma *246*, 15-24.

Zhai, Z., Gayomba, S.R., Jung, H.I., Vimalakumari, N.K., Pineros, M., Craft, E., Rutzke, M.A., Danku, J., Lahner, B., Punshon, T., *et al.* (2014). OPT3 is a phloem-specific iron transporter that is essential for systemic iron signalling and redistribution of iron and cadmium in Arabidopsis. The Plant Cell *26*, 2249-2264.

Zhang, M.-Y., Bourbouloux, A., Cagnac, O., Srikanth, C.V., Rentsch, D., Bachhawat, A.K., and Delrot, S. (2004). A novel family of transporters mediating the transport of glutathione derivatives in plants. Plant Physiology *134*, 482-491.

Zhang, Z., Xie, Q., Jobe, T.O., Kau, A.R., Wang, C., Li, Y., Qiu, B., Wang, Q., Mendoza-Cózatl, D.G., and Schroeder, J.I. (2016). Identification of *AtOPT4* as a plant glutathione transporter. Molecular Plant *9*, 481-484.

LIST OF FIGURES AND TABLES

SUPPLEMENTARY DATA

Appendix I: Shoot phenotyping of *gsh1* allelic series

Supplementary Figure 1: Potential quantum yield of PSII (Fv/Fm) of Arabidopsis wild-type and *gsh1* mutants grown under control and drought stress conditions. (A) Continuous recording of Fv/Fm during the entire growth period for control and drought-stressed plants **(B)** Fv/Fm on the last day of the drought period 37 days after stratification. **(C)** Fv/Fm at the end of the experiment 43 days after stratification. All values are means ± SD from ≥ 16 biological replicates. Asterisks in each graph indicates significant different with in the same genotype and letters in each graph indicate significant differences among the genotypes as determined by Two-way ANOVA with Tukey's multiple comparisons test; $p \leq 0.05$). For Col-0 and zir1 control plants and drought-treated plants were compared separately (indicated by index numbers).
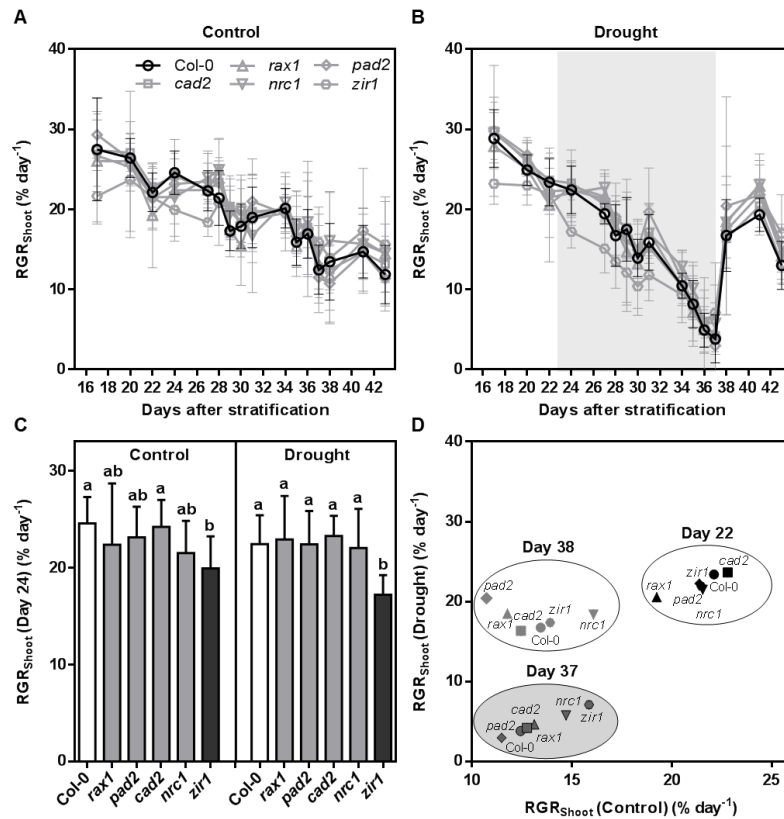
Supplementary Figure 2: Relative shoot growth rate (RGR$_{Shoot}$) in wild-type and *gsh1* mutants grown und control and drought-stress conditions. Continuous recording of RGR$_{Shoot}$ during the entire growth period for control (A) and drought-stressed plants (B). The period of water withdrawal for the drought-stressed population is indicated by a grey shadow. Water withdrawal ended when RGR$_{Shoot}$ approached zero on day 37. (C) RGR$_{Shoot}$ in wild-type and GSH deficient mutants one day after water withdrawal (24 DAS). (D) Comparison of relative growth rates for plants in well-watered and drought stressed populations at three critical time points during the experiment. Symbols for the different lines are used as described in panel A. Letters in each graph indicate significant differences among the genotypes as determined by Two-way ANOVA with Tukey's multiple comparisons test; $p \leq 0.05$).
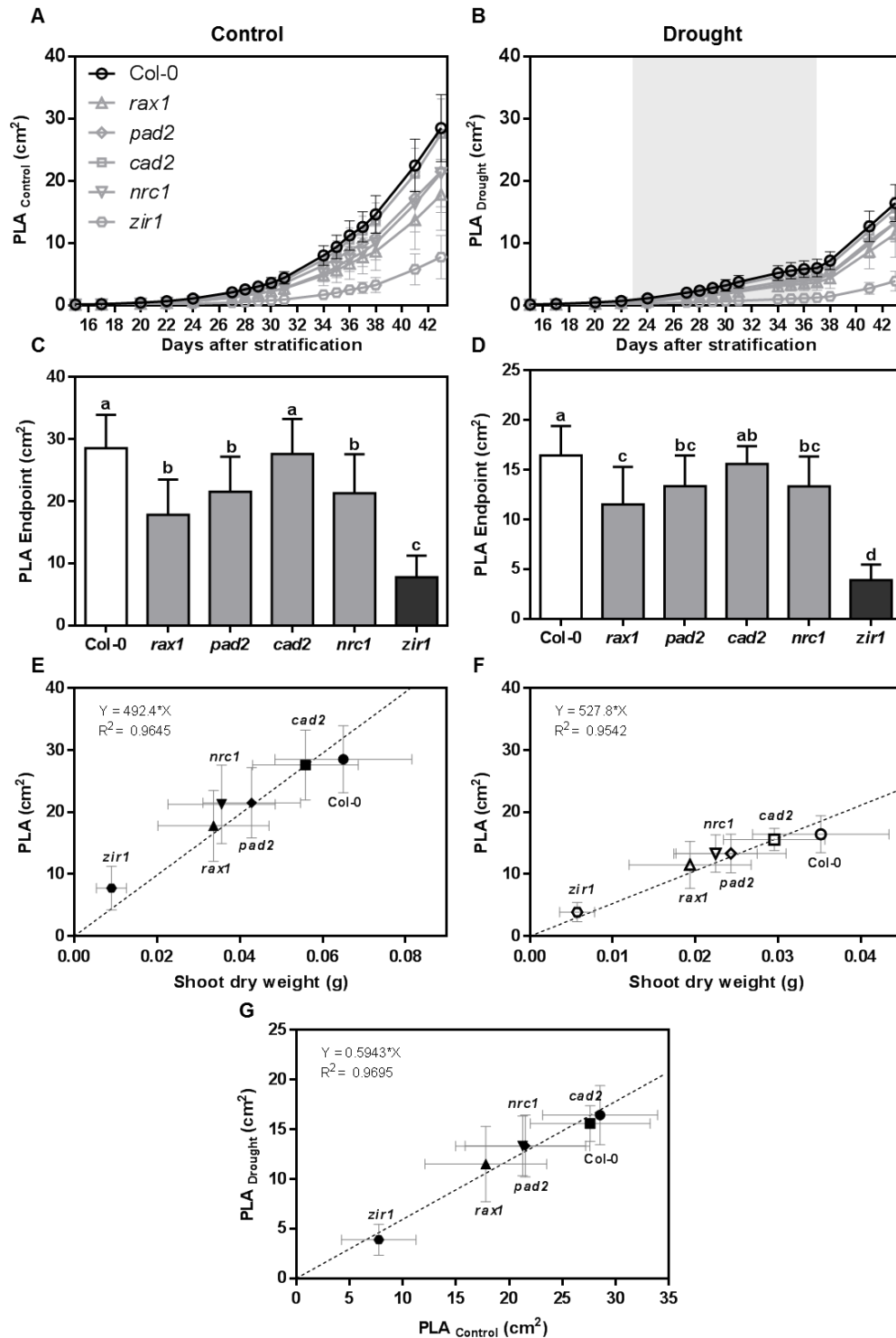
Supplementary Figure 3: Projected leaf area (PLA) in wild-type and *gsh1* mutants grown under control and drought stress conditions. (A, B) Continuous recording of PLA during the entire growth period for control (A) and drought-stressed plants (B). (C, D) PLA at the time of harvest 43 days after stratification for control (C) and drought-stressed (D) plants. (E, F) PLA for wild-type and all *gsh1* mutants under control and drought conditions measured at the end of the growth period. The linear relationships indicated by the trend lines show that the specific leaf area (PLA g^{-1} DW) is not affected by the glutathione content. For calculation of the regression the origin of co-ordinates (point 0/0) was included as an additional virtual data point. (G) Relative PLA. The calculated linear regression indicates a direct correlation between PLA under drought and control conditions for all plant lines under investigation. All values are means ± SD from ### plants randomly distributed on 8 trays.

142
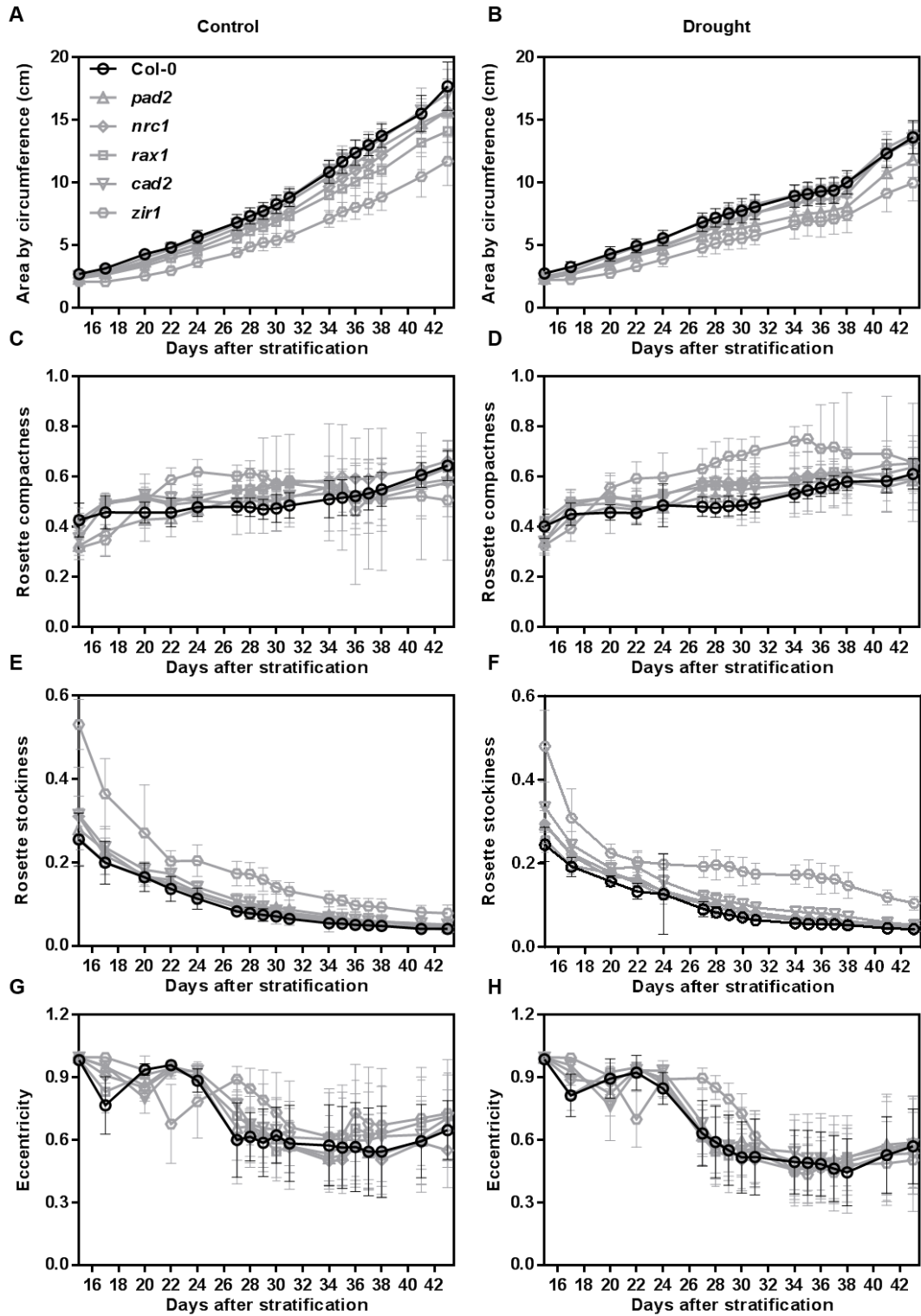
Supplementary Figure 4: Morphological characteristics of rosettes grown under control and drought-stress conditions.

Appendix II: Plant material generated in this project

Supplementary Table 1: Double mutant produced in this project

Double mutants	Purpose
gr1x zir1	GSH function
gr1x rml1	GSH function
bir6 x rml1	GSH function
bir6 x zir1	GSH function
atm3-4 (M29) x gr2 epc2	GSSG transport
ggct2;1-1zir1	GSH degradation
ggct2;1-1rml1	GSH degradation
ggct2;1-2zir1	GSH degradation
ggct2;1-2rml1	GSH degradation
opt4rml1	GSH transport
opt4gsh1	GSH transport
aux1-21rml1	GSH transport
aux1-21gsh1	GSH transport
gsh1_cGSH1xgsh2_ cGSH2	GSH compartmentation
gsh1_ cGSH1xgsh2_ TKTP-GSH2	GSH compartmentation

Supplementary Table 2: Complemented lines produced in this project

Line	Plasmid/Promoter	Construct	Targeted Compartments
gr1_cytoGSH1-GFP	pUBC/UB10	cytoGSH1-GFP	Cytosolic
gsh1-1_cytoGSH1-GFP	pUBC/UB10	cytoGSH1-GFP	Cytosolic
gsh1-1_cytoGSH1-RFP	pUBC/UB10	cytoGSH1-RFP	Cytosolic
gsh1-1_GSH1-GFP	pUBC/UB10	GSH1-GFP	Plastidic
gsh1-1_GSH1-RFP	pUBC/UB10	GSH1-RFP	Plastidic
gsh1-1-GFP-GSH1-SKL	pUBN/UB10	GFP-GSH1-SKL	Peroxisomal
gsh2-1_GSH2-GFP	pUBC/UB10	GSH2-GFP	Cytosolic (floral dipped, need to screen)
gsh2-1_GSH2-RFP	pUBC/UB10	GSH2-RFP	Cytosolic (floral dipped, need to screen)
gsh2-1_TKTP-GSH2-GFP	pUBC/UB10	GSH2-RFP	Plastidic (floral dipped, need to screen)
gsh2-1_TKTP-GSH2-RFP	pUBC/UB10	GSH2-RFP	Plastidic (floral dipped, need to screen)

144

Supplementary Table 3: roGFP2 reporter lines produced in this project

Line	Plasmid/Promoter	Construct	Targeted Compartments
Col-0	pBinCM,Ubi10	GRX1-roGFP2	Cytosol
rax1	pBinCM,Ubi10	GRX1-roGFP2	Cytosol
pad2	pBinCM,Ubi10	GRX1-roGFP2	Cytosol
cad2	pBinCM,Ubi10	GRX1-roGFP2	Cytosol
nrc1	pBinCM,Ubi10	GRX1-roGFP2	Cytosol
zir1	pBinCM,Ubi10	GRX1-roGFP2	Cytosol
rml1	pBinCM,Ubi10	GRX1-roGFP2	Cytosol
Col-0	pBinCM,Ubi10	TKTP-GRX1-roGFP2	Plastid
rax1	pBinCM,Ubi10	TKTP-GRX1-roGFP2	Plastid
pad2	pBinCM,Ubi10	TKTP-GRX1-roGFP3	Plastid
cad2	pBinCM,Ubi10	TKTP-GRX1-roGFP4	Plastid
nrc1	pBinCM,Ubi10	TKTP-GRX1-roGFP5	Plastid
zir1	pBinCM,Ubi10	TKTP-GRX1-roGFP6	Plastid
rml1	pBinCM,Ubi10	TKTP-GRX1-roGFP7	Plastid
Col-0	pBinCM,Ubi10	SHMT-roGFP2,GRX1	Mitochondria
rax1	pBinAR,35S	SHMT-roGFP2,GRX1	Mitochondria
pad2	pBinAR,35S	SHMT-roGFP2,GRX1	Mitochondria
cad2	pBinAR,35S	SHMT-roGFP2,GRX1	Mitochondria
nrc1	pBinAR,35S	SHMT-roGFP2,GRX1	Mitochondria
zir1	pBinAR,35S	SHMT-roGFP2,GRX1	Mitochondria
rml1	pBinAR,35S	SHMT-roGFP2,GRX1	Mitochondria
clt1,2,3	pBinCM,Ubi10	GRX1-roGFP2	Cytosol
clt1,2,3	pBinCM,Ubi10	TKTP-GRX1-roGFP2	Plastid
trxo-1	pBinCM,Ubi10	SHMT-roGFP2,GRX1	Mitochondria
nrtrab	pBinCM,Ubi10	GRX1-roGFP2	Cytosol
nrtrab	pBinCM,Ubi10	SHMT-roGFP2,GRX1	Mitochondria
sir-1cad2	pBinCM,Ubi10	GRX1-roGFP2	Cytosol
sir-1cad2	pBinCM,Ubi10	TKTP-GRX1-roGFP2	Plastid
ggct2;1-1	pBinCM,Ubi10	GRX1-roGFP2	Cytosol
ggct2;1-2	pBinCM,Ubi10	GRX1-roGFP2	Cytosol
opt4rml1	pBinCM,Ubi10	GRX1-roGFP2	Cytosol
aux1-21rml1	pBinCM,Ubi10	GRX1-roGFP2	Cytosol

LIST OF ABBREVIATIONS

ABA	Abscisic acid
ACO	Aconitase
Asp	Aspartate
ATP	Adenosine triphosphate
BSA	Bovine serum albumin
BSO	L-buthionine-(S, R)-sulfoximine
CLSM	Confocal laser scanning microscopy
Cys	Cysteine
dNTP	Deoxynucleotide triphosphates
DPS	4,4'-dipyridyl disulfide (Aldrithiol TM-4)
DTT	1,4-dithiothreitol
EDTA	Ethylenediaminetetraacetic acid
E_{GSH}	Glutathione redox potential
EtOH	Ethanol
Gln	Glutamine
Glu	Glutamate
Gly	Glycine
GSA	Glutathione sulfonic acid
GR	Glutathione reductase
GRX	Glutaredoxin
GSH	Reduced glutathione
GSSG	Oxidised glutathione, glutathione disulfide
HEPES	4-(2-hydroxyethyl)-1-piperazineethanesulfonic acid
His	Histidine
HPLC	High-performance liquid chromatography
IAA	Indole-3-acetic acid
IPTG	Isopropyl-D-1-thiogalactopyranoside
MCB	Monochlorobimane
MDH	Malatedehydrogenase
LB-medium	lysogeny broth - medium
MeOH	**Methanol**
MES	2-(N-morpholino)ethanesulfonic acid
MS-medium	Murashige-Skoog - **medium**
MSO	Methionine sulfoximine
NAA	1-naphthaleneacetic acid
NADH	β-nicotinamide adenine dinucleotide (reduced)

NADPH	β-nicotinamide adenine dinucleotide phosphate (reduced)
NPF	Nitrate transporter 1/ peptide transporter family
OD	Optical density
PCR	Polymerase chain reaction
PEG	Polyethylene glycol
pK$_a$	Acid dissociation constant
PMSF	Phenylmethane sulfonyl fluoride
PI	Propidium iodide
roGFP2	Redox-sensitive green fluorescent protein 2
RO/NS	Reactive oxygen/nitrogen species
SD	Standard deviation
SD medium	Synthetic defined medium
S-hexyl-GSH	S-hexyl-glutathione
T-DNA	Transfer deoxyribonucleic acid
TKTP	Transketolase transit peptide
Tris-HCl	Tris(hydroxymethyl)aminomethane hydrochloride
TRX	Thioredoxin
v/v	volume per volume
w/v	weight per volume
2,4-D	2,4-diclorophenoxyacetic acid

PUBLICATIONS

Part of the doctoral studies were published or submitted in the following publications:

Published:

Delorme-Hinoux V, **Bangash SAK**, Meyer AJ, Reichheld J-P (2016). Nuclear thiol redox systems in plants. Plant Science, 243, 84-95; doi: 10.1016/j.plantsci.2015.12.002.

Submitted:

Sajid A.K. Bangash, David Solbach, Kerstin Nagel, Marcus Jansen, Fabio Fiorani, Markus Schwarzländer, Stanislav Kopriva and Andreas J. Meyer (2017) Genetic depletion of glutathione does not cause increased drought sensitivity. Experimental Journal of Botany.

In preparation:

At low concentrations glutathione is more important as a cofactor than for redox control

Sajid A. K. Bangash, Anna Moseler, Kerstin Nagel, Marcus Jansen, David Solbach, Stephan Wagner, Markus Schwarzländer, Stanislav Kopriva, Andreas Meyer Stephan Krüger?

GENERAL STATEMENT

I declare that I am the sole author of this submitted dissertation. Where the work of others has been consulted, this is duly acknowledged in the thesis. I have not made use of any sources apart from those specifically referred to and all verbatim or referential use of the sources are indicated as such. I also affirm that this thesis has not been submitted in the same or similar form, or in extracts, within the context of another examination or institution.

------------------   --------------------------

Place, Date   Sajid Ali Khan Bangash

ACKNOWLEDGMENT